Using Organotypic Tumour Slices to Optimise 5T4 CAR-T Cell Therapy for Pancreatic Ductal Adenocarcinoma



Alice Evans

Keble College

University of Oxford

A thesis submitted for the degree of

Doctor of Philosophy

Trinity term, 2025

Supervised by Eric O'Neill and Hua Ye

Declaration

I declare that the work presented in this thesis is wholly my own, except where otherwise stated. It has not been submitted in whole, or in part, for consideration for any other degree or qualification in this or any other university.

Alice Evans

For Mum and Dad,

I am extraordinarily lucky to be your daughter.

Abstract

Pancreatic ductal adenocarcinoma (PDAC) has a 5-year survival rate of less than 10%. This is due to a combination of limited treatment options, late diagnosis due to subtlety of symptoms, and frequent metastatic spread. Systemic control of disease can be achieved with chemotherapy, but chemotherapeutic resistance and dose-limiting toxicities frequently lead to disease recurrence. There are currently no licenced immunotherapies for PDAC, due to the dense desmoplastic stroma and immunosuppressive microenvironment. Whilst these parameters are central to the immune 'cold' nature of most PDAC tumours, they are not accurately represented by preclinical models.

Chimeric antigen receptor (CAR) T cell therapy has markedly improved the prognosis of multiple forms of haematological malignancy. Despite this success, no CAR-T cell therapies are currently licensed for use in solid tumours. Lack of tumour infiltration, antigen escape, local microenvironmental suppression, and difficulties identifying tumour specific antigens all contribute to the challenge of translating CAR-T cell therapy beyond haematological cancers.

Organotypic tumour slices allow these challenges to be addressed by preserving the cellular heterogeneity, soluble signalling and stromal structure of the native tumour. This thesis aims to use PDAC tumour slices to evaluate the efficacy of a novel CAR-T cell construct targeting the oncofoetal antigen 5T4. The expression of 5T4 across pancreatic tumours and PDAC cell lines was characterised, confirming the suitability of the target. Anti-5T4 CAR-T cells displayed selective and efficient cytotoxicity against $5T4^+$ cell lines *in vitro* along with high levels of IFNγ, granzyme B and IL-2 release. Autologous patient CAR-T cells were applied to tumour slices showing co-localisation with $5T4^+$ cells. The lack of cytotoxicity seen *ex vivo*

prompted analysis of tumour slice-derived suppressive soluble factors and donor-specific T cell characteristics.

I demonstrate the utility of organotypic tumour slices in evaluating novel CAR-T cell therapies in a patient-relevant model prior to clinical trial.

Acknowledgements

First, I would like to thank my supervisor Professor Eric O'Neill - your support and guidance over the last four years has been brilliant. I am also very grateful to Professor Cathy Ye, Dr Kyriacos Mitrophanous, Dr Bernard Souberbielle, Dr Anna Ettorre and Dr Daniel Blount - it's been a pleasure to learn from you all. Additionally, I would like to thank The Medical Research Council and Oxford Biomedica for funding my project and providing some amazing experiences beyond the lab. This project would not have been possible without their support.

I am so grateful to the members of the O'Neill lab for being excellent colleagues and wonderful friends. Thank you to Tess and Simei for being an amazing support over the years; you are both brilliant scientists and even more brilliant people. To Ben, Giamp, Alex, Shannon, Elsita, Ash, Gift, Az and Tinos, thank you for brightening even the most disastrous of lab days. I'll really miss debating which media looks the most drinkable with you (it's definitely DMEM).

Thank you, Keaton, for your invaluable advice; your capacity for work will never cease to impress and terrify me in equal measure. Thank you Hala for always being such a generous mentor to so many people - Oncology is so lucky to have you. Thank you again, Giamp, for not only being a ray of sunshine but also a flow cytometry wizard - you've taught me so much. To Mayowa and Laura, thank you for all your support at OXB. I have loved my time there and am so grateful to have spent it learning from you both.

Thank you to all the HPB surgical team for your generous help with sample collection for this project. Martin, your help coordinating samples has been invaluable and your warmth and dedication to patients are so inspiring.

To the wonderful facilities team at Oncology; Caroline, Nicki, Andy, Sarah, Pash, Christopher, Saji, and Jiaqi, thank you for all you do for us. Your kindness and hard work are so appreciated.

To my wonderful Keble friends; Luke, Max, Ollie and Luca, thank you for the happiest home. I will miss our flat dinners very much. Thank you, Megan, for being both the most wonderful friend and inspiration - I'm beyond excited for the future members of The Payne Lab. Thank you, Claudia, for your love of 2000s club classics which founded our friendship. I want to be you when I grow up. To the brilliant friends I have made through the triathlon club; Rory, Emma, Jess, Ellie, Harriet, I can't wait for so many more years of adventuring with you.

To Dr Parkin and Mrs Keyes - thank you for inspiring me to pursue a career in science. I admire you both so much and am so grateful for your encouragement over the years.

Thank you to Emily for always being there for me, I can't wait to celebrate this phase of our lives along with so many others. Emma, you are the best adventure companion and I'm so excited for what the future holds for us both. I promise you don't actually have to read this thesis. Darling Fred, thank you for being there through thick and thin. I can't wait to drink my body weight in sangria with you.

To Mum and Dad, thank you for being my biggest cheerleaders. Thank you for four years of love and kindness in some particularly tough times. Mum, I am so in awe of your determination and utterly grateful for all that you do for me. Dad, I so admire your intellectual curiosity and am thrilled to have inherited your love of unorthodox dance moves. I really am so grateful for our little family.

Finally, to Harri, thank you for unwavering companionship, support and silliness throughout these last four years. Your kindness and love of adventure have made even the tough bits so much fun. I can't wait for the next chapter.

"A model is a lie that helps you see the truth."

Siddhartha Mukherjee

Contents

Abbreviations **xvi**

1 Introduction **1**

1.1 Pancreatic Cancer 1

1.1.1 Normal Biology of the Pancreas 1

1.1.2 Common Forms of Pancreatic Cancer 2

1.1.2.1 Pancreatic Ductal Adenocarcinoma 2

1.1.2.2 Pancreatic Neuoendocrine Tumours 3

1.1.2.3 Cholangiocarcinoma 3

1.1.3 Diagnosis and Early Detection 4

1.1.4 Current Mainline Treatment Strategies 5

1.2 Pre-Clinical Models of PDAC 7

1.2.1 Cell Lines 7

1.2.2 Murine Models 7

1.2.3 Organoids and Spheroids 9

1.2.4 Organotypic Tumour Slices 11

1.3 Immunotherapy 13

1.3.1 Immune Checkpoint Inhibitors 14

1.3.2 Adoptive Cell Therapies 15

1.3.3 CAR-T Cell Therapy 15

1.3.3.1 Early CAR-T Cell Development 15

1.3.3.2 Licenced Therapies 16

1.3.3.3 Adverse Events 18

1.3.3.4 Manufacturing Cost 19

1.3.3.5 Development of Allogeneic CAR-T Cells 20
1.3.3.6 Challenges Associated with Solid Tumours 21
1.3.3.6.1 Improvements to CAR-T Cell Receptor Sensitivity 22
1.3.3.6.2 Logic Gating to Exploit Antigen Combinations 24
1.3.3.6.3 TRUCKs and Engineered Outputs 24
1.3.3.6.4 Loco-Regional CAR-T Cell Delivery . . . 25
1.3.3.6.5 Clinical Trials in PDAC 26
1.4 Oncofoetal Antigens 28
1.4.1 Therapeutic Utility 28
1.4.2 Trophoblast Glycoprotein 29
1.4.2.1 Function in Development and Stemness 29
1.4.2.2 Potential as a Therapeutic Target 29
1.5 Study Aims 30

2 Materials and Methods 31

2.1 Cell and Tissue Culture 31
2.1.1 Acquisition of Tissue and Blood Samples 31
2.1.2 Sectioning and Culture of Live Tumour Slices 35
2.1.3 Tissue Digestion 36
2.1.4 Cell Culture 36
2.1.5 Purification of PBMCs from Whole Blood 37
2.1.6 CAR-T Cell Generation and Culture 37
2.2 Protein Expression Analysis 39
2.2.1 Western Blot 39
2.2.2 Histological Analysis – Immunohistochemistry (IHC) 40
2.2.3 5T4 ELISA 41
2.2.4 IL-6 ELISA 42
2.2.5 Cytokine Array 42
2.2.6 Cytokine Bead Array (CBA) 43

2.3 T Cell Migration and Cytotoxicity 44
2.3.1 Co-Culture - Flow Cytometry 44
2.3.2 Co-Culture - xCELLigence Impedance Assay) 45
2.3.3 Transwell Migration 46
2.3.4 CAR-T Cell Culture with IL-6 47
2.3.5 Tumour and Cell Line Conditioned Media Suppression . . . 48
2.4 Immunofluorescence and Imaging 48
2.4.1 Immunofluorescence (IF) 48
2.4.1.1 PDAC Slices with Jurkat T Cells 48
2.4.1.2 PDAC Slices with Matched Patient T Cells 50
2.4.1.3 PDAC Slices with Matched Patient CAR-T Cells . 50
2.4.1.4 Live Cell Imaging 51
2.4.1.5 Imaris Image Processing 53
2.5 Flow Cytometry 53
2.5.1 Flow Cytometry 53
2.5.2 Spectral Flow Cytometry 56
2.6 Statistical and Computational Analysis 59
2.6.1 Survival Analysis 59
2.6.2 AlphaFold Protein Mapping 59
2.6.3 Differential Expression Gene Analysis 59
2.6.4 Statistical Analysis 60
2.7 Ancillary Methods and Materials 61
2.7.1 qPCR 61
2.7.2 Reagents 62

3 Characterisation of 5T4 Antigen Expression in PDAC and Anti-5T4 CAR-T Cell Generation 63

3.1 Introduction 63
3.1.1 The 5T4 Antigen in PDAC 63
3.1.2 CAR-T Cell Targets in PDAC 64
3.1.3 Anti-5T4 CAR-T Cell Manufacturing Considerations 66

3.1.4 Aims . . . 67
3.2 Results . . . 68
3.2.1 Prognostic Impact of Antigen Expression in PDAC Patients 68
3.2.2 Antigen Expression Across Patient Cohorts . . . 69
3.2.3 Antigen Shedding and CAR Binding Site . . . 71
3.2.4 Antigen Surface Expression on Human Tumour Cells . . . 74
3.2.5 Total 5T4 Protein Expression in Pancreatic Cell Lines . . . 75
3.2.6 Antigen Surface Expression in Cell Lines . . . 77
3.2.7 Anti-5T4 CAR-T Cell Culture Condition Optimisation . . . 78
3.2.8 Anti-5T4 CAR-T Cell Generation, Transduction Efficiency, and Expansion . . . 81
3.2.9 CAR-T Cell Phenotyping . . . 82
3.3 Discussion . . . 84
3.3.1 Conclusion . . . 89

4 In Vitro Efficacy of Anti-5T4 CAR-T Cells 90
4.1 Introduction . . . 90
4.1.1 In Vitro Cytotoxicity Assays . . . 90
4.1.2 Cytokines Associated with CAR-T Cell Cytotoxicity . . . 91
4.1.3 Aims . . . 94
4.2 Results . . . 94
4.2.1 Selective Cytotoxicity of Anti-5T4 CAR-T Cells with OXB-Validated Cell Lines Using Flow Cytometry . . . 94
4.2.2 Cytokine Production from OXB-Validated Cell Line Co-Culture with CAR-T Cells . . . 96
4.2.3 Selective Cytotoxicity of 5T4+ PDAC Cell Lines by Anti-5T4 CAR-T Cells . . . 98
4.2.4 Cytokine Production from PDAC Cell Line Co-Culture with CAR-T cells . . . 101
4.2.5 Effect of IL-6 Supplementation on CAR-T Cell Viability, Proliferation, and Exhaustion . . . 102

4.2.6 Effect of IL-6 Supplementation on CAR-T Cell Cytotoxicity and Cytokine Production 104
4.3 Discussion 106
4.3.1 Conclusion 109

5 Ex Vivo Efficacy of Autologous Anti-5T4 CAR-T Cells Cultured with Organotypic Tumour Slices 110

5.1 Introduction 110
5.1.1 Use of 3D Models in Cancer 110
5.1.2 Organotypic Tumour Slice Culture 111
5.1.3 Organotypic Tumour Slice Analysis 112
5.1.4 Studying Immunotherapy Efficacy with Tumour Slices . . . 113
5.1.5 Live Imaging of CAR-T Cells and Tumour Slices 113
5.1.6 The Impact of the TME on T cells in PDAC 115
5.1.7 Aims 117
5.2 Results 117
5.2.1 Immunofluorescence Validation for Depth and Colocalisation Measurements of Exogenous T Cells in PDAC Slices 117
5.2.2 Activation of Autologous T Cells is Necessary for Adhesion to Slices 119
5.2.3 Autologous CAR-T Cell Treatment of PDAC Tumour Slices - Patient 1 121
5.2.4 Autologous CAR-T Cell Treatment of PDAC Tumour Slices - Patient 2 123
5.2.5 Autologous CAR-T Cell Treatment of Cholangiocarcinoma Tumour Slices - Patient 3 125
5.2.6 Effect of Tumour Slice Conditioning on CAR-T Cell Efficacy 127
5.2.7 RNAseq Analysis of Differentially Expressed Receptors for Soluble Factors in PDAC Tumour T Cells 130
5.2.8 Tumour Conditioned Media Cytokine Array - Part I 131
5.2.9 Tumour Conditioned Media Cytokine Array - Part II 133

5.3 Discussion 135
5.3.1 Conclusions 141

6 Spectral Flow Cytometry for Analysis of Patient and Healthy Donor-Derived CAR-T Cells 142

6.1 Introduction 142
6.1.1 Current Knowledge of Donor Fitness Impact on CAR-T Cell Therapy Efficacy 142
6.1.2 T Cell Exhaustion States 144
6.1.3 TCF1 and PD-1 Define a Progenitor Subset of Exhausted T Cells 145
6.1.4 The Role of TCF1 in CD4 T Cells 146
6.1.5 Suppressive Adenosine Signalling 147
6.1.6 Aims 148
6.2 Results 149
6.2.1 In Vitro Cytotoxicity of Healthy Donor and Patient-Derived CAR-T Cells 149
6.2.2 Marker Selection in Spectral Flow Cytometry Panel 150
6.2.3 Demographics of Patient PBMC Donors 152
6.2.4 Transduction Efficiency and CD4:CD8 of Patient and Healthy Donor-Derived T Cells 154
6.2.5 T Cell Phenotypic Variation Between Patient and Healthy Donors 156
6.2.6 Inhibitory Receptor Expression of Patient and Healthy Donor CAR T Cells 157
6.2.7 TCF1 Expression in Patient and Healthy Donor CAR-T Cells 159
6.2.8 CAR-T Cell Terminal Exhaustion 161
6.2.9 Suppressive Adenosine Signalling 162
6.2.10 UMAP Dimensionality Reduction 163
6.3 Discussion 165
6.3.1 Conclusions 169

7 Discussion **170**

7.1 Contribution to Knowledge 171

7.2 Opportunities and Limitations 174

7.3 Closing Remarks 178

Appendices

A Results 1: Appendix **180**

B Results 2: Appendix **184**

C Results 3: Appendix **187**

D Results 4: Appendix **193**

References **196**

Abbreviations

ADAM	a disintegrin and metalloproteinase
ADC	antibody-drug conjugate
ALL	acute lymphoblastic leukaemia
AML	acute myeloid leukaemia
ANOVA	analysis of variance
APP	amyloid precursor protein
AR	adenosine receptor
ATP	adenosine triphosphate
BACE	beta-site amyloid precursor protein cleaving enzyme 1
BCA	bicinchoninic acid
BMI	body mass index
BRC	Biomedical Research Centre
BSA	bovine serum albumin
BSG	basigin
CA	cancer antigen
CAF	cancer-associated fibroblast
CAR	chimeric antigen receptor
CAYA	children, adolescents, and young adults
CBA	cytokine bead array
CBD	cancer of the bile duct
CCL	C-C chemokine ligand
CCM	cell line-conditioned media
CCR	C-C chemokine receptor

CD	cluster of differentiation
CEA	carcinoembryonic antigen
CI	cell index
CLL	chronic lymphocytic leukaemia
CMFDA	5-chloromethylfluorescein diacetate
CMV	cytomegalovirus
CPTAC	Clinical Proteomic Tumor Analysis Consortium
CRC	colorectal cancer
CRR	complete response rate
CRS	cytokine release syndrome
CSC	cancer stem cell
CSF	cerebrospinal fluid
CTLA-4	cytotoxic T-lymphocyte-associated antigen
CXCL	C-X-C motif chemokine ligand
CXCR	C-X-C motif chemokine receptor
CysLTR	cysteinyl leukotriene receptor
DAB	diaminobenzidine
DAPI	diamidino-2-phenylindole
DC	distal cholangiocarcinoma/dendritic cell
DEG	differential gene expression
DMEM	Dulbecco's modified Eagle's medium
DMSO	dimethyl sulfoxide
DPX	dibutylphthalate polystyrene xylene
DTT	dithiothreitol
ECL	electrochemiluminescence
EDTA	ethylenediaminetetraacetic acid
ELISA	enzyme-linked immunosorbent assay
EMT	epithelial-mesenchymal transition
EMTR	elution microtubes RS

EOMES	eomesdermin
ERK	extracellular signal-regulated kinase
FACS	fluorescence-activated cell sorting
FBS	foetal bovine serum
FDA	Food and Drug Administration
FFPE	formalin-fixed paraffin-embedded
FMO	fluorescence minus one
FOLFIRINOX	folinic acid, fluorouracil, irinotecan and oxaliplatin
FSC	forward scatter
gDNA	genomic deoxyribonucleic acid
GEMM	genetically engineered mouse model
GM-CSF	granulocyte-macrophage colony-stimulating factor
GMP	good manufacturing practice
GR	glucocorticoid receptor
GvHD	graft versus host disease
HBSS	Hank's Balanced Salt Solution
HGF	hepatocyte growth factor
HLA	human leukocyte antigen
HNSCC	head and neck squamous cell carcinoma
HPV	human papilloma virus
HRP	horseradish peroxidase
hTERT	human telomerase reverse transcriptase
HvG	host versus graft
ICANS	immune effector cell-associated neurotoxicity syndrome
ICI	immune checkpoint inhibitor
IDO	indoleamine-pyrrole 2,3-dioxygenase
IF	immunofluorescence
IFN	interferon

IgG	immunoglobulin G
IHC	immunohistochemistry
IL	interleukin
IPMN	intraductal papillary mucinous neoplasms
ISG	interferon-stimulated gene
KPC	$Kras^{LSL.G12D+-}$; $Trp53^{LSL.R17H+-}$; Pdx1-Cre
KRAS	Kirsten rat sarcoma
LAG3	lymphocyte activation gene 3
LBCL	large B cell lymphoma
LCMV	lymphocytic choriomeningitis virus
LG	low glucose
LMA	low melting point agarose
LPS	lipopolysaccharide
LRR	leucine-rich repeat
MACS	magnetic-activated cell sorting
MAIT	mucosal-associated invariant T
MCL	mantle cell lymphoma
MCP	monocyte chemoattractant protein
MDSC	myeloid-derived suppressor cell
MFI	mean fluorescence intensity
MHC	major histocompatibility complex
MM	modified T cell medium/multiple myeloma
MMP	matrix metalloproteinase
MOI	multiplicity of infection
MOPS	4-morpholinepropanesulfonic acid
mRNA	messenger ribonucleic acid
NBF	neutral buffered formalin
NCI	National Cancer Institute

NCL	nucleolin
NFAT	calcineurin-dependent nuclear factor of activated T cells
NHS	National Health Service
NIHR	National Institute for Health and Care Research
NIR	near infrared
NK	natural killer
NoD	new-onset diabetes
OPG	osteoprotegerin
ORR	objective response rate
OS	overall survival
OXB	Oxford Biomedica
P4HB	protein disulphide isomerase
PanIN	pancreatic intraepithelial neoplasia
PBMC	peripheral blood mononuclear cell
PBS	phosphate-buffered saline
PCR	polymerase chain reaction
PD-L1	programmed cell death ligand 1
PD-1	programmed cell death protein 1
PDAC	pancreatic ductal adenocarcinoma
PDO	patient-derived organoid
PDX	patient-derived xenograft
PET	polyethylene terephthalate
PFA	paraformaldehyde
PFS	progression-free survival
PI3K	phosphoinositide 3-kinase
pLDDT	predicted local distance difference test
PMA	phorbol 12-myristate 13-acetate
PNET	pancreatic neuroendocrine tumours
POC	point-of-care

PP	pancreatic polypeptide
PSC	pancreatic stellate cell
PTGR	prostaglandin receptor
PVDF	polyvinylidene fluoride
qPCR	quantitative polymerase chain reaction
REC	research ethics committee
RIPA	radioimmunoprecipitation assay
ROP	research operating procedure
ROS	reactive oxygen species
RPM	revolutions per minute
RPMI	Roswell Park Memorial Institute
RPPH1	ribonuclease P RNA component H1
RT	room temperature
RTCA	real-time cell analyser
scFv	single chain variable fragment
SCT	stem cell therapy
SNIPR	synthetic intramembrane proteolysis receptor
SPIC	spiked PCR inhibition control
SSC	side scatter
$\mathbf{T_{CM}}$	central memory T cell
$\mathbf{T_{eff}}$	effector T cell
$\mathbf{T_{EM}}$	effector memory T cell
$\mathbf{T_{SCM}}$	T memory stem cell
TAA	tumour-associated antigen
TAM	tumour-associated macrophage
TBST	tris-buffered saline with Tween 20
TCF1	T cell factor 1
TCGA	The Cancer Genome Atlas

TCM	tumour-conditioned media
TCR	T cell receptor
$\mathbf{Tex_{term}}$	terminally exhuasted T cell
TGF	transforming growth factor
TGLU	Translational Gastroenterology and Liver Unit
Th	T-helper cell
TIGIT	T cell immunoreceptor with immunoglobulin and ITIM domain
TIL	tumour-infiltrating lymphocyte
TIM3	T cell immunoglobulin and mucin domain-containing protein 3
TM	thawing media
TME	tumour microenvironment
TNF	tumour necrosis factor
TOX	thymocyte selection-associated HMG BOX
TPBG	trophoblast glycoprotein
Tpex	progenitor exhausted T cell
TRAC	T cell receptor alpha constant
TRAIL	tumor necrosis factor-related apoptosis-inducing ligand
Treg	regulatory T cell
TRuC	T cell receptor fusion construct
TRUCK	T cells redirected for universal cytokine-mediated killing
TSA	tumour-specific antigen
TSG	Translational Sciences Group
UC	unconditioned
UMAP	Uniform Manifold Approximation and Projection
UTC	untransduced control
VCN	vector copy number
VEGF	vascular endothelial growth factor
VIP	vasoactive intestinal peptide
WT	wildtype

"Continuous improvement is better than delayed perfection"

Mark Twain

1 Introduction

1.1 Pancreatic Cancer

1.1.1 Normal Biology of the Pancreas

The pancreas (Figure 1.1) is divided anatomically into a head, body and tail and is located in the upper abdomen, posterior to the stomach. The head of the pancreas is surrounded by the duodenum while the tail extends towards the spleen. Up to 80% of the total cellular mass of the pancreas is dedicated to its exocrine function (Leung 2010). This is performed by acinar and ductal cells which secrete digestive enzymes and sodium bicarbonate respectively. These components form part of the iso-osmotic pancreatic juice, combining with mucus secreted by goblet cells (Karpińska and Czauderna 2022). The fluid is transported to the duodenum through the main pancreatic duct, joining the bile duct at the hepatopancreatic ampulla to enter via the major duodenal papilla. Distinct from the exocrine secretory cells are the Islets of Langerhans which perform the endocrine function of the pancreas. This involves the production of hormones including insulin, somatostatin, pancreatic polypeptide (PP), and glucagon. These hormones respond to fluctuations in blood glucose to control intracellular glucose uptake and release and maintain homeostasis (Leung 2010).

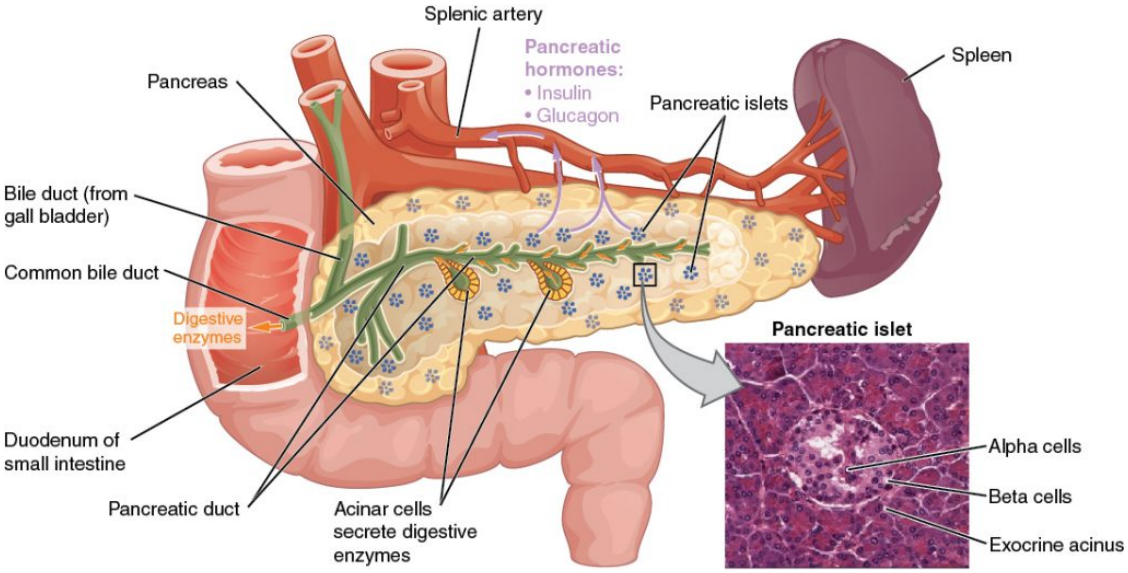


Figure 1.1: The anatomy of the pancreas. The pancreas has endocrine and exocrine functions facilitated by the islets of Langerhans and acinar cells respectively. The overall structure of the pancreas is depicted including its proximity to the spleen and connections to the gallbladder and duodenum via the bile duct. Figure taken from Anatomy and Physiology (Biga et al. 2019) which is open access under the Creative Commons Attribution-ShareAlike 4.0 International License.

1.1.2 Common Forms of Pancreatic Cancer

1.1.2.1 Pancreatic Ductal Adenocarcinoma

PDAC accounts for more than 90% of pancreatic malignancies. Tumours are classically thought to be derived from ductal cells but the exact cellular origins remain unknown (Backx et al. 2022). Patients often present to the clinic at a later stage due to the nonspecific symptoms associated with disease. This late-stage diagnosis in combination with ineffective therapies contributes to a high mortality rate. 5-year survival for PDAC is just 8% (Siegel, Miller and Jemal 2018) and it has recently become the third leading cause of cancer-related death in the US (Halbrook et al. 2023). PDAC arises from non-invasive precursor lesions including pancreatic intraepithelial neoplasias (PanINs) or intraductal papillary mucinous neoplasms (IPMNs) (Ren, Xiaoying Liu and Suriawinata 2019). These lesions progress slowly, with a model generated using data from National Cancer Institute (NCI)'s Surveillance, Epidemiology, and End Results program suggesting that it takes around 11-12 years for a high-grade PanIN to progress and become PDAC

(Peters et al. 2018). This process occurs sequentially with early events including Kirsten rat sarcoma *(KRAS)* mutation and *CDKN2A* loss (Kanda et al. 2012). *SMAD4* loss and *TP53* mutations are seen later in high-grade PanINs (Maitra, Adsay et al. 2003). The early development of activating *KRAS* mutants in neoplasias with limited progression potential (Carpenter et al. 2023) highlights the difficulty of using such genetic signatures as biomarkers (H. Kato and Bardeesy 2024).

1.1.2.2 Pancreatic Neuoendocrine Tumours

Pancreatic neuroendocrine tumours (PNETs) are the second most common pancreatic malignancy, constituting between 3-7% of pancreatic tumours (Singh et al. 2025). PNETs are diverse in their presentation with large variability in speed of tumour growth and hormone secretion profiles. The median survival time for patients diagnosed with PNETs is 4.1 years - approximately 8 times longer than those diagnosed with the more common PDAC (J. C. Brooks, Shavelle and Vavra-Musser 2019). While the majority of PNETs are 'non-functional' i.e. do not produce endocrine hormones, the subset of functional neoplasms frequently lead to severe hormonal symptoms such as hypoglycaemia (Okabayashi et al. 2013) or Zollinger-Ellison syndrome (Hain et al. 2016). These functional tumours display increased survival rates in the first few years following diagnosis, likely due to earlier detection facilitated by hormonal symptoms (J. C. Brooks, Shavelle and Vavra-Musser 2019).

1.1.2.3 Cholangiocarcinoma

While not a cancer of the pancreas, distal cholangiocarcinomas (DC) present with similar symptoms and are often confused with PDAC during diagnosis (Gkountakos et al. 2023). Both are classed as periampullary tumours and are treated with surgical resection with pancreaticoduodenecomy - known as the Whipple procedure (see Chapter 1.1.4). Mortality associated with cholangiocarcinoma is similarly high to PDAC with a 5-year survival of roughly 10% (Rizvi and Gores 2013). While these cancers are often treated synonymously, a recent retrospective multi-centre study showed that adjuvant chemotherapy ± radiation had no effect on survival for DC, unlike results seen in PDAC (Ethun et al. 2017). These results indicate

the importance of examining cholangiocarcinomas as a distinct disease and further refining post-surgery treatment strategies.

1.1.3 Diagnosis and Early Detection

Early detection of PDAC is currently limited due to a combination of subtle symptoms and rapid metastatic dissemination (Halbrook et al. 2023). Weight loss, abdominal pain and jaundice are the most common symptoms reported by patients. Given the non-specific nature of the first two symptoms, this often means that a pancreatic cancer diagnosis is slow to materialise. Whilst presentation with jaundice helps to direct diagnosis, jaundice usually indicates that the tumour is large enough to obstruct the bile duct or is already disseminated, hence the disruption to liver function (Ceniceros, Prados and Alvarez Gallego 2021). This lack of rapid diagnosis is known to reduce survival times; a study from Johns Hopkins showed a statistically significant increase in the number of surgical resections performed on patients who were diagnosed less than 60 days following their initial medical appointment (Deshwar et al. 2018).

One potential avenue to increase the proportion of PDAC cases diagnosed earlier is screening for at-risk groups. This particular strategy is currently employed for those over the age of 50 with either genetic risk due to syndromes such as hereditary pancreatitis, CDKN2A gene mutations or Lynch syndrome, or familial risk with at least two affected genetically related relatives (Elta et al. 2018; Aslanian, J. H. Lee and Canto 2020; Goggins et al. 2020). A meta-analysis of patients with a family history of PDAC who were regularly screened showed that only 20% of those diagnosed had metastatic disease - significantly lower than in the general population (Corral et al. 2019).

The diagnosis of new-onset diabetes (NoD) in patients over the age of 50 has been highlighted as cause for investigation and additional screening on those with familial risk of pancreatic cancer (Goggins et al. 2020). Patients with pancreatic cancer frequently develop diabetes prior to their cancer diagnosis, with causes thought to be linked to cancer-associated chronic inflammation and altered glucose

metabolism (Zhao Liu et al. 2023). Currently, multiple studies are investigating the link between NoD and pancreatic cancer, one such study includes performing regular MRIs to determine PDAC incidence in the 3 years following diagnosis of NoD (S. T. Chari et al. 2022; Maitra, Ayush Sharma et al. 2018; Frank et al. 2021). These investigations will better characterise the elevated risk in this group and hopefully facilitate the development of new screening programmes to prevent cancers being missed (Khalaf and Ali 2022).

1.1.4 Current Mainline Treatment Strategies

Surgery and chemotherapy are the primary treatment options for PDAC. However, due to the aforementioned prevalence of late diagnosis, only 10-15% of patients are eligible for surgery (Sarfaty et al. 2023; Siegel, Miller and Jemal 2018) and the majority present with disseminated or non-resectable disease. Non-metastatic cases are sub-divided into resectable, borderline resectable and locally advanced/unresectable disease.

All forms of the disease are treated with chemotherapy, along with immediate resection in cases of resectable disease and resection, if possible, following neoadjuvant (i.e prior to surgery) chemotherapy in borderline resectable disease. Treatment of locally advanced PDAC involves initial chemotherapy followed by chemoradiation in patients with good performance status. Patients with metastatic disease are treated with chemotherapy followed by either targeted treatment in cancers with *BRCA1* or *BRCA2* mutation or second-line chemotherapy (Y. Jiang and Sohal 2023).

FOLFIRINOX (a combination of oxaliplatin, leucovorin, irinotecan and 5-FU) is often given as the primary chemotherapeutic combination but frequently leads to adverse events and is not suitable for patients experiencing frailty. Alternative options include mFOLFIRINOX which has a reduced 5-FU dosage and the combination of nab-paclitaxel and gemcitabine (Netto et al. 2024). A recent phase III study investigated the efficacy of NALIRIFOX which uses liposomal irinotecan to prevent unwanted pro-drug metabolism and increase availability in tissue. The combination

demonstrated an improved overall survival (OS) and objective response rate (ORR) compared to nab-paclitaxel and gemcitabine (Wainberg, Melisi et al. 2023).

Surgical resection is carried out with the Whipple procedure, which is a complex surgery involving removal of the head of the pancreas, duodenum, gallbladder and bile duct. The gastrointestinal tract must then be reconstructed to restore function. It is a technically challenging surgery which poses significant risks including pancreatic leaks, postoperative infection and delayed gastric emptying (D'Cruz et al. 2025). Advances in surgical techniques such as laparoscopy (Y.-L. Jiang, R.-C. Zhang and Y.-C. Zhou 2019) or robotic assistance (Mantzavinou et al. 2022) have improved outcomes but the procedure is still associated with significant morbidity and mortality (Kimura et al. 2014).

Neoadjuvant chemotherapy is not used universally in PDAC but is an area of significant research interest due to its potential both to prolong survival in resectable patients and increase both resection and survival rates in borderline resectable patients. Given that recurrence rates following surgery are documented to be around 37.9% within a year of resection (Murakawa et al. 2023), achieving early control of potential systemic spread is vital to improving long-term outcomes. Given the invasive nature of the Whipple procedure, effective chemotherapy doses may be better tolerated prior to surgery (Seufferlein et al. 2023). These advantages must be balanced with the risks associated with delaying surgery, particularly for patients who do not respond to chemotherapy and therefore experience disease progression. A clinical trial with both borderline resectable and resectable patients indicated a modest but significant improvement in OS with neoadjuvant chemotherapy, despite the delay this causes to surgery (Versteijne et al. 2022). This regimen has not been confirmed to confer a significant survival advantage specifically in patients with resectable disease, meaning further trials are needed to confirm the best course of treatment for this subset of patients (Springfeld et al. 2023).

1.2 Pre-Clinical Models of PDAC

1.2.1 Cell Lines

The majority of early pre-clinical research in PDAC is performed using cell line monolayers. Commonly used cell lines are derived not only from primary tumours but also ascites fluid and metastatic sites. Each cell line also carries a distinct genetic profile, morphology and differentiation status leading to diverse phenotypic characteristics (Deer et al. 2010; Shichi et al. 2022). Even fundamental genetic changes seen widely throughout PDAC cases vary between cell lines; BxPC-3 are *KRAS* wildtype (WT) while Capan-1 and Capan-2 share a G12V mutation (Berrozpe et al. 1994). It is important that genetic and morphological variation is accounted for when selecting cell lines in order to represent the diversity of patient tumours.

1.2.2 Murine Models

Murine models provide the ability to study the development of cancers in a whole organism and observe the systemic effects of therapeutic interventions. Mouse models are segmented broadly into genetically engineered mouse models (GEMMs), patient-derived xenograft models (PDXs), chemically induced models, and syngeneic mouse models (Figure 1.2). Autochthonous GEMMs can spontaneously form tumours due to genetic mutations that predispose the mice to cancer. Certain GEMMs can also be induced, using an agent such as Tamoxifen, to genetically activate desired genes in the model. PDX models use immunocompromised mice injected with cells derived from patient tumours. PDX models are faster and tumour growth rates are more uniform throughout cohorts, while GEMMs provide the ability to observe the early stages of tumour establishment in the context of an intact host immune system. Syngeneic mouse models bridge this gap through the use of murine tumour cell injections allowing the use of immunocompetent hosts (Mallya et al. 2021; J. W. Lee et al. 2016).

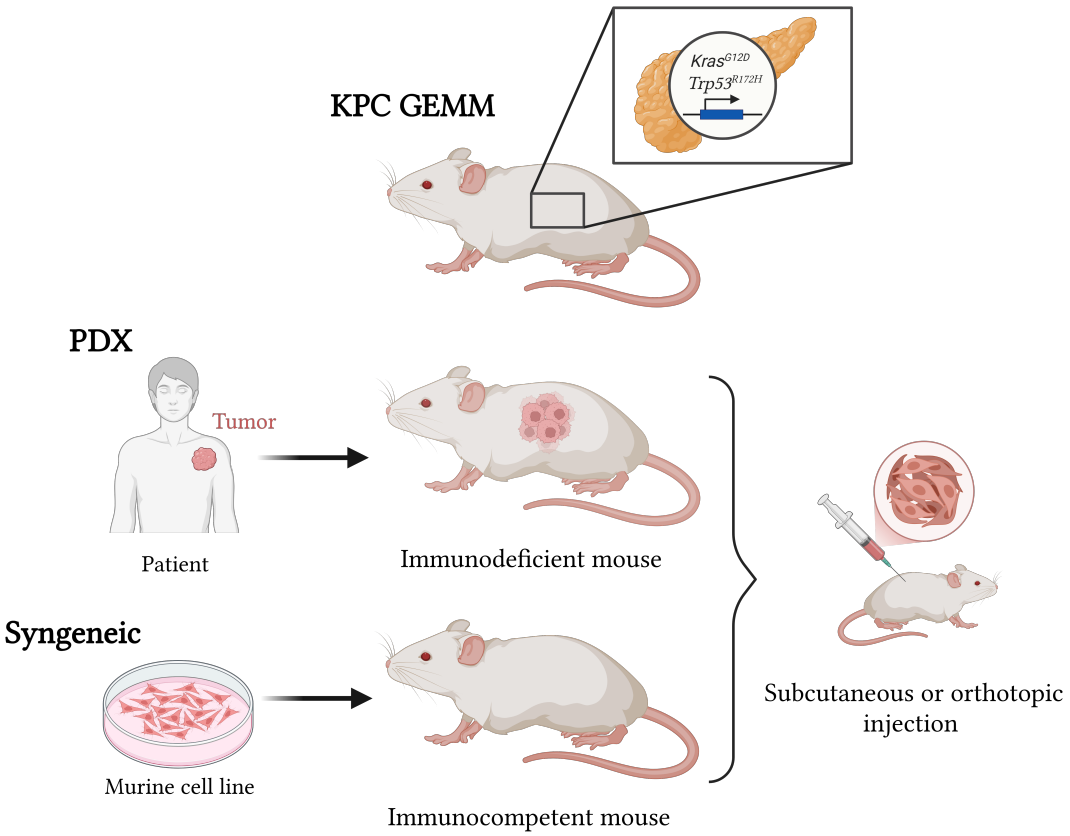


Figure 1.2: Murine models of PDAC. Commonly used murine models of PDAC split broadly into categories of GEMM, PDX and syngeneic. The KPC mouse with pancreas-specific *Kras* and *Tp53* mutations is regarded as the 'gold standard' of PDAC GEMMs. PDX and syngeneic mice differ in the source of the tumour cells and therefore the immunocompetence of the host. Both of these murine models can use subcutaneous or orthotopic injection of tumour cells with variation in the fidelity to human tumours and ease of monitoring. Created with Biorender.com.

One of the most widely studied murine models of PDAC includes site-specific *Kras* and *Tp53* mutations in the pancreas. The LSL-Kras$^{G12D/+}$;LSL-Tp53$^{R172H/+}$;Pdx1-Cre (KPC) mouse is widely used due to its fidelity to human tumours (Hingorani et al. 2005). The addition of the *Tp53* mutation was found to produce more aggressive tumours, thus recapitulating the rapid dissemination of PDAC seen in the clinic (Mallya et al. 2021). Alongside progress in the fidelity of GEMMs to human tumours, the movement from subcutaneous injection to orthotopic transplantation has improved PDX and syngeneic models. Orthotopic injection producing tumours in the pancreas of the host has been shown to produce highly stromal cancers (Horvat

et al. 2024) which better mimic human tumours (Fernandez et al. 2023) than those grown subcutaneously. These tumours also metastasise to the liver (J. W. Lee et al. 2016) and often cause ascites therefore better representing human clinical outcomes.

While mouse models are a valuable tool to investigate systemic effects of therapies, immunotherapies are a challenging modality to test in these systems. Immunocompromised mouse models can overestimate CAR-T cell efficacy due to a lack of immunosuppressive microenvironment while immunocompetent mice require either transgene expression of the human protein target or CAR modification to target the murine protein (E. N. Ahmed, Cutmore and Marshall 2024).

1.2.3 Organoids and Spheroids

Three-dimensional modelling of tumours represents a middle ground between murine models, which are slow and costly to generate, and 2D cell culture, which does not accurately represent the heterogeneity within tumours and between patients (Pampaloni, Reynaud and Stelzer 2007; Peng et al. 2025). The most widely used 3D models in oncology are tumour organoids which can be derived from patient material - patient-derived organoids (PDOs) or stem cells. The terms organoid and spheroid are often, incorrectly, used interchangeably. The main difference is that while organoids are grown with scaffolds to form structural units, spheroids are free-floating aggregates of cells with minimal organisation (Gunti et al. 2021).

Spheroids were first introduced in the 1970s (Sutherland, McCredie and Inch 1971) and the technique has since been applied across disease areas with both cell lines and tumour tissue-derived cell suspensions. Despite their simplicity, tumour spheroids are able to mimic properties of tumours effectively including cell-cell contacts (S. Xu et al. 2014). They are a useful tool for studying drug distribution in a poorly-vascularised tumour (Zoetemelk et al. 2019) and can also be used to study hypoxia if grown large enough to develop a necrotic core (Kirsh, Pascetta and Uniacke 2023).

The use of PDOs in cancer research began more recently, in around 2011 (Sato et al. 2011). These more complex structures involve the digestion (mechanical or

enzymatic) of tumour tissue which is plated within a matrix structure in nutrient-rich media. Organoids have been shown to replicate architectural features of the tumour and preserve some of the genetic heterogeneity (D. Gao et al. 2014) which is lost in 2D cell culture. In some cases, this similarity to patient tumours has been shown to enable prediction of therapy response (Ooft et al. 2019). Despite these advantages, the need for rapid growth and continual renewal in organoids means that many populations are lost (Boucherit, Gorvel and Olive 2020). These cells can be re-administered following organoid establishment (Yuki et al. 2020) but the initial interactions between native cellular subsets cannot be restored.

Developments in bioengineering have increased the complexity of organoid models by introducing microfluidic delivery of nutrients and removal of waste. These dynamic culture systems have also facilitated the communication of multiple tissues through organ-on-a-chip systems (Sontheimer-Phelps, Hassell and Ingber 2019). This technology has been used to study PDAC interactions with blood vessels, showing mechanisms of invasion and endothelial ablation (Nguyen et al. 2019). While multi-organ communication systems facilitate the study of complex biological mechanisms, high-throughput microfluidics approaches are also necessary for drug screening. B. Schuster et al. (2020) developed an automated microfluidics platform compatible with live imaging and matrigel culture of tumour organoids (B. Schuster et al. 2020). Larsen et al. (2021) describe their system which similarly focuses on high-throughput with optimisation of a pan-cancer system designed to enable AI-driven precision medicine (Larsen et al. 2021). Systems such as this which balance the use of a physiologically relevant tumour model with high-throughput may play an important role in the future of drug screening.

The profound impact that cellular composition and structure of tumour models can have on their properties is evidenced in work by Frances Balkwill's group. Their ovarian cancer spheroids were resistant to CAR-T cell killing when formed only of malignant cells but became increasingly susceptible following the addition of fibroblasts. This susceptibility was ablated by the culture of the dual population

spheroids in a collagen gel matrix, leading to a transforming growth factor (TGF)β-mediated inhibition of CAR-T cell cytotoxicity (Joy et al. 2024). The variability in treatment response added by each layer of complexity highlights the need for models to incorporate as many elements of the native tumour as possible in order to obtain results, *in vitro*, which are more likely to transfer into the clinic.

1.2.4 Organotypic Tumour Slices

While 3D culture of patient-derived cells recapitulates the tumour better than 2D models, digestion and long-term culture degrade the structure of the tumour and reduce cellular heterogeneity (Figure 1.3). Organotypic tumour slices, sometimes referred to as patient tumour slices, precision cut slices, or patient avatars are derived from patient tumour samples. Rather than digesting tumours into a single cell suspension, samples are cut into uniform slices and their structure is maintained (Misra et al. 2019; Salas et al. 2020; Martin et al. 2019). These platforms were first developed using fresh animal tissues in the early 1950s (Leighton 1951) and were extended to the use of human tumours in the 1980s (A. E. Freeman and Hoffman 1986).

The maintenance of the physical structure and the cellular heterogeneity of patient tumours makes organotypic tumour slices an attractive tool for the investigation of interactions in the tumour microenvironment (TME) and novel therapies, particularly those with an immunological focus. Immunofluorescence has been used to visualise immune cells within the tumour structure (X. Jiang et al. 2017), with live imaging techniques used to observe the cellular interactions determining immune cell migration (Salmon et al. 2012; Boutet et al. 2016; Peranzoni, Lemoine et al. 2018). Functional assessments of treatments have also been carried out including oncolytic viral infection (Runge et al. 2022) and immune modulation (Lim, J. H. Chang, W. S. Lee, J. Kim et al. 2021). While limited, the current strategies used to analyse cellular therapies using tumour slices are discussed in Chapter 5.1.

One issue associated with tumour slice culture is the limited timescale of slice viability. This problem is more pronounced with softer healthy tissues but is

still prevalent in stromal cancers such as PDAC, with reported viability windows varying from 5 to 12 days (Lim, J. H. Chang, W. S. Lee, K. M. Lee et al. 2018; Kokkinos et al. 2021). Multiple techniques have been used to attempt to extend this timeframe including dynamic culture (Hughes et al. 2024) and nanostructured scaffolds (Kallendrusch et al. 2017).

While the longevity of tumour slice culture can limit the scope of analysis, their rapid generation is advantageous for their use in a predictive capacity. Organoids require a minimum of 2-4 weeks to develop, whereas, a major boon of patient tumour slices is that slices can be generated on the same day as surgical resection (Abdullah et al. 2022; Broutier et al. 2016) . Majumder et al. (2015) used matrix-coated tumour slices to correlate *ex vivo* drug responses to patient clinical responses in head and neck squamous cell carcinoma (HNSCC) and colorectal cancer (CRC) (Majumder et al. 2015). A recent paper similarly investigated this predictive capacity in PDAC, identifying one patient response to gemcitabine in a palliative setting (Hughes et al. 2024) despite the 9-17% response rate to gemcitabine seen in clinics (Heinemann 2002) and particularly limited efficacy documented in late-stage treatment (Xinopoulos et al. 2008).

Tumour slice culture is increasingly being used alongside other analysis techniques to evidence the clinical relevance of preclinical findings. This integration of the model into larger workflows allows its limitations to be addressed while taking advantage of the unique fidelity of the slices to human tumours. As with organoid models, efforts are being made to combine organotypic slice culture with microfluidics platforms to enable high-throughput screening (Rodriguez et al. 2020), potentially facilitating multiplexed drug testing over a short timeframe to help influence clinical decision-making.

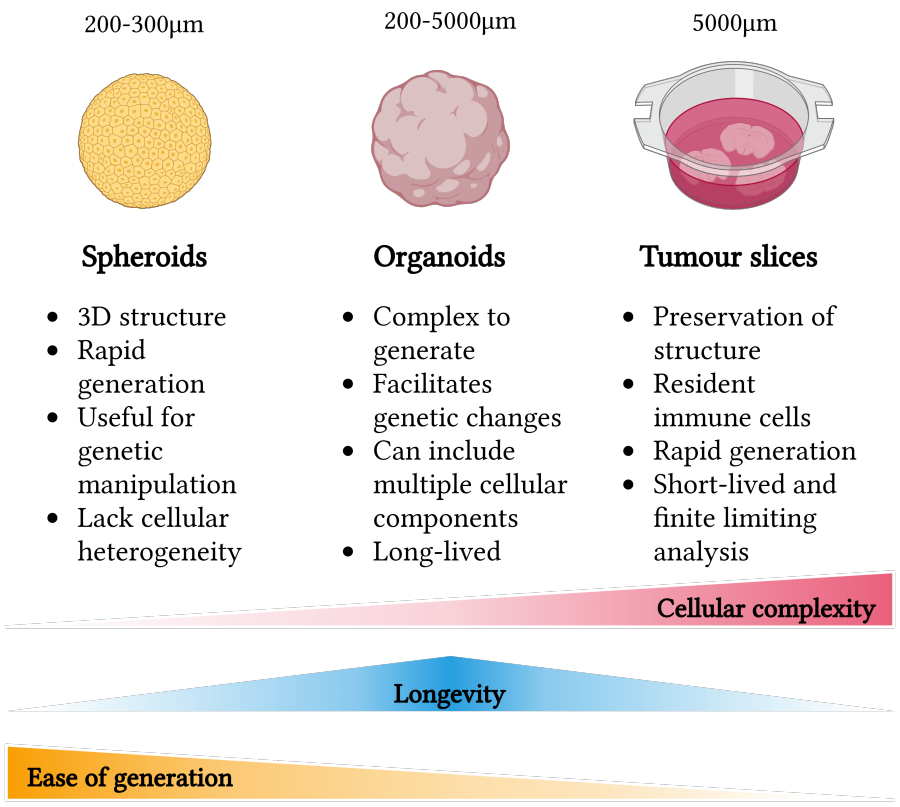


Figure 1.3: Characteristics of 3D tumour models. Spheroids, organoids and tumour slices are all commonly used to recapitulate tumours *ex vivo*. The ease of generation, scope for genetic manipulation, complexity, and longevity of the models vary, meaning that different models are optimal for different forms of investigation. Created with Biorender.com.

1.3 Immunotherapy

The overarching goal of immunotherapies is to enhance existing immunosurveillance to eliminate malignant cells. This relies on the ability of the immune system to recognise the structural changes brought about by genomic instability as 'nonself', triggering an immune response (Yuanyuan Zhang and Z. Zhang 2020). Current approaches are focused primarily on the activation and effector function of lymphocytes, although novel approaches recognise the importance of natural killer (NK) cells (Daher and Rezvani 2021), neutrophils (Y. Chang et al. 2023), dendritic cells (Suh et al. 2018) and macrophages (Klichinsky et al. 2020) in the immunological

response to cancer.

The first use of immunotherapy is attributed to William Coley who first observed that mixtures of live and inactivated bacteria could cause tumour regression in sarcoma patients (Starnes 1992; Coley 1893). This early discovery subsequently led to discoveries throughout the 1960s-80s regarding the role of immune cells and cytokines in producing an immune response to cancer (M. Zhang et al. 2025). Following controversy concerning the mechanisms of immune recognition in cancer, the discovery of the TCR in the 1980s (Reinherz, Hussey and Schlossman 1980; Haskins et al. 1983; Meuer et al. 1983) and the identification of the first human tumour antigen to be recognised by T cells in the 1990s (Bruggen et al. 1991) sparked decades of innovation.

1.3.1 Immune Checkpoint Inhibitors

Immune checkpoint inhibitors (ICIs) aim to overcome the immunosuppressive microenvironment through releasing 'brakes' on T cell function (Yuanyuan Zhang and Z. Zhang 2020). The first immune checkpoints cytotoxic T-lymphocyte-associated antigen (CTLA-4) and programmed cell death protein 1 (PD-1) were discovered by Pierre Goldstein (Brunet et al. 1987) and Tasuko Honjo (Ishida et al. 1992) respectively. CTLA-4 was subsequently found to bind CD80 and CD86 and Jeffrey Bluestone identified the protein as a directly negative regulator of T cell function (Walunas et al. 1994). Both proteins were shown to be expressed on activated T cells, leading to our current understanding of their respective roles (Chamoto et al. 2023; Bernard 2022). CTLA-4 is predominantly expressed by T cells in lymphoid tissues to regulate T cell priming and PD-1 is expressed upon antigen recognition in tissues regulating immunopathology (Bernard 2022).

The subsequent development of inhibitors for PD-1 (Iwai et al. 2002) and CTLA-4 (Leach, Krummel and Allison 1996) by Takusu Honjo and Jim Allison has led to the licencing of checkpoint inhibitors across tumour types (Petrelli et al. 2020) - representing an advance in the regulatory approval process from the traditional model of single disease indications. The widespread licencing of

checkpoint inhibitors targeting CTLA-4, PD-1 and its ligand follow clinical trials showing dramatic improvement to prognosis, including more than doubling of the previous 10-year survival rate with ipilimumab (Schadendorf et al. 2015) and a 50% response rate in combination with nivolumab in metastatic melanoma (Postow et al. 2015). Additional approval has more recently been granted in advanced melanoma for the use of the LAG-3 inhibitor relatlimab in combination with nivolumab after the phase 2-3 clinical trial showed a doubling in PFS with the combination when compared to nivolumab alone (Tawbi et al. 2022).

1.3.2 Adoptive Cell Therapies

Adoptive cell therapies also aim to improve T cell recognition of tumours through the expansion and re-infusion of T cells rather than removal an inhibitory signal in situ. Lymphokine-activated killer (LAK) cell therapy was the first form of this therapy pioneered by Steven Rosenberg. These cells comprised of subsets of T and NK cells derived from peripheral blood and selected due to their IL-2-mediated activation (S. Rosenberg 1985). This discovery was closely followed by Rosenberg's pioneering of tumour-infiltrating lymphocyte (TIL) therapy (S. A. Rosenberg, Spiess and Lafreniere 1986; S. A. Rosenberg, Packard et al. 1988) using tumour-derived lymphocytes. Rosenberg's work not only highlighted the potency of tumour-resident T cells but facilitated observations of long-term clonal persistence in T cell populations following TIL therapy (Dudley et al. 2002). The power of this clonality paved the way for the engineered TCR and CAR-T cells which now dominate the adoptive cell therapy landscape.

1.3.3 CAR-T Cell Therapy

1.3.3.1 Early CAR-T Cell Development

The first use of a receptor combining antibody-based variable domains with constant regions derived from the TCR is attributed to Yoshikazu Kurosawa in 1987. The group was able to produce antigen-specific stimulation of calcium responses in T cells, mimicking the activation of the TCR (Kuwana et al. 1987). A similar

approach was developed by Zelig Eshhar who designed the first single-chain variable fragment (scFv) fused to CD3ζ creating a construct that produced T cell activation independently of the conventional TCR complex (Eshhar et al. 1993). This form of receptor was the first instance of a first generation CAR-T cell (Mitra et al. 2023). Murine models using these constructs showed that they slowed tumour growth (Hwu et al. 1995; Moritz et al. 1994), but the results could not be replicated in clinical trials (Kershaw et al. 2006; Park et al. 2007) leading to the addition of co-stimulatory domains to constructs and the design of second generation CARs.

The addition of CD28 to the CAR construct provided the necessary co-stimulation needed to improve CAR-T cell effector function (Maher et al. 2002) by combatting issues with persistence that arose with first generation CARs (Savoldo et al. 2011). This persistence was further enhanced by the substitution of CD28 for the alternative co-stimulatory receptor 4-1BB. Each of these receptors confers different advantages, with CD28 CARs showing more cytokine release (Cappell and Kochenderfer 2021) and rapid tumour elimination and 4-1BB greater persistence (Zhao, Condomines et al. 2015; Guedan et al. 2018). These differences are thought to be due to differing signal strengths and downstream pathways (Salter et al. 2018; Lindner et al. 2020) leading to alterations to T cell subsets and concurrent alterations to predominant metabolic pathways (Kawalekar et al. 2016). Using a CD19-targeting CD3 and 4-1BB construct, Carl June's group reported complete or partial remission in 3 patients with advanced chronic lymphocytic leukaemia (CLL) in 2011. This major step demonstrated the clinical potential of CAR-T cell therapy (Porter et al. 2011).

1.3.3.2 Licenced Therapies

From 2017, the first anti-CD19 CAR-T cells were approved by the FDA for the treatment of multiple B cell malignancies. These were followed in 2021-22 by two anti-BCMA CAR-T cell therapies for multiple myeloma. The current FDA-approved CAR-T cell therapies are detailed in Table 1.1.

Therapy (company)	**FDA Approval**	**Antigen Target**	**Co-stimulatory Domains**	**Vector**	**Starting Cell Population**
Tisagenlecleucel/ Kymriah (Novartis)	Aug 2017 B-ALL (CAYA)	CD19	4-1BB + CD3ζ	Lentiviral	Enriched T cells
Axicabtagene ciloleucel/Yescarta (Kite)	Oct 2018 LBCL	CD19	CD28 + CD3ζ	Retroviral	PBMCs
Brexucabtagene autoleucel/ Tecartus (Kite)	Jul 2020 MCL	CD19	CD28 + CD3ζ	Retroviral	CD4/8 enriched T cells
Lisocabtagene maraleucel/Breyanzi (Juno)	Feb 2021 LBCL	CD19	4-1BB + CD3ζ	Lentiviral	CD4 and CD8 T cells separately
Idecabtagene vicleucel/Abecma (Bluebird)	Mar 2021 MM	BCMA	4-1BB + CD3ζ	Lentiviral	PBMCs
Ciltacabtagene autoleucel/Carvykti (J&J)	Feb 2022 MM	BCMA	4-1BB + CD3ζ	Lentiviral	Enriched T cells
Obecabtagene autoleucel/Obe-cel (Autolus)	Nov 2024 ALL	CD19	4-1BB + CD3ζ	Lentiviral	PBMCs

Table 1.1: FDA-approved CAR-T cell therapies. All CAR-T cell therapies currently approved by the FDA. 'FDA Approval' details the date of approval and the disease for which the treatment is approved. B-ALL = B cell acute lymphoblastic leukaemia, CAYA = children, adolescents, and young adults, LBCL = large cell B cell lymphoma, MCL = mantle cell lymphoma, MM = multiple myeloma.

Real-world data shows that CAR-T cell therapy has led to significant improvements in prognosis across many B cell malignancies. In B cell lymphomas, anti-CD19 CAR-T cell therapy transformed the complete response rate in chemotherapy-refractory disease (CRR) from 7%, previously recorded with conventional treatment (Abramson et al. 2020), to between 40-54% (Abramson et al. 2020; Neelapu et al. 2017; S. J. Schuster et al. 2019). Long term responses are experienced by a

subset of patients with predictive factors including the initial depth of remission, type of malignancy, tumour burden and initial levels of circulating CAR-T cells (Cappell and Kochenderfer 2023).

1.3.3.3 Adverse Events

While these results are transformative for a subset of patients with severe B cell malignancies, CAR-T cell therapy can also lead to a variety of severe adverse events. The acute adverse events associated with treatment are most commonly cytokine release syndrome (CRS) and immune effector cell-associated neurotoxicity syndrome (ICANS) (Yugu Zhang et al. 2023; Sheth and Gauthier 2021). CRS is a severe adverse event seen when CAR-T cell activation leads to increased cytokine levels in serum, inflammatory markers and generalised immune activation. In most patients the symptoms are mild and can be reversed but in severe cases it can cause multi-organ failure (Sheth and Gauthier 2021). Given that real-world data suggest that 55-75% of patients present with CRS, it is an important factor to consider when considering the effect of novel therapies (Shewade 2023). IL-6, IL-1, interferon (IFN)γ and tumour necrosis factor (TNF)α are the cytokines most elevated in CRS while IL-8, IL-10, monocyte chemoattractant protein (MCP)-1 and granulocyte-macrophage colony-stimulating factor (GM-CSF) are all also implicated (Silveira et al. 2022; J. Wang and Doran 2021).

The anti-IL-6 receptor antibody tocilizumab is most commonly used to treat CRS due to the central role that IL-6 plays (Ayuketang and Jäger 2022). Elevated levels stimulate cytokine release from surrounding immune cells such as macrophages, monocytes and dendritic cells (DCs), perpetuating existing inflammatory signalling (Yugu Zhang et al. 2023). Although ICANS is less well understood, the associated neurological symptoms are thought to arise from high concentrations of the aforementioned inflammatory cytokines in the cerebrospinal fluid (CSF). Symptoms range from headache, confusion and lethargy to seizures and cerebral oedema in the most severe cases (Sheth and Gauthier 2021). Tocilizumab, anakinra (the IL-1α antagonist) and corticosteroids are similarly used in treatment.

Long term treatment-associated adverse events include persistent B cell depletion, cytopenias and severe infections. B cell depletion and immunoglobulin depletion occur frequently due to the expression of CD19 on non-malignant B cells (Cappell and Kochenderfer 2023). Reduced humoral immunity, alongside other common immunological effects including neutropenia and lymphocytopenia, leads to an increased rate of infection particularly during the first 30 days of treatment but continuing for months following (Hill, D. Li et al. 2018). The exact cause of these infections is difficult to determine due to the immunological effects of prior chemotherapy and lymphodepletion used prior to CAR-T cell infusion. Additionally, use of corticosteroids and tocilizumab to treat the hyperinflammation caused by CRS also increases the risk of infection (Hill, Giralt et al. 2019; Hill and S. K. Seo 2020).

1.3.3.4 Manufacturing Cost

One of the major factors limiting the adoption of CAR-T cell therapy across geographies is the prohibitive cost of manufacturing. In the US, treatment is estimated to cost around $500,000 (Hernandez, Prasad and Gellad 2018) for patients who experience severe adverse effects. In the UK, these financial barriers mean that therapies have been made available through the Cancer Drugs Fund, reportedly costing the NHS just under £300,000 per patient (Williamson 2019). In comparison, month of checkpoint inhibitor therapy in the US costs between $11,000-$15,000 (Paul et al. 2024). There is no overall consensus for the optimal timeframe for checkpoint inhibitor therapy but patients demonstrating CR tend to be given around 6 months of treatment while those showing PR can be treated for around 2 years (J. Yin et al. 2022).

Potential solutions to reduce the cost of CAR-T cell therapy include use of non-viral vectors or point-of-care (POC) decentralized manufacturing (Abdo, Batista-Silva and Bonamino 2025). POC manufacturing was employed to deliver a second generation anti-CD19 CAR in a Phase I study in India, showing PFS in 80% of patients at the 15-month median follow-up (Palani et al. 2025). Whilst this

approach is cost effective (around $50,000 per patient), regulation of individual good manufacturing practice (GMP) facilities could become challenging.

1.3.3.5 Development of Allogeneic CAR-T Cells

To combat the issues of high costs associated with autologous CAR-T cell manufacturing, many groups are working to develop allogeneic CAR-T cell products. This would not only reduce the costs of treatment but prevent delays due to the time needed to manufacture and ship autologous CAR-T cells. The substantial variation between donors (discussed in detail in Chapter 6.1.1) leads to variable CAR-T cell batches, while an allogeneic product could facilitate greater standardisation (Depil et al. 2020). This standard healthy-donor derived product could potentially benefit patients whose own T cells have been previously depleted by treatments - a problem highlighted by the 9% failure rate for Kymriah manufacture in their clinical trial (Salmikangas, Kinsella and Chamberlain 2018).

In order to translate current CAR-T cell approaches for allogeneic therapy, the issues of graft-versus-host disease (GvHD) and rejection must first be overcome. It has been previously demonstrated in the context of allogeneic stem cell therapy (SCT) that T cells are central to GvHD (Abdelhakim, Abdel-Azim and Saad 2017), which is mediated by the interactions of the TCR with peptide-MHC complexes. The recognition of either polymorphic peptides by shared MHC or foreign MHC presenting different peptide sequences can lead to both GvHD and rejection. These two processes are due to the recognition by donor and host T cells respectively. Genetic editing to remove the T cell receptor (TCR) from T cells has shown promise in preventing GvHD, with the added advantages of allowing site-specific incorporation of the CAR at the TRAC locus (Eyquem et al. 2017). Additional genetic editing allows selective depletion of host T cells prior to therapy (Poirot et al. 2015). The first clinical trial results show promising initial complete remission prior to SCT (Qasim et al. 2017) but longer-term studies are needed to evaluate efficacy compared to autologous therapy.

1.3.3.6 Challenges Associated with Solid Tumours

Alongside challenges associated with delivering therapy to patients with B cell malignancies, CAR-T cell therapy is not currently licensed for the treatment of any solid tumours. Major challenges include a lack of infiltration into the tumour, the immunosuppressive microenvironment and antigenic heterogeneity (Flugel et al. 2023; A. J. Hou, L. C. Chen and Y. Y. Chen 2021; Du et al. 2025). The complexity of this challenge requires innovation across aspects of CAR design and delivery (Figure 1.4).

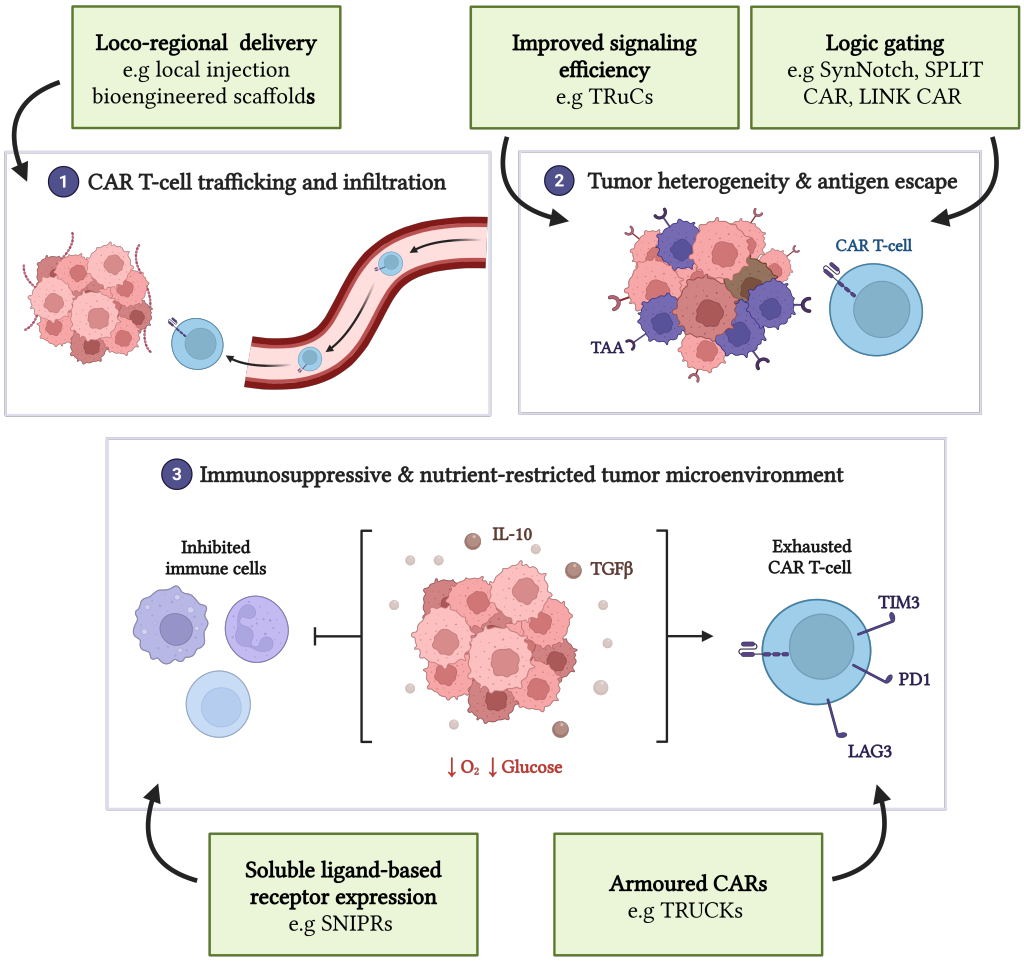


Figure 1.4: Challenges and development strategies for CAR-T cell therapy use in solid tumours. Multiple challenges that have so far prevented the translation of CAR-T cell therapy success in haematological cancers to solid tumours. These include (1) lack of infiltration which is being combatted through use of local delivery strategies. (2) Antigenic heterogeneity which can be tackled through improved receptor signalling increasing antigen discrimination and logic gating targeting multiple antigens. (3) The immunosuppressive microenvironment which can be used to improve CAR-T cell targeting through ligand-based receptor expression or combatted through use of armoured CARs. Created with Biorender.com.

1.3.3.6.1 Improvements to CAR-T Cell Receptor Sensitivity

A fundamental difference between strategies targeting B cell malignancies and solid tumours is the choice of antigen target. CD19 and BCMA are both expressed on normal B cells and plasma cells as well as on malignant cells (K. Wang, Wei and D. Liu 2012; Salem et al. 2018) meaning that all current licenced CAR-T cell therapies deplete B cell populations indiscriminately. This strategy is not possible when

targeting solid tumours - targets must be selected on the basis of sufficient tumour-specific restriction. Tumours do not widely express completely unique proteins (Flugel et al. 2023) so targeting strategies must either be focused on proteins with limited healthy expression and frequent upregulation in malignant cells or proteins with alternative glycosylation (Raglow et al. 2022). The most commonly used targets are those which are significantly overexpressed in tumours which poses challenges in receptor design sensitivity (Flugel et al. 2023). Low affinity receptors risk a lack of sufficient effector function whilst high affinity receptors risk on-target off-tumour toxicities (Caruso et al. 2015).

Antigen density discrimination is complex, with activation thresholds determined by factors including scFv affinity, the size of the extracellular portion and the use of accessory receptors (Lindner et al. 2020). Traditional CAR designs are 10-100 fold less sensitive than TCRs with the same recognition domains (Harris et al. 2018). These differences are primarily attributed to inefficient utilisation of LFA-1 and CD2 accessory receptors and can be restored by replacing parts of the CAR construct with TCR-derived sequences (J. I. D. Burton et al. 2023) to create T cell receptor fusion constructs (TRuCs). Increased efficiency can also be conferred by matching the length of the CAR in complex with the antigen with the length of the CD2/CD58 complex (J. Burton et al. 2025). Tuning the efficiency of CAR signalling is essential for successful antigen density discrimination as it increases the likelihood of antigen recognition leading to T cell activation, thereby allowing scFv affinity to be tuned more effectively.

Alongside improving the efficiency of the CAR construct, expression of multiple receptors also allows target density discrimination. Hernandez-Lopez et al. (2021) demonstrated this effect using a low affinity Notch receptor to induce expression of a high affinity CAR, both binding to HER2. This receptor combination yielded a sigmoidal relationship between antigen density and target cell lysis, demonstrating finely tuned HER2 density discrimination (Hernandez-Lopez et al. 2021).

1.3.3.6.2 Logic Gating to Exploit Antigen Combinations Rather than relying on antigen density discrimination, logic-gated CAR-T cells take advantage of the differential expression of multiple antigens to control activation (Zhao and Sadelain 2023). These receptor combinations can be categorised broadly into 'OR-gate', 'NOT-gate' and 'AND-gate'. The latter receptor combination is particularly useful as it relies on expression of two independent tumour-associated antigens (TAAs) but is challenging as neither receptor should independently produce activation.

Tousley et al. (2023) recently described a dual CAR design bypassing the need for CD3 or co-stimulatory signalling domains. LAT and SLP-76 intracellular regions were used instead due to their role downstream of ZAP-70 and lack of independent activation signal transduction. The cells displayed more efficient dual antigen discrimination than previous platforms including SPLIT CARs and a SynNotch system (Tousley et al. 2023).

1.3.3.6.3 TRUCKs and Engineered Outputs Alongside tackling the initial challenge of specific and efficient tumour cell recognition, durable responses remain challenging for CAR-T cells in solid tumours due to the immunosuppressive TME. A new generation of CAR constructs are designed to combat suppressive signalling through the release of pro-inflammatory cytokines upon CAR ligation. These T cells redirected for universal cytokine-mediated killing (TRUCKs) can be engineered to produce cytokines designed to enhance persistence, improve trafficking and modify the TME (L. Tang et al. 2023). Phase I clinical trials have shown that this approach with IL-18 (Svoboda et al. 2023) or IL-7 and CCL19 in combination (Lei et al. 2022; Duan et al. 2021) can yield effective disease control with a manageable safety profile.

An alternative approach to combating TME-induced suppression involves using a novel synthetic intramembrane proteolysis receptor (SNIPR) platform which is activated by soluble ligands. These cells are, therefore, able to use the suppressive context of the microenvironment to enhance CAR-T cell specificity and prevent on-target off-tumour toxicity. Piraner et al. (2025) demonstrate the ability of SNIPR

cells to activate in response to TGF-β signalling triggering expression of a HER2 CAR and control of tumour growth. The cells were shown to localise the response to the tumour site, showing no systemic toxicity in murine models (Piraner et al. 2025).

1.3.3.6.4 Loco-Regional CAR-T Cell Delivery Intravenous infusion of CAR-T cells is performed for all licenced therapies, but is less effective when targeting frequently poorly vascularised solid tumours. For that reason, many clinical trials have explored the possibility of locoregional delivery of CAR-T cells facilitating better accumulation. The higher concentration of CAR-T cells at the tumour site and not in circulation may also potentially reduce the frequency of on-target off-tumour effects and systemic adverse events (R. C. Sterner and R. M. Sterner 2021).

The most commonly used method of delivery is injection into the tumour site. This technique has been used in clinical trials for head and neck cancer (Papa et al. 2023), glioma (Brown et al. 2024) and pleural mesothelioma (Adusumilli et al. 2021). The lack of delivery-associated complications in these trials indicate the safety and feasibility of this approach. The superior efficacy of local injection has also been demonstrated in studies comparing local and systemic approaches. N. Tang et al. (2020) demonstrated complete elimination of tumours with local injection of CAR-T cells, but not with the same product administered intravenously (N. Tang et al. 2020).

Alongside the delivery of CAR-T cells, Agliardi et al. (2021) used intratumoral delivery of IL-12 to boost cytotoxicity and remodel the TME in a murine glioblastoma model (Agliardi et al. 2021). This approach is not dissimilar to Rosenberg's original administration of IL-2 alongside TIL therapy in the 1980s (S. A. Rosenberg, Spiess and Lafreniere 1986) but uses local delivery and an alternative cytokine to prevent the systemic toxicities experienced with high dose IL-2 infusion (Julve et al. 2025).

Due to an increase in development of biocompatible materials over the last decade, bioengineered scaffolds can now be used to support local delivery of CAR-T cells. These structures can facilitate simultaneous delivery of cytokines and antibodies (D. K. Y. Zhang et al. 2025; T. T. Smith et al. 2017) designed to activate CAR-T cells in situ, whilst containing activation to the delivery site to further

reduce the possibility of systemic inflammation (Grosskopf et al. 2022). No clinical trials have yet been initiated using these modalities, but preclinical studies continue to yield promising improvements over traditional infusion-based approaches.

1.3.3.6.5 Clinical Trials in PDAC PDAC is a challenging target for CAR-T cell therapy due to the dense desmoplastic stroma (Alrifai, Sarker and Maher 2016) and prevalence of protumorigenic immune cells such as tumour-associated macrophages (TAMs) and myeloid-derived suppressor cells (MDSCs) (Siret et al. 2019). Due to this complexity, relatively few CAR-T cell approaches have progressed beyond Phase I trials for pancreatic cancer. The current Phase II CAR-T cell clinical trials for PDAC are listed in Table 1.2.

Trial ID/Sponsor	Status	Target	CAR Design	Treatment Regimen
NCT06006390 Chongqing Precision Biotech	Recruiting	CEA	N.A.	IV infusion or peritoneal cavity infusion
NCT05538195 Chongqing Precision Biotech	Recruiting	CEA	N.A.	IV infusion or peritoneal cavity infusion
NCT04581473 CARsgen Therapeutics	Recruiting China-based	Claudin 18.2	Isoform-specific targeting	N.A.
NCT05736731 A2 Biotherapeutics	Active	CEA with HLA-A*02 loss	Logic-gated	Manufacture upon disease progression, prior lymph-odepletion
NCT06051695 A2 Biotherapeutics	Recruiting	MSLN with HLA-A*02 loss	Logic-gated	Manufacture upon disease progression, prior lymph-odepletion
NCT04404595 CARsgen Therapeutics	Active US-based	Claudin 18.2	Isoform-specific targeting	N.A.
NCT02830724 NCI	Recruiting	CD70	Retroviral vector	2 rounds of infusion 6 months apart
NCT05795595 CRISPR Therapeutics	Recruiting	CD70	Allogeneic CRISPR-edited	IV infusion following lymphodeple-tion

Table 1.2: Ongoing Phase II CAR-T cell therapy clinical trials in PDAC. All currently active clinical trials for CAR-T cell therapy in PDAC are listed. Where trials are sponsored by the same company and use the same CAR construct the trial region is listed under 'status'. 'CAR Design' describes information provided about the nature of the construct including whether the CAR-T cells are autologous or allogeneic. N/A indicates that information was not provided on ClinicalTrials.gov or the website of the sponsor.

1.4 Oncofoetal Antigens

Tumour antigens are primarily separated according to the specificity of their expression. TAAs are self-proteins also expressed on tumours while tumour-specific antigens (TSAs) are exclusively expressed on tumour cells. TAAs include proteins which are overexpressed, have abnormal post translational modifications or mutations causing abnormal isoforms. Additionally, proteins which are expressed in reproductive tissues (cancer testis antigens) or are expressed during development (oncofoetal antigens) also fall under the TAA classification. TSAs include oncoviral antigens derived from viruses which cause oncogenic transformation and neoantigens arising from genetic mutations (Zarour et al. 2003; Feola et al. 2020).

1.4.1 Therapeutic Utility

Given that TSAs are unique to cancers, they are the ideal target for therapy. This is evidenced by the success of vaccination against human papillomavirus (HPV) which is estimated to have reduced rates of cervical cancer by 87% in the UK (Torjesen 2021). This demontrates that the use of a TSA in immunisation can produce a robust protective immune response against cancer. Neoantigens provide a greater challenge due to their individual nature. These antigens are mostly unique to patients and vary within tumours, meaning that personalised vaccines with combinations of peptides are needed (Goloudina et al. 2025). Increased research into 'public' or shared antigens has formed the basis for universal vaccines, but clinical trials are yet to show evidence of long-term responses (Rappaport et al. 2024).

Widespread similarities between embryonic and malignant tissues were observed as early as the 1960s (Gold and Freedman 1965). Since then, oncofoetal antigens have been discovered across tumour types, making up some of the most common diagnostic and therapeutic markers in use today (Ankur Sharma et al. 2022). These include carcinoembryonic antigen (CEA), which is used in colorectal cancer management (Shinkins et al. 2017), and cancer antigens (CA) 19.9 and 125 which are widely used in the management of pancreatic (E. Poruk et al. 2013) and ovarian (Charkhchi et al. 2020) cancers respectively.

1.4.2 Trophoblast Glycoprotein

1.4.2.1 Function in Development and Stemness

Trophoblast glycoprotein (gene name TPBG), also known as 5T4, is primarily expressed on the syncytiotrophoblast cells of the human placenta (Alam et al. 2018). The protein was discovered in 1988 and was found to have expression across diverse tumour cell lines and restricted normal tissue expression (Hole and P L Stern 1988). Early work with 5T4 observed the correlation between its expression in colorectal and gastric malignancies and their metastatic spread (Starzynska, Rahi and P L Stern 1992). This correlation is also linked to a worse prognosis (Starzyńska et al. 1994; Naganuma et al. 2002) with subsequent work revealing that 5T4 interferes with Wnt-mediated β-catenin signalling and activates non-canonical Wnt signalling pathway (Kagermeier-Schenk et al. 2011).

The function of 5T4 in normal development remains unclear, but it has been postulated that its role in epithelial-mesenchymal transition (EMT) could indicate a function in regulating the invasion and proliferation of trophoblasts (Alam et al. 2018).

1.4.2.2 Potential as a Therapeutic Target

Although the expression of 5T4 is not completely limited to malignant tissues, its overexpression across solid tumours makes it an attractive target for therapeutics (Southall et al. 1990). The lack of systemic toxicity produced by the Trovax 5T4 vaccine when it was administered alongside chemotherapy supports the safety of the target (Harrop, Drury et al. 2008). A similar 5T4 vaccine approach was used in early stage prostate cancer, showing evidence of 5T4-reactive TILs after vaccination (Cappuccini et al. 2020). Tumour control has not been demonstrated using these approaches, but it is unclear whether this is as a result of the target or the treatment modality. Alternative therapeutics targeting 5T4 including tribodies (Passariello et al. 2025), antibody-drug conjugates (ADCs) (Schmitt et al. 2024) and CAR-NK cells (NCT05137275,NCT05194709) are currently in development.

Previous studies using the anti-5T4 CAR produced by Oxford Biomedica have demonstrated IFNγ release in response to autologous ovarian tumour cells (Owens et al. 2018). More recently, the same CAR-T cells showed efficacy in acute myeloid leukaemia (AML) both *in vitro* and *in vivo* (Harrop, Blount et al. 2024). This foundation, combined with the elevated 5T4 expression documented in PDAC (R. Wang et al. 2018), provides a rationale for investigating anti-5T4 CAR-T cell therapy in PDAC.

1.5 Study Aims

This thesis aims to explore the use of organotypic tumour slices to evaluate the efficacy of anti-5T4 CAR-T cell therapy in pancreatic ductal adenocarcinoma. This will be accomplished through the completion of the following aims -

1.Determine the expression of 5T4 in patient tissue across pancreatic malignancies and healthy pancreatic samples and in PDAC cell lines.

2. Optimise methods to generate autologous patient anti-5T4 CAR-T cells within a timeframe compatible with clinical timelines.

3. Investigate the *in vitro* cytotoxicity of anti-5T4 CAR-T cells co-cultured with pancreatic cell lines.

4. Develop methods to interrogate the interactions between organotypic patient tumour slices and autologous CAR-T cells.

5. Analyse tumour-associated and donor-intrinsic factors inhibiting CAR-T cell efficacy with a view to development of future targeting strategies.

2
Materials and Methods

The methods listed in this chapter were developed either at Oxford University or by the Translational Sciences Group (TSG) at Oxford Biomedica (OXB). The relevant research operating procedures (ROPs) are quoted for all validated experimental procedures performed at OXB.

2.1 Cell and Tissue Culture

2.1.1 Acquisition of Tissue and Blood Samples

The initial collection of tissue and blood was approved by the Oxford Radcliffe Biobank (REC number 19/A056). Collection of specimens was supported by the Oxford Centre for Histopathology Research and biopsy samples were taken by the pathologist at the John Radcliffe hospital following surgery provided that clear surgical margins could be determined. This ethical approval was granted initially to Dr Daniel Hughes in October 2018 with amendments made at the conception of this project (October 2021) and ran until August 2023. Additional ethics were granted by the Translational Gastroenterology and Liver Unit (TGLU) in March 2023 to facilitate the direct collection of tissue from surgery (21/YH/0206) thus reducing the viability loss from surgery to culture. This study was supported by the National Institute for Health and Care Research (NIHR) Biomedical Research

Centre (BRC) Oxford, through the BRC Oxford GI Biobank. This ethical approval ran until October 2025.

Both studies were approved for the collection of tumour and healthy pancreatic tissue with matched blood samples. All elective pancreatic surgeries were eligible for collection with tumour tissue primarily derived from PDAC patients with additional ampullary tumours and cholangiocarcinomas collected. Healthy tissue was obtained from pancreatitis cases. All patients recruited to the study provided written consent confirming voluntary participation and permission for tissue and blood donation for research. Bloods up to 50 ml were obtained prior to surgery and transported in ethylenediaminetetraacetic acid (EDTA) prior to processing. All patient tissues and bloods were processed and stored in designated areas with anonymised records kept of sample location, analysis and disposal.

Patient Identifiers were kept constant throughout experiments (Table 2.1). Tissue samples were labelled according to the tissue of origin as PDAC (P), healthy pancreatic tissue (H), cholangiocarcinoma (C) and ampullary cancer (A). When referring to blood samples, the identifier denotes patient-derived (p) or healthy donor-derived (d) blood. Only samples used to create data referenced within this thesis are listed in the table below. Other samples were collected and used for additional projects under the same ethical approvals.

Donor ID	Tissue	Date of Collection	Assay Usage
P001	PDAC	05JAN2022	CAR-T antigen IHC
P002	PDAC	07MAR2022	CAR-T antigen IHC
H001	Healthy	21MAR2022	CAR-T antigen IHC
P003	PDAC	07APR2022	CAR-T antigen IHC
P004	PDAC	21JUN2022	Jurkat IF co-culture
P005	PDAC	14DEC2022	5T4 IHC
P006	PDAC	30JAN2023	5T4 IHC
A001	Ampullary	21MAR2023	H&E, Ki67, Caspase
P007	PDAC	13APR2023	5T4 IHC
P008	PDAC	06JUL2023	5T4 IHC, conditioned media, 5T4 flow
P009	PDAC	11JUL2023	5T4 IHC
P010	PDAC	24JUL2023	5T4 flow
P011	PDAC	14AUG2023	5T4 flow, 5T4 IHC
P012	PDAC	31AUG2023	Conditioned media
p001	Blood	21NOV2023	IF matched T cell
P013	PDAC	21NOV2023	IF matched T cell
P014	PDAC	18JAN2024	IF matched T cell (no activation)
p002	Blood	18JAN2024	Spectral flow
p003	Blood	21FEB2024	Spectral flow
P015	PDAC	28FEB2024	Matched CAR-T P1, cytokine array, conditioned media
p004	Blood	18MAR2024	Single cell proteomics trial, spectral flow
P016	PDAC	18MAR2024	Single cell proteomics trial
P017	PDAC	25APR2024	Conditioned media
p005	Blood	11JUL2024	Spectral flow
P018	PDAC	17JUL2024	Matched CAR-T P2, Conditioned media
p006	Blood	07AUG2024	Proteomics
p007	Blood	05SEP2024	Spectral flow
p008	Blood	25SEP2024	Spectral flow
P019	PDAC	03OCT2024	Conditioned media
p009	Blood	16DEC2024	Spectral flow
C001	Cholangiocarcinoma	30DEC2024	Matched CAR-T P3

Table 2.1: Patient samples including pancreatic ductal adenocarcinoma (PDAC), cholangiocarcinoma, ampullary cancer, healthy pancreatic biopsies and blood.

Peripheral blood mononuclear cells (PBMCs) listed in Table 2.2 were obtained from both Oxford Biomedica and Oxford University. PBMCs used at Oxford Biomedica were obtained from the commercial organisation CTL who collect healthy donor blood under a Food and Drug Administration (FDA) licence (Registration Number 3004200746, Licence Number 1141). PBMCs used at Oxford University were obtained from blood cones obtained via the ethics of Dr Kerry Fisher, granted by the London Westminster REC (19/LO/1848) and the ethics of Dr Sim Paulkin, R83151/RE001. These samples were provided by NHS Blood and Transplant.

Donor ID	**Date of generation**	**Assay usage**
d001	MAR2023	Transduction, expansion and phenotype
d002	MAR2023	Transduction, expansion and phenotype
d003	JUN2023	CAR-T generation optimisation, co-culture
d004	DEC2023	IL-6 culture, spectral flow
d005	FEB2024	IL-6 culture, spectral flow
d006	FEB2024	IL-6 culture, spectral flow
d007	JAN2025	Spectral flow
d008	JAN2025	Spectral flow
d009	JAN2025	Spectral flow

Table 2.2: PBMC samples used at Oxford Biomedica (OXB) and Oxford University (OXF) to generate CAR-T cell batches.

Patient data was acquired in an anonymised format from the Translational Gastoenterology and Liver Unit (TGLU). Demographic information, diagnosis, preoperative chemotherapy and staging records were obtained. Staging data was derived both from pre-operative radiology and post-operative pathology. Details of staging for pancreatic cancer are shown in Table 2.3.

Tumour Size	**Meaning**
T0	No evidence of primary tumour
T1	Tumour <2cm in greatest dimension
T2	Tumour <4cm but >2cm
T3	Tumour >4 cm in greatest dimension
T4	Involvement of coeliac axis, superior mesenteric artery and/or common hepatic artery
Tx	Primary tumour cannot be assessed
Nodal Involvement	
N0	No evidence of nodal involvement
N1	1-3 regional node metastases present
N2	4+ regional node metastases present
Nx	Nodes cannot be assessed
Vascular Involvement	
V0	No vascular involvement
V1	Observation of vascular involvement
Lymphatic Involvement	
L0	No lymphatic involvement
L1	Observation of lymphatic involvement
Metastasis	
M0	No evidence of metastases
M1	Distant metastases present
Mx	Presence of metastases cannot be assessed

Table 2.3: Staging used to describe the extent of spread of pancreatic malignancies.

2.1.2 Sectioning and Culture of Live Tumour Slices

Samples were transported on ice in unsupplemented Gibco low glucose (LG) Dulbecco's modified Eagle's medium (DMEM) prior to suspension in agarose scaffolds. Following a manual wash in LG DMEM, biopsy punches were suspended in 4% low melting point agarose (LMA) and cooled. The agarose scaffold structure was generated by melting the solution, cooling, and suspending the slice in a small embedding mold (Leica Biosystems). 250 µm tumour sections were generated using the Leica Biosystems VT1200 vibratome (blade angle +21°C, speed 1.5 mm/s, amplitude 2 mm) in a bath of ice-cold phosphate-buffered saline PBS and transported in LG DMEM on ice. Short-term culture of tumour slices was

conducted using static culture in 6-well plates (Corning). LG DMEM complete pancreatic medium (Table 2.13) was used and plates were incubated at +37°C and 5% CO_2 for the duration of culture.

2.1.3 Tissue Digestion

Digestion of tumour biopsies was performed using the GentleMACS tissue dissociator (Miltenyi Biotec) with the Tumour Dissociation Kit, human (Miltenyi Biotec) designed to preserve viability and surface epitopes. Dissociation was carried out as per the Miltenyi protocol for tough tumours. Briefly, tumour slices were cut into small pieces and placed in GentleMACS C-tubes containing the pre-prepared enzyme mix. The C-tubes were placed on the dissociator and run using the 37C_h_TDK_3 program. The sample was then centrifuged and passed through a 70 µm strainer (Corning) into a 50 ml Falcon tube (SARSTEDT) and the strainer was washed with DMEM (Gibco). Cells were then centrifuged and the supernatant aspirated. Single cell suspension was counted using the haemocytometer and subsequently stained for flow cytometry or plated for co-culture with CAR-T and untransduced control (UTC) cells.

2.1.4 Cell Culture

Pancreatic cell lines were cultured in DMEM (Gibco) supplemented with 10% foetal bovine serum (FBS) (Gibco), 1% L-glutamine (Gibco) and 1% pen-strep (Gibco) (100 U/ml). Jurkat cells were cultured in Roswell Park Memorial Institute (RPMI) 1640 medium (Gibco) supplemented with 10% FBS, 1% L-glutamine and 1% pen-strep. Cells were kept in an incubator at +37°C and 5% CO_2 for the duration of culture and split at 90% confluency using 0.25% Trypsin-EDTA (Sigma-Aldrich) solution (or TrypLE (Gibco) solution if examining surface epitopes). Cells were frozen in freezing medium containing 90% (v/v) FBS and 10% (v/v) Dimethyl sulfoxide (DMSO). All cryovials were stored for 24 h in -80°C in a Mr Frosty (Nalgene), followed by long-term storage in liquid nitrogen.

2.1.5 Purification of PBMCs from Whole Blood

Patient blood was purified by isolating PBMCs from whole blood donated in EDTA tubes. Blood was transferred to 50 ml Falcon tubes (SARSTEDT) and diluted 1:1 with sterile PBS. Diluted blood was layered onto Lymphoprep (STEMCELL) with 15 ml of Lymphoprep used for every 20 ml of blood processed. The suspension was centrifuged using minimal deceleration. The cloudy white interface was then pooled using sterile Pasteur pipettes, topped up with sterile PBS and spun using low deceleration. Isolated cells were then washed twice with chilled magnetic-activated cell sorting (MACS) buffer (Table 2.13) by centrifugation. Cells were counted using the haemocytometer and frozen down in heat-inactivated FBS (Gibco) with 10% DMSO (Sigma Aldrich) at $1x10^7$ cells/ml. Cells were frozen at -70°C for 24 h in a Mr Frosty (Nalgene) and then transferred to liquid nitrogen for long term storage. Cells were retrieved from liquid nitrogen to thaw using OXB thawing medium (TM) (Table 2.13).

2.1.6 CAR-T Cell Generation and Culture

CAR-T cells were generated from donor PBMCs under REC approvals in experiments conducted at the University of Oxford and through the commercial supplier CTL at OXB. Protocols for CAR-T generation and culture were previously optimised by TSG at OXB (ROP069).

The CAR is a second generation construct comprising of 4-1BB and CD3ζ domains. The plasmid was designed at OXB and its structure is confidential.

On Day 0 (the day before transduction), PBMCs were thawed at +37°C following cryopreservation in serum-free CTL-CryoABC Serum-free Freezing Medium and transferred to 15 ml Falcon tubes (SARSTEDT) using a transfer pipette to minimise shear stress. 1 ml of TM (Table 2.13) was added to rinse the cryovials and the Falcon tubes were topped up to 10 ml with TM. Cells were centrifuged and the pellet resuspended in 10 ml of TM. Following an additional centrifugation step, cells were resuspended in 4 ml TM per cryovial and counted using the Chemometec NucleoCounter NC-3000 automated cell analyser (OXB) or manually using a

haemocytometer (University of Oxford). Cells were centrifuged and resuspended at 2x10^6 viable cells/ml in modified T cell medium (MM) (Table 2.13). Cells were plated at 1.5x10^6 viable cells/well in 24-well plates (Corning) with additional sample kept for staining controls.

Dynabeads Human T-Expander cluster of differentiaion (CD)3/CD28 (Thermo Fisher Scientific) were prepared at a 1:1 bead:cell ratio in PBS with 1% human AB serum (Sigma). Beads (1x10^8 beads/ml stock) were vortexed for 30 secs and the desired volume transferred to a 15ml Falcon with an equal volume of buffer (at least 1 ml). Beads were separated with the STEMCELL EasySep cell separation magnet and resuspended in MM at equal volume to that removed from the vial, topped up with MM to produce a solution of 2x10^6 beads/ml. Dynabeads were added to PBMCs at 1.5x10^6 beads/well and 10 ng/ml of interleukin (IL)-7 (Miltenyi Biotec) and IL-15 (Miltenyi Biotec) were added prior to incubation at +37°C/5% CO_2.

On Day 1 anti-H8 CAR lentiviral vector aliquots were thawed at +37°C and stock dilutions were created giving a final multiplicity of infection (MOI) of 2.0 based upon calculated HEK293T polymerase chain reaction (PCR) titre. Cell harvest was variably performed on Day 4 or Day 7 depending on the assay. For Day 7 harvest assays, on Day 4 viability was calculated as previously and medium volume was adjusted to maintain cells at 5x10^5 viable cells/ml.IL-7 and IL-15 were replenished to 1:1000 prior to incubation at +37°C/ 5% CO_2. For harvest, cells were transferred to Falcon tubes and centrifuged prior to resuspension in 2-5 ml for removal of beads with the STEMCELL EasySep magnet. Cells were centrifuged in fresh Falcon tubes and counted as previously. Cell concentration was then corrected to 1x10^6 viable cells/ml and aliquots of 1x10^6 total cells were taken for PCR or 9x10^5 viable cells for T cell phenotyping. Any additional cells were centrifuged and resuspended at 1x10^7 viable cells/ ml in cell freezing medium. 1 ml cryovials were then stored in a cell freezing unit (OXB) / Mr Frosty (University of Oxford) at -80°C for 18-24 h prior to transfer to liquid nitrogen for long-term storage.

2.2 Protein Expression Analysis

2.2.1 Western Blot

Cell lysates were obtained from adherent cells by removal of culture medium and PBS wash prior to addition of radioimmunoprecipitation assay (RIPA) lysis buffer (Thermo Fisher Scientific) with cOmplete protease inhibitor (Roche) and PhosSTOP phosphatase inhibitor (Roche) and 5 min incubation on ice. A cell scraper was used to collect lysates which were then centrifuged and transferred to fresh Eppendorf tubes for analysis. Protein was quantified using a bicinchoninic acid (BCA) protein assay kit (Thermo Fisher Pierce). Absorbance of samples and standards was read at 562 nm using the POLARstar Omega microplate reader following 30 min incubation of samples with the working reagent. GraphPad Prism version 10 was used to interpolate protein concentrations which were then normalised through dilution with sample buffer.

Gel electrophoresis was performed using 10% Bis-Tris gels (Thermo Fisher Scientific) with 50 µg protein in each well. Samples were diluted in RIPA buffer with NuPAGE LDS sample buffer (Thermo Fisher Scientific) and 1 mM dithiothreitol (DTT) before running at 150V for 90 mins in 4-morpholinepropanesulfonic acid (MOPS) buffer. Following electrophoresis, transfer was achieved using a polyvinylidene difluoride (PVDF) membrane Immobilon-P (Millipore) which was activated in 100% methanol prior to use. Tris-glycine buffer (Table 2.13) was used for transfer, run at 30 V for 90 mins on ice. Membranes were blocked with tris-buffered saline with tween (TBST) with 5% bovine serum albumin (BSA) (Sigma Aldrich) at room temperature (RT) for 1 h and incubated with primary antibodies (Table 2.4) diluted in TBST with 1% BSA overnight at +4°C. Following three TBST washes, secondary horseradish peroxidase HRP antibody was applied (1:5000 dilution in TBST with 1% BSA) for 45 mins. Electrochemiluminescence (ECL) (Millipore) was applied after three further TBST washes and images were taken using the LICOR Odyssey Imaging System.

Target	Catalogue number	Dilution
5T4 (TBGP)	Proteintech 29394-1-AP	1:1000
Mesothelin	CST 99966	1:1000
Muc1	CST 4538	1:1000
Prominin (CD133)	CST 64326	1:1000
β-actin	Proteintech 60008-1-1g	1:5000

Table 2.4: Primary antibodies used for Western Blot.

Protein expression was quantified using ImageJ (National Institutes of Health). Individual bands were quantified, and protein expression was calculated relative to the housekeeper protein using ImageJ. Biological replicates were conducted by obtaining lysates from different passages of each cell line, run on individual gels.

2.2.2 Histological Analysis – Immunohistochemistry (IHC)

Samples were fixed in 4% neutral buffered formalin (NBF) for 12 h and stored in 70% ethanol prior to processing and embedding in paraffin wax (Epredia). To prevent loss of the small tissues during processing, each slice was placed into a Cellsafe biopsy insert (Electron Microscopy Science) inside the processing/embedding cassette (Histosette). 4-5 µm microtome sections were generated and mounted on negatively charged slides (Epredia). Slides were kept overnight at +50°C prior to rehydration in Citroclear (Leica Biosystems) and decreasing concentrations of ethanol. After ethanol steps (100%, 100%, 70%, 50%), slides were submerged in ddH_20.

Following rehydration, an antigen retrieval step was performed to improve staining quality. Retrieval was optimised for individual antibodies (Table 2.5) with slides in staining bins incubated in a pressure cooker which was set to reach +125°C for 2 mins and +90°C for 1 min prior to cooling. Staining bins were kept on ice for 1 h before a hydrophobic PAP pen (Invitrogen) was used to circle the specimens.

Target	Manufacturer	Antigen retrieval	Dilution
5T4 (TBGP)	Proteintech 29394-1-AP	Citrate	1:2000
Mesothelin	CST 99966	Citrate	1:250
Muc1	CST 4538	Citrate	1:4000
Prominin (CD133)	CST 64326	Citrate	1:300
Cleaved caspase 3	CST 9661S	Citrate	1:200

Table 2.5: Primary antibodies used for IHC.

Samples were then blocked for 15 mins with dual endogenous enzyme block (Dako) and 45 mins with 5% goat serum in PBS to reduce non-specific binding. Primary antibodies (Table 2.5) were applied and samples were kept overnight at +4°C in a humid chamber. All antibodies were diluted in antibody diluent (Abcam) and were optimised for specific experiments (see Appendix A.2) or had previously been optimised by a member of the lab. Slides were washed three times in staining bins prior to 45 min incubation with secondary antibody HRP (Dako/CST) at RT in the humid chamber.

Staining was visualised through short exposure to diaminobenzidine (DAB) diluted 1:50 in diluent before the reaction was stopped by submersion in distilled water. Slides were then counterstained with 20 sec immersion in haematoxylin Gill (Leica Biosystems), washed and dehydrated. Following xylene (Leica Biosystems) submersion, coverslips were applied using dibutyl phthalate polystyrene xylene (DPX) mountant (Sigma Aldrich) and slides were dried in the fume hood for 48 h prior to imaging at 20x magnification using the Aperio Brightfield Slide Scanner or the Mica (Leica Biosystems).

2.2.3 5T4 ELISA

The 5T4 enzyme-linked immunosorbent assay (ELISA) (Assay Genie) was carried out as per manufacturer's instructions. Briefly, samples were diluted at a minimum of 1:1 with sample dilution buffer and standard dilution was prepared. Samples and standards were applied to the pre-coated ELISA plate followed by 90 min incubation. The plate was washed twice, and then biotin-detection antibody

solution was added for 60 mins. After three washes, SABC working solution was added, incubated for 30 mins and then washed five times. TMB substrate was added for 10 mins, and the reaction was terminated with stop solution when the first three standards turned visibly blue. The absorbance was read using the POLARstar Omega microplate reader at 450 nm and concentrations of 5T4 in the samples were interpolated from the standard curve.

2.2.4 IL-6 ELISA

The Ella (Protein Simple) platform was used to carry out an ELISA of IL-6 in media samples previously analysed in the cytokine array, Gareth Price (OXB) assisted with acquisition. The Simple Plex cartridge kit general protocol was followed. Samples were diluted up to 1:1000 in sample diluent to ensure that IL-6 values would fall within the standard curve. 1 ml of wash buffer was added into cartridge buffer inlets and 50 µl of diluted sample was added to each sample well. A positive IL-6 control (Protein Simple) was loaded as well as negative control wells using sample diluent alone. The Simple Plex Runner application was used to run the plate and the Simple Plex Explorer to analyse the data.

2.2.5 Cytokine Array

The RayBiotech C1000 Human Cytokine array was used to assess soluble factors present in tumour conditioned media (TCM). This kit was chosen as it contained most factors identified by the ligand identification analysis performed by Constantinos Demetriou (O'Neill lab, Department of Oncology, University of Oxford).

Conditioned media samples were used immediately upon thawing without dilution as per the manufacturer's instructions. Prior to completing the full C1000 array, a C6 array kit was used to optimise sample incubation times for both full biopsy (full tumour biopsy used to condition medium for 72 h) and slice (single 250 µm tumour slice incubated for 24 h) conditioned media samples.

The kit was used as per the manufacturer's instructions. C6 and C7 membranes were incubated in blocking buffer prior to overnight incubation at +4°C with slice

TCM samples. Full biopsy samples were added the next day for a 3 h incubation at RT. After sample incubation the streptavidin conjugated antibody was applied for 2 h followed by HRP-conjugated secondary and a final substrate step. Washes were carried out after each step following the sample incubation. The ChemiDoc gel imaging system was used to image the membranes and images were subsequently analysed using ImageJ (National Institutes of Health).

Gintare Smagurauskaite (Bhattacharya group, Centre for Human Genetics, University of Oxford) provided the method for analysis of the array data. Images were cropped to contain only one membrane with each membrane enlarged to allow sufficient detection area. The Protein Array Analyser plugin developed by Gilles Carpentier was used in ImageJ. Background was subtracted and spot identification circles were set to have a radius of 6 throughout analysis. Grid models were generated and grid intensity measurements exported.

2.2.6 Cytokine Bead Array (CBA)

The cytokine bead array (CBA) assay used the BD CBA Human Soluble Protein Flex Set System to detect multiple analytes at concentrations between 10 to 2500 pg/ml (ROP050). Media samples were profiled for levels of IL-2, IL-6, IFNγ, IL-10, IL-1β, TNFα, and IL-12p70 – different combinations were used in different assays and are detailed in the results. For each protein being analysed, a set of standards was prepared (Table 2.6) through reconstituting the lyophilised standard with 4 ml of Assay Diluent. A serial dilution was then performed using 500 µl Assay Diluent per condition down to 1:256 dilution.

Dilution	Top Standard	1:2	1:4	1:8	1:16	1:32	1:64	1:128	1:256
Protein (pg/ml)	2,500	1,250	625	312.5	156.25	78.13	39.06	19.53	9.77

Table 2.6: Standard dilution series used in the CBA Human Soluble Protein Flex Set System.

The filter plate used for the assay was washed in 100 µl Wash Buffer per well which was removed using a vacuum manifold. After aspiration, 50 µl of the Flex

Set standards were added along with 50 µl of the samples. All unknown samples were diluted 1 in 7.14 prior to addition to the plate, in order to mitigate against the presence of protein concentrations above the range of the standards.

50µl of diluted Capture Beads were added to each well and the plate was mixed at 500 RPM for 5 mins before RT incubation for 1 h. 50 µl of PE Detection Reagent was then added with a further mix and 2 h RT incubation. The plate was then vacuum rinsed and 150 µl of wash buffer was added to each well. A further 500 RPM mix was performed before the samples were transferred to a 96-well U bottom plate (Thermo Fisher Scientific) for analysis.

The BD FACSverse was used to read the wells and subsequent analysis was performed using the FCAP array software (BD Biosciences). Values for concentration of each cytokine were interpolated from the standard curves with values for each individual cytokine defined by the distinct fluorescence profiles of the beads.

2.3 T Cell Migration and Cytotoxicity

2.3.1 Co-Culture - Flow Cytometry

Flow cytometry was performed at OXB following previously optimised protocols (ROP049). CAR-T cells and matched donor UTCs were thawed in complete RPMI-10 (10% FBS (Gibco), L-glutamine (Gibco), pen-strep (Gibco)), washed, counted and plated at 2x10^6 cells/ml in 6-well plates (Corning). On the same day, target cells were labelled with CellTrace Far Red (Thermo Fisher Scientific) (1 µl/2 ml cell suspension with cells at 1x10^6 cells/ml) and incubated at +37°C/5% CO_2 for 5mins. An equal volume of complete RPMI was added before a further 5 min incubation at +37°C/5% CO_2. Cells were washed, resuspended in complete RPMI and plated at 1x10^6 cells/ml in 6-well plates.

After 24 h, cells were resuspended, pooled and counted. Following centrifugation, cells were resuspended at 1x10^6 cells/ml and 100 µl of each effector and target cell type transferred into relevant wells of a round-bottom 96-well plate (Thermo Fisher Scientific). Cells were plated in triplicate with medium-only and effector/target cell

only controls. For 'cell only' controls, 100 µl of the alternative cell medium was added to ensure that the medium would not affect subsequent measurements.

After 24 h of co-culture at +37°C/5% CO_2, 50 µl of medium was removed from each well without disturbing cells and transferred to a 96-well plate stored at -80°C for CBA analysis.

At 48 h, the 96-well plate containing the co-culture was centrifuged. The cells were washed with 150 µl of PBS (adherent SKOV3 cells were lifted with TrypLE (Gibco) prior to this) and then re-suspended in 100 µl Aqua LIVE/DEAD Fixable Cell Stain viability dye (Thermo Fisher Scientific) diluted 1 in 1000 in PBS. The cells were incubated for 30 mins RT in the dark and washed with stain buffer after which point centrifugation steps were conducted at +4°C. In experiments including 5T4 staining, 2.5 µl of the PE conjugated H8 antibody (supplied by OXB) were added to each sample at this point. Cells were incubated for 30 mins at +4°C in the dark. Cells were washed twice with stain buffer before being resuspended in 100 µl of stain buffer and analysed using the BD FACSverse flow cytometer.

2.3.2 Co-Culture - xCELLigence Impedance Assay)

Impedance assays were carried out using the ACEA xCELLigence real-time cell analyser (RTCA) system. First, tumour cells were titrated using protocols developed by Tess Stanley and Will Jackson (O'Neill Lab, Department of Oncology, University of Oxford). Numbers were selected based upon plateau at 24h with 10,000 cells/well determined optimal for all target tumour cell lines. Prior to plating, cells were washed and lifted with TrypLE (Gibco) and resuspended in DMEM pancreatic cell line medium (Table 2.13) to give desired concentrations. E-Plate 96 polyethylene terephthalate (PET) plates (Agilent) were used to read impedance with an initial 50 µl of medium added to calibrate the RTCA. Cells were then plated in triplicate using a range of concentrations, left to rest for 30 mins and the RTCA was run overnight analysing impedance at 15 min intervals for 1000 sweeps.

CAR-T cells and UTC were thawed in RPMI (Gibco) accounting for 50% loss on Day 2 of culture. Cells were centrifuged, counted and resuspended at $2x10^6$

cells/ml in RPMI and transferred to a 6-well plate (Corning). CAR-T cells were left overnight in a humidified incubator at +37°C and 5% CO_2. After 18-24 h incubation, CAR-T cells were diluted to the desired concentrations. The RTCA was paused and 100 µl of CAR-T cells were added to each well and left to rest for 30 mins before returning and acquiring.

Analysis of cytotoxicity of healthy donor and patient-derived CAR-T cells was carried out as above using 10,000 target cells/well and CAR-T cells at 1:10, 1:5, 1:2, 1:1, 2:1, 5:1 and 10:1 effector:target ratios. Percentage cytotoxicity was calculated using the average cell index (CI) of the target cell line cultured without effector cells.

For cytokine analyses, media samples were harvested after 24 h of co-culture and analysed using the CBA assay (see section 2.2.6).

2.3.3 Transwell Migration

Migration assays were performed using the Corning transwell 96-well permeable support. Guidance in the setup and optimisation of the system was provided by Megan Payne (Bhattacharya Group, Centre for Human Genetics, University of Oxford) and Bruno Beernaert (Parkes Group, Department of Oncology, University of Oxford).

T cells were thawed at +37°C 24 h prior to migration. Cells were thawed into TM and centrifuged. Cells were counted and plated at $2x10^6$ cells/ml in 6-well plates (Corning) before being rested overnight in the incubator at +37°C and 5% CO_2. T cells were washed twice in PBS to minimise serum carryover from culture before being suspended in migration medium (Table 2.13) at $1.33x10^6$ cells/ml.

75 µl of cell suspension was pipetted into the upper chamber of the transwell plate followed by 235 µl of migration medium into the lower chamber. In test wells, the migration medium contained 100 ng/ml C-X-C motif chemokine ligand (CXCL)12 (Miltenyi Biotec), negative controls contained no chemokine and positive controls used normal T cell line medium containing 10% FBS (Gibco). Chemokine concentration (100 ng/ml) was chosen based upon optimisation experiments (Appendix C.2) using both CXCL10 (Miltenyi Biotec) and CXCL12. Cells were incubated at +37°C/5% CO_2 for 4 h.

Following incubation, the upper chamber was removed from the plate and the cell suspension from the lower chamber was transferred into a round-bottom 96-well plate (Thermo Fisher Scientific) for analysis. Cells were centrifuged and washed twice with fluorescence-activated cell sorting (FACS) buffer. Cells were analysed using the Attune flow cytometer (Thermo Fisher) using volumetric counting with 100 µl acquisition volume. Forward scatter (FSC) and side scatter (SSC) were measured and used to gate whole cells.

2.3.4 CAR-T Cell Culture with IL-6

Healthy donor PBMCs were thawed in TM and spun before counting and resuspension at 5x10^7 cells/ml in PBS with 2% FBS (Gibco) and 100 µg/ml DNAse I solution (suggested buffer). The STEMCELL EasySep Cell Separation magnet was used for T cell isolation using negative selection (as per manufacturer's instructions). A manual count was performed with the resulting enriched cell suspension and cells were plated in MM at 2x10^6 cells/ml in 0.75 ml per well of a 24-well plate (Corning).

Thermo Fisher Dynabeads human T cell activator CD3/CD28 beads were used at a 1:1 ratio with T cells. Beads were washed in PBS with 1% BSA (Sigma Aldrich) using the EasySep magnet and resuspended in an equal volume of MM to the total of the previous cell suspension. 0.75 ml of beads were added to all wells except no activation controls which were topped up with MM. Cytokines (Miltenyi Biotec) were added to wells at 10 ng/ml.

Cells were counted on Day 4 and maintained at 5x10^5 cells/ml through addition of MM. Cytokines were added to maintain original concentrations. On Day 7, cells were centrifuged and resuspended in 3 ml MM before the EasySep magnet was used to remove beads. The cell suspension was washed, counted, and then samples were analysed for viability using the haemocytometer. CD3 percentage, programmed cell death protein 1 (PD-1) expression and T cell phenotype were assessed using flow cytometry panels (see section 2.5.1). Media samples were collected on Day 0, Day 4 and Day 7 and analysed using the CBA assay performed at OXB.

2.3.5 Tumour and Cell Line Conditioned Media Suppression

Conditioned media samples were generated from cell lines (CCM) through culture of cell lines in T75 (Corning) flasks until 95% confluency. Media was then collected and centrifuged and stored at -20°C until use. Slice media samples were obtained through collection of media from slices cultured over 24 h. Biopsy media samples were generated through collection of media from culture of slices generated from a total biopsy cultured over 72 h. Media were centrifuged and stored at -80°C until use.

CAR-T cells were generated as per the previous protocol. On Day 6 of culture (12/24 h before harvest), cells were centrifuged and resuspended in either TCM or CCM (maintaining a concentration of $2x10^6$ cells/ml). The exposure time was optimised through exposure of Dynabead-activated T cells (with and without Dynabead removal) for 12/24 h in T cell line medium and tumour slice medium. After exposure to conditioned media (with T cell line and tumour slice base medium controls), CAR-T cells were washed and plated for downstream analysis.

Cytotoxicity was analysed as per the xCELLigence impedance assay protocol using $1x10^5$ tumour cells/well and ratios of 1:1 and 1:2 effector:target cells. Migration was assessed as per the migration assay protocol and PD-1 expression through flow cytometry as detailed previously. The Beckman Coulter CytoFLEX Flow Cytometer was used to analyse expression with subsequent analysis carried out using FlowJo.

2.4 Immunofluorescence and Imaging

2.4.1 Immunofluorescence (IF)

2.4.1.1 PDAC Slices with Jurkat T Cells

Jurkat activation was carried out in RPMI medium at $1x10^6$ cells/ml. Cells were incubated for 1 h at +37°C/5% CO_2 with Cell Stimulation Cocktail (eBioscience) added at 1:500 followed by resuspension in fresh RPMI. This activates cells using a combination of phorbol 12-myristate-13-acetate (PMA), ionomycin and Brefeldin A. 5-chloromethylfluorescein diacetate (CMFDA) (Thermo Fisher Scientific) incubation was carried out in Hank's Balanced Salt Solution (HBSS). 1mM CMFDA was diluted

1:100 in an equal volume of HBSS and then combined with cells for 15 mins. Cells were resuspended in RPMI at a final concentration of $1x10^7$ cells/ml and 10 µl of suspension was added to each slice to give $1x10^5$ cells/slice. The suspension was concentrated in an aluminium washer placed over the specimen and incubated for 1 h at +37°C/5% CO_2 before manual washing in LG DMEM (Gibco).

Target	**Manufacturer**	**Conjugate**	**Dilution/Conc**
Fibronectin	Stratech BS-13455R-A594-BSS/ Abcam ab201800	Alexa Fluor 594/DyLight 550	1:100
EpCAM	Abcam ab237396/ Abcam ab201799	Alexa Fluor 647/DyLight 488	1:100
Exogenous T cell	Santa Cruz sc-396581/ Thermo Fisher C34564	CMFDA/CellTrace Far Red	10µM
Nucleus	Invitrogen D1306	DAPI	2µg/ml
5T4	Thermo Fisher PA5-116062	DyLight 488/unconjugated	1:100
T cell activation	Thermo Fisher F14201	Fluo4 AM	1µM

Table 2.7: Primary antibodies and markers used to stain tumour slices and T cells for IF.

Following Jurkat incubation, PDAC slices were fixed for 12 h in 4% paraformaldehyde (PFA) prior to blocking in PBS containing 1% BSA (Sigma Aldrich) and 10% FBS (Gibco) for 12 h at +4°C. Slices were then incubated with antibodies (Table 2.7) diluted in PBS with 0.5% BSA and 2% human AB serum (Thermo Fisher Scientific) overnight at +4°C. 1 µl of 100 µg/ml diamidino-2-phenylindole (DAPI) was added to each sample at the time of antibody incubation. Slices were then washed three times in PBS with 1% BSA and 0.1% sodium azide. Finally, slices were mounted on negatively charged glass slides (Epredia) and coverslips (Scientific Laboratory Supplies) were mounted with ProLong Gold mounting medium (Invitrogen). The ZEISS LSM 710 confocal microscope system was then used for imaging. Spectral unmixing was conducted using the ZEN 2011 (ZEISS) software package with single colour controls used to define individual stain spectra.

2.4.1.2 PDAC Slices with Matched Patient T Cells

For tumour slice incubation with primary T cells, PBMCs were purified from whole blood as described. T cell isolation was performed using the STEMCELL EasySep Negative T cell selection kit (as per manufacturer's instructions). Cells were counted and resuspended in MM at $2x10^6$ viable cells/ml, plated in 0.75 ml medium per well of 24-well plates (Corning). Dynabeads Human T-Expander CD3/CD28 (Thermo Fisher Scientific) were washed (as per manufacturer's instructions) and added at a ratio of 1:1 beads:cells. IL-7 (Miltenyi Biotec) and IL-15 (Miltenyi Biotec) were added at a working concentration of 10 ng/ml and the T cells were incubated at +37°C/5% CO_2 until PDAC tumour slices were generated.

Prior to slice incubation, T cells were resuspended in PBS at $1x10^6$ cells/ml and incubated with 1 µM CellTrace Far Red Tracker Dye (Thermo Fisher Scientific) for 20 mins at +37°C/5% CO_2 in the dark. Five times the original volume of PBS was added to quench the dye and incubated for a further 5mins. Cells were pelleted and resuspended in fresh medium with a further 10 min incubation at +37°C/5% CO_2. Finally, cells were spun and resuspended at $1x10^7$ cells/ml and 10 µl was added to the surface of each tumour slice. The suspension was concentrated in an aluminium washer placed over the specimen and incubated for 1 h at +37°C/5% CO_2 before manual washing in LG DMEM.

PDAC slices were fixed following T cell incubation as previously with Jurkat cells. Staining and washing was also carried out as previously. Once slides were washed and mounted on glass slides, the Andor Dragonfly confocal microscope was used to generate Z-stacks and tile scan images of the slices and Imaris was used to analyse images.

2.4.1.3 PDAC Slices with Matched Patient CAR-T Cells

For application of autologous CAR-T cells to patient tumour slices, PBMCs were purified from whole blood (as previously) at least 7 days prior to sample collection. After MACS buffer wash steps, PBMCs were plated as described in section 2.1.6 and a 7-day transduction was carried out. If surgery was scheduled more than 8

days after PBMC isolation, CAR-T cells were frozen at 1x10^7 cells/ml in FBS with 10% DMSO (Sigma Aldrich) after Dynabead removal on Day 7.

Prior to slice incubation, CAR-T cells and matched UTC were resuspended in PBS at 1x10^6 cells/ml and incubated with 1 µM CellTrace Far Red Tracker Dye for 20 mins at +37°C in the dark. Five times the original volume of PBS was added to quench the dye and incubated for a further 5 mins. Cells were pelleted and resuspended in fresh medium with a further 10 min incubation at +37°C. Finally, cells were spun and resuspended at 1x10^7 cells/ml and 10 µl was added to the surface of each tumour slice. The suspension was concentrated in an aluminium washer placed over the specimen and incubated for 1 h at +37°C before manual washing in LG DMEM.

PDAC slices were fixed following T cell incubation as previously. Antibody staining, washes and mounting were also performed as previously. Imaging was carried out using the Andor Dragonfly as with matched patient T cells and image analysis was also repeated using Imaris.

2.4.1.4 Live Cell Imaging

Live cell imaging experiments were performed using the Zeiss LSM980 Airyscan 2 upright microscope in the Micron imaging facility (Oxford University). Experimental setup, execution and analysis were aided by Lior Pytowski and Niloufer Irani (The Micron Imaging Facility, Oxford University). The protocol was adapted from (Espie et al. 2023) with advice from the first author David Espie (French Institute of Health and Medical Research).

CAR-T cells and UTC cells were generated from autologous patient blood as described previously. Cells were washed twice with HBSS and resuspended in HBSS containing 1 µM Fluo-4 AM (Thermo Fisher Scientific) at 1x10^6 cells/ml. Cells were incubated for 30 mins at +37°C/5% CO_2 in the dark. Cells were then washed twice in XVIVO (Lonza) and kept in the dark at +4°C while slices were prepared.

Tumour slices were prepared as previously described (maintaining the agarose around the edge of the slice) and placed in a 6-well plate (Corning) containing

1 ml of tumour slice medium per well for staining. A washer was placed on top of each slice and 40 µl of 5T4 antibody solution (1:100 unconjugated antibody) added to the slice surface. The slice was incubated for 30 mins at +37°C protected from light, washed in tumour slice medium and the secondary antibody was added (anti-rabbit immunoglobulin G (IgG), Alexa 594/647, 1:200) for a further 30 mins at +37°C/5% CO_2 protected from light. Slices were then washed in tumour slice medium and kept at +4°C in the dark prior to imaging.

The ZEISS LSM980 was configured with a 20x water objective immersion lens and the temperature set to +37°C prior to imaging. A 35 mm petri dish (Thermo Fisher Scientific) was placed on the imaging stage with the tissue slice secured with butyl cyanoacrylate tissue glue (applied with a pipette tip). A washer was placed around the slice and a meniscus created by adding 200 µl of complete medium to the surface of the slice. The objective lens was lowered into the meniscus and brightfield used to focus on the cut surface of the slice and a region of interest selected using the 5T4 stain.

Imaging was carried out using the following parameters: time lapse with one image every 10 secs (1 time point) for 10-15 mins. Acquisition for the channel recording Fluo-4 at every time point with the 5T4 staining recorded every 5 time points. 10 z-steps with a z-stack thickness between 5-10 µM.

Prior to imaging CAR-T cells and UTC cells were resuspended in 10 µl of XVIVO medium. The cells were added to the medium droplet on top of the tumour slice and the camera turned on. Recording was commenced when the first CAR-T cells landed on the slice. Images were analysed using Imaris using the 'surfaces' feature with thresholding to locate single T cells. T cells in contact with $5T4^+$ cells were then selected and their fluorescence intensity over time was analysed. Intensity was calculated as a ratio over the course of the experiment relative to the intensity at the beginning of imaging when the T cell was first visible.

2.4.1.5 Imaris Image Processing

Processing and quantification of Z-stack IF images were conducted using Imaris. Imaris file converter was used to create IMS files from the CZI images obtained on the Zeiss 710/Andor Dragonfly. Surfaces were used in Imaris analysis to define tumour (EpCAM), target (5T4), nuclei (DAPI), stroma (fibronectin) and T cells (CMFDA/CellTrace Far Red). Surfaces were defined using a consistent surface detail size using 'absolute intensity' and background subtraction to remove false positive staining detection. Thresholding used to define the surfaces was kept consistent throughout samples within each experiment and was calculated independently to account for variation in staining intensities between different patient samples. Z-depth of T cells was calculated by subtracting the Z-depth of each individual object from the T cell-rich surface of the slice while colocalisation was defined using the shortest distance from each T cells to the nearest target cell. All data was exported to Excel prior to analysis using GraphPad Prism version 10.

Live imaging analysis was carried out using protocols described in (Espie et al. 2023). CAR-T and UTC cells were selected due to their persistence in the imaging field for a sufficient duration to measure calcium flux. For analysis of P018 (Table 2.1), CAR-T cells were identified based upon their contact with 5T4 protein while UTC cells were chosen at random due to a lack of antigen in the UTC-treated sample. Calcium flux was measured by dividing each Fluo-4 intensity throughout the time course by the initial intensity when the T cells were first applied to the slice.

2.5 Flow Cytometry

2.5.1 Flow Cytometry

Flow cytometry was carried out at both Oxford University and OXB.

Target	Manufacturer	Conjugate	Dilution
Human 5T4 (ONC)	R&D FAB49751R	Alexa fluor 647	1:40
Human 5T4 (H8)	Oxford Biomedica	PE	1:40
Human 5T4 (2E4)	Oxford Biomedica	PE	1:40
Isotype control (PE)	Thermo Fisher 12-4714-82	PE	1:40
Isotype control (APC)	Thermo Fisher 51-4714-81	Alexa fluor 647	1:40
Fixable Viability Dye eFluor 506	Thermo Fisher 65-0866-14	Dye (eFluor™ 506)	1:1000
Human PD-1	BioLegend	PE Dazzle 594	1:100

Table 2.8: Antibodies and markers used at Oxford University for flow cytometry of CAR-T cells and tumour slice-derived single cell suspensions.

At Oxford University, adherent cells were harvested using TrypLE (Gibco) to preserve surface antigen expression. Counting was performed using the haemocytometer and 2.5-5x10^5 cells were plated per sample in a 96-well plate (Thermo Fisher Scientific). Cells were centrifuged and washed with ice cold PBS prior to staining with fixable live/dead dye (Thermo Fisher Scientific) diluted in PBS for 30 mins at +4°C protected from light. Following washing twice in fluorescence-activated cell sorting (FACS) buffer (Table 2.13) cells were stained with antibodies (Table 2.8) at concentrations determined through prior titration using a range of concentrations from 0.1 µl to 10 µl (Appendix A.3. Stain indices were calculated in FlowJo using the formula:

$$\frac{\mathrm{MFI}_{\mathrm{positive}} - \mathrm{MFI}_{\mathrm{negative}}}{2 \times \mathrm{SD}}$$

Staining was carried out for 30 mins at +4°C protected from light, alongside isotype controls and staining of compensation beads for compensation of individual fluorophores and setting live/dead thresholds. Following staining, cells were washed three times in FACS buffer before acquisition using the CytoFLEX flow cytometer (Beckman Coulter). All analysis was carried out using FlowJo with graphs generated in GraphPad Prism version 10. Gating thresholds were determined by live/dead and compensation beads.

Flow cytometry experiments performed at Oxford Biomedica had previously been optimised by members of TSG. Transduction efficiency was analysed using the FACSverse flow cytometer (BD Biosciences) through assessment of CD3 positivity and vector product (anti-H8 CAR) surface expression (ROP062). T cell phenotype was assessed using the Attune flow cytometer (Thermo Fisher Scientific) through expression of CD4, CD8, CD45RA, CD95 and CD62L (ROP070). Cell viability was also assessed during both processes.

Target	**Manufacturer**	**Conjugate**	**Dilution**
Human CD3	BioLegend # 300441	PE	1:20
Human H8	Fleet Bioprocessing	AF488	1:200
Human CD4	BioLegend # 300546	BV510	1:100
Human CD8	BioLegend # 344712	PE Cy7	1:100
Human CD45RA	Thermo # 61-0458-42	PE EFluor 610	1:50
Sytox advanced	Thermo # S10274	Read in PerCP-Cy5.5	1:1000
Human CD95	BD Biosciences 563132	BV711	1:100
Human CD62L	BD Biosciences 555544	PE	1:20

Table 2.9: Antibodies and markers used at OXB for flow cytometry of CAR-T cells

For each test, $5x10^5$ cells were collected and pelleted in a round bottom 96-well plate (Thermo Fisher Scientific). Cells were washed twice in staining buffer (BD Biosciences) and spun to pellet. Prior to surface marker staining, SYTOX (Thermo Fisher Scientific) live-dead stain was added in 200 µl of stain buffer per test. Antibody cocktails (Table 2.9) were made up in a total of 100 µl per test in staining buffer and added to pelleted cells. These were then incubated in the dark at +4°C for 60 mins. For each antibody, an additional cell sample with fluorescence minus one (FMO) and single stain controls were set up. Compensation beads were also used with single stains added to each bead sample, incubated for 5 mins before addition of negative beads and dilution in sample buffer. Samples were run and gated using thresholds determined by FMO controls. The Attune (Thermo Fisher Scientific) and FACSverse (BD Biosciences) flow cytometers were used for acquisition.

Populations were defined as follows:

1. Naïve T cell: $CD45RA^{+}$ $CD62L^{+}$ $CD95^{-}$
2. Stem cell-like memory T cell: $CD45RA^{+}$ $CD62L^{+}$ $CD95^{+}$
3. Central memory T cell: $CD45RA^{-}$ $CD62L^{+}$ $CD95^{+}$
4. Effector memory T cell: $CD45RA^{-}$ $CD62L^{-}$ $CD95^{+}$
5. Effector T cell: $CD45RA^{+}$ $CD62L^{-}$ $CD95^{+}$

2.5.2 Spectral Flow Cytometry

Spectral flow cytometry was carried out using the Cytek Aurora 4 laser (UV/V/B/R) cytometer. The panel used was adapted from Biolegend's 'Human T Cell Differentiation and Exhaustion' optimised panel (Table 2.10) with guidance from Eva Zemlickova (Sr. Strategic Commercial Manager, Biolegend). Antibodies for the CAR and T cell factor 1 (TCF1) were added, provided by Oxford Biomedica and Matthew Jackson (Parkes lab, Department of Oncology, University of Oxford) respectively. Details of the function of each target in the panel are provided in Chapter 6 (Table 6.1). Giampiero Valenzano (O'Neill lab, Department of Oncology, University of Oxford) and Matthew Jackson assisted with experimental design and Giampiero Valenzano assisted with acquisition and data analysis.

CAR-T cells generated from PDAC patients and healthy blood donors were thawed as previously described and seeded at $2x10^{6}$ cells/ml in 6-well plates (Corning). Cells were rested overnight in the incubator at +37°C/5% CO_2. Staining was carried out in round-bottom 96-well plates (Thermo Fisher Scientific) with $1x10^{6}$ cells/well plated per sample with extra cells used as unstained controls. Single stains were initially carried out using cells, but rare populations defined by some markers led to a lack of separation. BioLegend compensation beads were therefore used for all single stains apart from Zombie near infrared (NIR) viability dye where cells were used.

Cells were washed with PBS and fixable viability dye solution was added (1:2000 dilution in PBS). Cells were incubated at +4°C and protected from light

for 30 mins. Cells were then washed twice with 200 µl of staining buffer and resuspended in staining buffer with 5 µl of Human TruStain FcX and True-Stain Monocyte Blocker and incubated at RT for 10 mins. Without washing, antibody mastermix or single stains were added to samples which were incubated at +4°C protected from light for 30 mins.

Following two washes with staining buffer, cells were fixed for intracellular staining using the Foxp3 / Transcription Factor Staining Buffer Set (eBioscience). Fixation buffer was added to cells with 15 min incubation at RT. Permeabilisation buffer was added, cells were washed once with Permeabilisation buffer and resuspended in 50 µl of TCF1 antibody solution (1:1000 in Permeabilisation buffer). Following overnight incubation at +4°C protected from light, cells were washed twice in Permeabilisation buffer and were resuspended in staining buffer for acquisition. At least 100,000 cells were acquired per sample and unmixing was performed on the Cytek Aurora using single colour control beads and unstained cells. During acquisition, a gate was applied to filter out debris, ensuring that only whole cells were captured.

Manual analysis and unsupervised clustering were both performed using FlowJo. The compensation matrix was manually edited prior to manual gating using FMOs where relevant (gating strategy detailed in Figure D.2). Diagrams were generated using the layout editor with either density or pseudocolour plots and statistics were obtained using the table editor.

All patient and healthy donor samples were concatenated prior to the use of Uniform Manifold Approximation and Projection (UMAP) clustering. UMAP dimensionality reduction was applied to concatenated samples and pre-defined manually-gated populations were then overlaid onto UMAP plots. Additional plots were generated overlaying the fluorescence intensity of each marker onto the UMAP plot. Protocols for clustering were obtained from (Valenzano et al. 2024).

Target	Clone	Fluorophore	Volume/test	Manufacturer
Anti-5T4 CAR	H8	AF488	0.50	OXB
TCF-1	C63D9	AF647	0.05	CST
CD19	HIB19	Spark UV 387	0.50	BioLegend
CD27	O323	APC Fire 750	1.25	BioLegend
CD28	CD28.2	Pacific Blue	1.25	BioLegend
CD45RA	HI100	Spark NIR 685	1.25	BioLegend
HLA-DR	L243	APC Fire 810	1.25	BioLegend
CD39	A1	Pe Cy7	1.25	BioLegend
CD244	C1.7	PerCP Cy5.5	1.25	BioLegend
TCR γ/δ	B1	PE Fire 700	1.25	BioLegend
CD4	SK3	Spark YG 581	1.25	BioLegend
CD8	Sk1	Spark Blue 550	1.25	BioLegend
CD3	OKT3	BV510	1.25	BioLegend
TIM3	F38-2E2	BV650	1.25	BioLegend
CD127	A019D5	BV570	1.25	BioLegend
CCR7	G043H7	BV421	1.25	BioLegend
CD25	M-A251	PE Cy5	1.25	BioLegend
CXCR5	J252D4	BV750	1.25	BioLegend
KLRG1	MAFA	PE Fire 810	1.25	BioLegend
CD45	2D1	Spark Blue 574	1.25	BioLegend
CTLA4	BNI3	BV605	1.25	BioLegend
TIGIT	A15153G	PE Fire 640	1.25	BioLegend
PD-1	A17188A	PE	1.25	BioLegend
CD57	QA17A04	BV785	1.25	BioLegend
CD14	S18004B	Spark UV 387	1.25	BioLegend
CD95 (Fas)	DX2	PE Dazzle 594	1.25	BioLegend
CD73	AD2	BV711	1.25	BioLegend
LAG3	7H2C65	APC	1.25	BioLegend
TCR v/α7.2	3C10	Spark Red 718	1.25	BioLegend
Live/dead	n.a.	Zombie NIR	1.00	BioLegend

Table 2.10: Antibodies and markers used in the spectral flow panel adapted from the BioLegend Human T Cell Differentiation and Exhaustion optimised panel.

2.6 Statistical and Computational Analysis

2.6.1 Survival Analysis

Survival curves were generated using an R script designed by Constantinos Demetriou (O'Neill lab, Department of Oncology, University of Oxford). Analysis was conducted using The Cancer Genome Atlas (TCGA) and Clinical Proteomic Tumor Analysis Consortium (CPTAC) databases and the Oxford-Kidani cohort - FFPE samples obtained from the Oxford Radcliffe Biobank and analysed in house through microarray. Segregation was performed using the MAXSTAT function which determines the optimal cutoff point based upon outcome significance.

2.6.2 AlphaFold Protein Mapping

The structure of 5T4 was retrieved from AlphaFoldv2 using Gene Name: TPBG, UniProt: Q13641. Alexander Hasson (O'Neill lab, Department of Oncology, University of Oxford) processed the images using ChimeraX, removing residues with predicted local distance difference test (pLDDT) ≤ 50. The binding region of the H8 antibody was determined from a prior publication (Shaw et al. 2002). UniProt Feature Viewer was used to identify the transmembrane, proximal disulphide bonds and leucine-rich repeat (LRR)(-2) which were annotated on the AlphaFold structure. These regions were originally identified as encompassing the H8 binding site when the antibody was first characterised (Shaw et al. 2002). Matrix-associated 5T4 peptide sequences obtained by Dr Daniela Pankova (Pankova et al. 2019) were retrieved by Dr Iolanda Vendrell. These sequences were then annotated on the AlphaFold structure.

2.6.3 Differential Expression Gene Analysis

Receptor and ligand analysis was carried out by Constantinos Demetriou (O'Neill lab, Department of Oncology, University of Oxford). Single cell sequencing data from the single cell atlas (data derived from an amalgamation of 9 separate studies) was analysed using differential expression gene (DEG) analysis for CD4 and CD8 T cell states within PDAC tumours and adjacent normal pancreatic tissue. Wilcoxauc

was used for this analysis from the presto R package. Genes were filtered based on the following cutoffs:

pct_in > 0.2 & logFC > 0.2 & padj < 0.05

Pct_in: percentage of cluster (of interest) expressing the gene >20%

LogFC: Log fold change of cluster (of interest) vs rest of clusters > 0.2

Padj: adjusted p value < 0.05

CellChat was then used to filter for ligands in the categories 'Secreted Signaling' or 'Non-protein signaling' in order to obtain soluble ligands and receptors for ligands which could be detected in conditioned media.

2.6.4 Statistical Analysis

All statistical testing was performed using GraphPad Prism version 10 unless otherwise stated. Statistical tests used are described in the relevant figures or tables. The Shapiro-Wilk test was used throughout to determine Normalcy of data. Comparisons of the differences between two means with Normal distributions were made using t-tests while Normally distributed data comparisons of three or more means were made using Analysis of Variance (ANOVA) with multiple comparisons post-hoc testing. Alternative tests used for data determined not to be Normally distributed are detailed in figure legends. Graphs are displayed with mean ± standard deviation with all individual data points displayed. All statistical test results are displayed as follows: * = p< 0.05; ** = p< 0.01; *** = p< 0.001, **** = p< 0.0001, ns = not significant (p>0.05).

Number of replicates are detailed in all figure legends and are defined for individual experiments. Where possible biological replicates were carried out using distinct donors or cell line passages. Assay replicates were carried out if biological replicates were not possible. Technical replicates were incorporated into all assays where possible, these were used instead of assay replicates only in experiments where clinical sample quantities were limited.

2.7 Ancillary Methods and Materials

2.7.1 qPCR

Quantitative PCR (qPCR) analysis was carried out at OXB. The QIAcube HT instrument was used to perform gDNA extraction from samples prior to PCR. Samples were processed in a QIAamp 96-well plate with an additional elution microtubes RS (EMTR) plate loaded prior to running. Cell pellets were first resuspended in 200 µl of RNase A in PBS with an additional enzyme-only control also plated. Proteinase K was then added to Buffer VXL in dilutions previously optimised by TSG at OXB (ROP016_B) and added to the appropriate reagent trough. The QIAcube 'DNA extraction V2' protocol was run and, upon completion, the EMTR plate was removed.

To perform qPCR according to ROP016_C, primers (Table 2.11) and probes (Table 2.12) were combined with the TaqMan gene expression Master Mix, diluted with nuclease-free water. Along with samples and controls, plasmid standard dilutions were prepared. 20 µl of PCR mix was used per sample with 17.5 µl used for corresponding spiked PCR inhibition control (SPIC) PCR mixes. 5 µl of each template DNA sample was added directly to the mix and the plate sealed with adhesive film. The plate was then centrifuged and the reaction carried out using the QuantStudio 6 Flex System. Cycling parameters were as follows; initial +95°C hold for 10 mins followed by 40 cycles of +95°C for 15 secs and +60°C for 1 min.

OXB Primers		
Target	**Forward sequence**	**Reverse sequence**
EIAV	5' ATTGGGAGACCCTTTGA-CATTG 3'	5' ACCAGTAGTTAATTTCT-GAGACCCTTGTA 3'
HIV-Ψ	5' TGGGCAAGCAGGGAGCTA 3'	5' TCCTGTCTGAAGGGATGGT-TGT 3'
RPPH1	5' CCCTAGTCT-CAGACCTTCCCAAG 3'	5' GCGGAGGGAAGCTCATCAG 3'

Table 2.11: Primers for qPCR used at OXB.

OXB Probes	
Target	Sequence
EIAV	5' FAM-CACCTTCTCTAACTTCTTGAGCGCCTTGCT-TAMRA 3'
HIV-Ψ	5' FAM-AACGATTCGCAGTTAATCCTGGCCTGTT-TAMRA 3'
RPPH1	5' VIC-CCACGAGCTGAGTGCGTCCTGTCA-TAMRA 3'

Table 2.12: Probes for qPCR used at OXB.

2.7.2 Reagents

Reagent	**Composition**
LG DMEM complete pancreatic medium	DMEM (1g/L glucose), 0.5% FBS, 1% pen-strep-neo (PSN), 1% soybean trypsin inhibitor (SBTI), 1% L-glutamine and 0.4% amphotericin B
DMEM pancreatic cell line medium	DMEM, 10% FBS, 1% pen-strep, 1% L-glutamine
RPMI T cell line medium	RPMI, 10% FBS, 1% pen-strep, 1% L-glutamine
FACS buffer	PBS, 2% FBS, 1mM EDTA, 0.1% sodium azide
DC MACS buffer	PBS, 2mM EDTA, 0.5% BSA
Tris-EDTA antigen retrieval buffer	Distilled water, 10mM Tris-Cl (pH 8.0), 1mM EDTA (pH 8.0)
Citrate antigen retrieval buffer	Distilled water, 0.0825M sodium citrate dihydrate, 0.0175M citric acid (pH 6.0)
Transfer buffer	Distilled water, 190mM glycine, 25mM Tris-HCL, 10% v/v methanol
TM - Thawing medium (OXB)	X-VIVO TM 15, 10% Human AB serum, 2mM GlutaMax, 20mM HEPES, 1mM sodium pyruvate, 1% MEM Vitamin Mix, 100ug/ml pen-strep
MM - CAR-T cell medium (OXB)	X-VIVO TM 15, 2.5% Human AB serum, 2mM GlutaMax, 20mM HEPES, 1mM sodium pyruvate, 1% MEM Vitamin Mix, 100ug/ml pen-strep
Dynabead buffer	PBS, 1% BSA (sterile filtered)
T cell isolation buffer	PBS, 2% FBS
Migration medium	RPMI, 1% FBS, 1% pen-strep, 1% L-glutamine

Table 2.13: Composition of reagents used including media supplementation.

"Could your medicine be a cell, not a pill? Could your medicine be an organ that's created outside the body? Could your medicine be an environment?"

Siddhartha Mukherjee

3

Characterisation of 5T4 Antigen Expression in PDAC and Anti-5T4 CAR-T Cell Generation

3.1 Introduction

3.1.1 The 5T4 Antigen in PDAC

The oncofoetal antigen 5T4 has been implicated in the regulation of stemness and Wnt signalling (discussed in more detail in Chapter 1.4.2.1) and is reported to have minimal expression on most healthy adult tissues (Peter L Stern and Harrop 2017). Its upregulation across multiple solid tumours makes it an attractive target for cellular therapy, capable of reducing risk of on-target off-tumour side effects. The documentation of 5T4 expression on cancer stem cells (CSCs) increases its utility as a target (Harper et al. 2017) as these cells are associated with poor prognosis due to their ability to profilerate and promote metastasis (X. Chu et al. 2024). The role that 5T4 plays in disrupting Wnt signaling could be hypothesised to contribute to the altered metastatic potential of CSCs (Peter L Stern and Harrop 2017) although the exact mechanisms underpinning this should be investigated further.

There is evidence of 5T4 expression in PDAC (R. Wang et al. 2018), but data are limited to a small number of patients and does not include data regarding the

surface expression of 5T4 that is necessary for CAR-T cell engagement. Given that antigen internalisation and intra-tumoral heterogeneity frequently limit the efficacy of solid tumour CAR-T strategies, this investigation is crucial. Additionally, due to the scarcity of human samples, there is a lack of expression data for less common malignancies such as PNETs and ampullary cancers. Healthy pancreatic tissue samples are similarly scarce but act as an important control in determining the restriction of the antigen to cancerous cells alone.

3.1.2 CAR-T Cell Targets in PDAC

Alongside 5T4 there are many other CAR-T targets which have reached clinical trials for PDAC including mucin-1, mesothelin and prominin-1/CD133 (Akce et al. 2018). Given that there are no licenced adoptive cell therapies for PDAC, these existing candidates provide a useful comparison to evaluate the potential of 5T4 as a target. Existing clinical-stage CAR-T cell antigens were therefore incorporated into initial analyses of patient survival impact and antigen expression in human tissue and cell lines. This data provides information about the relative inter-patient heterogeneity and lack of expression in healthy tissue of the proteins, thus indicating their relative potential as clinical candidates.

Similarly to 5T4, mucin-1 (MUC1) is overexpressed in a range of epithelial tumours including breast and ovarian cancer (Uhlen et al. 2017). It is also known to increase the metastatic potential of malignant cells (Hull et al. 2020). Mucin-1 is also expressed on the apical surfaces of normal epithelial cells including breast, uterus and airway passages. Due to this lack of tumour specificity, those creating therapeutics have developed strategies to improve the selectivity of targeting. Multiple groups have developed constructs targeting the 'Tn glycoform' of the protein; first an HMFG2-derived scFv (Wilkie et al. 2008), then a 5E5 construct (Posey et al. 2016) and more recently a TAB004-based therapeutic (Yazdanifar et al. 2019). These constructs specifically target the aberrantly glycosylated isoform which is frequently found on mucin-1 in cancer, thus reducing the potential for healthy tissue toxicity (Wilkie et al. 2008; Posey et al. 2016; Yazdanifar et al. 2019). While these novel

strategies show promise, trials are yet to demonstrate clinical efficacy. Two trials of anti-mucin-1 CAR-T cells in pancreatic cancer are currently ongoing or have unknown status (NCT02587689, NCT04025216) while a third (NCT04025216) was terminated due to unfavourable risk/benefit analysis.

Mesothelin (MSLN) is a membrane protein known to be highly expressed in many solid cancers, with additional lower expression in other tissues such as the peritoneum, pericardium and pleural membrane (H. Jiang et al. 2017). Given the widespread low levels of expression risking on-target off-tumour side effects, June's group developed a strategy to transiently induce expression of anti-mesothelin CARs on autologous patient T cells using mRNA electroporation. The transient expression was hypothesised to reduce the likelihood of on-target off-tumour toxicities although no mechanistic explanation was given to support this claim. This strategy is one of two clinical trials with published results for anti-mesothelin CAR-T cell therapy in PDAC (NCT01897415), showing modest responses in two out of six patients (Beatty et al. 2018). The other study (NCT02159716) was conducted by a similar group showing good tolerance but 'limited clinical activity' (Haas et al. 2019).

Prominin-1 or CD133 is a widely expressed protein which is overexpressed in epithelial malignancies and is speculated to be a marker of CSCs although evidence is conflicting (Glumac and LeBeau 2018). Prominin-1 isoforms 1 and 2 are also present across healthy tissues and exist both at the plasma membrane and subcellularly (Röper, Corbeil and Huttner 2000). Much like 5T4, there have been reports implicating prominin-1 in downregulating canonical Wnt signalling and stem-like phenotype (Rappa et al. 2013). This effect is not limited to CSCs, as the marker is also present on prostate (Richardson et al. 2004), neural (Tamaki et al. 2002) and haematopoietic (A. H. Yin et al. 1997) stem cells. The only clinical trial (NCT02541370) targeting this antigen in metastatic solid tumours showed a good safety profile and a median progression-free survival (PFS) of five months. No further trials have been initiated.

3.1.3 Anti-5T4 CAR-T Cell Manufacturing Considerations

The initial selection of 5T4 as a candidate antigen by OXB stemmed from its relative restriction to tumour tissue and its role in stemness and metastasis. OXB have previously published their generation of two CAR-T constructs - H8 and 2E4 against human 5T4 protein, analysing pre-clinical CAR-T cell efficacy in ovarian cancer cell lines and mouse models. Both constructs were shown to be transduced effectively into human T cells without affecting proliferation or viability. The H8 epitope was demonstrated to have a higher binding affinity to 5T4 and elicit the strongest effector response *in vitro* compared to 2E4 (Owens et al. 2018), leading to the selection of this CAR construct for investigation in PDAC. The 'anti-5T4 CAR-T cells' referred to throughout this thesis contain the construct that targets the H8 epitope.

Anti-5T4 CAR-T cells are generated using both CD4 and CD8 T cells. This is clinically relevant as all currently approved therapeutics are manufactured from a mixture of T cells. Variations exist in methods of selection, with traditional manufacture using unfractionated PBMCs but the recently approved Lisocabtagene maraleucel (or liso-cell) instead using individual populations of selected CD4 and CD8 cells (Abramson et al. 2020). Use of both subsets in therapy is important for efficacy and has been shown to be mechanistically advantageous (Bove, Maher and Glover 2024).

The cytotoxic function of CD8 T cells is well-characterised but the role of CD4 T cells in cancer is less well understood beyond their capacity as 'helper cells'. Alongside cytokine release and DC licensing, CD4 T cell-mediated maintenance of CD8 effector function has been shown to involve direct receptor interactions including CD40L-CD40 and CD70-CD27 (S. Y. Lee et al. 2023). As well as supporting the cytotoxic role of CD8 T cells, there is evidence that CD4 T cells are able to kill tumour cells directly through release of perforin and granzyme (Liadi et al. 2015; Cachot et al. 2021). Following infusion, CD4 T cell help has been shown to be crucial for the longevity of CAR-T cell responses in leukaemia (Melenhorst et al. 2022). The cooperation of the two cell types is crucial from the earliest stages of CAR-T cell generation to establishing *in vivo* persistence and durable tumour control.

T cell subset selection has been found to be a particularly important factor in determining the duration of CAR-T cell responses (Wherry, Teichgräber et al. 2003). Many clinical trials in solid tumours require multiple CAR-T infusions and, even when initial tumour control is established, this frequently fails to persist when the T cells become exhausted. Although this effect is also seen in some haematological malignancies, it is much more common in solid tumours and is therefore hypothesised to be partially dictated by microenvironmental factors (Rodriguez-Garcia et al. 2020). To improve longevity, current manufacturing methods aim to select for greater T cell stemness over more differentiated effector cells (Gattinoni, Klebanoff and Restifo 2012). These stem-like subsets include CD45RA^{+} CD62L^{+} CD95^{+} T_{SCM} and CD45RA^{-} CD62L^{+} CD95^{+} T_{CM} subsets (Turtle et al. 2016). Base media, serum source and concentration and cytokine supplementation all play a role in this selection process (Colina et al. 2024) and have been optimised to balance advantageous T cell subset selection with efficient manufacturing.

3.1.4 Aims

This chapter aims to characterise the expression of 5T4 in human PDAC, other pancreatic lesions and healthy human pancreas. These investigations serve to establish the suitability of 5T4 as a target antigen in PDAC using a larger and more varied cohort than is available in current literature. Human PDAC tumours (alongside other pancreatic malignancies and healthy pancreatic tissue) were analysed initially using IHC to observe expression patterns of total protein across tissue and explore heterogeneity between patients. Flow cytometry of disaggregated PDAC tissue was then used to confirm cell surface expression of the 5T4 protein.

Cell lines were investigated for their total and surface 5T4 protein levels through Western blot and flow cytometry. This investigation was used to select 5T4^{hi}, 5T4^{lo} and 5T4^{-} cell lines for future *in vitro* efficacy testing. A murine model of PDAC was also investigated to understand the feasibility of potential *in vivo* experiments.

Anti-5T4 CAR-T cells were generated at OXB using previously developed protocols under the guidance of Mayowa Soyombo (TSG, OXB). The existing

protocols were adapted to suit rapid CAR-T cell generation for use in future assays using autologous patient-derived PBMCs. Expansion, transduction efficiency and T cell phenotyping was performed following CAR-T cell generation from PBMCs derived from multiple healthy donors.

3.2 Results

3.2.1 Prognostic Impact of Antigen Expression in PDAC Patients

While 5T4 expression across some cancers has been documented, its impact on tumour progression is not well characterised. As previously described, 5T4 is associated with CSCs and implicated in migration and stemness, but the impact of its expression on survival has yet to be explored.

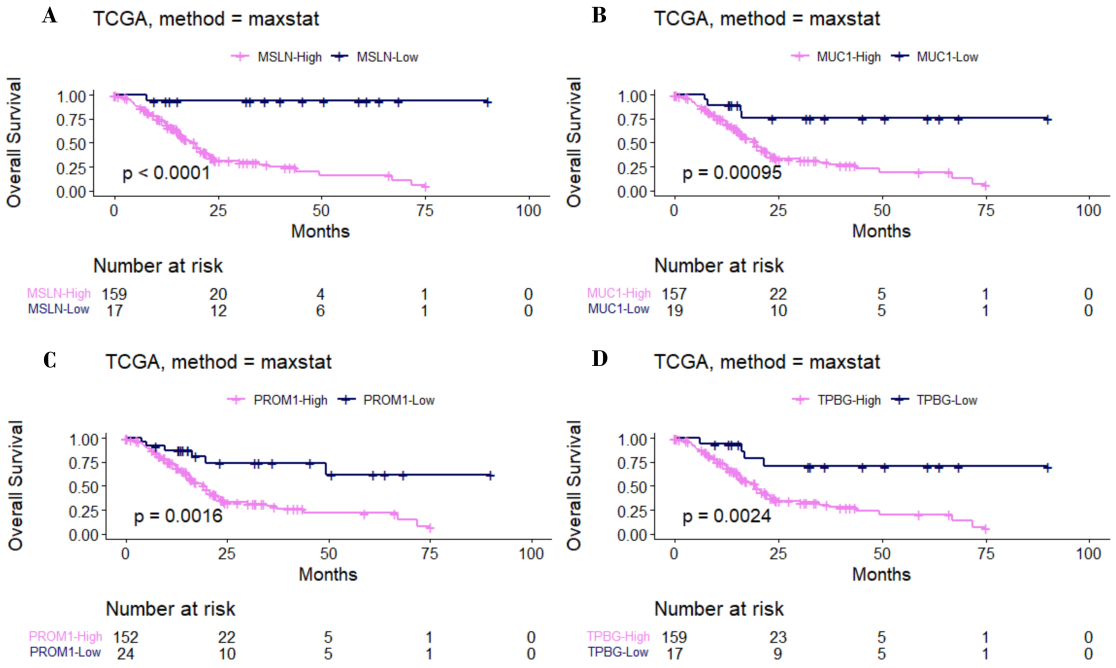


Figure 3.1: Survival curves for expression of CAR-T target antigens in PDAC patients. Expression data obtained from The Cancer Genome Atlas (TCGA) for (A) MSLN, (B) MUC1, (C) PROM1, and (D) TPBG (5T4) and segregated using the MAXSTAT function. 'Number at risk' details surviving patients in each cohort at the corresponding timepoints. Analysis was performed by Constantinos Demetriou.

To investigate this, genomic data was used from three independent cohorts; The Cancer Genome Atlas (TCGA), Clinical Proteomic Tumor Analysis Consortium

(CPTAC) and the Kidani cohort (sequenced in house). Expression level of 5T4 along with clinical stage CAR-T antigens mucin-1, mesothelin and prominin-1 was classified as 'high' or 'low' across patients with segregation performed using the MAXSTAT R package. This function determines an optimal cut-off point for selected continuous variables (CAR-antigen expression level) which corresponds to the most significant relationship with outcome (survival) (Hothorn 2001).

Overall survival was calculated for 'high-' (pink) and 'low-' (blue) expressing groups with a significant reduction in survival in the high expression groups of all four antigens using TCGA data (Figure 3.1). In the CPTAC cohort (Appendix A.1A.i-D.i) prominin-1 gene expression level was not found to significantly affect survival and in the Kidani cohort (Appendix A.1A.ii-D.ii) neither prominin-1 or mucin-1 expression significantly impacted patient survival. These factors can partly be linked to the relative sizes of the cohorts with n=176 for TCGA, n=135 for CPTAC and n=83 for Kidani. Despite differences between cohorts, the overall poor outcomes experienced by patients with high expression of the antigens provides initial validation that they are promising therapeutic targets.

3.2.2 Antigen Expression Across Patient Cohorts

Having determined that the high expression of the selected antigens impacts survival, their expression was validated in PDAC, other pancreatic malignancies and in healthy pancreas. IHC was used to observe the spatial distribution of 5T4, mucin-1, mesothelin and prominin-1 antigen expression. All antibodies were titrated prior to staining (Appendix A.2) to prevent excessive background staining.

The expression of 5T4, Mucin-1, Mesothelin and prominin-1 was interrogated across three PDAC patients and a healthy control pancreas (Figure 3.2A). 5T4 and mucin-1 displayed high expression across these patients (notably with different distributions) while prominin-1 showed more inter-patient variation and mesothelin was expressed at relatively low levels throughout. Mucin-1 and prominin-1 could both be seen in the healthy control which raises questions about their potential to cause on-target off-tumour effects.

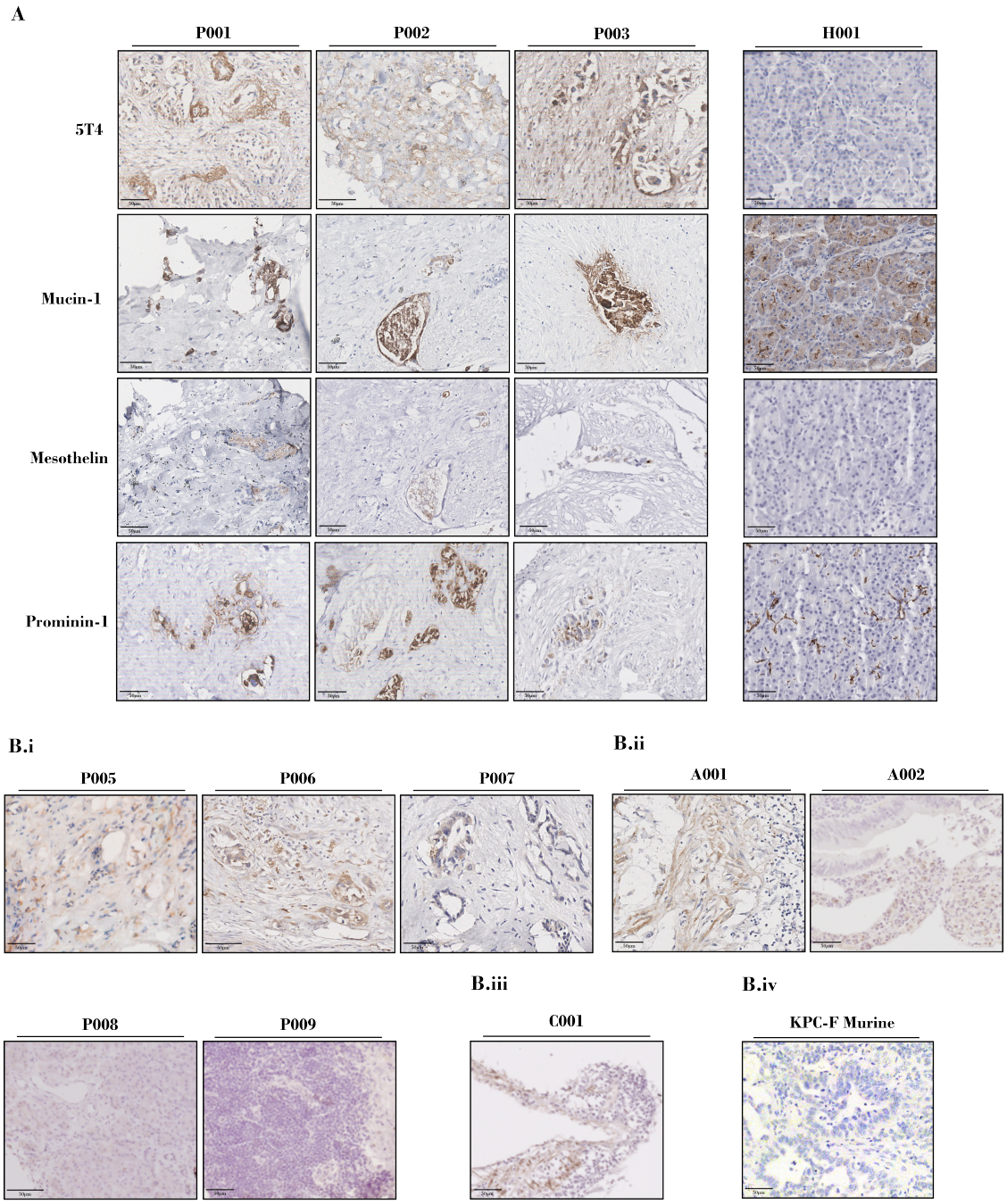


Figure 3.2: Patient tumour expression of clinical stage CAR-T cell target antigens and 5T4. (A) Immunohistochemistry showing expression of 5T4, mucin-1, mesothelin and prominin-1 in PDAC tumour slices. Slices were derived from three PDAC patients (P001-P003) and one healthy pancreatic sample (H001) from an acute pancreatectomy. (B) Extended panel of pancreatic lesions analysed for 5T4 expression including (B.i) PDAC (P005-P009), (B.ii) ampullary (A001-A002), and (B.iii) cholangiocarcinoma (C001) samples and (B.iv) KPC murine orthotopic tumours. IHC images were produced using the Aperio Brightfield Slide Scanner and the Leica Mica.

Additional profiling of 5T4 expression was carried out with a further five PDAC

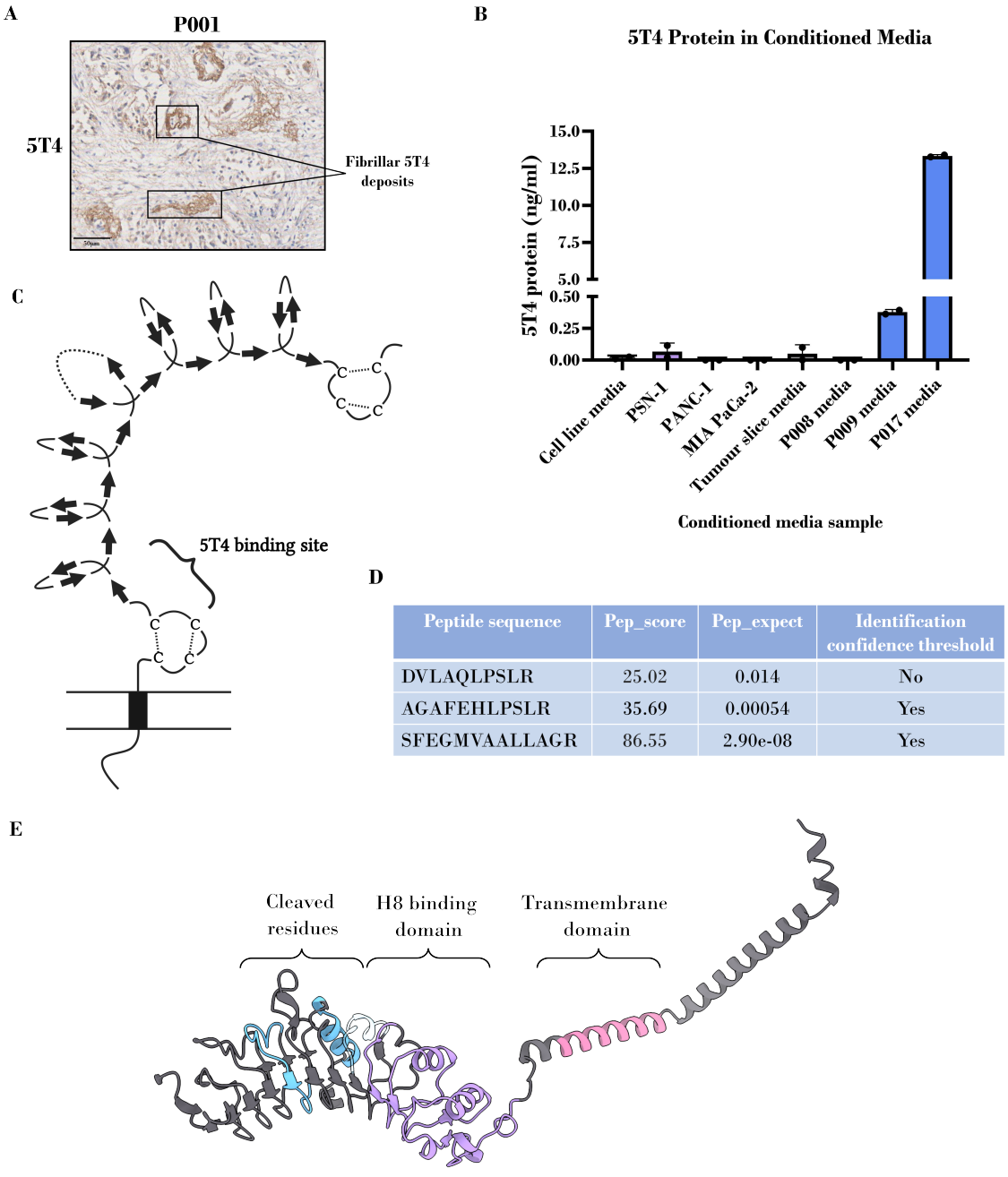
samples (Figure 3.2B.i), two ampullary cancers (Figure 3.2B.ii), a cholangiocarcinoma (Figure 3.2B.iii) and with a KPC-F murine tumour (Figure 3.2B.iv). High 5T4 expression was seen in P005 and P006 with reduced expression in P007-P009. Both the ampullary tumours and cholangiocarcinoma expressed 5T4 while the KPC-F murine tumour showed no antigen expression (despite both human and murine antibody reactivity).

KPC mice are genetically engineered using the Cre-Lox expression system (chapter 1.2.2) and develop spontaneous pancreatic tumours. Cells from KPC-F mice can subsequently be injected into immunocompetent, MHC-compatible mice, either subcutaneously or orthotopically, to study tumour progression in a more controlled timeframe than with the spontaneous tumour formation displayed by GEMMs. The tumour of an orthotopically injected mouse was initially profiled (Figure 3.2B.iv) to investigate the potential of using the model for future *in vivo* work; however, no 5T4 expression was seen. A recombinant KPC-F cell line altered to express 5T4 would need to be generated in order to facilitate these experiments.

3.2.3 Antigen Shedding and CAR Binding Site

IHC images of 5T4 staining demonstrated heterogeneous antigen distribution (Figure 3.3A). Discrete cellular staining was combined with large fibrillar bundles that did not appear to be cell associated (an observation replicated in later IF analysis). Both IF and IHC were conducted using polyclonal antibodies binding to multiple epitopes of the protein.

To investigate whether this expression pattern was due to a staining artefact or the shedding/cleavage of 5T4 antigen, an ELISA (polyclonal antibody) of the supernatants from tumour slice culture was performed (Figure 3.3B). Variable levels of 5T4 protein were observed from the slice media and no protein was seen in $5T4^+$ cell line supernatants or media controls. 5T4 shedding was particularly evident in the concentrated biopsy media sample generated from the continuous culture of an entire biopsy for 72 h. Although there was substantial variation between patient-derived slices, 5T4 was present in the media in some cases.



Peptide sequence	Pep_score	Pep_expect	Identification confidence threshold
DVLAQLPSLR	25.02	0.014	No
AGAFEHLPSLR	35.69	0.00054	Yes
SFEGMVAALLAGR	86.55	2.90e-08	Yes

Figure 3.3: Mapping the binding site of the anti-H8 5T4 CAR-T cells following evidence of 5T4 antigen shedding. (A) Immunohistochemistry (IHC) of 5T4 in patient tumour slice showing fibrillar deposit patterns. (B) ELISA for 5T4 conducted with cell line and tumour slice conditioned media. (C) Binding site of the H8 antibody epitope (adapted from (Shaw et al. 2002)). (D) Existing evidence of 5T4 peptide presence in lung cancer cell line matrix (data obtained from (Pankova et al. 2019)) with identified peptide sequences obtained by Dr Iolanda Vendrell. (E) AlphaFold structure of 5T4 edited by Alexander Hasson to display the transmembrane region (pink), total potential H8 binding region (purple) and peptides previously identified as matrix-associated acellular fragments (blue).

3. Characterisation of 5T4 Antigen Expression in PDAC and Anti-5T4 CAR-T Cell Generation

CAR-T cell efficacy would only be impacted by this unbound antigen if the binding site of the CAR lay within the cleaved regions. This would reduce the efficacy of the therapy as CAR-T cells would bind to soluble antigen and fail to engage with target cells. The anti-5T4 CAR-T cells utilise the H8 antibody epitope in their scFv - an epitope initially characterised by Peter Stern and colleagues (Shaw et al. 2002). A peptide structure for the binding site has not been elucidated, but Shaw et al. (2002) characterised the structural motifs present in the site through analysing antibody binding to various truncated forms of 5T4 protein. Figure 3.3C details the known binding region of H8 as described in Stern's original publication.

There is limited documentation in the literature of 5T4 being shed from the cell surface, particularly in the context of PDAC. Investigation into matrix-associated proteins by a previous lab member, Daniella Pankova, led to detection of 5T4 peptide sequences in a cell-free environment (Pankova et al. 2019). These sequences were detected in the extracellular matrix deposits isolated from H1299 lung cancer cells (Figure 3.3D). While the latter two sequences meet the threshold for confidence in origin identification, the third identified peptide falls below this threshold and therefore cannot be confidently assigned to be derived from 5T4. Although the peptides were not detected in PDAC, they provide a cancer-derived set of peptides associated with cleavage/shedding.

To determine whether the anti-5T4 CAR would bind to shed 5T4 peptides, each of the cleaved residues, the H8 binding site, and the transmembrane domains were mapped onto the experimentally validated AlphaFold V2 structure for 5T4 (Figure 3.3E). Mapping demonstrated that the previously identified matrix-associated peptides lie further from the transmembrane domain than the H8 binding site. This arrangement means that, based upon previously documented cleavage events, the efficacy of the H8 CAR would not be reduced by antigen shedding.

3.2.4 Antigen Surface Expression on Human Tumour Cells

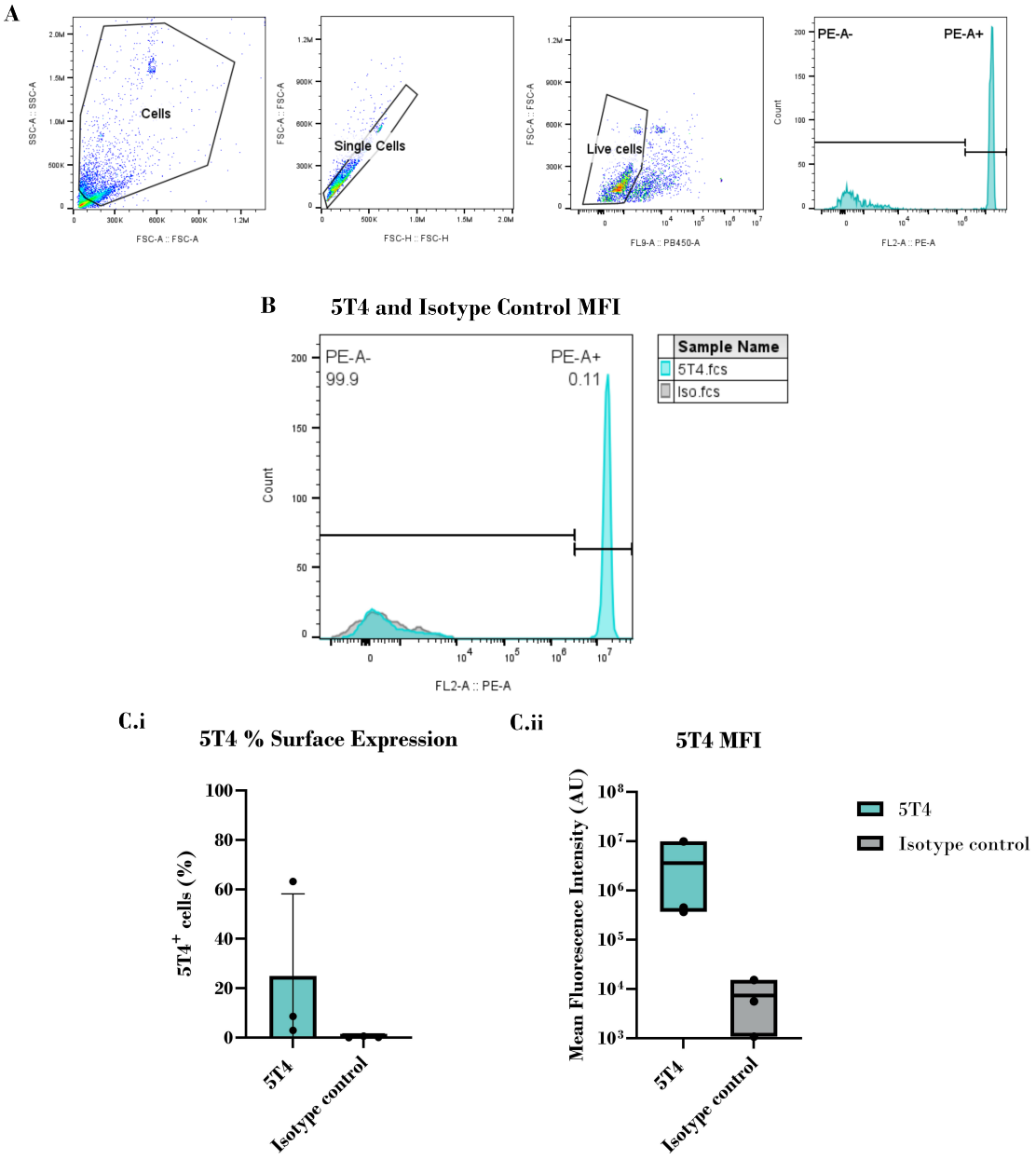


Figure 3.4: 5T4 (H8 epitope) surface expression on cells isolated from disaggregated tumour slices measured by flow cytometry. (A) Gating strategy showing selection of cells, single cells and live cells prior to 5T4 expression analysis. (B) Representative 5T4 (blue) and isotype control (grey) fluorescence intensity profiles for disaggregated tumour slice. (C.i) $5T4^+$ percentage of total cells and (C.ii) MFI analysed with paired t-test and Wilcoxon matched pairs signed rank test respectively ($ns = p > 0.05$). Independent PDAC tumours were used for n=3 biological replicates.

While IF demonstrated widespread expression of 5T4 antigen throughout the human tumour slices, flow cytometry was needed to confirm the surface expression of the protein and therefore its accessibility to CAR binding. Tumour biopsies were dissociated to create single cell suspensions containing both tumour cells and all other cells present in the TME. These cells were then stained for the H8 epitope of 5T4 or an isotype control and gated for viability (Figure 3.4A).

In each of the three patient tumours, a proportion of cells were highly positive for surface 5T4 (Figure 3.4B), along with a large $5T4^-$ population. This bimodal distribution captures the heterogeneity of cells present in the tumour slices; not all cell populations would be expected to express 5T4. There was substantial variation in the size of the $5T4^+$ fraction seen across tumour samples (Figure 3.4C.i) indicating that the proportion of $5T4^+$ cells in tumours can vary substantially between patients. These observations were mirrored in later autologous CAR-T cell experiments using IF to characterise 5T4 expression (see Chapter 5). Mean fluorescence intensity (MFI) was calculated for each tumour sample for 5T4 and isotype control (Figure 3.4C.ii).

3.2.5 Total 5T4 Protein Expression in Pancreatic Cell Lines

Analysing the efficacy of anti-5T4 CAR-T cells on live human tumour samples requires prior *in vitro* analysis using cell lines to generate suitable reference controls. The PSN-1, PANC-1 and MIA PaCa-2 cell lines were selected due to their extensive use in PDAC research. These cell lines were derived from the ductal cells isolated from primary PDAC tumours in the 1970s-1980s (Lieber et al. 1975; Yunis, Arimura and Russin 1977; Yamada et al. 1986). DEC hTERT is a normal pancreatic epithelial cell line immortalised through virally induced expression of human telomerase reverse transcriptase (hTERT). The cells are able to maintain their telomere ends, preventing them from entering replicative senescence. This line was generated in house and used throughout as a cell line proxy for normal pancreatic tissue.

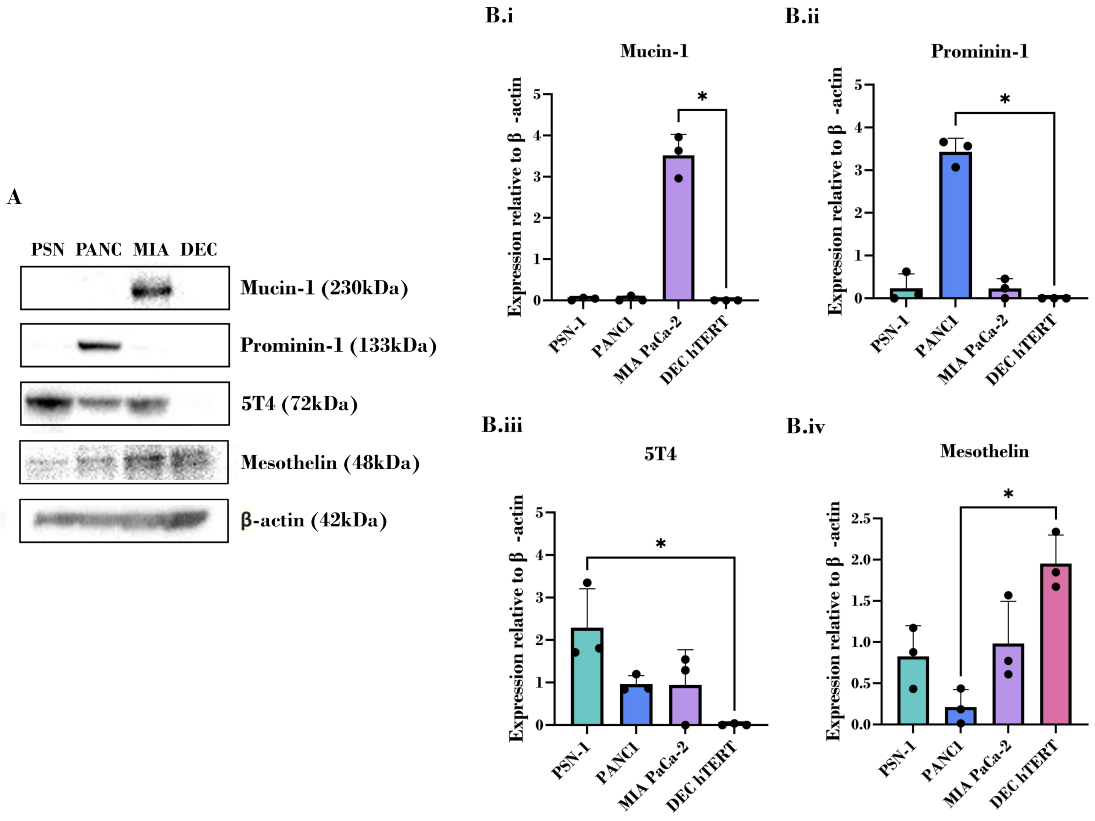


Figure 3.5: Cell line expression of PDAC clinical stage CAR-T cell target antigens. (A) Western blot for mucin-1, prominin-1, 5T4, mesothelin and β-actin (loading control) in PSN-1, PANC-1 and MIA PaCa-2 PDAC cell lines and the DEC hTERT normal pancreatic epithelial line. Representative blot image, band intensity quantified across three biological replicates for (B.i) mucin-1, (B.ii) prominin-1, (B.iii) 5T4, (B.iv) mesothelin, n=3 biological replicates using different cell line passages. The Kruskal-Wallis test with multiple comparisons was used to assess differences in expression between cell lines. $^{*}p < 0.05$.

Western blots for 5T4, mucin-1, mesothelin and prominin-1 total protein expression (Figure 3.5A) were quantified relative to the β-actin housekeeper protein (Figures 3.5B.i-iv). Only MIA PaCa-2 demonstrated significantly elevated mucin-1 expression while prominin-1 was only significantly expressed in PANC-1 cells. Mesothelin and 5T4 displayed more widespread expression across the cell lines. DEC hTERT displayed the highest mesothelin expression with modest trends towards increased expression in both PSN-1 and MIA PaCa-2. 5T4 was expressed to some degree in all PDAC cell lines but not DEC hTERT cells. PSN-1 protein levels were the highest relative to β-actin, with PANC-1 and MIA PaCa-2 both showing lower levels of protein expression.

3.2.6 Antigen Surface Expression in Cell Lines

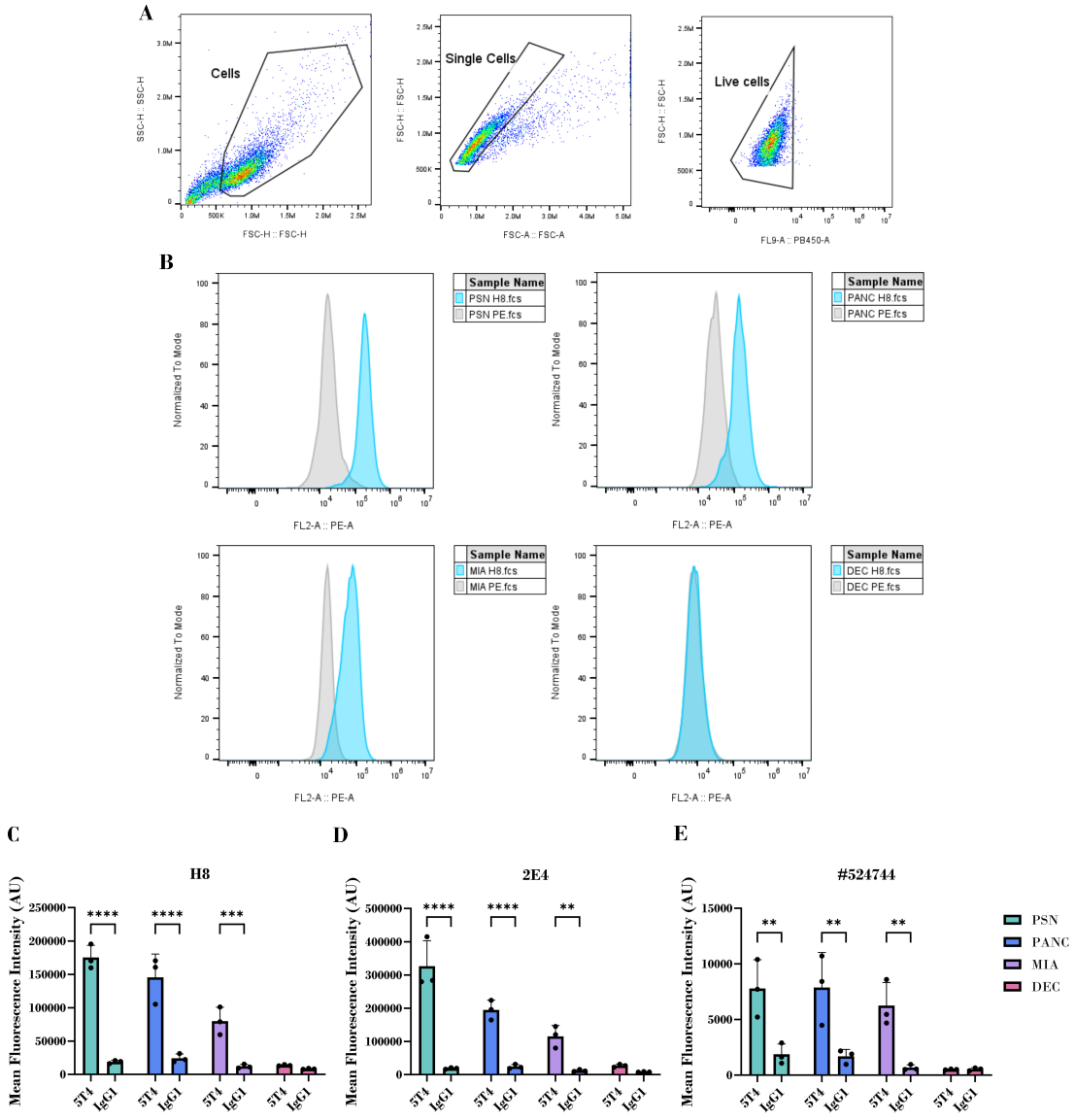


Figure 3.6: Surface expression of 5T4 on pancreatic cell lines. Flow cytometry was used to assess surface expression of 5T4 epitopes on PSN-1 (PSN), PANC-1 (PANC) and MIA PaCa-2 (MIA) PDAC cell lines and DEC hTERT (DEC) healthy pancreatic epithelial cells. (A) Gating strategy to select for cells, single cells and live cells. (B) Representative image of H8 epitope and isotype control MFI in all four cell lines. Quantification of MFI using (C) H8, (D) 2E4 and (E) #524744 epitopes. Statistical analysis using 2-way ANOVA and Šidák multiple comparisons test. $^{****}p < 0.0001$, $^{***}p < 0.001$, $^{**}p < 0.01$. n=3 biological replicates using cell line passages.

As with tumour slices, analysing surface expression of 5T4 on cell lines was necessary to predict CAR-T cell accessibility. Cell lines were profiled using alternative

antibodies 2E4 and 'ONC' alongside H8. 2E4 is the lower affinity alternative epitope tested by Oxford Biomedica in their original ovarian cancer CAR-T cell studies (Owens et al. 2018). ONC is a commercially available antibody derived from the #524744 antibody clone which was generated using an immunogen derived from the extracellular portion of the human 5T4 protein. All three antibodies were used at this stage to determine whether the H8 flow cytometry antibody would provide the superior signal-to-noise for future experiments. Each antibody was titrated prior to use (Appendix A.3) and dilutions were selected based upon separation indices.

Analysis of 5T4 expression was performed on gated live single cells (Figure 3.6A). Fluorescence profiles for the H8 antibody (blue) are shown (Figure 3.6B) for PSN-1, PANC-1, MIA PaCa-2 and DEC hTERT compared to isotype control (grey). The MFI was calculated for each antibody epitope (Figure 3.6C-E) allowing comparison between antibodies. Similarly to Western blot data, PSN-1 cells showed the highest 5T4 expression with PANC-1 and MIA PaCa-2 cells also showing signficant expression compared to the isotype control. DEC hTERT showed no signficant expression. The ONC antibody produced a lower MFI than H8 and 2E4 throughout assay replicates and did not demonstrate the elevated expression of the PSN-1 cells, unlike the other two epitopes. Based on these results, future experiments excluded the use of the ONC antibody.

3.2.7 Anti-5T4 CAR-T Cell Culture Condition Optimisation

TSG at Oxford Biomedica optimised a culture protocol for anti-5T4 (H8) CAR-T cells to maximise CAR-T cell expansion, $CD3^+$ cell selection and vector incorporation. Factors which had been previously optimised to increase viability and expansion include base media formulation (Figure 3.7A) and human serum concentration (Figure 3.7B). Results from these assays led to the selection of XVIVO TM 15 (referred to as XVIVO throughout) media and 2.5% human serum supplementation, which produced superior expansion to other conditions. This data was generated by members of TSG.

3. Characterisation of 5T4 Antigen Expression in PDAC and Anti-5T4 CAR-T Cell Generation

In the established protocol, PBMCs were used without prior selection for CD3 positivity. This method was selected due to a reduction in $CD3^+$ CAR^+ yield with prior CD3 negative selection because of handling-associated losses of $CD3^+$ cells in the process. Dynabead stimulation throughout the course of the 7-day generation process was sufficient to produce >95% CD3 positivity therefore negating the need for an initial selection step.

Given that *ex vivo* experiments rely on the collection of patient blood prior to surgical biopsy specimen collection, developing the shortest possible CAR-T cell generation protocol was desired. The protocol was therefore trialled without CD3 selection, harvesting on Day 4 and Day 7 and using flow cytometry to measure the CD3 positive fraction and transduction efficiency (Figure 3.7C-D). Although the proportion of $CD3^+$ transduced cells was largely unchanged between these conditions, Day 4 harvest yielded a substantially greater $CD3^-$ fraction than Day 7 harvest.

Given these results, the final 7-day protocol was decided as previously established by TSG (Figure 3.7E).

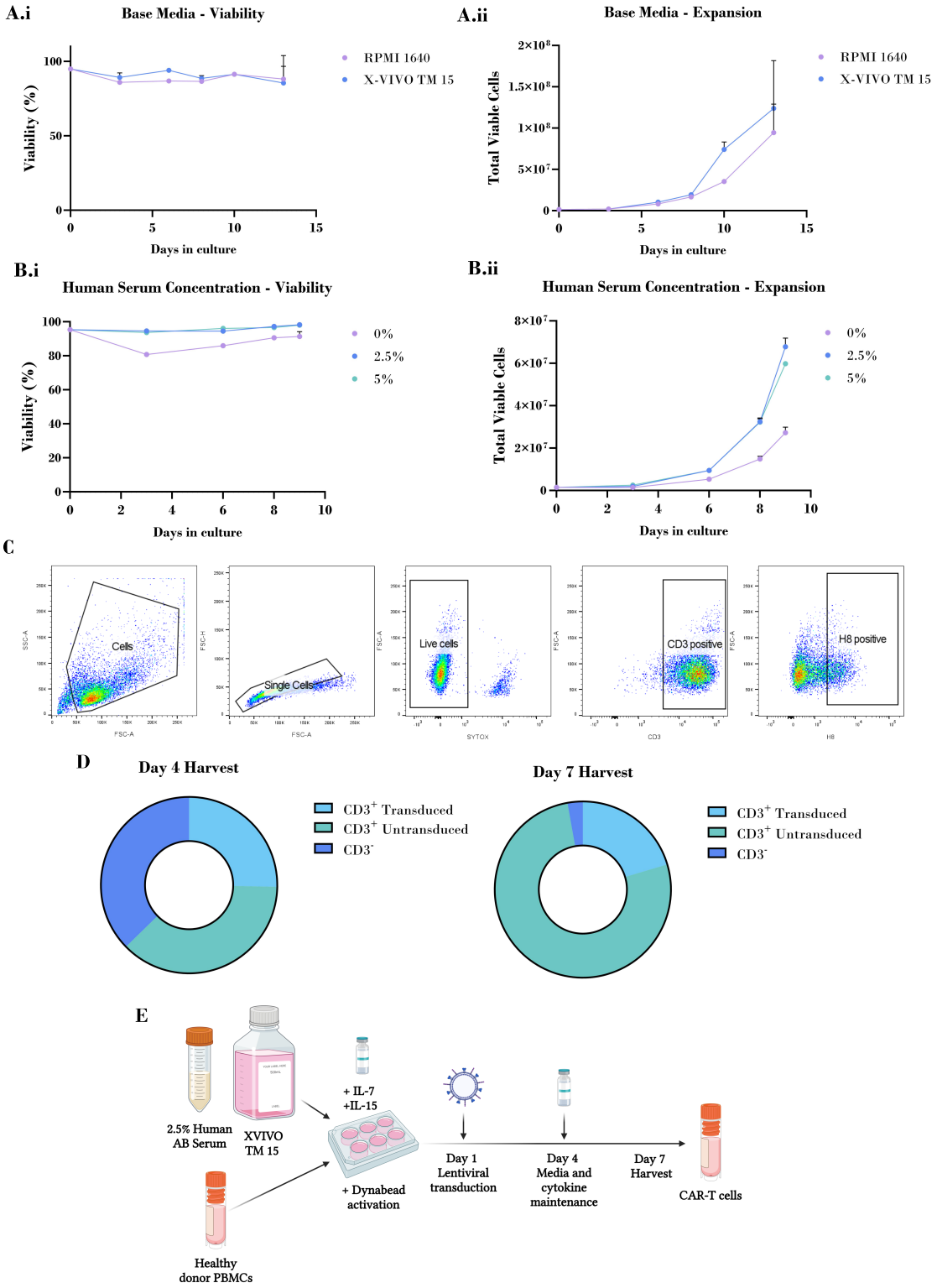
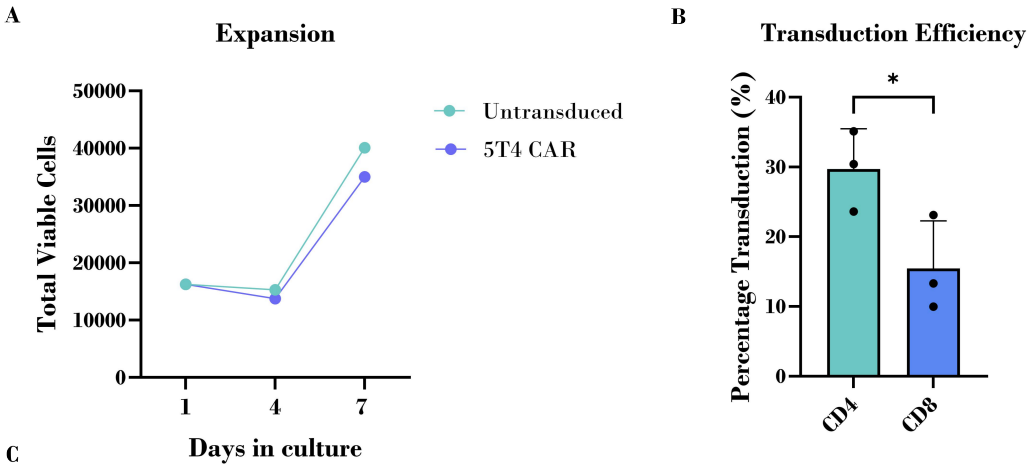


Figure 3.7: Protocol optimisation for CAR-T cell generation. Media formulation analysis comparing XVIVO TM 15 and RPMI 1640 for T cell (A.i) viability and (A.ii) expansion. Human AB serum concentration analysis for (B.i) T cell viability and (B.ii) expansion. Efficiency of $CD3^+$ selection and 5T4 CAR vector transduction with 4-day and 7-day protocols. (C) Flow cytometry gating strategy, (D) proportions of $CD3^+$ and transduced cells at the time of harvest. (E) Summary of optimal culture conditions for generation of 5T4 CAR-T cells. All parameters used n=1 biological replicate, media formulation with n=6 and Human AB Serum with n=2 technical replicates.

3.2.8 Anti-5T4 CAR-T Cell Generation, Transduction Efficiency, and Expansion

Multiple healthy donor PBMC samples were used to generate CAR-T cells according to the optimised protocol. The previously discussed variation in CAR-T cell products seen between donors demonstrates the importance of using multiple donors whenever possible.



C

Sample	Mean Copies		Cells/Reaction (Mean RPPH1/2)	VCN (Mean HIV/cells)
	RPPH1	HIV		
UTC1	11944	0	5971.87	0
UTC2	21816	0	10908.15	0
UTC3	9191	0	4595.51	0
TDN1	52638	28787	26319.23	1.094
TDN2	13773	7879	6886.58	1.144
TDN3	15818	8571	7909.19	1.084
			Mean VCN	1.107

Figure 3.8: Transduction efficiency and expansion of CAR-T cells during 7-day generation. (A) Expansion of live CAR-T and UTC cell populations throughout duration of CAR-T cell generation. (B) Transduction efficiency of T cell subsets assessed by flow cytometry and (C) vector incorporation assessed by PCR. For PCR and flow cytometry analysis, n=3 biological replicates, for expansion n=1 biological replicate. Transduction efficiency was analysed using a paired two-tailed t-test, $^{*}p < 0.05$.

The expansion (Figure 3.8A) of CAR-T and UTC cells was assessed using cell counts, transduction efficiency (Figure 3.8B) using flow cytometry and vector copy

number (VCN) (Figure 3.8C) using PCR. Cell counts were taken on day 1, day 4 and day 7 of culture, while flow cytometry and PCR were carried out on day 7 after harvest. Over 7 days of culture, both UTC and CAR-T cells expanded more than two-fold with little difference in final cell count. Transduction efficiency was significantly higher for CD4 cells than CD8 cells. This data is in line with previous findings from OXB showing that in healthy donor-derived PBMCs, CD4 cells were more efficiently transduced than CD8 cells, while in patient blood, transduction efficiency was higher in CD8 cells than CD4 cells (Owens et al. 2018).

VCN was calculated for both CAR-T and UTC cells to ensure that there was no contamination in the UTC condition. The Ribonuclease P RNA Component H1 (RPPH1) gene was used to calculate the number of cells per reaction as 2 copies are present in each cell. This cell number was then used to calculate the VCN/cell. VCN was consistent between CAR-T replicates and no copies of HIV were detected in UTC cells, indicating that there was no contamination between CAR-T and UTC cells. This confirmed that the lentiviral vector and transduction process developed by OXB was reliable and that none of the culture conditions led to contamination of the products.

3.2.9 CAR-T Cell Phenotyping

Due to the importance of T cell stemness in producing durable CAR-T cell responses, subset polarisation induced by CAR-T cell generation was analysed. The protocol used supplementation of CAR-T cell media with IL-7 and IL-15 rather than conventional IL-2. This combination has been shown to increase T_{SCM} proportions as well as stimulating proliferation and producing greater release of IL-2 by CAR-T cells *in vitro* (Amatya et al. 2024).

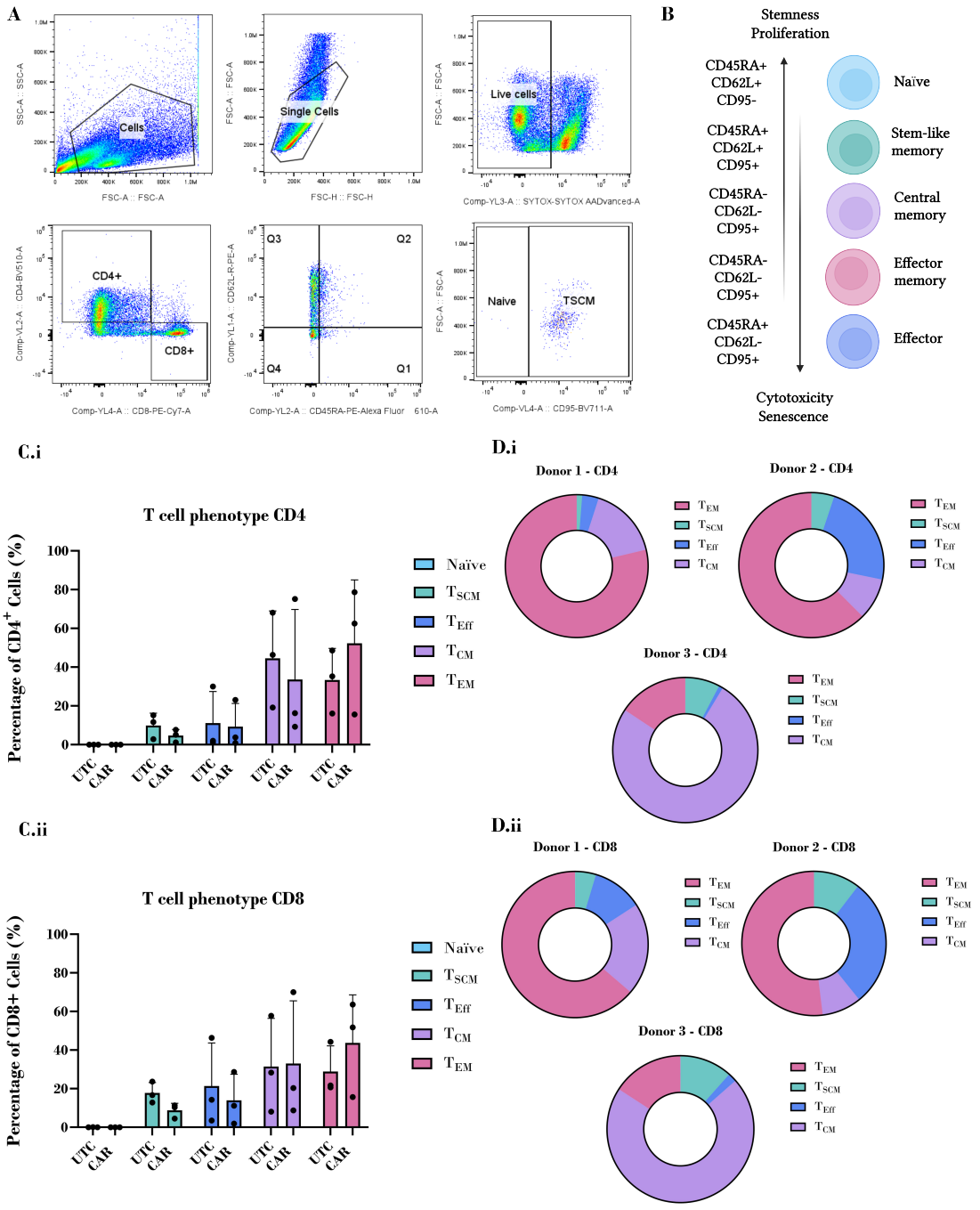


Figure 3.9: Phenotyping of T cell subsets produced in CAR-T cell generation from healthy donor PBMCs assessed using flow cytometry. (A) Gating strategy and (B) T cell subset classification, identifying markers and corresponding properties. Overall proportions of T cell subsets in CAR transduced (CAR) and untransduced (UTC) controls across three donors for (C.i) CD4 and (C.ii) CD8 T cells. 2-way ANOVA with multiple comparisons was used in analysis. Individual distribution of T cell subsets in transduced donor CAR-T populations for (D.i) CD4 and (D.ii) CD8 T cells. Phenotyping was carried out with n=3 biological replicates.

3. Characterisation of 5T4 Antigen Expression in PDAC and Anti-5T4 CAR-T Cell Generation

T cell subsets were defined by surface markers CD45RA, CD62L and CD95 (Figure 3.9B) and gated accordingly (Figure 3.9A). Overall, the T_{EM} subset was the most dominant in both CD4 (Figure 3.9C.i) and CD8 subsets (Figure 3.9C.ii) of CAR-T cell culture with high levels of T_{CM} in addition. In CD8 UTC cells from the same donors there was a trend towards fewer T_{EM} and higher levels of T_{CM} cells. In CD4 UTC cells there was a similar trend towards reduction in T_{EM} cells, but this was largely due to an increase in T_{eff} cells. Due to the variation between donors these overall differences were not statistically significant.

Individual proportions of each subset within CD4 (Figure 3.9D.i) and CD8 (Figure 3.9D.ii) populations were characterised for the CAR-T cells generated from three healthy donors, demonstrating the heterogeneity in CAR-T cell products that exists due to pre-existing donor variation. While Donors 1 and 2 had T_{EM} dominance, Donor 3 had higher T_{CM} with almost no T_{eff} cells. Subset predominance was largely consistent for each donor between the CD4 and CD8 fractions with greater T_{eff} fractions seen in CD4 cells of Donors 1 and 2.

These results indicate that the current culture methods cannot standardise individual donor differences and could be further optimised to produce greater T_{SCM} fractions across donors.

3.3 Discussion

5T4 was established as a rational CAR-T cell target for use in PDAC. H8 was demonstrated to be a useful epitope for targeting due to its proximity to the transmembrane domain of the protein. Along with validating expression in primary human samples, cell lines were identified expressing high and low levels of 5T4 and negative controls were established for *in vitro* experiments. Finally, it was demonstrated that anti-5T4 CAR-T cells could be reliably generated from patient blood in 7 days. These findings indicated that the anti-5T4 CAR-T cell product could be analysed for *in vitro* and *ex vivo* efficacy.

The negative impact of high levels of 5T4 along with mucin-1, prominin-1 and mesothelin on patient survival provided a rationale for targeting cells displaying

those markers. The correlation with worse survival does not necessarily implicate these proteins in carcinogenesis but does indicate that eradication of the cells expressing them may lead to increased survival. This is supported by existing literature detailing the association of 5T4 and prominin-1 with CSCs and the roles of 5T4 and mucin-1 in increasing cancer cell migration and thus metastatic potential.

A further rationale for targeting the 5T4 antigen came from its expression across the majority of PDAC patient samples and lack of expression in healthy pancreas. Further investigation is needed to determine whether any other healthy tissues express 5T4 as the Human Protein Atlas reports expression across a wide variety of healthy tissues as well as across malignancies. The lack of 5T4 expression in the healthy pancreatic sample as well as in the immortalised healthy pancreatic cell line indicate that local toxicity is unlikely but this should be repeated with more patients. Provided that expression in other tissues is sufficiently lower than in PDAC, improving CAR sensitivity or use of loco-regional delivery could reduce the risk of on-target off-tumour effects.

The expression of mucin-1 and prominin-1 in the healthy pancreas is supported by existing literature documenting widespread expression across both healthy and malignant tissues (Tabu et al. 2013; Nath and P. Mukherjee 2014; Holmberg Olausson et al. 2014). As discussed in this chapter's introduction, June and Maher's groups have previously demonstrated that isoform-specific targeting of mucin-1 can fine-tune responses to target only cancer-associated antigen variants. Alongside local administration and antigen density discrimination, isoform selectivity provides an additional mechanism to limit CAR-T cell responses to tumour cells.

The variability in proportions of tumour cells expressing 5T4 seen in Figures 3.2 and 3.4 requires further investigation. If antigen expression is insufficient within the tumour this would limit the ability of CAR-T cells to induce substantial killing. In contrast to the safety concerns associated with healthy tissue protein expression, heterogeneity of antigen expression in tumours provides logistical challenges in terms of patient selection and raises questions about the viability of both clinical trial and treatment production. The NCI estimated that as of 2022, 25% of cancer

clinical trials failed to enrol enough patients. Particularly in a relatively rare cancer such as PDAC, further stratifying patients may lead to insufficient recruitment and trial failure. This was the case with Rosenberg's anti-mesothelin CAR-T trial which recruited just 15 eligible patients over its 6-year duration (Castelletti et al. 2021).

Having seen that the patterns of expression varied between patients, the possibility of protein shedding was investigated. Shedding is a well-characterised process associated with normal physiological functions such as growth factor and cytokine release (Shirakabe et al. 2017). These cleavage events are mediated by enzymes known as 'sheddases' which are subdivided further into families including a disintegrin and metalloproteinase (ADAM), beta-site amyloid precursor protein (APP) cleaving enzyme 1 (BACE) and matrix metalloproteinases (MMP) (Hayashida et al. 2010). Two of the most common sheddases; ADAM10 and ADAM17 are expressed widely and frequently overexpressed in cancers (Saftig and Reiss 2011). This is advantageous as it allows aberrant cleavage of oncogenic substrates and can cause drug resistance.

A recent study used sheddase knockdowns to investigate mesothelin cleavage, finding that ADAM10, ADAM17, BACE1, BACE2 and MMP15 were all implicated (Xiufen Liu et al. 2020). Despite the prevalence of these cleavage events, shedding is not frequently discussed in CAR-T cell literature. Xiufen Liu et al. (2020) advocate for the use of sheddase inhibitors to sensitise cells to mesothelin targeting therapeutic strategies. Inhibitors such as Lanabecestat could be incorporated into treatment regimens to inhibit BACE activity. The drug has previously been used in Alzheimer's clinical trials (NCT02245737 and NCT02783573) and is well tolerated (Wessels et al. 2020).

Inhibiting 5T4 cleavage is only necessary if the therapeutic binds to the protein downstream of the cleavage sites. Xiufen Liu et al. (2020) mapped cleavage sites using mass spectrometry of fragments isolated from pulldown using cell supernatants, similar to the mass spectrometry Dr Pankova carried out using decellularised matrix deposits from the H1299 cell line. Given the limited frequency of tumour samples and small volumes obtained from media conditioning, data could not be obtained

about the specific amino acid sequences of 5T4 shed in the PDAC samples. This data should be collected if additional samples were available to further validate the suitability of the H8 binding site. The current sequences cannot be guaranteed to be relevant to PDAC due to the difference in sheddase expression documented between cancers and between cell lines derived from the same cancer (Arai et al. 2023). Despite this, the data demonstrates a need for sheddase activity to be considered during the design of therapeutic antibodies targeting membrane proteins.

Cell line selection was needed for initial *in vitro* validation to establish basic CAR-T functionality prior to investigation of the therapy in a more physiologically relevant setting. Analysis of expression from total and surface protein allowed comprehensive comparison between cell lines and established DEC hTERT as negative for the marker. Given that the surface protein levels relate most directly to interactions with CAR-T cells, classifications of antigenicity were based primarily on flow cytometry data. This led to the classification of cell lines with PSN-1 - $5T4^{hi}$, PANC-1 - $5T4^{mid}$, MIA PaCa-2 - $5T4^{lo}$ and DEC hTERT - $5T4^{-}$. This segmentation facilitated efficacy evaluation for varying degrees of target expression prior to testing on heterogeneous patient samples.

To generate CAR-T cells for testing in PDAC, the protocol needed to be adapted and verified for use with patient PBMCs isolated from whole blood prior to Whipple surgery and tumour sample collection. The PBMC layer isolated from whole blood using Ficoll contains T cells, B cells, NK cells and monocytes, all of which are mononuclear. From this pool, T cells are usually selected through magnetic bead-based sorting (Agarwal et al. 2023) but can also be enriched through Dynabead stimulation alone (Abraham-Miranda et al. 2022). While MACS is widely documented to produce high purity and viability (Weiss et al. 2021), TSG found that the process involves a loss of $CD3^{+}$ cells. Using Dynabeads alone prevented this loss, but required a 7 day stimulation to produce sufficient $CD3^{+}$ selection, thus preventing product contamination. This timeframe was incorporated into the *ex vivo* workflow with blood sampling occurring at least 7 days prior to tumour sampling for autologous patient CAR-T testing.

3. Characterisation of 5T4 Antigen Expression in PDAC and Anti-5T4 CAR-T Cell Generation

Alongside CD3 percentage, transduction efficiency is important for ensuring therapeutic efficacy. The efficiency of lentiviral transduction is dictated by the properties of the virus, vector, target cells, culture conditions, and the multiplicity of infection (MOI) at which the virus is administered to the cells. An MOI of two was determined to be optimal by TSG, balancing the cost of vector production and need for a low VCN with a high transduction efficiency. This balance is needed as the FDA recommends a VCN of <5 copies per genome to prevent elevated risk of oncogenesis (A. Chen, Velickovic and Rasko 2020). Incorporating a FACS sorting step into the process would facilitate selection of a pure population of transduced cells however this was not logistically possible. Selection for transduced cells alone is generally not included in CAR-T manufacturing and clinical trial protocols (N. Ahmed et al. 2015; X. Wang and Rivière 2016; Amatya et al. 2024) and therefore the unsorted product generated in these protocols does not differ from current clinical CAR-T products.

Finally, CAR-T cell phenotype was investigated due to the aforementioned link between central memory subsets (T_{SCM} and T_{CM}) and durable tumour control. The established protocol using 10 ng/ml IL-7 and IL-15 led to a variable selection of T_{EM} and T_{CM} subsets with a smaller pool of T_{SCM} cells seen across healthy donors. Variation between donors has been previously documented (Joedicke et al. 2022) and has been shown to affect patient outcomes in CLL. CR was correlated with elevated $CD27^{+}CD45RO^{-}$ (T_{SCM}) frequency and memory related gene expression profiles, including IL-6/STAT3 signatures (Fraietta et al. 2018). There have been multiple strategies suggested for improving the consistency of CAR-T cell batches, such as stimulating with only CD3 antibodies rather than the CD3 and CD28 combination present on Dynabeads (Kranz et al. 2022). Other approaches include metabolic manipulation via the S-2HG metabolite, which is endogenously upregulated upon TCR activation and has been linked to TET2-mediated CAR-T memory formation (Foskolou et al. 2020). Use of 4-1BB as a costimulatory domain as opposed to CD28 (used in the anti-5T4 CAR construct) has also been documented to increase CAR-T cell functionality and specifically enhance proportions of central memory T cells (Roselli et al. 2021; G. J. Chu et al. 2023).

3.3.1 Conclusion

In this chapter 5T4 was shown to be a relevant target for CAR-T cell therapy in PDAC and preclinical models were selected to test *in vitro* efficacy. Peptide mapping indicated that the H8 epitope present in the anti-5T4 CAR construct is ideally situated to limit the risk of binding to shed antigen and limiting efficacy. Evaluation of the TSG protocol for anti-5T4 CAR-T cell generation and confirmed its suitability for future autologous patient CAR-T generation and functional analysis.

"Do something. If it works, do more of it. If it doesn't, do something else"

Franklin Roosevelt

4

In Vitro Efficacy of Anti-5T4 CAR-T Cells

4.1 Introduction

4.1.1 In Vitro Cytotoxicity Assays

In vitro cytotoxicity assays are necessary to determine the efficacy of cellular therapies such as CAR-T cell therapy. These assays are generally conducted using cell lines expressing the antigen of interest and facilitate investigation of parameters including the necessary effector:target ratio, the timeframe of response and the cytokine levels associated with response. The most common assays include chromium release, luciferase-based assays, impedance, and flow cytometry (Kiesgen et al. 2021).

Chromium release was first described by Brunner et al. (1968) and uses radioactive chromium released into media upon target cell death (Brunner et al. 1968). The assay requires a radiation licence and the ability to safely store and dispose of radioisotopes and thus is not widely used anymore. The luciferase assay involves transduction of target cells with the luciferase transgene which is only expressed in live cells (Karimi et al. 2014). While this method is higher throughput and more easily automated than chromium release, it requires stable transduction of target cells with the luciferase transgene (Kiesgen et al. 2021) and is therefore not convenient for screening multiple cell lines.

Impedance-based approaches do not require any labelling, instead using the adhesion of target cells to the bottom of the plate to generate electrical impedance. As the target cells are killed, they lift off the plate and thus the impedance drops (Xi et al. 2019). This parameter can be measured throughout the duration of the experiment and assays are not limited by the half-life of the reporter so can be continued over the course of several days (Peper et al. 2014). Finally, flow cytometry allows measurement of cell death using staining with viability dyes. Effector cells can be differentiated from target cells through prior staining of either population with an additional tracker dye (Jedema et al. 2004; Q. Jin et al. 2018). This method provides versatility in study design through incorporation of additional antibodies but is limited to a single time point (Kiesgen et al. 2021).

4.1.2 Cytokines Associated with CAR-T Cell Cytotoxicity

Alongside analysis of cytotoxicity, measuring the cytokines released by CAR-T cells during killing can provide valuable insights. IFNγ is a potent proinflammatory signal which facilitates the induction of tumour cell apoptosis through both direct signalling via caspase activation (Y. Zhou et al. 2008) and reactive oxygen species (ROS) production (Rakshit et al. 2014), and indirect upregulation of Fas/Fas ligand (X. Xu et al. 1998) and TRAIL/DR5 (Shin et al. 2001). The cytokine has potent anti-tumour effects through induction of Th1 polarisation, stimulation of cytotoxic T cell activity and inhibition of T regulatory cells (Tregs) (Jorgovanovic et al. 2020). The immunomodulatory effects of the cytokine also include MHC upregulation and the facilitation of antigen spreading (Qdaisat et al. 2025; Yelei Guo et al. 2023). Despite this, there is also evidence of IFNγ inducing programmed cell death ligand 1 (PD-L1) and indoleamine-pyrrole 2,3-dioxygenase (IDO) expression on tumour tissue, limiting antitumour immunity (Abiko et al. 2015). Notably, IFNγ has been reported to be more important in CAR-T cell cytotoxicity in solid tumours than in $CD19^+$ liquid tumours (Larson et al. 2021; Bailey et al. 2022). The group demonstrated that in solid tumours, including ovarian and pancreatic cancers, knocking out the IFNγR led to resistance to CAR-T cell killing while the same resistance was not observed

in leukaemia, lymphoma or multiple myeloma. This resistance was attributed to the lack of ICAM-1 upregulation in the absence of IFNγR signalling preventing sufficient T cell adhesion to allow cytotoxicity (Larson et al. 2021).

Granzyme B is a member of the serine protease family of granzymes (Cigalotto and Martinvalet 2024) which are key to T cell cytotoxicity in both cancer and infection (Hay and Slansky 2022). While some CD8 T cells express both granzymes A and B at rest, stimulation of T cells induces substantial expression of granzyme B alone in both CD4 and CD8 T cells (Grossman et al. 2004). Both Granzymes and perforin are stored and trafficked in cytotoxic granules in order to protect the T cell from degradation. Upon T cell activation, the granules are released at the immunological synapse and induce cell death in the target cell (Bossi and Griffiths 2005). While cytotoxic granule release was previously attributed solely to CD8 T cells, increasing evidence has shown that CD4 T cells can directly kill tumour cells via this mechanism provided that the tumours express MHC class II (Haabeth et al. 2014). This pathway is the major axis mediating direct killing of target cells by CAR-T cells (Benmebarek et al. 2019) with additional mechanisms including cytokine-mediated sensitisation of other immune cells and Fas-FasL interactions.

IL-2 is a polyfunctional cytokine which was first identified due to its role in driving expansion of activated T cell populations. Alongside proliferation induction, IL-2 has been shown to be vital for Treg production as well as subset determination of both CD4 and CD8 T cells (Shouse, LaPorte and Malek 2024). IL-2 is predominantly produced by CD4 T cells but signals via high affinity receptors which are present on all activated T cells (Robb, Munck and K. A. Smith 1981) along with other immune cell populations. While IL-2 is commonly used for the *ex vivo* expansion of CAR-T cells, it is also important for persistence *in vivo*. CD8 T cell memory and effector functions are influenced by levels of IL-2 signalling and CD4 T cells are driven towards T helper (Th)1, Th2, Th9 and Treg states (Spolski, P. Li and Leonard 2018). Given the multifaceted role of IL-2 in antitumour immunity, a wide range of therapeutic agents are being used to modify signalling in clinical trials (Levin et al. 2012; Sockolosky et al. 2018).

TNFα is another cytokine which plays a complex role in cancer immunity being both pro- and anti-inflammatory. It is primarily produced by activated macrophages, T and NK cells and acts through the low affinity TNFR-1 and high affinity TNFR-2. The latter receptor is expressed primarily on immune cells and lacks the death domain that is present in the TNFR-1 (Aggarwal 2003). The role of TNFα in cancer is varied as it can both contribute to carcinogenesis, EMT and treatment resistance (Cruceriu et al. 2020; Mercogliano et al. 2020; Gong et al. 2021) and has been used to treat cancers, although with limited success due to toxicity profiles and lack of clinical efficacy (Roberts et al. 2011). T cells are able to both produce and respond to TNFα through the TNFR2 receptor. TNFα binding has been shown to enhance TCR-dependent activation (Aspalter, Eibl and Wolf 2003) and augment IL-2R expression to enhance proliferation (Scheurich et al. 1987). Long-term effects include aiding memory cell formation and divergent roles either reducing Treg suppressive capacity (Valencia et al. 2006) or enhancing proliferation (Govindaraj et al. 2013).

Elevated levels of the aforementioned cytokines can indicate effective T cell activation and cytotoxicity but high levels can also be indicative of an uncontrolled immune response. This widespread activation can lead to toxicities such as CRS and ICANS (discussed in Chapter 1.3.3.3).

IL-6 is both a key marker of uncontrolled immune activation in CRS but is also produced by cells in the TME. In PDAC, pancreatic stellate cells (PSCs), inflammatory cancer-associated fibroblasts (iCAFs) and tumour cells are all able to synthesise IL-6, contributing to the maintenance of the desmoplastic stroma, angiogenesis, metastasis and cancer progression (Öhlund et al. 2017; Fu et al. 2018; Duijneveldt, Griffin and Putoczki 2020). High levels of IL-6 are reported during and even preceding tumorigenesis (Duijneveldt, Griffin and Putoczki 2020), contributing to the chronic inflammation which facilitates the development of tumours (Taher, Davies and Maher 2018). Despite the pro-tumorigenic role of IL-6, the cytokine also has a profound effect on anti-tumour immunity through the induction of T cell expansion under inflammatory conditions (B. Li, Jones and Geiger 2018). The

positive effect of IL-6 can also be seen clinically by the upregulation of IL-6/STAT3 signatures seen in the CAR-T cells and high serum IL-6 of CLL patients who respond well to therapy (Fraietta et al. 2018). While IL-6 is widely documented to have a proliferative effect on T cells, there is also evidence of induction of exhaustion in chronic settings. In patients with chronic cytomegalovirus (CMV) infections, high IL-6 was detected in serum and IL-6R blockade led to a 5-fold increase in CMV-specific T cells (T. Kato et al. 2011). Investigation is needed to understand the context-specific release and effect of IL-6 and its potential impact on CAR-T cell function both *in vitro* and *ex vivo*.

4.1.3 Aims

This chapter aims to characterise the *in vitro* efficacy of anti-5T4 CAR-T cells using both cell lines previously validated by OXB and pancreatic cell lines evaluated for their expression of 5T4 in the previous chapter. This characterisation employed the use of flow cytometric assays to analyse antigen density on target cell populations and impedance-based assays to measure the dynamics of the response.

In combination with measurements of cytotoxicity, media from each assay was collected for cytokine analysis. This was used to assess cytokine profiles of both CAR-T and UTC cells as well as cytokine release by cancer cells in response to CAR-T cell killing.

4.2 Results

4.2.1 Selective Cytotoxicity of Anti-5T4 CAR-T Cells with OXB-Validated Cell Lines Using Flow Cytometry

Prior to testing the 5T4 CAR-T cells against pancreatic cell lines, the efficacy of the cells was evaluated against a panel of cell lines used at OXB. AML-193 and Kasumi-1 are both suspension cell lines derived from acute myeloid leukaemia (AML) samples. These cell lines were evaluated in relation to the previous work at OXB testing the 5T4-CAR in AML (Harrop, Blount et al. 2024). In previous assays the AML-193 cells were determined to be 5T4 negative while Kasumi-1 cells

were $5T4^{lo}$. SKOV-3 cells were incorporated as a known $5T4^{hi}$ line to assess the ability of the CAR-T cells to kill target cells with varying antigen densities.

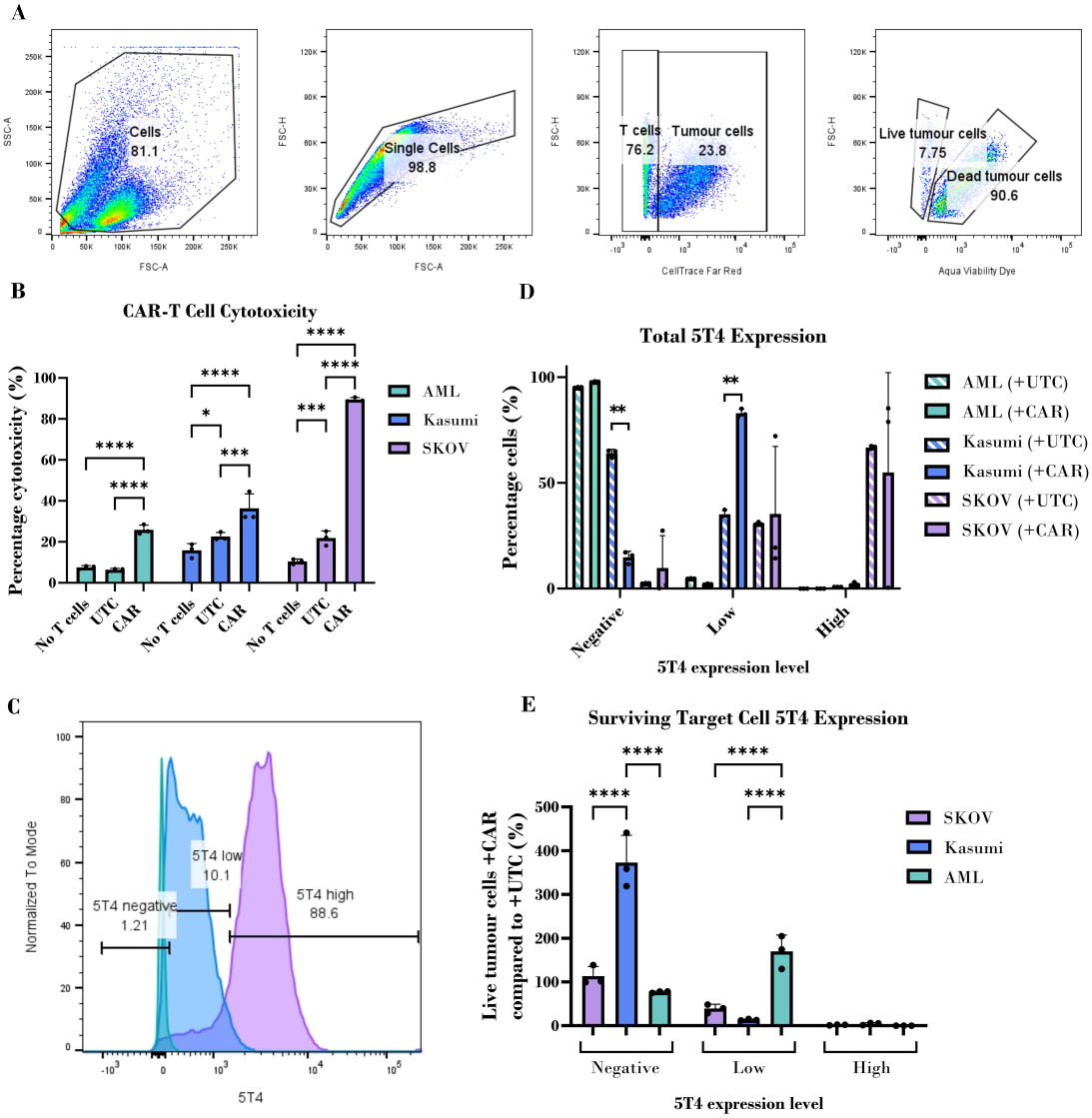


Figure 4.1: *In vitro* cytotoxicity of CAR-T cells with OXB-validated AML-193 (AML) and Kasumi-1 (Kasumi) leukaemia cell lines and SKOV-3 (SKOV) ovarian cancer cell line. (A) Gating strategy separating T cells and target cells. (B) Percentage cytotoxicity after 48 h co-culture with either untransduced (UTC) donor T cells or anti 5T4-CAR transduced (CAR) donor T cells. (C) MFI thresholds set for 5T4 levels in live target tumour cells based upon known expression in cell lines. (D) Total expression of 5T4 in all tumour cell lines in co-culture samples. (E) Live tumour cells classified based upon 5T4 expression remaining after 48 h co-culture with 5T4 CAR T cells as a proportion of live tumour cells cultured with UTC T cells from the same donor. All results were analysed using Two-way ANOVA with Tukey's multiple comparisons test, n=3 technical replicates. $^{****}p < 0.0001$, $^{***}p < 0.001$, $^{**}p < 0.01$, $^{*}p < 0.05$.

Cells were separated through CellTrace Far Red selection of target cells and then

assessed for viability (Figure 4.1A). Viability of target cells was assessed for each cell line cultured 1:1 with UTC and CAR-T cells as well as without T cells (Figure 4.1B). Low levels of cytotoxicity were observed in the AML-193 and Kasumi-1 cell lines with a slight (but statistically significant) increase in Kasumi-1 cell death in the UTC condition compared to no T cells. A similar non-specific killing was seen in the SKOV-3 cells between UTC and no T with efficient killing by CAR-T cells.

In addition to viability, target cells were also stained for their expression of 5T4 to allow stratification of killing among individual $5T4^{-}$, $5T4^{lo}$ and $5T4^{hi}$ groups within cell lines (Figure 4.1C). Percentage expression of total tumour cells for each cell line was quantified (Figure 4.1D) indicating that AML-193 cells were mostly negative for 5T4 but contained some low expressing cells. Kasumi-1 were primarily low expressing and SKOV-3 were primarily high expressing. Percentage change of the proportions of live tumour cells remaining in the sample after co-culture with CAR-T cells compared to the same cell line with UTC cells (Figure 4.1E) demonstrated efficient killing of $5T4^{hi}$ cells in all lines. In the AML-193 sample, a higher proportion of the surviving cells were $5T4^{lo}$ in the CAR condition than the UTC while SKOV-3 showed a reduction in the surviving $5T4^{lo}$ proportion but not a complete eradication.

4.2.2 Cytokine Production from OXB-Validated Cell Line Co-Culture with CAR-T Cells

Supernatant was harvested after 24 h of co-culture and assessed for levels of cytokine using the CBA assay. Distinct fluorescence profiles (Figure 4.2A) were generated for each cytokine allowing simultaneous analysis of multiple analytes in a single supernatant. A panel of cytokines was used within the assay to capture both CD4 and CD8 effector functions and cancer cell line cytokine release (Figure 4.2B). Given the fact that multiple cells release and bind to the same cytokines, the signals could not always be attributed to a single cell type, but gave an overall indication of the signalling landscape.

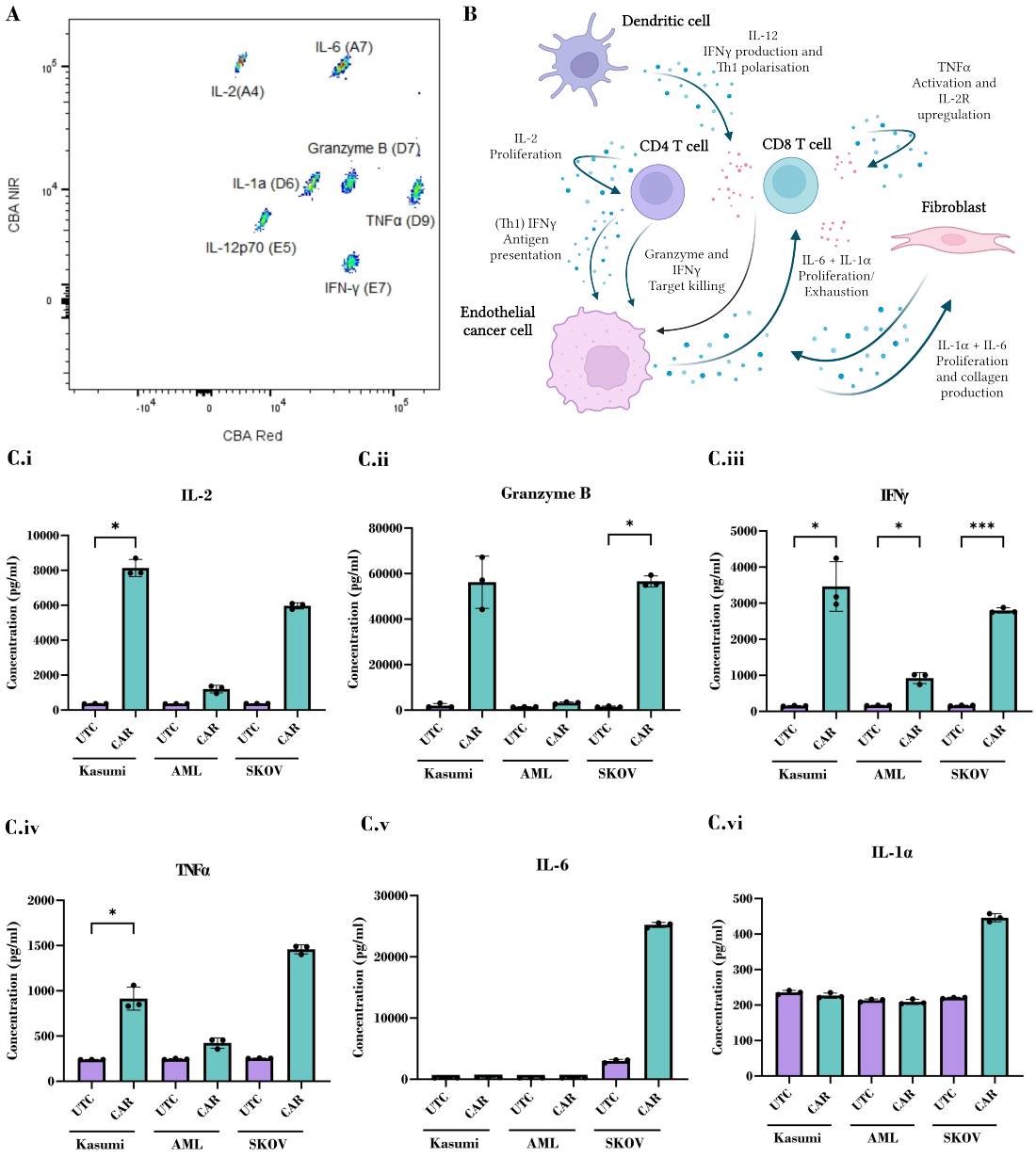


Figure 4.2: Expression of key cytokines in CAR-T cell co-culture with OXB validated target cell lines measured by cytometric bead array (CBA) assay. (A) Flow cytometric layout of bead array generated with Red and NIR clustering parameters using the PE reporter system. (B) Signalling pathways and effects of assessed cytokines in the context of cancer. Profiles of individual cytokines in AML-163 (AML), Kasumi-1 (Kasumi) and SKOV-3 (SKOV) cell lines. Mean fluorescence intensity (MFI) interpolated from standard curves and used to plot concentration of (C.i) IL-2 , (C.ii) Granzyme-B, (C.iii) IFNγ, (C.iv) TNFα, (C.v) IL-6, and (C.vi) IL-1α in media. Cell lines cultured for 24 h with untransduced (UTC) donor T cells or 5T4 CAR transduced (CAR) donor T cells. For co-culture technical replicates n=3, analysis using one-way ANOVA with Šidák's multiple comparisons test for IFNγ and Kruskal-Wallis test with multiple comparisons for all cytokines. $^{***}p < 0.001$, $^{*}p < 0.05$.

Concentrations of each of the cytokines were determined by interpolation using standard curves. Cytokine levels were read for each of the cell lines in the killing assay in combination with both CAR-T and UTC cells. IL-2 (Figure 4.2C.i) was assessed as a measure of CAR-T cell activation and proliferative signaling, showing significant production in Kasumi and a trend towards high levels in SKOV co-culture conditions. Granzyme-B (Figure 4.2C.ii) and IFNγ (Figure 4.2C.iii) indicate CAR-T cell effector function. Substantial release of both Granzyme B and IFNγ was measured in Kasumi and SKOV cell lines with a lower but significant release of IFNγ in AML culture with CAR-T cells.

TNFα (Figure 4.2C.iv) is another measure of CAR-T cell activation and was significantly expressed in Kasumi and high in SKOV co-culture but present at lower concentrations than the previous cytokines. IL-6 (Figure 4.2C.v) and IL-1α (Figure 4.2C.vi) were incorporated due to their aforementioned role in CRS and the high levels documented to be released by epithelial tumours as well as by CAR-T cells themselves. High levels of IL-6 were seen in the SKOV CAR-T cell co-culture only with a slight elevation in the UTC condition. IL-1α was also elevated in SKOV co-culture with CAR-T cells but the increase was far smaller than IL-6.

4.2.3 Selective Cytotoxicity of 5T4+ PDAC Cell Lines by Anti-5T4 CAR-T Cells

To test the efficacy of the anti-5T4 CAR-T cells in the context of PDAC, co-culture was performed with PDAC cell lines. These cells were previously assessed for their 5T4 expression (Figure 3.6) with PANC-1 determined to be $5T4^{mid}$, MIA PaCa-2 $5T4^{lo}$ and DEC hTERT $5T4^{-}$. Impedance assays were used to determine efficiency and selectivity of CAR-T cell killing with CAR-T and UTC cells seeded at ratios between 1:10 and 10:1 into wells of adherent target cells. Cell index (CI) was measured at 48 h following CAR-T cell addition (this timepoint is used frequently in the literature (Roselli et al. 2021; Abraham-Miranda et al. 2022)) and percentage killing was calculated using the following formula:

$$\text{Percentage cytotoxicity} = \left(\frac{\text{CI}_{\text{co-culture}} - \text{CI}_{\text{target cell}}}{\text{CI}_{\text{co-culture}}} \right) \times 100$$

The CI (Fig 4.3A) indicates the density of adherent cells remaining in each well and is used as a measure of live target cells. PANC-1 cells were significantly reduced in their viability at CAR-T cell: tumour cell ratios of 2:1, 5:1 and 10:1 while MIA PaCa-2 viability was significantly reduced at 5:1 and 10:1 CAR-T cells:target cells. No concentration of CAR-T cells induced a significant reduction in DEC hTERT viability. There was variation between the cell indices observed in different experiments which is due both to slight variations in growth rate between cell line passages and differential effector function of CAR-T cells derived from different healthy donors. Calculating percentage killing (Figure 4.3B) accounts for passage differences by using the baseline growth of the target cells alone to contextualise the CI for each condition. This showed significant cytotoxicity of PANC-1 between CAR-T cell ratios of 1:2-10:1 and of MIA PaCa-2 cells between 1:1-10:1. There was no significant death of DEC hTERT cells at any CAR-T cell concentration indicating 5T4-dependent cytotoxicity.

(Figure 4.3C) shows the total 48 h timecourse for all co-culture conditions. Measurements were taken from the point of CAR-T cell addition to co-culture. CI changes over time were plotted at each effector:target ratio. PANC-1 cells were killed more efficienty at earlier timepoints than MIA PaCa-2 cells while DEC hTERT cells showed no drop in CI at any timepoint.

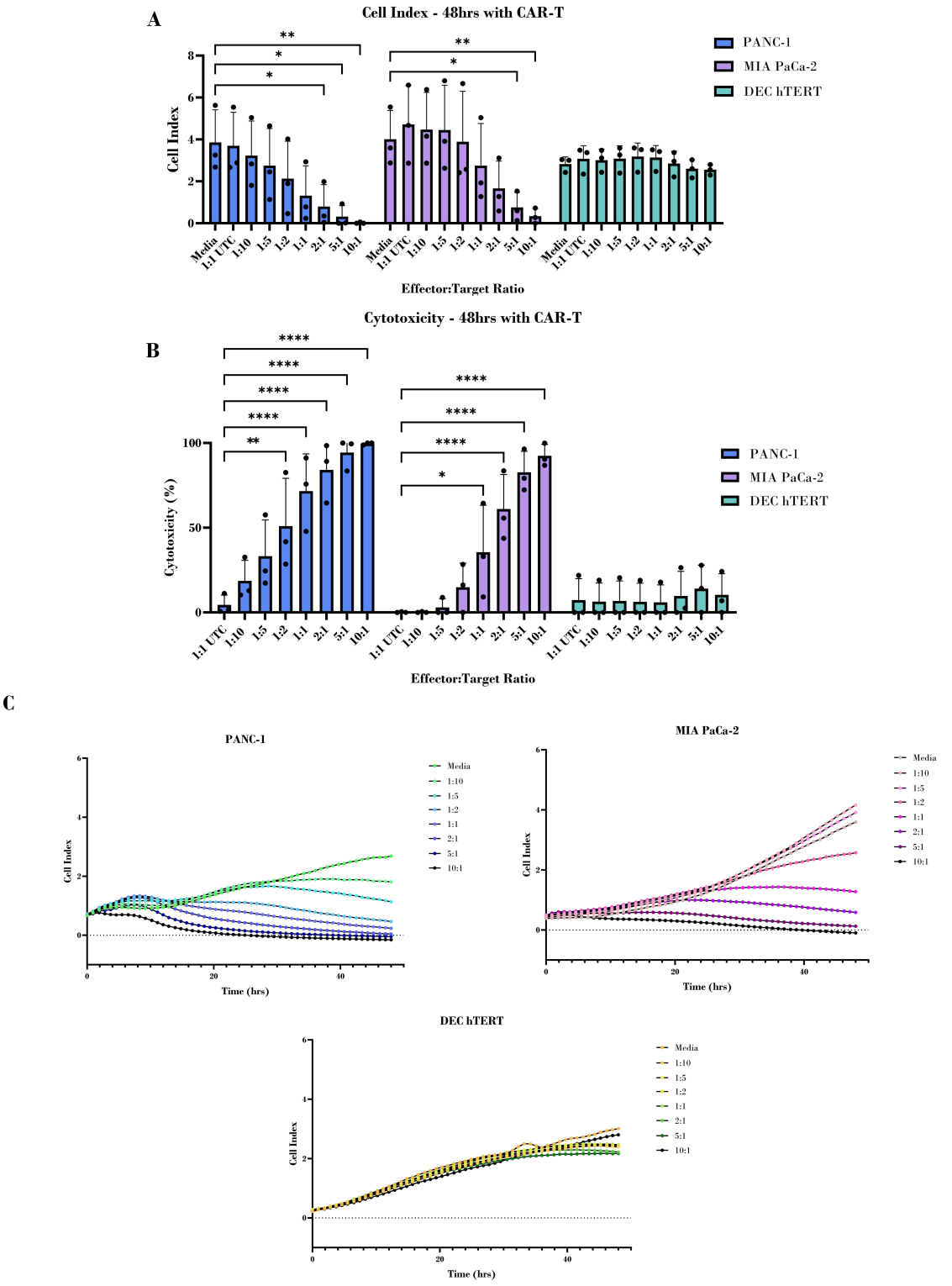


Figure 4.3: Healthy donor-derived CAR-T cell cytotoxicity with pancreatic cell lines expressing mid (PANC-1), low (MIA PaCa-2) and no (DEC hTERT) 5T4. (A) Cell index and (B) percentage cytotoxicity at 48 h of co-culture of PDAC cells and CAR-T cells with increasing effector:target cell ratios from 1:10 - 10:1. Two-way ANOVA with Dunnett's multiple comparisons test used for all analyses. (C) Individual time course plots showing cell index from CAR-T cell addition to 48 h of co-culture. n=3 biological replicates using different CAR-T cell donors and cell line passages. $^{****}p < 0.0001$, $^{**}p < 0.01$, $^{*}p < 0.05$.

4.2.4 Cytokine Production from PDAC Cell Line Co-Culture with CAR-T cells

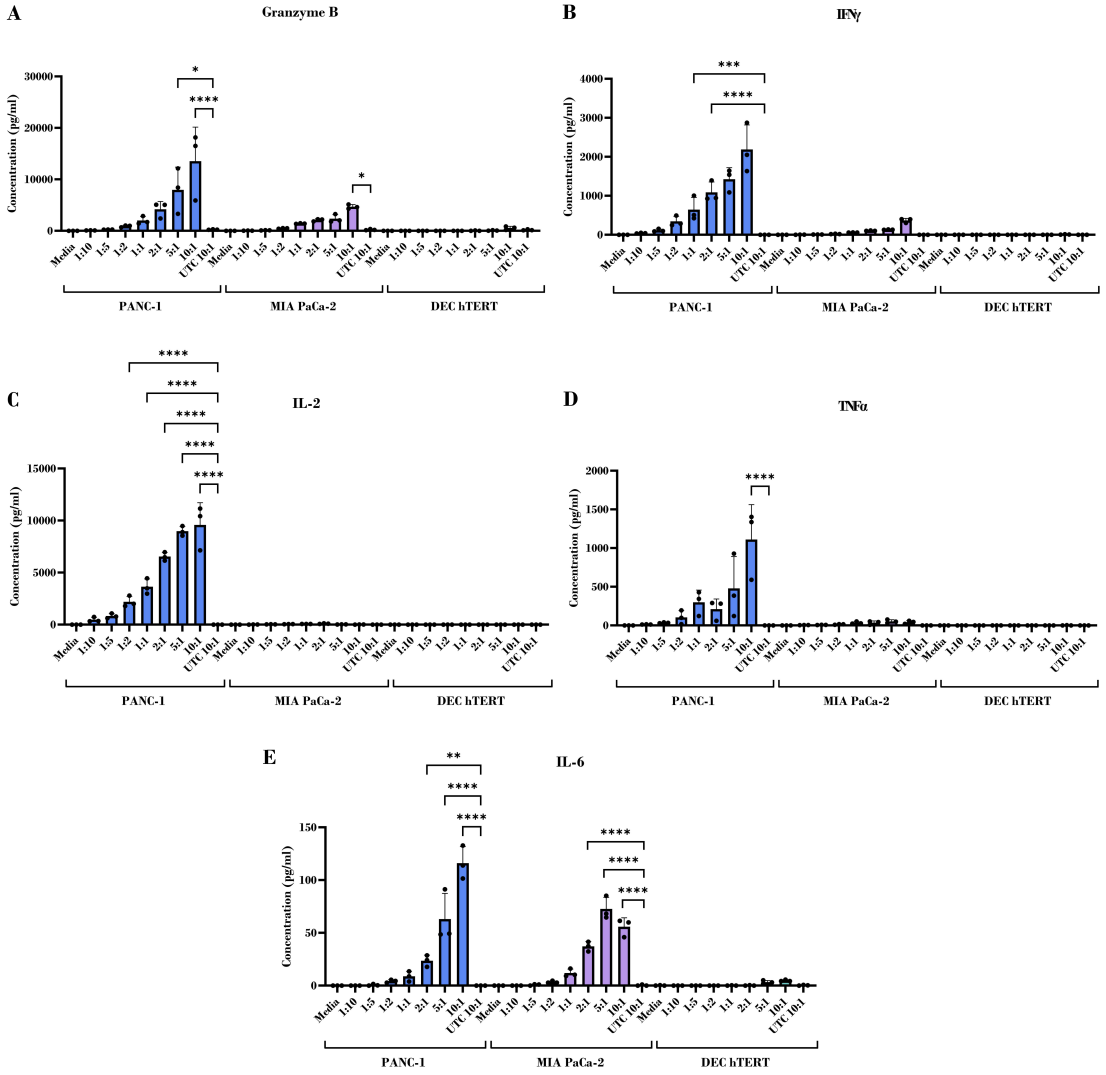


Figure 4.4: Expression of key cytokines in CAR-T cell impedance-based cytotoxicity assay with PDAC cell lines measured by cytometric bead array (CBA). Profiles of individual cytokines in PANC-1, MIA PaCa-2 and DEC hTERT cell line co-culture with CAR-T cells or UTC T cells for 48 h. Mean fluorescence intensity (MFI) interpolated from standard curves and used to plot concentration of (A) Granzyme B, (B) IFNγ, (C) IL-2, (D) TNFα and (E) IL-6 in media. One-way ANOVA with Dunnett's multiple comparisons test used for analysis with UTC 10:1 used as the control group for each cell line. CBA was performed using the n=3 technical replicates from n=1 co-culture assay. $^{****}p < 0.0001$, $^{**}p < 0.01$, $^{*}p < 0.05$.

Supernatant was harvested after 24 h of co-culture and assessed for levels of cytokine using the CBA assay as previously. Levels of Granzyme B (Figure 4.4A)

were significantly elevated in PANC-1 co-culture with CAR-T cells in 5:1 and 10:1 CAR-T cells:target cells and in the 10:1 CAR-T cells:MIA PaCa-2 target cells condition but no other ratio produced a significant increase. IFNγ (Figure 4.4B) was similarly only elevated in PANC-1 co-culture with significant elevation at ratios of 5:1 and 10:1 CAR-T cells:target cells. IL-2 (Figure 4.4C) and TNFα (Figure 4.4D) were also only significantly increased in PANC-1 co-culture with CAR-T cells; IL-2 was significantly elevated with CAR-T cell ratios from 1:2-10:1 and TNFα in 10:1 CAR-T cells:tumour cells only.

IL-6 (Figure 4.4E) was significantly elevated in both PANC-1 and MIA PaCa-2 co-culture between ratios of 2:1-10:1 CAR-T cells:tumour cells. This elevation was in line with the previously measured elevation of IL-6 in CAR-T cell co-culture with SKOV-3 cells (Figure 4.2C.vi) as both PANC-1 and MIA PaCa-2 are epithelial cell lines. The lack of IL-6 expression in the DEC hTERT line supports the need for CAR-T cell activation to produce the response previously demonstrated by the lack of significant elevation previously seen in the UTC conditions.

4.2.5 Effect of IL-6 Supplementation on CAR-T Cell Viability, Proliferation, and Exhaustion

In both co-culture experiments there was significant elevation of IL-6 when CAR-T cells were cultured with $5T4^+$ epithelial cell lines. The effect of IL-6 supplementation on CAR-T cells was investigated given the documented expression in PDAC and the conflicting roles that the cytokine can play in both activation and exhaustion of T cells. CAR-T cells were generated from PBMCs (Chapter 2.1.6) and cultured in combinations of cytokines over the course of the 7 day protocol (Figure 4.5A). All cytokines were added at 10ng/ml in line with the standard protocol developed at OXB and maintained at this level throughout the culture period. Expansion (Figure 4.5B) and viability (Figure 4.5C) were calculated based on measurements taken on Day 0, Day 4 and Day 7 of culture while phenotype (Figure 4.5D) and PD-1 expression (Figure 4.5E) were assessed on Day 7 using flow cytometry.

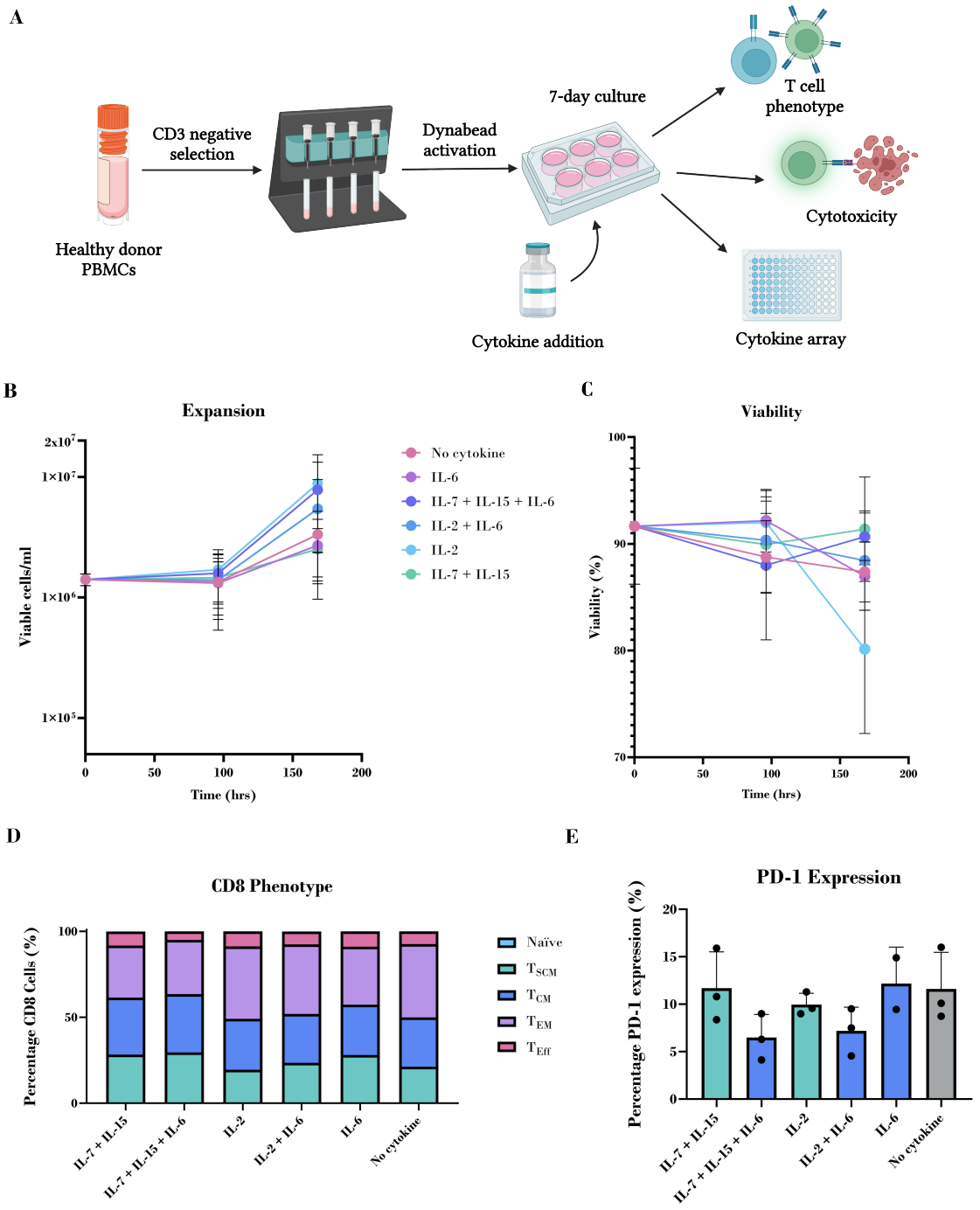


Figure 4.5: The *in vitro* effects of IL-6 on primary T cell function. (A) Workflow from patient sample to downstream analysis. (B) Expansion and (C) viability of T cells cultured in the presence of different cytokine combinations measured through viable cell counts at Day 1, Day 4 and Day 7 of culture. (D) CD8 T cell phenotype and (E) PD-1 expression measured by flow cytometry at Day 7. Phenotype analysed using 2-way ANOVA with Tukey's multiple comparisons test. PD-1 expression was analysed using a Mixed Effects Model (insufficient replicates in all conditions for ANOVA) with Tukey's multiple comparisons test. For all analyses n=3 healthy donors were used. $ns = p > 0.05$.

Viability and expansion of the cells across culture conditions was consistent, with no significant reduction or expansion seen with any cytokine combination. The phenotype of the CAR-T cells was similarly unchanged in all conditions, with no naïve cells present on Day 7 of culture and comparable levels of all other subtypes. This was consistent across both CD8 cells (Figure 4.5D) and CD4 cells (Appendix B.1). PD-1 expression was also not significantly altered across any of the conditions.

4.2.6 Effect of IL-6 Supplementation on CAR-T Cell Cytotoxicity and Cytokine Production

The effector function of CAR-T cells generated in different cytokine conditions was assessed through analysis of baseline cytokine production with supernatant collected at Days 0, 4 and 7 (described in Chapter 2.2.6) and analysed using the CBA assay. An impedance-based cytotoxicity assay (as in Figure 4.3) was also used to investigate potential impacts on cytotoxicity. PANC-1 cells were used as target cells as these were killed the most efficiently in previous assays.

Cytokine release varied throughout the time in culture (Appendix B.2). Day 4 cytokine release is represented as levels of all cytokines peaked at this time point. No significant differences were seen in the levels of Granzyme B (Figure 4.6A), IFNγ (Figure 4.6B), IL-2 (Figure 4.6C) or TNFα (Figure 4.6D) released by CAR-T cells cultured in different cytokine combinations. There is substantial variation between donors in cytokine production levels but no significant change is induced by the addition of IL-6 to culture alone or with either IL-7 and IL-15 or IL-2.

The cytotoxicity assay displayed differences between individual conditions at each effector:target ratios with a significant reduction in cytotoxicity in the IL-7, IL-15 and IL-6 combination at 1:10 and 1:2 effector:target cells and in IL-6 alone at 1:1 and 2:1. Overall no individual combination led to a consistent reduction in CAR-T cell cytotoxicity.

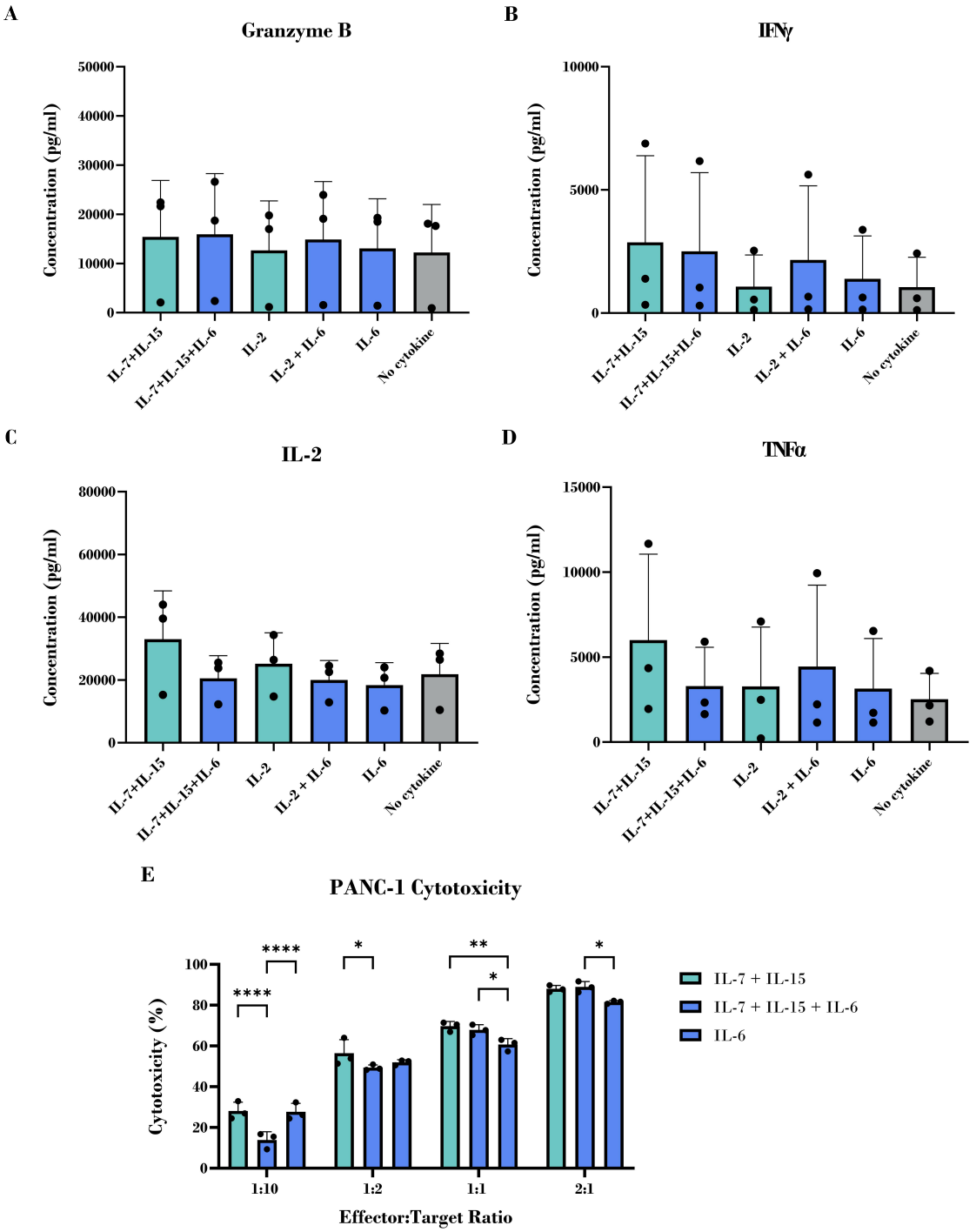


Figure 4.6: The *in vitro* effects of IL-6 on primary T cell cytokine secretion and target cell killing. Cytokine bead array (CBA) analysis of supernatants collected from T cells at Day 4 of culture. Levels of (A) Granzyme B, (B) IFNγ, (C) IL-2 and (D) TNFα detected in supernatants of T cells maintained in 10 ng/ml of each cytokine. Cytokine data analysed using 1-way ANOVA with Tukey's multiple comparisons test, n=3 healthy donor PBMC samples. (E) xCELLigence impedance-based killing of PANC-1 cells by healthy donor T cells cultured +/- IL-6. Percentage cytotoxicity calculated from impedance values after 48 h co-culture. For cytotoxicity, n=1 healthy donor PBMC sample with n=3 technical replicates. For analysis, 2-way ANOVA with Tukey's multiple comparisons test was used. $^{****}p < 0.0001$, $^{**}p < 0.01$, $^{*}p < 0.05$.

4.3 Discussion

Both flow cytometry of OXB-validated cell lines and impedance assays using PDAC cell lines indicated that anti-5T4 CAR-T cells kill target cells efficiently and selectively. Cytokine release was consistent with effector response throughout and high IL-6 seen in CAR-T cell co-culture with $5T4^{+}$ epithelial cancer lines did not substantially affect CAR-T function.

The $5T4^{hi}$ SKOV-3 cell line was killed efficiently by the CAR-T cells. Low levels of non-specific killing were evident due to the significantly higher cytotoxicity observed in the UTC condition when compared to the tumour cells alone. Kasumi-1 cells, which express a lower level of 5T4, were killed less efficiently at a similar level to the AML cell line which was previously documented to be $5T4^{-}$. Despite this previous categorisation, the 5T4 staining (Figure 4.1C-E) indicated that a proportion of the AML cells did express low levels of 5T4. Alternatively, the expression of 5T4 may be below the detection limit of flow cytometry but sufficient to trigger CAR-T cell activation. This has been previously documented with CD19 (Patel et al. 2024). This would explain the increased cytotoxicity of CAR-T cells compared to UTC cells co-cultured with the AML cell line.

The increased proportion of $5T4^{-}$ surviving cells in the CAR-T cell condition of the Kasumi-1 cells was indicative of both $5T4^{hi}$ and $5T4^{lo}$ populations being targeted. In the $5T4^{lo}$ cell populations, the increased surviving proportion seen in the AML cell line compared to Kasumi and SKOV was potentially due to the increased effector function of the CAR-T cells exposed to $5T4^{hi}$ cells in the latter cell lines leading to more effective eradication of lower 5T4 expressing cells. This was supported by the low levels of cytokine release seen in the AML co-culture.

The cytokine array demonstrated that the CAR-T cells were able to proliferate and kill target cells through the release of IFNγ and Granzyme B. These responses were not seen in the UTC conditions and were therefore not the result of non-specific T cell activation and rely on CAR signalling to occur. Notably, the Kasumi-1 co-culture produced comparable levels of Granzyme B and IFNγ to the SKOV-3 co-culture despite a marked reduction in cytotoxicity. The elevated IFNγ signalling

seen in the CAR-T cell coculture with the $5T4^-$ AML cell line compared to that of UTC cells with AML aligns with the observation of the presence of $5T4^{lo}$ cells and the low levels of killing observed.

IL-6 and IL-1α were only elevated in the SKOV cell line co-culture with CAR-T cells. This could be attributed to release by either the tumour cells or the CAR-T cells but is unique to the epithelial cell line. The lack of release of CAR-T with Kasumi-1 cells could indicate that the interaction is dependent on the malignancy being solid rather haematological, and therefore that the cytokine is cancer cell-derived rather than T cell-derived. This is supported by existing literature documenting SKOV-3 production of IL-6 (Rabinovich). Given the fact that IL-6 production is documented in both solid (Rašková et al. 2022) and haematological malignancies (Fayad et al. 2001) including AML (Saadi et al. 2021; D. Hou et al. 2023) this difference could also be due to the lower levels of 5T4 in Kasumi-1 and AML leading to a reduced CAR-T cell effector response and therefore less CAR-T cell-derived IL-6 production. Additionally, a feedback loop involving both tumour cell and CAR-T cell mediated IL-6 production is possible.

Impedance-based cytotoxicity of PDAC cell lines confirmed the ability of the CAR-T cells to discriminate between $5T4^+$ and $5T4^-$ lines and demonstrated that the efficiency of cytotoxicity varies with the extent of 5T4 positivity of the target. The effector:target ratio required to kill PANC-1 cells was less than needed to produce the equivalent level of cytotoxicity with MIA PaCa-2 cells. Target density was also reflected in the dynamics of the response, with PANC-1 cell viability beginning to drop around 5-20 h after CAR-T cell addition depending on effector:target ratio and MIA PaCa-2 only dropping before 20 h in the 10:1 and 5:1 effector:target cell conditions. In this setting, the same levels of non-specific killing were not seen as with Kasumi-1 and AML-193; UTC cells did not significantly reduce the viability of target cells compared to media with any cell line.

Although 5T4 expression differs between the cell lines thus impacting the ability of the CAR-T cells to exert a cytotoxic effect, other variations between the lines may also impact CAR-T cell responses. The expression of adhesion molecules

such as ICAM-1 and LFA-3 have been documented to alter CAR-T cell engagment through the formation of sub-optimal immune synapses (Yan et al. 2022). Additional differences in apoptotic resistance including the expression of FasL (Houston and O'Connell 2004) could also mediate altered CAR-T cell potency. Systematically modifying the expression of 5T4 within a single cell line would bypass these sources of variation and demonstrate that 5T4 surface expression level is the sole factor altering CAR-T cell cytotoxicity.

While cytokine release in co-culture with PANC-1 mirrored that of the SKOV-3 cells, the MIA PaCa-2 co-culture showed comparably low levels of Granzyme-B, IFNγ, TNFα and IL-2. This discrepancy could potentially have been due to the dynamics of the cytotoxic effect seen in Figure 4.3C. Media was taken 24 h after the addition of CAR-T cells to culture therefore capturing the CAR-T cell killing of PANC-1 long after initiation, but capturing the MIA PaCa-2 response in its very early stages, or even before initiation at lower effector:target ratios. The fact that IL-6 was significantly elevated in both PANC-1 and MIA PaCa-2 co-culture supernatants at this time point is potentially another sign that the cytokine was cancer-derived rather than CAR-T cell derived.

IL-6 had no significant effect on T cell viability, proliferation, PD-1 expression, or phenotype at 10 ng/ml. There were significant variations seen in cytotoxicity between the conditions, although these were not consistent to a single cytokine combination and, although statistically significant, they represent a relatively small reduction in percentage killing.

The 10 ng/ml concentration of IL-6 was chosen so as to be comparable with the existing concentrations of IL-7 and IL-15 used to supplement the CAR-T cell media. This concentration was roughly 10-fold higher than the concentration detected in the CAR-T cell co-culture with PANC-1 cells thus indicating that the IL-6 produced in this setting did not impact the functionality of the CAR-T cells. While this concentration did not impact the CAR-T cells, the cytokine was later investigated at concentrations relevant to PDAC tumours (Appendix C.5), due to detection in

tumour slice eluates (see Figure 5.8). This later investigation supported the findings in a setting much more applicable to the *ex vivo* platform used throughout Chapter 5.

Given that exhaustion is one of the documented negative effects of IL-6 on T cells, the experimental procedure using a 7-day exposure time could potentially be insufficient to study the long term effects of the cytokine on the CAR-T cell population. For the purposes of evaluating the potential of IL-6 to impact CAR-T cell function in relation to *ex vivo* slice culture, this timeframe is sufficient, as it aligns with the period of slice viability previously determined by the lab (Hughes et al. 2024). The impact of chronic cytokine exposure in clinical settings may require longer term assays. The potential for induction of CRS indicated by high IL-6 would also require a different model system to investigate due to the systemic nature of the reaction. Comparing IL-6 levels in cell culture supernatant upon co-culture with a variety of CAR constructs could determine whether the anti-5T4 CAR-T cells induce particularly high IL-6 in comparison to other CARs.

4.3.1 Conclusion

Together, these findings confirm that the anti-5T4 CAR-T cells are able to discriminate between $5T4^{+}$ and $5T4^{-}$ cell lines across cancers and specifically in PDAC. Given the widespread use of *in vitro* killing assays, this provides a measure of efficacy which can be readily compared to alternative CAR-T cell therapies in the literature. Validation in this simplified setting provided a rationale for pursuing more physiologically relevant testing using live tumour slices.

"All cancers are alike but they are alike in a unique way"

Siddhartha Mukherjee

5

Ex Vivo Efficacy of Autologous Anti-5T4 CAR-T Cells Cultured with Organotypic Tumour Slices

5.1 Introduction

5.1.1 Use of 3D Models in Cancer

Although *in vitro* efficacy studies provide valuable information about the sensitivity and specificity of CAR-T cell responses, two-dimensional systems fail to replicate the environment that the cells will encounter in the native tumour. As discussed in Chapter 1.1.2, three-dimensional models are frequently used to more accurately represent solid tumours. Both organoids and organotypic tumour slices have advantages over cell culture monolayers as they replicate the complexity of the cellular interactions that occur in a solid mass (Peng et al. 2025).

While 3D culture generally facilitates more physiological modelling, the addition of the stroma is particularly important in the context of PDAC, given that it can comprise up to 90% of the tumour mass (Geyer et al. 2023). The stroma is key in altering tumour cell behaviour due to increased environmental stiffness (Kpeglo et al. 2022) and has been shown to impact diverse aspects of tumour biology including metastatic potential (Wullkopf et al. 2018; Ray et al. 2022) and

drug resistance (Rice et al. 2017). When using PDOs, the stromal component of tumours is sometimes incorporated through co-culture with PSCs (Geyer et al. 2023), CAFs (Schuth et al. 2022) or collagen matrix embedding (Lahusen et al. 2024). When using tumour slices, the stroma is preserved (Hughes et al. 2024), facilitating investigation without additional culture components.

5.1.2 Organotypic Tumour Slice Culture

Organotypic slices effectively represent the native tumour but are not currently widely used in preclinical testing. Due to their disparate use, a wide variety of methods is used to culture and analyse the slices *ex vivo*. Generally, slices are cultured in media compositions similar to those used in cell culture. The addition of FBS to media formulations is common in organotypic slice culture protocols despite the lack of physiological relevance and unknown effects on metabolism (Barroso et al. 2022). Static culture is also generally used to maintain tumour slices, although our group previously showed that the use of perfusion culture can extend the viability of PDAC tumour slices (Hughes et al. 2024), giving researchers a greater window for therapeutic intervention. Similar advantages using perfusion have been demonstrated with the culture of murine brain slices (Romero-Leguizamón et al. 2019) and a group has since applied the approach in human glioblastoma (Olubajo, Achawal and Greenman 2020).

Despite their different biologies, groups working with brain tissue and HNSCC use similar techniques to those working with PDAC (Gerlach et al. 2014) such as vibratome sectioning (Ravi et al. 2019) and culture at the air interface using porous membranes. These techniques are not universal, with some using collagen scaffolds (X. Jiang et al. 2017) or porous sponges (Kokkinos et al. 2021) as the basis for culture, but these long-term platforms are generally constructed to achieve maintenance of nutrient delivery and waste removal. In order to maintain oxygen delivery throughout the slice, studies tend to use sections between 200-500 µm thick. Generating sections <200 µm is technically challenging due to their fragility while >500 µm risks necrosis at the core of the tissue due to the lack of intact

vasculature. There was no evidence of this necrosis seen in a study by Kokkinos et al. (2021) despite their use of 1-2 mm diameter tumour fragments rather than slices. Although the authors reported a lack of positive TUNEL staining after 9 days in culture, it is unclear whether histology sections were taken from the perimeter or the core of each fragment (Kokkinos et al. 2021).

5.1.3 Organotypic Tumour Slice Analysis

Alongside differences in culture methodology, the outputs analysed following treatment of tumour slices also vary. Immunohistochemistry is the most commonly used analysis method, with cell death frequently assessed through caspase cleavage and proliferation with Ki67 staining (Lim, J. H. Chang, W. S. Lee, K. M. Lee et al. 2018; Martin et al. 2019; Misra et al. 2019; Kokkinos et al. 2021). This output can be adapted for different markers but cannot be used to visualise multiple markers on the same section (unless multiplexed IHC is used) or to image a section greater than 5-6 µm in thickness. Non-spatial techniques such as RNAseq have also been used to evaluate the global effects of drug treatment (Moro et al. 2022) but need to be combined with more direct measures of cytotoxicity in order to infer any meaningful therapeutic effect.

One of the advantages of using tumour slices is the ability to observe cells within their native architecture and thus to understand the ability of a therapy to penetrate into the structure of the tumour. The importance of the microenvironment in determining T cell motility has been demonstrated in this setting, through live imaging showing a reduction in resident T cell motility and tumour island infiltration following contact with TAMs (Peranzoni, Lemoine et al. 2018). In the case of CAR-T cell therapy, the model is particularly useful for observing the interactions between CAR-T cells, target cells and the TME - interactions which can be observed in 3D using IF. X. Jiang et al. (2017) used this technique to visualise the distribution of macrophages and fibroblasts in the TME, as well as the distribution of autologous PBMCs applied to the surface of slices as a proof-of-concept for use of the platform in testing autologous cell therapies (X. Jiang et al. 2017).

5.1.4 Studying Immunotherapy Efficacy with Tumour Slices

Although it is a growing area of interest, organotypic tumour slices are not widely used for the study of immunotherapies and specifically cellular therapies in solid tumour settings. Some groups have investigated using checkpoint blockade (Sivakumar et al. 2019; Voabil et al. 2021) with organotypic tumour slices to facilitate clinical response prediction. The fact that the slices are not able to capture systemic immunological effects of therapy may limit the utility of applying agents such as anti-PD-1/L1 alone in this setting. No publications document the use of the platform to test TIL therapies and only a few groups document their use in CAR-T cell therapy and oncolytic virotherapy (Runge et al. 2022). In virotherapy organotypic slices are particularly useful given the scarcity of available immunocompetent murine models for some oncolytic viruses (such as adenoviruses) which do not generally infect mice as effectively as humans (Otero-Mateo et al. 2025).

In one of the few demonstrations of CAR-T cell culture with tumour slices, Bandara et al. (2024) document use of ovarian tumour slices recovered after cryopreservation. They show relatively low caspase staining in control samples and significant increase in cell death following CAR-T cell therapy (Bandara et al. 2024). This finding indicates that long-term storage may be possible with this type of sample, but further investigation is needed comparing results between fresh and frozen samples directly.

5.1.5 Live Imaging of CAR-T Cells and Tumour Slices

Donnadieu and colleagues developed a series of protocols to investigate the migration of both in situ (Salmon et al. 2012; Bougherara et al. 2015; Peranzoni, Bougherara et al. 2017) and exogenous (Kantari-Mimoun et al. 2021; Espie et al. 2023) T cells through tumour slices using live imaging. The group used a diverse range of staining and imaging techniques to observe the ability of T cells to navigate the tumour architecture (Salmon et al. 2012), interact with other cells in the TME (Peranzoni, Lemoine et al. 2018) and (in the case of CAR-T cells) to activate upon engagement with a target antigen (Kantari-Mimoun et al. 2021; Espie et al.

2023). Many of the protocols were used to inform methods (detailed in Chapter 2.4) used within this chapter. Similar techniques were also recently described by another group applying exogenous T cells to murine pancreatic tumour slices; the group also stained the tissue and T cells prior to imaging and were therefore able to map T cell trajectories within the structure (Rodríguez-Merced, Callaway and Provenzano 2023). The paper highlights challenges associated with live-imaging requiring balance of image frequency and z-depth given the rapid movement of T cells within the structure. These constraints are particularly relevant to T cell activation imaging as the events occur over a short timeframe.

While the Donnadieu group have analysed the interactions of CAR-T cells with tumour slices, they used CAR-T cells generated from healthy blood donors rather than from the same patient (Kantari-Mimoun et al. 2021). This approach is used generally in the literature due to the limited availability of blood samples from matched donors prior to surgery. Despite the logistical challenges, using autologous CAR-T cells ensures that none of the effects seen is a consequence of either GvHD or host versus graft (HvG) allorejection. GvHD is caused by the TCR of the allogeneic CAR-T cells which has the potential to recognise 'foreign' peptides in the patient and target their healthy tissues (Moradi, Omidkhoda and Ahmadbeigi 2023). HvG, on the other hand, is due to HLA mismatch leading to the patient's immune cells destroying the CAR-T cells thus limiting their efficacy. This has been shown to lead to a reduction in clinical efficacy even with haploidentical CAR-T cells rather than full HLA matching (X. Jin et al. 2020; T. C. Y. Tang et al. 2022). As allogeneic CAR-T cell therapy development progresses, more strategies are being developed to combat both GvHD and HvG and facilitate both safe and effective treatment with donor cells (discussed in Chapter 1.3.3.5). It is therefore important that, when testing a CAR-T cell therapy which has not been modified for use with allogeneic T cells, the cells used preclinically are autologous so as to obtain the most accurate reflection of their potential in the clinic.

5.1.6 The Impact of the TME on T cells in PDAC

As discussed in Chapter 1.3.3.6, solid tumours are a challenge for CAR-T cell therapy. One major contributor is the milieu of immunosuppressive soluble mediators secreted by tumour cells, CAFs and other immune cells. The effects that these cells have on T cell infiltration and effector function are also mediated by receptor interactions including checkpoint inhibitors which are discussed further in Chapter 6. The term 'soluble mediators' encompasses a broad range of factors which have previously been identified to suppress T cell function in PDAC - these largely fall into groups of cytokines, chemokines and metabolites.

Although chemokines generally promote the migration of immune cells towards their source, they can also be linked to cell exclusion. Fibroblast-derived CXCL12 was found to exert this effect in PDAC (Feig et al. 2013) prompting a clinical trial (NCT02179970) blocking its receptor CXCR4. This mechanism is not entirely understood; some hypothesise that high concentrations of CXCL12 leads to 'fugetaxis' or repulsion of T cells (Vianello et al. 2006) while others demonstrate that stromal secretion could sequester T cells away from tumour islands (Ene-Obong et al. 2013; Malik et al. 2021). Y. D. Seo et al. (2019) demonstrate that in a tumour slice model, CXCR4 blockade combined with anti-PD-1 therapy leads to lymphocyte expansion, infiltration into juxtatumoural areas and tumour cell apoptosis, thus illustrating the negative role that the receptor plays in antitumour immunity (Y. D. Seo et al. 2019). CCL2 and CXCL5 are also implicated in T cell suppression through their recruitment of MDSCs and other regulatory immune cells (Loyher et al. 2016; Nywening et al. 2018; Deng et al. 2022). The impact of these molecules demonstrates the importance of favouring recruitment of antitumor immune cell subsets and preventing a pro-tumourigenic microenvironment from forming.

Cytokine-mediated suppression is prevalent in PDAC, with a number of cytokines found to be consistently upregulated. As mentioned in Chapter 4, IL-6 is known to be high in the TME and exerts a diverse array of effects on the immune population and on the tumour itself. In addition to its ability to induce T cell expansion, IL-6-mediated recruitment of MDSCs (Weber et al. 2021) and Th17/Treg polarisation

(Ware, El-Rayes and Lesinski 2020) are also documented. A recent clinical trial combining IL-6R blockade (tocilizumab) with chemotherapy showed no significant difference to OS (I. M. Chen et al. 2023). This, combined with the termination of another trial using tocilizumab in combination with radiation and checkpoint inhibitors (NCT04258150) due to not reaching primary endpoint, calls into question our ability to target this axis beneficially in clinic. TGFβ is another highly expressed factor for which blockade shows preclinical promise but a lack of efficacy in clinical trials (Metropulos, Munshi and Principe 2022). Alongside IL-10, TGFβ is secreted by Tregs (as well as M2-like macrophages and PSCs) inducing T cell anergy and preventing tumour trafficking (Gunderson et al. 2020). Development of synthetic receptors to subvert this negative signalling is ongoing in CAR-T cells (A. J. Hou, L. C. Chen and Y. Y. Chen 2021). The mechanistic importance of these factors contrasted by lack of clinical efficacy induced by their blockade highlights the complexity of cytokine regulation.

Recently there has been increased focus on the effects of the metabolic environment on cellular function, particularly in the context of T cells. Factors particularly pertinent to PDAC include adenosine signalling (discussed in Chapter 6) and adipokines, both of which are known to modulate antitumour immunity (Procaccini et al. 2013; Schneider et al. 2021). Adipokine levels have been shown to be altered to pancreatic cancer with a significant increase in adiponectin observed in PDAC patients (Ismaiel et al. 2024). The effect of adiponectin on T cells is unclear. Some papers show induction of T cell apoptosis (Wilk et al. 2011) and Treg polarisation by adiponectin-treated DCs (Tsang et al. 2011) while others indicate that it can enhance Th1 differentiation and pro-inflammatory cytokine production in CD4 T cells and macrophages (Cheng et al. 2012). Given the association between PDAC and metabolic diseases including diabetes and obesity, the links between adipokine levels and antitumor immunity warrant further investigation.

5.1.7 Aims

This chapter aims to establish a reproducible protocol for the analysis of autologous patient CAR-T cells interacting with tumour slices. Both fixed and live microscopy were used to interrogate the infiltration, colocalisation with $5T4^+$ target cells, and in situ activation of the anti-5T4 CAR-T cells.

Multiple assays were used to characterise the interactions between the autologous CAR-T cells and the tumour. Combinations of fixed and live IF, IHC, and cytokine analysis were used to assess the abundance of 5T4 in the tumour and the behaviour of the T cells from their first application to the surface of the slice to their long-term cytotoxicity. These assays aimed to provide an overall picture of how the CAR-T cells perform in a clinically relevant model, including their ability to penetrate the dense stromal matrix and overcome the immunosuppressive TME.

5.2 Results

5.2.1 Immunofluorescence Validation for Depth and Colocalisation Measurements of Exogenous T Cells in PDAC Slices

Prior to carrying out co-culture using autologous CAR-T cells, it was necessary to validate a staining panel to visualise both the structure of the PDAC tumour slice and the localisation of the exogenous T cells within the structure. Jurkat T cells were utilised as a proxy for primary T cells at this stage due to their widespread availability. Methods (Espie et al. 2023) were used to concentrate pre-stained Jurkat T cells on top of tumour slices. The staining panel was modified throughout development to minimise spectral overlap and ensure that staining was clear throughout the slice structure.

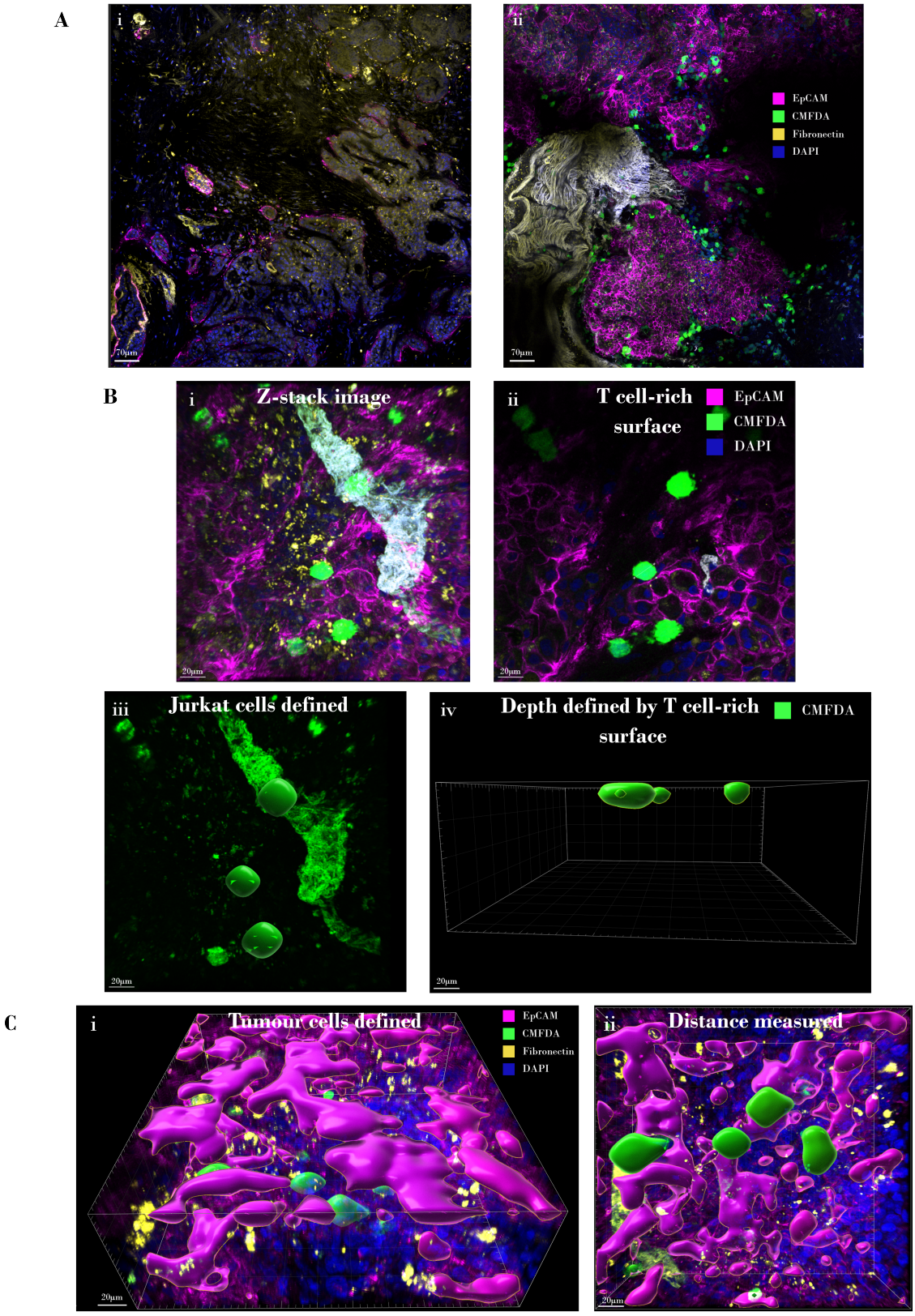


Figure 5.1: Development of analysis methods for exogenous T cell interaction with tumour slices. (A) Macro images of tumour slices stained for tumour (EpCAM, pink), stroma (fibronectin, yellow) and nuclei (DAPI, blue) without (A.i) and with (A.ii) exogenous Jurkat T cells (CMFDA, green). (B) Workflow for T cell depth analysis performed using Z-stacks with Imaris. (B.i) Z-stacks were loaded, (B.ii) the T cell-rich surface identified and (B.iii) cell surfaces classified. (B.iv) Cell surface depth was measured relative to the tissue surface. (C) Colocalisation was determined using a second tumour cell surface (C.i) measuring T cell distance to the nearest tumour cell (C.ii).

Images were captured (Figure 5.1A) of the surface of the tumour slices incubated with (Figure 5.1A.ii) and without (Figure 5.1A.i) Jurkat cells. Images show Jurkats (CMFDA, green), stromal regions (fibronectin, yellow), tumour cells (EpCAM, pink) and nuclei (DAPI, blue). Figure 5.1B details the process of determining T cell penetration depth from Z-stack images using Imaris. Z-stack images (Figure 5.1B.i) were assessed to locate the Jurkat-rich tumour slice surface (Figure 5.1B.ii) and Jurkat T cells (Figure 5.1B.iii) were defined. Depth into the slice was measured as the distance of the individual Jurkat cell from the Jurkat-rich slice surface (Figure 5.1B.iv). Figure 5.1C details the colocalisation measurement methodology which used EpCAM (in later figures 5T4) staining to define a second set of tumour cells (Figure 5.1C.i) and then used the shortest distance from each T cell to the nearest tumour cell (Figure 5.1C.ii) to define whether T cells were colocalised with tumour cells.

No quantification of tumour penetration depth or tumour cell colocalisation was performed during this optimisation period due to the lack of physiological relevance of Jurkat cells. The cells have been shown to have limited expression of chemokine receptors (Jost et al. 2016) and therefore may not migrate into the tumour tissue similarly to primary T cells. Despite the lack of quantification, validation with Jurkat cells demonstrated feasibility of analysis of T cell location within tumour slices. This process was therefore applied to autologous T cells.

5.2.2 Activation of Autologous T Cells is Necessary for Adhesion to Slices

Although autologous CAR-T cell generation requires blood samples 7 days prior to surgery, autologous untransduced T cells could be generated on the day of resection. These samples were used to test the conditions required to visualise T cell migration throughout the tumour slice.

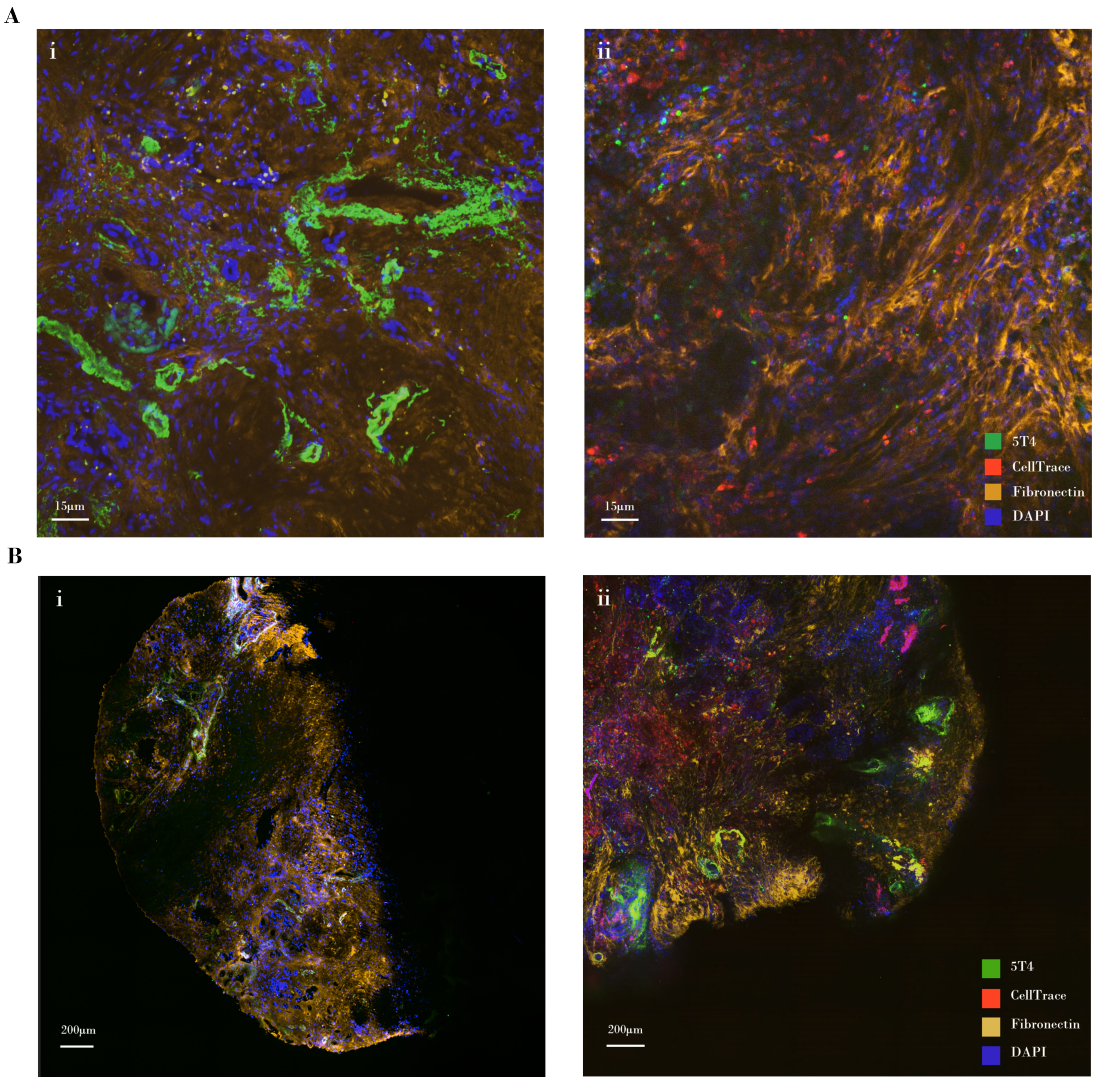


Figure 5.2: Primary T cells require Dynabead activation to infiltrate tumour slices *ex vivo*. (A) Autologous primary T cells applied to the surface of tumour slices for 1 h prior to immunofluorescence. Primary T cells (red) without (A.i) and with (A.ii) prior Dynabead stimulation. (B) Tilescan images show whole slices without (B.i) and (B.ii) Dynabead activation. Representative images shown of n=3 slices per patient.

Tumour slices were visualised with single frame (Figure 5.2A) and whole slice scan (Figure 5.2B) images. Staining shows autologous T cells (Cell Trace Far Red, red), stromal regions (fibronectin, yellow), target cells (5T4, green) and nuclei (DAPI, blue). Co-culture with autologous untransduced T cells was performed with (Figure 5.2A.ii and 5.2B.ii) and without (Figure 5.2A.i and 5.2B.i) prior Dynabead activation. T cells which were not activated prior to co-culture were not present in the tumour slice structure following washing, fixation and staining.

5.2.3 Autologous CAR-T Cell Treatment of PDAC Tumour Slices - Patient 1

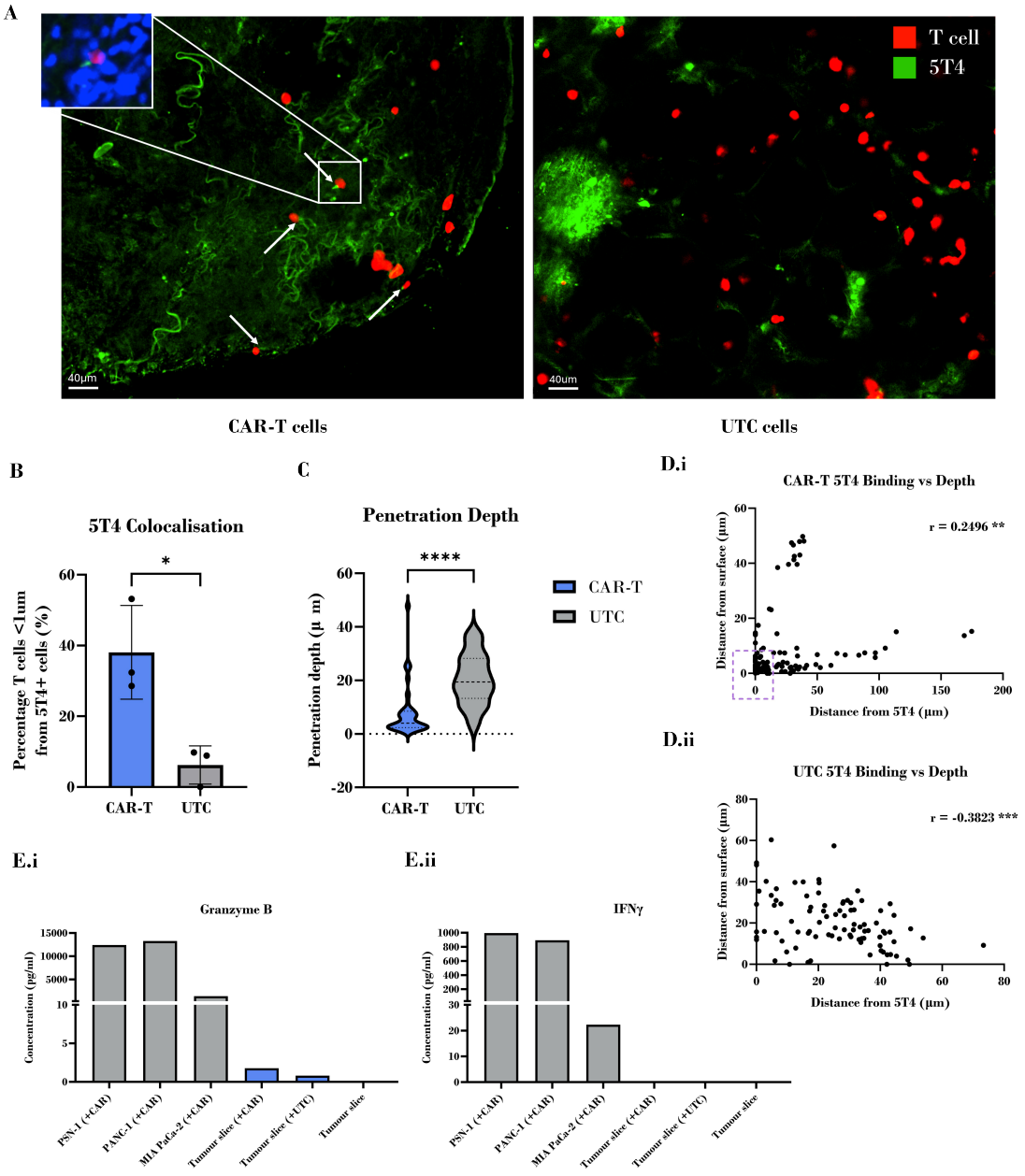


Figure 5.3: Patient 1 autologous CAR-T cells cultured *ex vivo* with live tumour slices. (A) CAR-T cells (left) and UTC (right) cells (red) and 5T4 (green) in patient tumour slices. (B) Colocalisation of CAR-T and UTC with 5T4 target cells analysed using unpaired t-test. (C) Penetration depth of UTC and CAR-T cells into tumour slices analysed using Mann-Whitney test. (D) Correlation of depth and target engagement of CAR (D.i) and UTC (D.ii) cells calculated using Pearson's R. (E) Analysis of Granzyme B (E.i) and IFNγ (E.ii) in slice supernatant compared with cell line co-culture. n=3 slices were used for IF and n=1 slice was used for supernatant analysis.$^{****}p < 0.0001$, $^{***}p < 0.001$, $^{**}p < 0.01$, $^{*}p < 0.05$.

Autologous patient CAR-T cells and matched untransduced T cells were generated using the protocol detailed in Chapter 2. Patient 1 refers to the first autologous CAR-T cell sample applied to tumour slices, this corresponds to samples P015 and p003 (Table 2.1). The transduction efficiency for each autologous CAR-T cell batch is detailed in Appendix C.1.

Figure 5.3A shows the colocalisation of CAR-T cells (left) with $5T4^+$ target cells and a lack of colocalisation of UTC cells (right) with $5T4^+$ cells. Panel includes markers for target cells (5T4, green), CAR-T cells (Cell Trace Far Red, red) and nuclei (DAPI, blue). Fibronectin was also incorporated into the staining panel but was not included in images to improve the clarity of the interactions between T cells and target cells.

Colocalisation and depth analysis were performed as in the methods developed in Figure 5.1. CAR-T cells colocalised (Figure 5.3B) with $5T4^+$ cells significantly more than UTC cells. Colocalisation was defined as a distance of less than 1 µm from each T cell to the nearest $5T4^+$ cell. Depth (Figure 5.3C) measurements indicated that CAR-T cells were significantly closer to the T cell-rich surface of the tumour slice than UTC cells. In order to understand the difference in depth, matched data for each T cell was used to evaluate the correlation (Figure 5.3D) between the depth of the cell within the slice and its proximity to the nearest $5T4^+$ target cell. Pearson's R (0.2496 **) indicated that CAR-T cell (Figure 5.3D.i) proximity to 5T4 was significantly positively correlated with proximity to the T cell-rich surface while UTC cell (Figure 5.3D.ii) proximity to the nearest $5T4^+$ cell was significantly negatively correlated with proximity to the T cell-rich surface. The dashed box on the origin of Figure 5.3D.i indicates the substantial population of CAR-T cells both in contact with 5T4 and at the surface of the slice. This population was not seen in the UTC cells.

Having shown that autologous CAR-T cells were able to engage with target cells in tumour slices, we then investigated their release of cytokines associated with cytotoxicity in this setting. To interrogate this, co-culture was carried out for 48 h, in line with *in vitro* experimental timelines used in Chapter 4. Media was taken after

24 h and assessed for levels of IFNγ and Granzyme B using the CBA assay used previously in Chapter 4. The comparison of IFNγ (Figure 5.3E.i) and granzyme B (Figure 5.3D.ii) levels with those from previous cell line co-culture showed that negligible IFNγ or Granzyme B could be detected from the tumour slice co-culture. This indicated that there was limited CAR-T cell effector function in this setting.

5.2.4 Autologous CAR-T Cell Treatment of PDAC Tumour Slices - Patient 2

Patient 2 refers to the second autologous CAR-T cell sample applied to tumour slices; this corresponds to samples P018 and p005 (Table 2.1).

IF was performed as previously (Figure 5.4A); however, a lack of 5T4 in both CAR-T and UTC co-culture tumour slices prevented measurement of colocalisation. Depth (Figure 5.4B) was calculated for both CAR-T and UTC cells. CAR-T cells were found to be significantly closer to the tumour slice surface than UTC cells despite the lack of target engagement seen previously. No correlation could be calculated due to lack of colocalisation measurement. IHC (Figure 5.4C) validated a lack of 5T4 expression in line with the IF tumour slices. Caspase activation (Figure 5.4D) was also negative in both CAR-T (left) and UTC (right) co-culture conditions.

5. Ex Vivo Efficacy of Autologous Anti-5T4 CAR-T Cells Cultured with Organotypic Tumour Slices

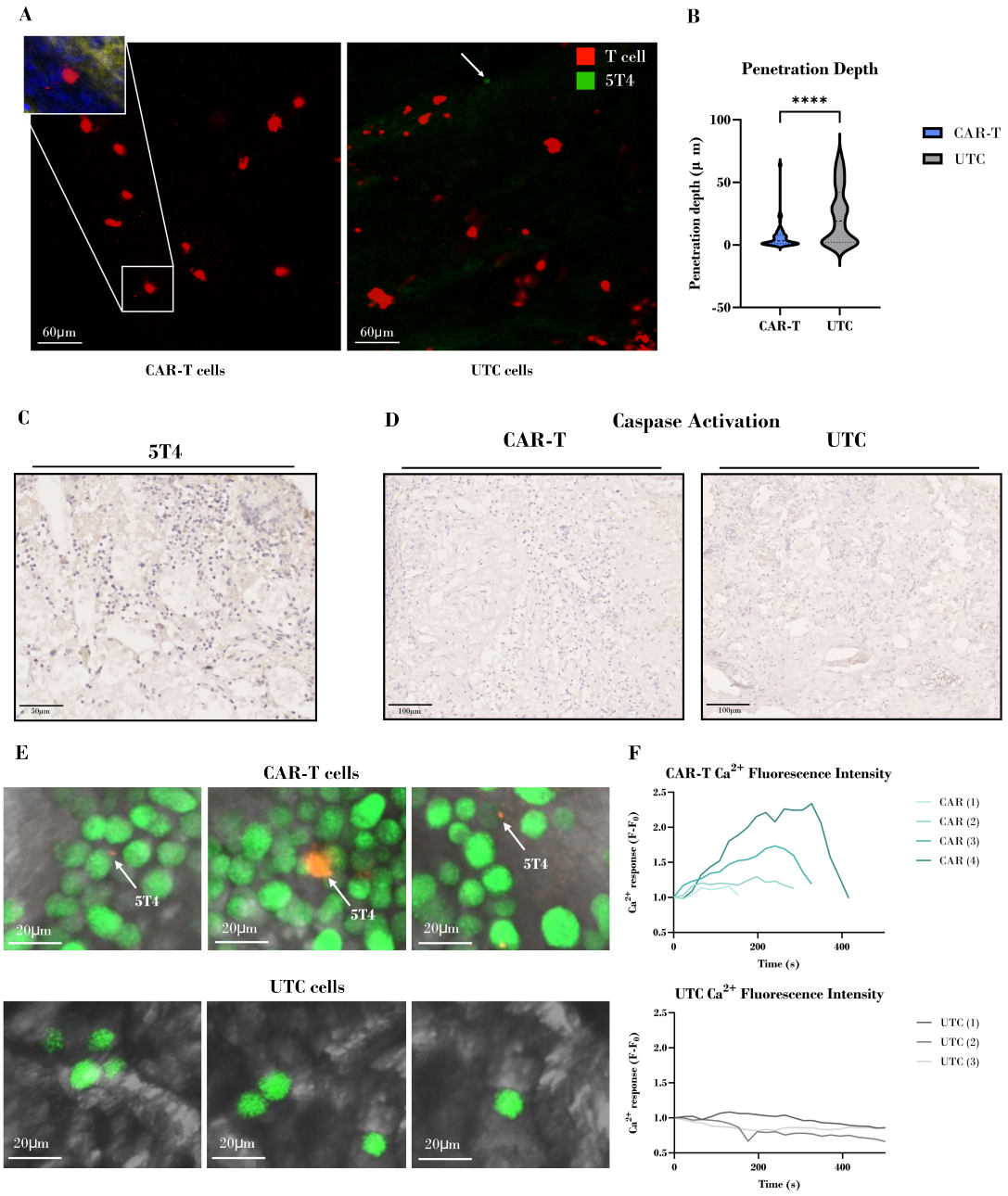


Figure 5.4: Patient 2 autologous CAR-T cells cultured *ex vivo* with live tumour slices. (A) Immunofluorescence images of CAR transduced cells (left) and UTC (right) cells and 5T4 (green) in patient tumour slices. (B) Penetration depth of CAR-T and UTC cells in tumour slices analysed using Mann Whitney test. (C) Images of 5T4 IHC staining in tumour slice and (D) cleaved caspase 3 staining of slices cultured with CAR-T (left) or UTC (right) cells for 48 h. (E) Live imaging of Fluo-4 tagged CAR-T and UTC cells (green) interacting with 5T4 (orange). (F) Traces of calcium flux over time of CAR-T and UTC cells (green) in contact with 5T4 positive cells (orange). For IF n=3 slices were used, n=1 slices were used for IHC and n=1 slices were used for live imaging.$^{****}p < 0.0001$.

In order to assess whether the previous lack of effector function seen in autologous patient 1 was as a result of a lack of CAR-T cell activation, live imaging of CAR-T cell calcium influx was introduced into the workflow. Live imaging (Figure 5.4E) was performed with Fluo-4 calcium dye (green) measuring T-cell calcium flux. 5T4 staining (orange) was carried out prior to live imaging to visualise the initial CAR-T cell contact with $5T4^+$ target cells. Imaging was carried out using a water immersion lens in a droplet of media suspended on top of the slice. Images were captured as CAR-T cells were pipetted into the media droplet and hit the surface of the slice. While there was no 5T4 present in the slice with UTC cells added, CAR-T cell calcium flux was analysed for cells in contact with $5T4^+$ cells. For each CAR-T cell making sustained contact with a $5T4^+$ cell, fluorescence intensity was measured over time; the flux was defined by the intensity at each timepoint divided by the intensity when the T cell was first visible. CAR-T cells displayed variable but visible flux (Figure 5.4F, top) when in contact with $5T4^+$ cells indicating that the cells were activated. The UTC cells did not show the same calcium flux indicating a lack of activation (Figure 5.4F, bottom).

5.2.5 Autologous CAR-T Cell Treatment of Cholangiocarcinoma Tumour Slices - Patient 3

Patient 3 refers to the third autologous CAR-T cell sample applied to tumour slices, this corresponds to samples C001 and p009 (Table 2.1). This was the only autologous culture performed with a cholangiocarcinoma sample. Tumour slices were analysed using the same techniques as previously although live imaging could not be performed due to facility availability.

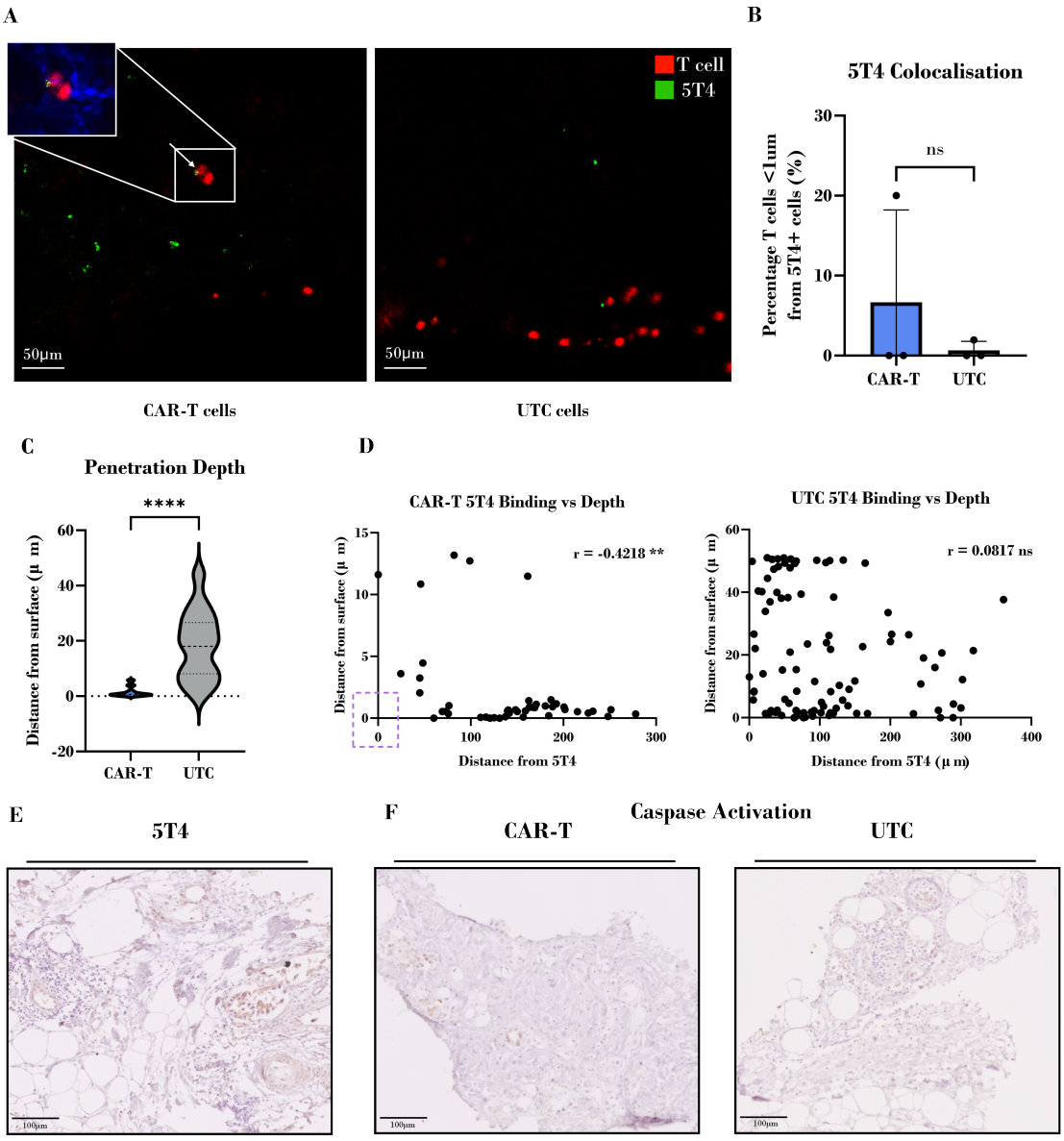


Figure 5.5: Patient 3 autologous CAR-T cells cultured *ex vivo* with live tumour slices. (A) CAR transduced cells (left) and untransduced control (right) T cells and 5T4 (green) in patient tumour slices. (B) Colocalisation of CAR-T and UTC with 5T4 target cells (defined as proximity of <1µm) analysed with unpaired t-test. (C) Penetration depth of autologous UTC and CAR-T cells into tumour slices analysed with Mann-Whitney test. (D) Correlation between depth and target engagement in CAR (left) and UTC (right) conditions calculated using Pearson's R. IHC staining of 5T4 (E) and cleaved caspase 3 (F) in tumour slices co-cultured with CAR-T cells (left) or UTC cells (right) for 48 h. N=3 slices were used for IF and n=2 for IHC. $^{****}p < 0.0001$, $^{**}p < 0.01$.

IF (Figure 5.5A) visualised colocalisation of CAR-T cells (left) and UTC cells (right) with $5T4^+$ target cells. Minimal 5T4 expression was seen throughout the slices. Quantification of this colocalisation (Figure 5.5B) showed a non-significant

increase in CAR-T cell colocalisation over UTC, indicating a lack of significant target recognition. Depth analysis (Figure 5.5C) showed that CAR-T cells were significantly closer to the T cell-rich slice surface than UTC cells. Correlation analysis of depth and proximity to 5T4 (Figure 5.5D) showed a significantly negative correlation (r = -0.4218) for CAR-T cells (top) and no significant correlation for UTC cells (bottom). The dashed box indicates a lack of CAR-T cells at the origin unlike those seen Patient 1.

5T4 staining with IHC showed sections of positive staining among larger areas of weak or negative staining (Figure 5.5E). This indicated that there were small regions of high 5T4 expression in a tumour otherwise lacking 5T4. IHC for cleaved caspase (Figure 5.5F) showed weakly positive signals in both CAR-T (left) and UTC (right) but no discernable difference between the conditions.

5.2.6 Effect of Tumour Slice Conditioning on CAR-T Cell Efficacy

A lack of CAR-T cell-mediated cytotoxicity was observed *ex vivo* despite evidence of target engagement and T cell activation, prompting exploration of various factors which could contribute to the suppression of effector function. Conditioned media was collected from slices where possible and used to assess the impact of PDAC tumour-derived soluble factors on CAR-T cell function. Due to the low volumes of TCM collected from each tumour, assays could only be carried out with a single CAR-T cell donor, technical replicates were used to calculate statistics.

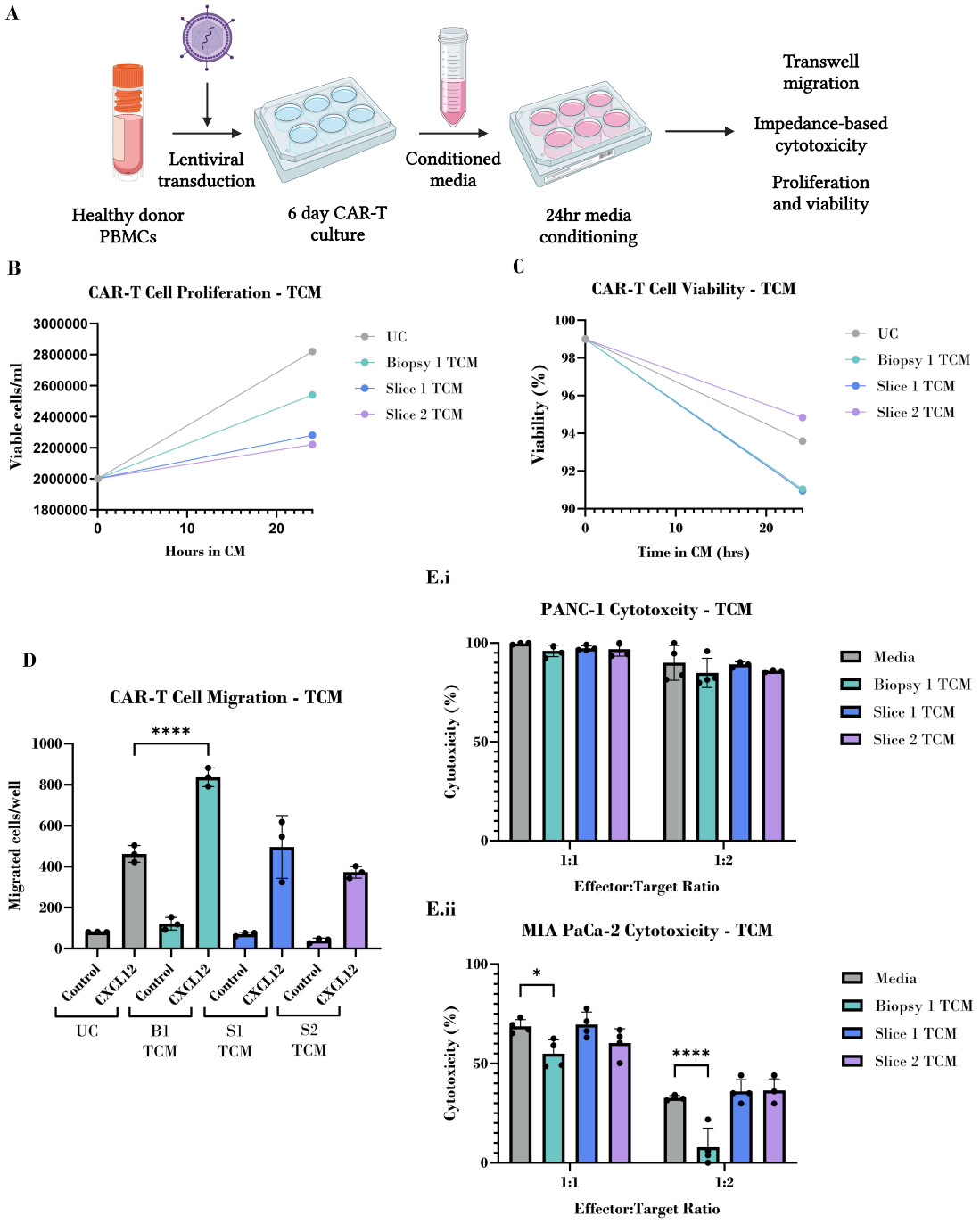


Figure 5.6: The *in vitro* effects of tumour conditioned media (TCM) on CAR-T cell growth and functionality. (A) Workflow indicating TCM exposure timeframe and stage in CAR-T cell generation process. (B) Expansion and (C) viability of CAR-T cells exposed to TCM. Viability and expansion measured pre- and post- TCM exposure. (D) CAR-T cell migration measured by flow cytometry and (E) cytotoxicity measured by xCELLigence impedance on Day 7. Co-culture with PANC-1 E.i) and MIA PaCa-2 (E.ii) cells. Migration was analysed using 1-way ANOVA and cytotoxicity was measured using 2-way ANOVA both with Tukey's multiple comparisons test. For all analyses n=3 tumour samples were used to generate TCM and cultured with n=1 healthy PBMC donor-derived CAR-T cells. $^{****}p < 0.0001$, $^{*}p < 0.05$.

5. Ex Vivo Efficacy of Autologous Anti-5T4 CAR-T Cells Cultured with Organotypic Tumour Slices

The workflow described in Figure 5.6A combined the normal CAR-T cell generation protocol with a 24 h conditioned media exposure prior to functional analysis. CAR-T cell viable cell count (Figure 5.6B) was calculated before and after TCM exposure, showing a reduction in the expansion of CAR-T cells when exposed to conditioned media. The unconditioned (UC) media used was complete tumour slice media (Table 2.13) in order to rule out differences in expansion due to the different formulations of CAR-T cell and tumour slice media. Percentage viability before and after TCM exposure (Figure 5.6C) showed that biopsy 1 and slice 1 TCM reduced the percentage viability of CAR-T cells while slice 2 TCM did not. Whilst CAR-T cells cultured with biopsy 1 and slice 1 TCM exhibited reduced viability and cell counts, those cultured with slice 2 TCM exhibited reduced cell count with no impact on viability indicating that, rather than increased levels of cell death, there was merely a reduction in proliferation in this condition.

In vitro migration (Figure 5.6D) was conducted using CXCL12 as the chemoattractant. CXCL12 showed greater migration induction than CXCL10 and was therefore selected following optimisation (Appendix C.2). CAR-T cells conditioned with biopsy 1 TCM showed a significant increase in CXCL12-mediated migration. Cytotoxicity assays with PANC-1 (Figure 5.6E.i) and MIA PaCa-2 (Figure 5.6E.ii) target cells showed no significant difference in CAR-T cell PANC-1 cytotoxicity with exposure to conditioned media but a significant reduction in CAR-T cell MIA PaCa-2 cytotoxicity after exposure to biopsy 1 TCM. As well as varying the target cell type, both 1:1 and 1:2 effector:target ratios were used to increase the window of variation in cytotoxicity.

In order to establish suitable controls for cytokine arrays, cell line conditioned media (CCM) was also used to treat CAR-T cells for 24 h (Appendix C.3). These assays used media harvested from confluent flasks of PSN-1, PANC-1 and MIA PaCa-2 cell lines. All CCM conditions suppressed CAR-T cell expansion (Appendix C.3B) but none reduced viability (Appendix C.3C) when compared to cell line media. CXCL12-mediated migration (Appendix C.3D) was significantly elevated in CAR-T cells exposed to PANC-1 TCM only. CAR-T cell cytotoxicity was reduced for

both PANC-1 (Appendix C.3E.i) and MIA PaCa-2 (Appendix C.3E.ii) cell killing following exposure to MIA PaCa-2 conditioned media. Due to these results, the cytokine array was carried out using PSN-1 media (CCM) as a negative control as it had no effect on CAR-T cell functionality.

5.2.7 RNAseq Analysis of Differentially Expressed Receptors for Soluble Factors in PDAC Tumour T Cells

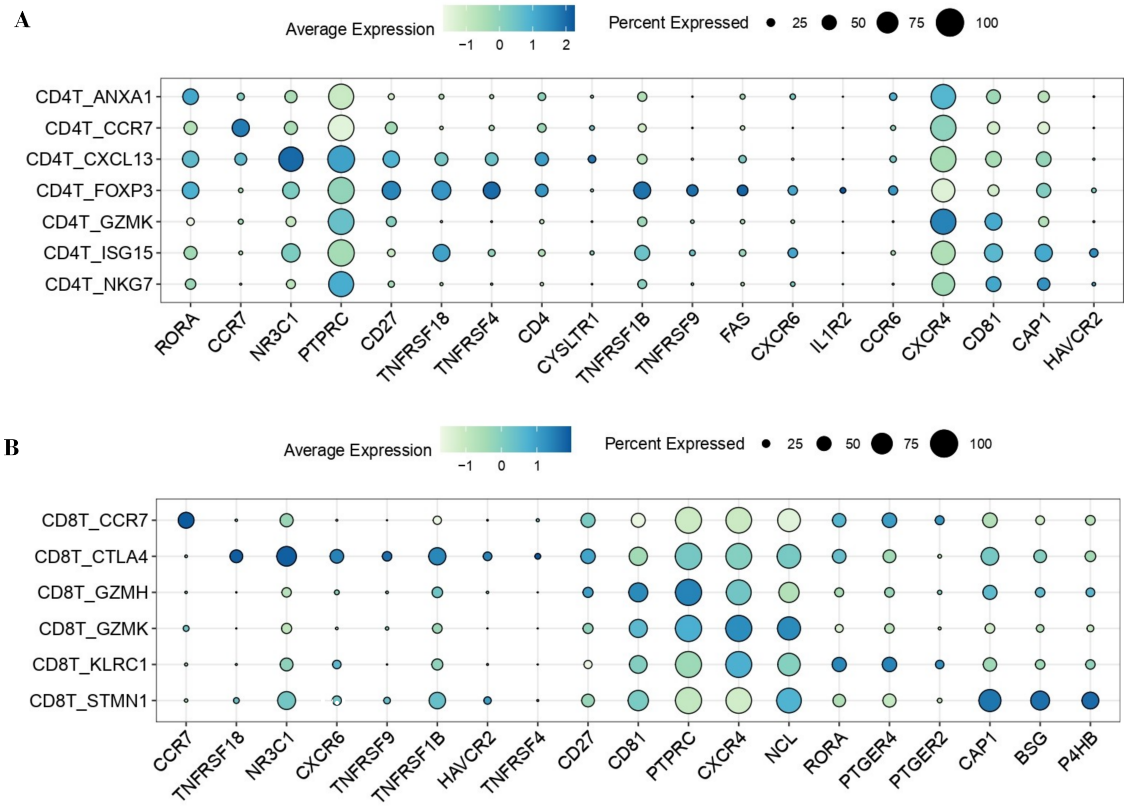


Figure 5.7: Differential expression of receptors for soluble factors in PDAC patients. Differentially expressed receptors for (A) CD4 and (B) CD8 T cells in PDAC tumours and healthy adjacent tissue obtained from single cell RNAseq data. T cells are segemented into subsets using defining genes from unsupervised clustering. Receptors were filtered for 'secreted signalling' and 'non-protein signalling' using CellChat. Significant genes are shown, calculated from a Wilcoxon rank sum test. Analysis carried out by Constantinos Demetriou.

Given the complexity of soluble factor signalling in the TME, a rationale was needed for the selection of a PDAC-relevant array to analyse TCM samples. Single cell RNAseq data from PDAC tumours was used to interrogate the most differentially

expressed receptors in CD4 (Figure 5.7A) and CD8 (Figure 5.7B) T cells. This provided a basis to understand which factors could prompt T cell signalling and therefore potentially affect function.

For both CD4 and CD8 T cells, common chemokine receptors were among the most differentially expressed, including CXCR4, CXCR6, CCR6, CCR7. Key proteins involved in receptor activation and costimulation such as CD45 (PTPRC), CD4, CD27, OX40, 4-1BB, GITR and CD81 were significantly differentially expressed in both CD4 and CD8 cells as well as key regulatory proteins such as the glucocorticoid receptor GR (NR3C1) and the checkpoint receptor TIM3 (HAVCR2). Along with the primarily activatory members of the TNF superfamily mentioned previously, TNFR2 (TNFRSF1B) was significantly upregulated in both regulatory CD4 populations and exhausted CD8 cells, aligning with literature reports of its association with Treg function and CD8 T cell exhaustion (Y. Gao et al. 2023). Fas, IL1R2 and the cysteinyl leukotriene receptor CysLTR1 were all differentially expressed solely in CD4 T cells while nucleolin (NCL), prostaglandin receptors PTGR2/4, basigin (BSG) and protein disulphide isomerase (P4HB) were solely differentially expressed in CD8 T cells.

The ligands for the receptors identified in RNAseq analysis formed the basis for selecting a panel of microenvironmental signalling proteins for use in the cytokine array.

5.2.8 Tumour Conditioned Media Cytokine Array - Part I

The Ray Biotech C1000 cytokine array (comprised of C6 and C7 components) was selected based upon its broad range of analytes including cytokines, chemokines and other soluble factors. Relative intensities of each analyte were calculated using the negative control for background subtraction and the positive control to normalise. This positive control normalisation allowed comparison between multiple arrays.

A

	C1	C2	C3	C4	C5	C6	C7	C8	C9	C10	C11	C12	C13	C14
L1-2	Positive control	Positive control	Negative control	Negative control	Blank	Angiogenin	BDNF	CXCL13	BMP-4	BMP-6	CCL23	CNTF	EGF	CCL11
L3-4	CCL24	CCL26	FGF-6	FGF-7	Flt-3 ligand	CX3CL1	CXCL6	GDNF	GM-CSF	CCL1	IFN-gamma	IGFBP-1	IGFBP-2	IGFBP-4
L5-6	IGF-1	IL-10	IL-13	IL-15	IL-16	IL-1 F1	IL-1 F2	IL-1 F3	Il-2	Il-3	Il-4	IL-5	IL-6	Il-7
L7-8	Leptin	LIGHT	CCL2	CCL8	CCL7	CCL13	M-CSF	CCL22	CXCL9	CCL15	CCL20	CXCL7	NT-3	CCL18
L9-10	PDGF-BB	RANTES	SCF	SDF-1 alpha	CCL17	TGF-beta 1	TGF-beta 3	TNF alpha	TNF beta	Blank	Blank	Blank	Blank	Positive control

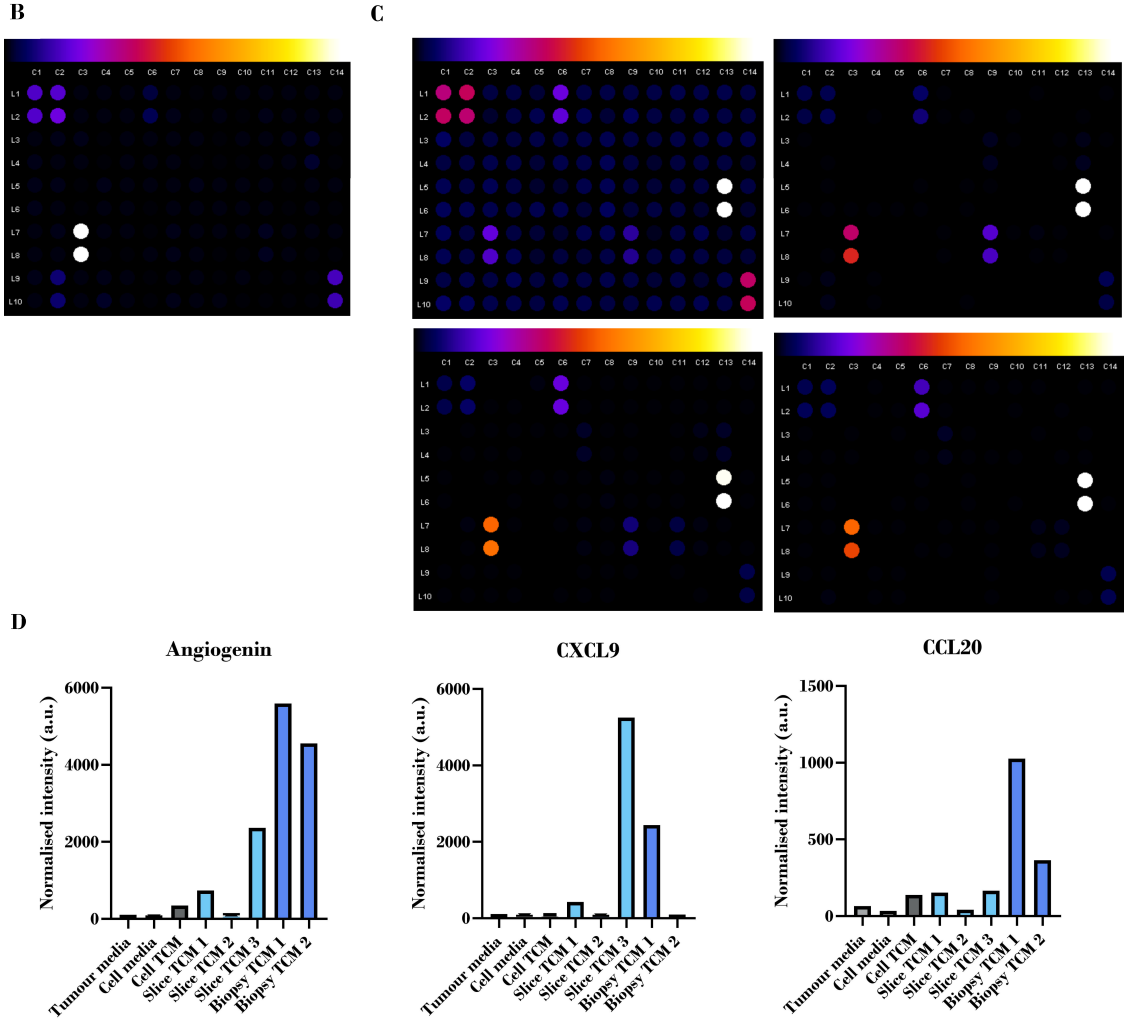


Figure 5.8: Cytokine array of tumour and cell line conditioned media part I. (A) Layout of C6 cytokine array. Heatmaps generated from array images of (B) cell line and (C) tumour slice conditioned media. Slice TCM 1 and 3, Biopsy TCM 1 and 2 shown. (D) Relative expression of highly expressed factors in Biopsy 1 TCM (known to suppress T cell cytotoxicity) without expression in CCM, cell line media, tumour slice media, slice 1 TCM or slice 2 TCM which do not suppress CAR-T cell cytotoxicity. N=2 technical replicates per media sample.

The array layout (Figure 5.8A) used duplicates of each analyte in the C6 half of the array set. The cell line conditioned media array (Figure 5.8B) was used to rule out suppressive cytokines due to the previous lack of suppression demonstrated by Appendix C.3. Unconditioned media samples of both cell line and tumour slice media were also used (not pictured) as negative controls to confirm that no analytes were present in basal media formulations.

Tumour conditioned media arrays (Figure 5.8C) were quantified and relative levels of factors were compared between samples. Factors expressed highly in biopsy 1 conditioned media, but not in cell line, slice 1, or slice 2 samples, were highlighted (Figure 5.8D) due to their potential to contribute to the CAR-T cell suppression seen in Figure 5.6. In the C6 portion of the array kit these were angiogenin, CXCL9 and CCL20.

Although IL-6 was elevated in slice 2 TCM as well as biopsy 1 TCM (and therefore would not otherwise have been considered), the high levels detected across the media samples (Appendix C.5A) led to quantification of IL-6 concentration using an ELISA (Appendix C.5B). The impact on *in vitro* cytotoxicity was assessed using concentrations detected in the ELISA (Appendix C.5C). Even at the highest TCM-relevant concentration, no significant difference was seen in CAR-T cell cytotoxicity.

5.2.9 Tumour Conditioned Media Cytokine Array - Part II

The C7 half of the array set was analysed as previously. Figure 5.9A shows the duplicate analytes present in each array. Cell line conditioned media (Figure 5.9B) and tumour conditioned media (Figure 5.9C) heatmap plots show relative expression of each analyte with positive and negative controls. The mostly highly expressed factors present in biopsy 1 TCM but absent in cell line, slice 1 and slice 2 TCM media samples were highlighted (Figure 5.9D) for further investigation. In the C7 portion of the array these were CXCL5, adiponectin, hepatocyte growth factor (HGF) and osteoprotegerin (OPG).

A

	C1	C2	C3	C4	C5	C6	C7	C8	C9	C10	C11	C12	C13	C14
L1-2	Positive control	Positive control	Negative control	Negative control	Blank	Adiponectin	AgRP	ANGPT2	AR	Axl	bFGF	beta-NGF	BTC	CCL28
L3-4	CCL27	Dtk	EGFR	CXCL5	Fas	FGF-4	FGF-9	G-CSF	GITR	GITR ligand	GRO a/b/g	GRO alpha	CCL16	HGF
L5-6	ICAM-1	ICAM-3	IGFBP-3	IGFBP-6	IGF-1R	IL-1 R4	IL-1 R1	IL-11	IL-12 p40	IL-12 p70	IL-17a	IL-2R alpha	IL-6R	IL-8
L7-8	CXCL11	Lymphotactin	MIF	MIP-1 alpha	MIP-1 beta	MIP-3 beta	MSP alpha/beta	NT4	OPG	OSM	PLGF	gp130	TNFRII	TNFRI
L9-10	CCL25	TIMP-1	TIMP-2	TPO	TRAIL R3	TRAIL R4	uPAR	VEGF-A	VEGF-D	Blank	Blank	Blank	Blank	Positive control

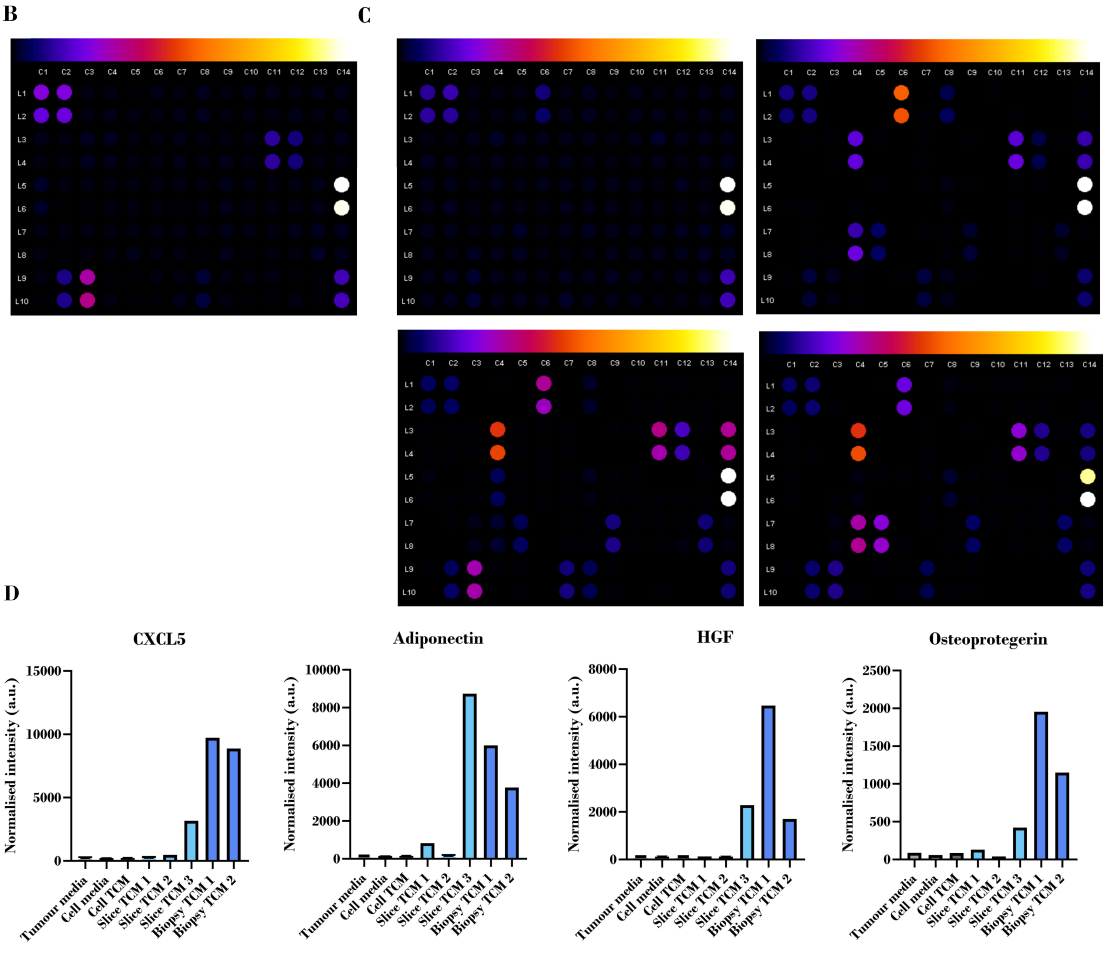


Figure 5.9: Cytokine array of tumour and cell line conditioned media part II. (A) Layout of C7 cytokine array. Heatmaps generated from array images of (B) cell line and (C) tumour slice conditioned media. Slice TCM 1 and 3, Biopsy TCM 1 and 2 shown. (D) Relative expression of highly expressed factors in Biopsy 1 TCM without expression in CCM, cell line media, tumour slice media, slice 1 TCM or slice 2 TCM which do not suppress CAR-T cell cytotoxicity. N=2 technical replicates per media sample.

5.3 Discussion

Autologous CAR-T cell culture with live tumour slices showed that anti-5T4 CAR-T cells can penetrate through the dense stromal matrix and colocalise with $5T4^+$ target cells *ex vivo*. Activation was seen upon target binding evidenced by transient calcium flux detected by live imaging. Despite this engagement and activation, there was no evidence of cytotoxicity either through IFNγ and granzyme B detection in culture media or cleaved caspase IHC of tumour slices following co-culture with CAR-T cells.

Fixed imaging of tumour slices allowed analysis of CAR-T cells moving throughout the structure of the tumour. This allowed observation of T cell localisation and the impact of stromal barriers on their ability to engage with target cells (Salmon et al. 2012; Ene-Obong et al. 2013; Blando et al. 2019). In creating tumour slices, this stromal barrier is compromised, thus exposing tumour cells present on the cut surface of the slice. This surface creates an artificial layer of exposed tumour cells for CAR-T cells to recognise which does not mimic the normal process of extravasation and stromal navigation when the therapy is administered intravenously. Tumour slice encapsulation techniques to combat this and the potential for local implantation are discussed in Chapter 7.

Imaging tumour slices presents challenges including opacity limiting imaging depth and background autofluorescence which is particularly noticeable in stromal structures such as in Figure 5.1. Collagen and other matrix proteins are widely documented to cause this signal (Monici 2005). Spectral unmixing can be used in some cases to minimise this signal, although the function is not available on all microscopes. Where spectral unmixing is not possible, manual thresholding can be used in Imaris to prevent detection of artefacts which may confound analysis due to background fluorescence.

While methods were standardised for the analysis of patient tumour slices, the disparity in target antigen expression in each patient's tumour prevents direct comparison between patients. The inter-patient heterogeneity highlighted in this chapter is a challenge when assessing the efficacy of a therapy with only small numbers of samples but is also vital in assessing the variation in treatment response

likely among a patient population. As well as inter-patient heterogeneity there is also a degree of intra-patient heterogeneity. This is demonstrated by Figure 5.4 where slices used for IF (Figure 5.4A) contained almost no 5T4 but the slice used for live imaging with the CAR-T cells (Figure 5.4E top) showed some 5T4 expression. While this variation is also important in determining how widely distributed the antigen is within the tumour, it also presents challenges in terms of the number of analyses that can be achieved with each sample. In their publication, Kokkinos et al. (2021) culture sections from the top, middle and bottom of a biopsy to account for these differences (Kokkinos et al. 2021). While selection of multiple slices from different regions of the biopsy was generally carried out in this thesis, sample size can prevent this being possible in all assays.

The variation in 5T4 expression between patients as well as the diversity of the tumour structure as also obstacles in determining the exact effector:target ratio when applying CAR-T cells to tumour slices. In their CAR-T cell culture with tumour slices the Donnadieu group uses 1-2x10^6 CAR-T cells per slice (Kantari-Mimoun et al. 2021; Espie et al. 2023) which can be considered as a proxy for a 1:1 ratio. This range roughly aligns with the number of $5T4^+$ cells which can be estimated to be present in a tumour slice using the total number of cells extracted from a biopsy, the number of slices per biopsy and the proportion of $5T4^+$ cells in each biopsy.

Through the tumour slice co-culture, multiple stages of CAR-T cell effector function were investigated including migration through the tumour, target colocalisation, activation, cytokine release, and induction of target cell apoptosis. Patient 1 could be considered to have high 5T4 expression, patient 2 little to no 5T4 and patient 3 had low 5T4. In the high 5T4 tumour, efficient colocalisation of CAR-T cells with $5T4^+$ target cells was evident within 1 h of co-culture. In the low 5T4 tumour there was a trend towards colocalisation but no statistical significance and in the $5T4^-$ tumour this could not be quantified. Notably, in all three of these tumours, CAR-T cells were significantly closer to the surface of the tumour than the UTC cells which migrated further into the tumour. In the high 5T4 tumour this was explained by a significant proportion of the CAR-T cells which were both colocalised with $5T4^+$

cells and at the surface of the tumour (Figure 5.3D), but the same population of CAR-T cells was not present in the other two samples. Given that the CAR-T and UTC cells were identical other than the lentiviral transduction and expression of the CAR, this difference was surprising. One potential explanation could be that the expression of 5T4 was below the detection limit of the IF but sufficient to produce CAR-T cell adhesion and thus prevent further movement through the tissue.

In all tumours there was no evidence of CAR-T cell-mediated cytotoxicity over a 48 h period. Cytotoxicity would not be expected for the 5T4 scarce patient 2 tumour but was surprising in both patient 1 and 3. In patient 1, the lack of IFNγ and Granzyme B at the 24 h time point indicated a lack of effector function. Even when considering the differences in effector cells per unit volume, there should have been no more than a 2-fold reduction in the tumour slice media concentration of cytokines compared to the *in vitro* co-culture media (Figure 5.3E). In patient 3, there was a lack of increase in cleaved caspase staining in the CAR-T cell co-culture compared to UTC. This could have been due to a lack of CAR-T cell effector function or low levels of 5T4 in the tumour (Figure 5.5A/D). Additional complexity arose when analysing patient 3 due to the low levels of transduction achieved with this particular donor (Appendix C.1). The lack of cytotoxicity in this instance was likely due to a combination of the aforementioned factors along with low frequencies of CAR^+ cells.

Autologous CAR-T cell assays showed that anti-5T4 CAR-T cells were able to bind to $5T4^+$ target cells in patient tumours. This binding was also demonstrated to cause a calcium flux. In future experiments it would be useful to use a positive control for live imaging such as the addition of PMA and ionomycin (Chatila et al. 1989) to provide an indiscriminate T cell activation response during live imaging. Using a positive control known to induce robust activation would allow assessment of the maximum amount of flux produced by activation, and therefore whether the flux seen upon localisation with $5T4^+$ target would be sufficient to trigger degranulation (Benmebarek et al. 2019). Additional assays assessing both CAR-T cell degranulation and cytotoxicity are discussed in Chapter 7.

In the live imaging performed in Figure 5.4D there was sufficient 5T4 in the tumour slice with CAR-T cells to observe the interactions between effector and target. There was no 5T4 detected on the surface of the UTC slice which means that this was not possible with the negative control. Given that UTC cells did not induce *in vitro* cytotoxicity of any $5T4^+$ PDAC cell line or bind to $5T4^+$ cells in tumour slices, it is reasonable to assume that they would not be activated in response to encountering $5T4^+$ tumour cells. Their lack of calcium flux when applied to the slices therefore provides a useful negative control showing that the signal seen when CAR-T cells encounter 5T4 is not seen at baseline.

As well as being useful tools for investigating the efficacy of CAR-T cell therapy in a clinically relevant model, tumour slices provide a platform to interrogate potential challenges associated with CAR-T cell efficacy in solid tumours. One well-documented challenge is the immunosuppressive cytokine milieu in the TME. Exposure to TCM allowed analysis of the potential suppressive effects of these soluble factors. Both slice and biopsy media were used due to the need to collect conditioned media from multiple different experimental setups in order to obtain sufficient samples; the conditions used to generate each sample are detailed in Chapter 2.2.5. Only biopsy 1 TCM had a significant impact on CAR-T cell function, both increasing the CXCL12-mediated migratory capacity and reducing the cytotoxicity of CAR-T cells to MIA PaCa-2 cells. The change in cytotoxicity could have been due to a combination of cytokines and metabolic factors reducing the effector function of the T cells through nutrient depletion and exhaustion (Ju et al. 2024). The increase in migration was potentially due to differences in CXCR4 expression as this receptor binds to CXCL12. The upregulation of chemokine receptors in response to pre-conditioning with chemokine-rich media has been previously documented with mesenchymal stem cells (Pesaresi et al. 2021) and could also apply to T cells. A similar, roughly 2-fold increase in migration, seen after TCM exposure, was also seen after exposure to PANC-1 conditioned media. The reduction in cytotoxicity was less pronounced following CCM exposure than after biopsy 1 TCM conditioning.

To evaluate this suppression with a view to identifying potential causative factors, a semi-quantitative array was selected. In order to identify a panel which would allow detection of cytokines relevant to the PDAC TME, single cell RNAseq data was used to determine the receptors of soluble signals upregulated in resident T cells. Information was also gathered about T cell expressed ligands (Appendix C.4). In terms of potential candidates for the cytokine array, this analysis identified chemokines CXCL12 (CXCR4), CXCL16 (CXCR6), CCL20 (CCR6), and CCL19 (CCR7). Glucocorticoids were also considered due to the upregulation of the GR in both CD4 and CD8 T cells and the complex outcomes of GR signalling on T cell function (Acharya et al. 2020; Taves and Ashwell 2021). The other anti-inflammatory mediators identified were leukotrienes and prostaglandins, although the roles of their receptors in T cell function in cancer is not well characterised. The inflammatory cytokines TNFα, IL-1α and IL-1β were also identified and formed part of the selected panel.

As a result of the varied selection of cytokines, chemokines and inflammatory mediators identified, the RayBiotech C1000 array was chosen. The C1000 cytokine array (composed of C6 and C7 components) revealed the substantial variation in factors present between TCM samples. Given the results of the previous cytotoxicity assay (Figure 5.6E), demonstrating suppressed cytotoxicity with biopsy 1 TCM exposure, factors elevated in this sample were highlighted. Those also high in slice 1 or 2 TCM, cell-conditioned media, cell line or tumour slice basal media were ruled out. From this selection process, factors mediating suppression were identified including the cytokines CXCL9, CXCL5, CCL20 and HGF. CXCL9 is unlikely to be a negative regulator of T cell efficacy given its well-documented role in T cell recruitment (Kohli, Pillarisetty and T. S. Kim 2022) and ability to augment antitumour immunity when used to armour CAR-T cells (Tian et al. 2022). As mentioned in the introduction to this chapter, CXCL5 is implicated in the recruitment of MDSCs and other protumourigenic cell types and therefore should be investigated further. Given that only CAR-T cells were exposed to the TCM, this mechanism would not be evident; however, CXCL5 has also been shown

to actively suppress T cell migration in some settings (Tu et al. 2025). CCL20 is a known chemoattractant with known high expression in PDAC (Kadomoto, Izumi and Mizokami 2020). As well as contributing to the metastatic potential of tumour cells, CCL20 is known to recruit Tregs (D. Wang et al. 2019; Rutihinda et al. 2021) - a role supported by the high expression shown on $CD4^+$ Tregs in the RNAseq analysis. Finally, HGF is known to cause CD8 T cell apoptosis in the liver through ligation of its receptor c-Met which subsequently binds to and activates Fas (Q. Chen et al. 2023). The impact of HGF in PDAC and its effects on therapeutic response are widely discussed (Rizwani, A. E. Allen and Trevino 2015; Pothula et al. 2020; Modica et al. 2021) but its role in T cell apoptosis induction has not been studied in this setting.

Adipokines and pro-angiogenic factors were similarly identified in the array. As discussed, adiponectin is known to be highly expressed in PDAC, but its effect on T cell function is not clear. In contrast, osteoprotegerin has been identified to interfere with tumor necrosis factor-related apoptosis-inducing ligand (TRAIL)-induced PDAC tumour cell apoptosis (Kanzaki et al. 2013). OPG is also a proangiogenic factor (Benslimane-Ahmim et al. 2013), a group of molecules whose inhibition has been demonstrated to synergise with checkpoint inhibitors to increase vessel normalisation and prolong T cell infiltration (E. Allen et al. 2017; Teleanu et al. 2019). While at present only vascular endothelial growth factor (VEGF) blocking therapeutics have been FDA approved in combination with checkpoint inhibitors (Huinen et al. 2021) there is the potential to expand to other angiogenic factors - particularly relevant here as VEGF was not as highly elevated in the tumour conditioned media as either angiogenin or osteoprotegerin (Figure 5.9).

While these targets should be investigated further, the array could potentially also have identified absent factors which have contributed to reduced effector function. The most highly concentrated factors are not necessarily those which had the most substantial effect on T cell function, and therefore many other factors detected at lower levels in the media could have been contributing to T cell dysfunction. Moreover, given the interplay of cytokines, chemokines, and metabolites, it is likely

that a combination of factors influenced anti-tumour immunity, even in this simplified setting. Moving forward, it will be important to investigate the selected hits from the array, but also to consider that they are part of a complex biological network.

5.3.1 Conclusions

CAR-T cells were able to recognise and colocalise with $5T4^+$ cells in tumour slices. Contact with $5T4^+$ cells induced calcium flux in CAR-T cells but not UTC cells, indicating activation. No evidence of cytotoxicity was seen in tumour slices co-cultured with CAR-T cells. Further investigation into T cell degranulation and cytotoxicity with live imaging would clarify the extent of CAR-T cell efficacy in this setting. Preconditioning with tumour slice conditioned media both enhanced the CXCL12-induced migration and reduced the cytotoxicity of CAR-T cells. The cytokine array highlighted the potential role of CXCL9, CXCL5, CCL20, HGF, OPG, adiponectin and angiogenin in mediating these effects. These factors should be further investigated to understand their prevalence in PDAC and effect on CAR-T cell function.

"There are only the pursued, the pursuing, the busy and the tired"

F. Scott Fitzgerald

6

Spectral Flow Cytometry for Analysis of Patient and Healthy Donor-Derived CAR-T Cells

6.1 Introduction

6.1.1 Current Knowledge of Donor Fitness Impact on CAR-T Cell Therapy Efficacy

Development of increasingly complex pre-clinical models is an important part of bridging the gap to clinical trials for CAR-T cells. Another factor to address in early-stage testing is the source of PBMCs from which CAR-T cells are derived. Since the first CAR-T cell therapy was approved by the FDA in 2017 (Mitra et al. 2023), studies have observed variations in treatment success as a result of an intrinsic lack of fitness of T cells in subsets of patients (Akce et al. 2018). In 2018, Fraietta et al. (2018) performed genomic, phenotypic and functional profiling of CAR-T cells derived from patients who had variable responses to treatment for CLL. A total of 41 patients with heavily pretreated CLL were given the anti-CD19 CAR-T cell therapy, only 5 of whom were categorised as complete responders. Common factors such as the initial magnitude of CAR-T expansion and persistence were highlighted as correlating with response, but the group also found that memory

cell predominance was important throughout treatment. The frequency of T_{SCM} cells present even prior to *ex vivo* expansion was found to be predictive of clinical response (Fraietta et al. 2018).

These potential biomarkers could be used in pre-screening for CAR-T cell therapy eligibility or used to develop enrichment strategies during *ex vivo* expansion. The latter technique was employed to prevent terminal differentiation in the CAR-T cells of B-cell ALL patients using a phosphoinositide 3-kinase (PI3K)δ inhibitor and vasoactive intestinal peptide (VIP) antagonism to increase the $CD27^+CD28^+$ CAR-T cell fraction (Petersen et al. 2018). Despite the demonstrated importance of T cell phenotype in the clinical outcomes of CAR-T cell therapy, comparisons are rarely made between clinical cohorts and healthy donors. Fraietta et al. (2018) showed superior tumour clearance and survival in a murine leukemia model when mice were treated with healthy donor CAR-T cells compared to even complete responding patient CAR-T cells, but did not perform phenotypic analysis on the healthy cells to investigate the reasons underpinning this difference (Fraietta et al. 2018).

Ledergor et al. (2024) recently performed analysis of MM patient PBMCs, comparing them with those of age-matched osteoarthritis patients. This comparison revealed both an expansion of CD8 effector T cells in the MM group as well as enrichment of non-classical monocytes in MM patient bone marrow thought to contribute to CD4 T cell exhaustion (Ledergor et al. 2024). Chronic inflammation is observed in osteoarthritis meaning that the T cells observed in these patients may not reflect a 'healthy' phenotype (Moulin et al. 2025) but the insights into the heavily pre-treated MM patient PBMCs are still useful when assessing the potential efficacy of CAR-T cell therapy in this group. Given that factors as simple as CD4:CD8 ratio can influence clinical outcomes (Baguet, Larghero and Mebarki 2024), it is important to consider how they may influence the results of preclinical testing using healthy donor PBMCs.

6.1.2 T Cell Exhaustion States

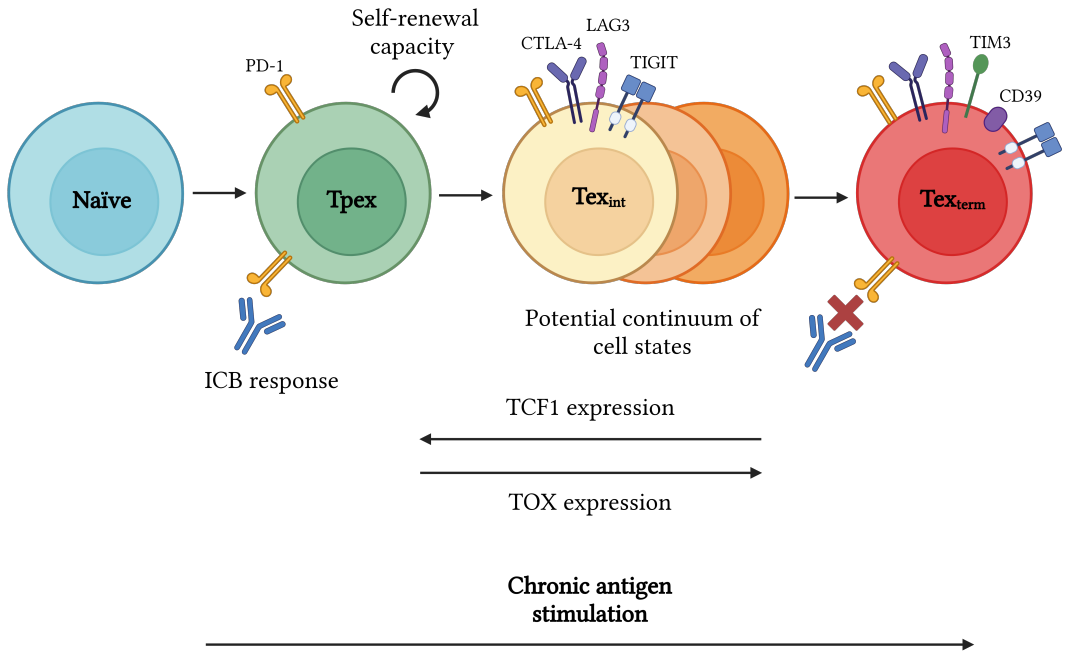


Figure 6.1: The spectrum of CD8 T cell exhaustion. Upon experiencing chronic antigen stimulation, T cells progress through progenitor exhausted (Tpex), intermediate exhausted (Tex_{int}) and terminally exhausted (Tex_{term}) states. These are defined by their expression of transcription factors (including TCF1 and TOX) and inhibitory receptors (PD-1, CTLA-4, TIM3, LAG3, TIGIT, CD39).

While both the need for a sufficient CD4:CD8 ratio (Chapter 3.1.3) and high proportions of T_{CM} and T_{SCM} subsets (Chapter 3.3) have previously been discussed, a lack of exhaustion is also key to successful CAR-T cell antitumour immunity. T cell exhaustion is a term that refers to the process by which effector T cells lose capacity to secrete cytokines and increase expression of inhibitory receptors (Blank et al. 2019). The processes underpinning exhaustion involves repeated TCR stimulation leading to transcriptional upregulation of inhibitory immune checkpoint proteins including PD-1, CTLA-4, TIM3, LAG3 and CD39 (Wherry, Ha et al. 2007). Exhaustion is frequently described as a binary state, but is now known to involve a spectrum of metabolic and epigenetic profiles resulting in a range of cell states (Figure 6.1). These range from highly proliferative stem-like cells known as 'progenitor exhausted' T cells (Tpex), to cells with complete loss of

both effector function and proliferative capacity known as 'terminally exhausted' T cells (Tex_{term}) (Blank et al. 2019).

The concept of exhaustion was first discovered in 1998 in relation to lymphocytic choriomeningitis virus (LCMV), where tetramers were used to track virus-specific CD8 T cells and observe their inability to clear the pathogen (Zajac et al. 1998; Gallimore et al. 1998). Concurrent to this discovery, the labs of Jim Allison and Tasuku Honjo demonstrated roles of CTLA-4 (Leach, Krummel and Allison 1996) and PD-1 (G. J. Freeman et al. 2000) in reducing antitumour immunity. These findings were linked by Baitsch et al. (2011) who demonstrated an 'exhaustion profile' for melanoma-reactive TILs including both CTLA-4 and PD-1 (Baitsch et al. 2011).

Given the prevalence of relapse across indications for CAR-T cell therapy, it is particularly important to understand exhaustion in this context. In both a murine melanoma model (J. Chen et al. 2019) and CLL patient blood (Kong et al. 2021), $TIM3^+PD\text{-}1^+$ CAR-T cell populations associated with exhaustion have been detected. Notably, these cells were enriched in patients who had inferior clinical outcomes. Similar correlations with negative outcomes could be found when assessing proportions of $PD\text{-}1^+$ and $LAG3^+$ CAR-T cells prior to infusion (Fraietta et al. 2018). These patterns have also been observed with transcription factors associated with exhaustion through analysing differentially expressed genes between patients with short and long CAR-T cell persistence times. G. M. Chen et al. (2021) found that factors associated with less persistence included interferon response genes such as *IRF7*, *RSAD2* and *IFIT3* whilst the highest positive predictor was *TCF7* (G. M. Chen et al. 2021).

6.1.3 TCF1 and PD-1 Define a Progenitor Subset of Exhausted T Cells

While the expression of inhibitory receptors associated with T cell exhaustion is predominantly thought to lead to negative outcomes, there is a widespread crossover between these exhaustion-associated genes and genes linked to tumour reactivity (Gros et al. 2015; Thommen et al. 2018). This duality means that it

can be challenging to assess where T cells lie along the scale of exhaustion based solely on the expression of inhibitory receptors.

Looking below the surface at the transcriptional regulation of exhaustion allows a greater understanding of whether surface marker expression indicates a lack of functionality. These factors include the calcineurin-dependent nuclear factor of activated T cells (NFAT), thymocyte selection-associated HMG BOX (TOX) families, eomesodermin (EOMES) and *TCF7*-encoded T cell factor 1 (TCF1).

The expression of TCF1 is exclusively associated with the Tpex population and lost in Tex_{term} cells. The factor has been demonstrated to be important in solid tumour immunity in CD8 T cells, with $\text{TCF1}^{+}\text{PD-1}^{+}$ CD8 TILs associated with improved survival in melanoma (Siddiqui et al. 2019) and predictive of a positive outcome in those undergoing checkpoint therapy (Sade-Feldman et al. 2018). This is potentially due to their increased proliferative response to TCR stimulation when compared to other CD8 T cells expressing inhibitory receptors (Miron et al. 2018). Despite being primarily associated with lymph node-resident CD8 T cells, this marker can also be found in Tpex populations in peripheral blood (Escobar, Mangani and Anderson 2020).

6.1.4 The Role of TCF1 in CD4 T Cells

In CD4 T cells, the role of TCF1 is more unclear. Studies using germline *Tcf7* knockout show increased IFNγ production by Th1 cells but with overall negative regulation of Th1 development, favouring instead Th2 differentiation (Yu, Archna Sharma, Oh et al. 2009). This could be functionally advantageous in a CAR-T cell setting due to GATA3 activity (the master regulator of the Th2 subtype) being positively correlated with *in vivo* CAR-T cell persistence (G. M. Chen et al. 2021). An additional predisposition towards Th17 differentiation is evident in the presence of constitutively active β-catenin signalling (Keerthivasan et al. 2014) but absent in *Tcf7* germline knockouts. In the germline mutated mice, a lack of TCF1 expression increased IL-17A production but overall Th17 lineage commitment was unaffected (Yu, Archna Sharma, Ghosh et al. 2011).

Exhaustion generally is not as well-characterised for CD4 T cells as for their CD8 counterparts. Despite this, it has been shown to be important, particularly in the context of the mixed CD4 and CD8 populations present in CAR-T cell products. In a paper observing the outcomes of varying CD4 T cell clonal abundance in a murine melanoma adoptive transfer model, high levels of inhibitory receptor expression and EOMES were observed in the cells administered at low clonal abundances (Malandro et al. 2016). These cells were less cytotoxic and produced more IL-21; a hallmark of chronic stimulation in CD4 T cells (Elsaesser, Sauer and D. G. Brooks 2009).

In a murine LCMV chronic infection setting, it was found that CD4 T cells show sustained PD-1 expression and higher CTLA-4 than CD8 cells. Additionally, CD4 T cells showed similar increase in transcription factors such as *Eomes*, yet did not display the same *Tcf7* reduction (Crawford et al. 2014), potentially indicating that TCF1 may not play the same role in CD4 T cell progenitor maintenance. This is contradicted by recent work in murine chronic tuberculosis indicating an increase in $TCF1^{-}TIM3^{+}$ CD4 T cell populations over the course of the infection (E. Chang, Cavallo and Behar 2025). In a cancer setting, CD4 T cell terminal exhaustion was found to be characterised by the same TCF1 loss seen in CD8 cells but with the upregulation of CD39 rather than TIM3. These cells were found to have a reduced capacity for cytokine production, higher expression of inhibitory receptors and high TOX expression. Despite this characteristic phenotype, the authors show successful reinvigoration of the population with PD-1 blockade (Balança et al. 2021) - a capacity not normally retained by terminally exhausted populations (Ghoneim et al. 2017).

6.1.5 Suppressive Adenosine Signalling

While chronic antigen stimulation and suppressive cytokines such as TGFβ are the main drivers of exhaustion, adenosine signalling also contributes to this phenotype in a protective mechanism to avoid overactivation (Huang et al. 1997; Lappas, Rieger and Linden 2005; Himer et al. 2010). Adenosine is produced by dephosphorylation of adenosine triphosphate (ATP) mediated by ectonucleotidases including CD39 and CD73 (Taylor, Glover and Maher 2024). Extracellular ATP is upregulated in

the TME due to inflammation, necrosis, apoptosis and hypoxia (Di Virgilio et al. 2018) thus increasing adenosine production rates. Additionally, cancers including PDAC express high levels of both CD39 (Lenzo et al. 2021) and CD73 (Wainberg, Manji et al. 2024) - a factor that is predictive of poor prognosis (X.-R. Wu et al. 2012; Loi et al. 2013; J. Wu et al. 2020; Jacoberger-Foissac et al. 2023). Not only are the enzymes present on the surface of cancer cells and CAFs but they are also upregulated in T cell exhaustion. CD39 is additionally expressed on Tregs, contributing to their immune modulatory function (Deaglio et al. 2007).

T cells express four adenosine receptor (AR) subtypes but their biology is thought to be primarily influenced by their expression of A2AR (Lukashev et al. 2003; Cekic et al. 2013). Activation of this receptor has been shown to limit cytokine production, proliferation and cytotoxicity in adoptively transferred CAR-T cells (Beavis et al. 2017; Fallah-Mehrjardi et al. 2020; G. Liu et al. 2021). These inhibitory effects mean that studying CD73 and CD39 expression is important, not only to understand more about the exhaustion status of CAR-T cells, but also to assess their susceptibility to adenosine-mediated suppression in the TME.

6.1.6 Aims

This chapter aims to use spectral flow cytometry to interrogate the intrinsic differences between CAR-T cells derived from healthy donors and cancer patient PBMCs. Multiple factors have been identified as determinants of response to therapy in clinical cohorts, including memory-related genes and low levels of exhaustion. These factors have not previously been compared between pools of healthy donor and cancer patient-derived CAR-T cells.

A spectral flow panel was selected to assess both changes in T cell subsets and in inhibitory receptors for CD4 and CD8 T cells. TCF1 was incorporated into the panel to provide additional granularity to the exhaustion status of T cells in patient and healthy populations. Given that the Tpex population demonstrates superior responses to checkpoint inhibitor blockade (Im et al. 2016) it was important to understand whether there were differences in this subset and the severely

hypofunctional Tex_{term} population between patient and healthy donor-derived CAR-T cells. The anti-5T4 CAR was incorporated into the panel to allow comparisons of receptor expression in global T cell populations and specifically on transduced cells.

Manual gating using FMO controls was initially used to investigate receptor expression. Dimensionality reduction with Uniform Manifold Approximation and Projection (UMAP) was then used to generate clusters based on global similarity. These methods were used to facilitate a global analysis of individual populations within both patient and healthy donor samples as well as to interrogate the relationships between the populations.

6.2 Results

6.2.1 In Vitro Cytotoxicity of Healthy Donor and Patient-Derived CAR-T Cells

Given the lack of *ex vivo* cytotoxicity of the patient-derived anti-5T4 CAR-T cells, direct comparison between patient-derived and healthy donor-derived CAR-T cells was made *in vitro*. An impedance-based assay (Chapter 2.3.2) was used, as previously, with $5T4^{mid}$ PANC-1 (Figure 6.2A) and $5T4^{lo}$ MIA PaCa-2 (Figure 6.2B) target cells.

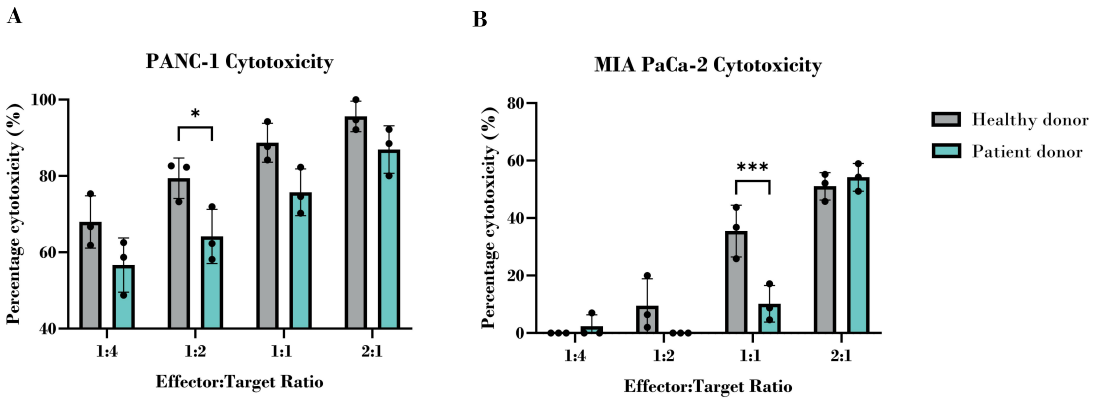


Figure 6.2: The *in vitro* cytotoxicity of healthy donor and patient CAR-T cells. CAR-T cell cytotoxicity in co-culture with PANC-1 (A) and MIA PaCa-2 (B) cells measured by xCELLigence impedance assay. Data analysed using 2-way ANOVA with Tukey's multiple comparisons test. For all analyses n=3 healthy donor and patient donor PBMC samples were used to generate CAR-T cells and n=3 technical replicates were performed per donor. $^{***}p < 0.001$, $^{*}p < 0.05$.

A significant reduction in the cytotoxicity of patient CAR-T cells was seen at effector:target ratios of 1:2 with PANC-1 target cells and 1:1 with MIA PaCa-2 target cells. Trends towards reduced target killing by the patient CAR-T cells were additionally seen across all effector:target ratios with PANC-1 cells and at 1:2 with MIA PaCa-2 cells. No change was seen DEC hTERT co-culture (Appendix D.1. This significant reduction in efficacy in a simplified system prompted the exploration of phenotypic differences between patient-derived and healthy donor-derived CAR-T cells.

6.2.2 Marker Selection in Spectral Flow Cytometry Panel

The BioLegend 27 colour Human T Cell Differentiation and Exhaustion panel was chosen as a starting point for characterising the patient and healthy donor CAR-T cells due to its combination of phenotypic and exhaustion markers. The panel was designed for use with PBMC samples and therefore also contained markers necessary for removing additional cell populations such as myeloid cells and B cells.

Eva Zemlickova (Sr. Strategic Commercial Manager, BioLegend) advised on modifications to the panel to allow the addition of antibodies against the anti-5T4 CAR and TCF1. CAR detection was integrated to determine whether differences seen globally between cohorts could also be seen in the transduced population. The addition of TCF1 (provided by Matthew Jackson, Parkes Lab, Department of Oncology, University of Oxford) allowed investigation of subsets of exhausted T cells, facilitating analysis beyond expression of inhibitory receptors.

Table 6.1 details the markers incorporated into the panel and the function of each marker. These include those commonly used to define broad populations such as CD45 for lymphocytes and CD19 for B cells to specific inhibitory and activatory receptors. Details of antibody epitopes and fluorophores can be found in Table 2.10.

Target	**Function**
Anti-5T4 CAR	Transduced cells expressing the CAR construct targeting the 5T4 protein
TCF-1	Transcription factor facilitating self-renewal in exhausted T cell populations, defines Tpex along with PD-1
CD19	Expressed on all B cells, marker of activation and differentiation
CD27	Co-stimulatory checkpoint molecule expressed on T cells, binds to CD70, marker of T cell memory
CD28	Responsible for second signal necessary for activation alongside TCR ligation, binds CD80/CD86, marker of T cell memory
CD45RA	Found on naïve and T_{SCM} cells, downregulated after activation
HLA-DR	MHCII receptor displayed on antigen presenting cells
CD39	Production of adenosine, associated with T cell exhaustion and highly expressed on Tregs
CD244	Expressed in response to repeated antigen exposure, at low levels activatory and high levels inhibitory
TCR γ/δ	Defines the gamma delta T cell population
CD4	Co-receptor for the TCR used to define the CD4 T cell population
CD8	Co-receptor for the TCR used to define the CD8 T cell population
CD3	Signalling complex associated with the TCR expressed on all T cells
TIM3	Marker of activation, sustained expression leads to T cell exhaustion
CD127	Expressed on naïve and central memory T cells, low expression on Tregs
CCR7	Expressed on naïve, T_{SCM} and T_{CM} cells
CD25	The α chain of the IL-2 receptor, upregulated by T cell activation and used as a marker for Tregs with CD127
CXCR5	Marker of circulation involved in stimulation of B cell antibody production
KLRG1	An inhibitory marker on late differentiated effector and T_{EM} CD8 T cells
CD45	Expressed on all leukocytes involved in signal transduction regulation during haematopoiesis
CTLA4	Marker of activation, sustained expression leads to T cell exhaustion
TIGIT	Marker of activation, sustained expression leads to T cell exhaustion
PD-1	Marker of activation, sustained expression leads to T cell exhaustion
CD57	Marker of terminal differentiation, indicates cytotoxic function
CD14	Expressed on macrophages, involved in detection of bacterial LPS
CD95 (Fas)	Regulator of T cell homeostasis, marker of activation
CD73	Production of immunosuppressive adenosine, highly expressed on Tregs
LAG3	Marker of activation, sustained expression leads to T cell exhaustion
TCR v/α7.2	Expressed on mucosal associated invariant T (MAIT) cells
Live/dead	Reacts with amines on compromised membranes staining dead cells

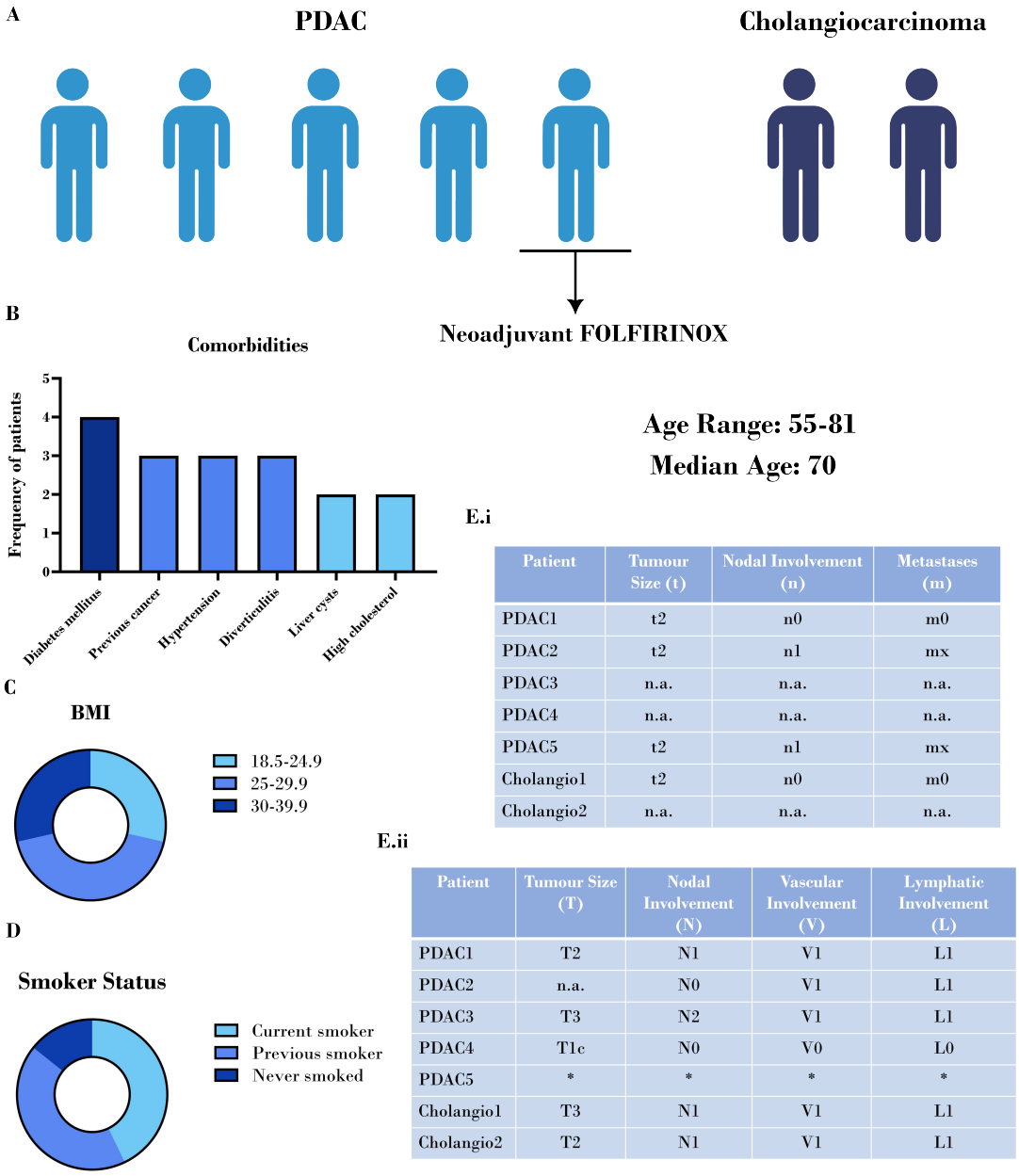
Table 6.1: Markers used in spectral flow cytometry panel and their function.

6.2.3 Demographics of Patient PBMC Donors

PBMC samples were collected from seven independent patients undergoing surgery for cancers of the pancreas and bile duct. Demographic and tumour staging information was obtained in an anonymised format from the TGLU.

Five PDAC and two cancer of the bile duct (CBD) patients were consented for the study (Figure 6.3A) between the ages of 55-81 at admission. Only one PDAC patient was given chemotherapy prior to surgery and PBMC collection (discussed in Chapter 1.1.4). Comorbidities (Figure 6.3B) shared between two or more patients included diabetes mellitus, previous cancer at a different site, hypertension, diverticulitis, liver cysts and high cholesterol. The body mass index (BMI) and self-reported smoker status were also obtained for all patients at pre-operative appointments. BMI (Figure 6.3C) indicated that only 28.5% of patients fell within a healthy range, while a further 28.5% were classed as obese. Self-reported smoker status (Figure 6.3D) indicated that only one patient had never smoked, with 42.9% of patients being current smokers.

Tumour staging was performed prior to surgery by radiology (Figure 6.3E.i) for all patients except PDAC3, PDAC4 and Cholangio2. The tumour size (t), lymph node involvement (n) and metastases (m) were measured according to the standard guidelines associated with HPB tumour staging (see Table 2.3). Following surgery, local staging was repeated by a pathologist (Figure 6.3E.ii) confirming the tumour size (T) and nodal involvement (N). The vascular (V) and lymphatic (L) involvement were also investigated at this stage. PDAC5 was not assessed by a pathologist as the surgery was aborted due to discovery of metastasis.



E.i

Patient	Tumour Size (t)	Nodal Involvement (n)	Metastases (m)
PDAC1	t2	n0	m0
PDAC2	t2	n1	mx
PDAC3	n.a.	n.a.	n.a.
PDAC4	n.a.	n.a.	n.a.
PDAC5	t2	n1	mx
Cholangio1	t2	n0	m0
Cholangio2	n.a.	n.a.	n.a.

E.ii

Patient	Tumour Size (T)	Nodal Involvement (N)	Vascular Involvement (V)	Lymphatic Involvement (L)
PDAC1	T2	N1	V1	L1
PDAC2	n.a.	N0	V1	L1
PDAC3	T3	N2	V1	L1
PDAC4	T1c	N0	V0	L0
PDAC5	*	*	*	*
Cholangio1	T3	N1	V1	L1
Cholangio2	T2	N1	V1	L1

Figure 6.3: CAR-T cell donor patient demographics. (A) Infographic detailing the tumour types and neoadjuvant chemotherapy of patients whose blood was used to generate CAR-T cells for spectral flow cytometry panel. (B) Co-morbidities present in more than one patient, (C) BMI and (D) smoker status at the time of preoperative assessment. (E) Tumour staging performed at (E.i) pre-operative radiology appointment or (E.ii) post-operative pathology. * indicates that surgery was unsuccessful hence no pathology was reported, n.a. indicates a lack of reporting. Tumour size (t pre-operative, T post-operative), nodal involvement (n pre-operative, N post-operative), metastases (m), vascular involvement (V) and lymphatic involvement (V) were reported.

6.2.4 Transduction Efficiency and CD4:CD8 of Patient and Healthy Donor-Derived T Cells

The 29 colour panel described in Table 6.1 was used to stain CAR-T cells generated from the seven patients and seven healthy blood donors. These samples were analysed using the Cytek Aurora 4 laser (UV/V/B/R) flow cytometer. Gating strategies for all following analyses including FMOs are detailed in Appendix D.2.

CAR-T cell transduction efficiency frequently varies between donors so was investigated in both healthy and patient donor T cells (Figure 6.4A.i). Density plots of the $CD3^+$ T cell population show expression of the anti-5T4 CAR indicating successful transduction. The efficiency of transduction was found to be significantly lower in patient T cells than in those of healthy donors (Figure 6.4A.ii).

Due to the importance of CD4:CD8 ratio in clinical outcomes (Baguet, Larghero and Mebarki 2024), this parameter was investigated in the patient and healthy CD3 T cell populations. There were no significant differences found between the total CD4 and CD8 T cell proportions between patient and healthy donor cells (Figure 6.4B) when total $CD3^+$ cells were measured. Additionally, no significant differences were found in the CD4 and CD8 T cell proportions of transduced cells (Figure 6.4C). Given that anti-5T4 CAR-T cell transduction was previously found to be significantly more efficient in CD4 T cells (Figure 3.8B) than CD8 T cells, it was important to confirm a lack of preferential CD4 T cell transduction in this setting.

There was substantial variation in the total proportions of CD4 and CD8 T cells between individual patient samples in contrast to healthy donors who all demonstrated relatively high CD4:CD8. Finally, no significant differences were seen in either the total or CAR^+ CD4:CD8 ratios (Figure 3.8D) between patient and healthy-donor derived T cells.

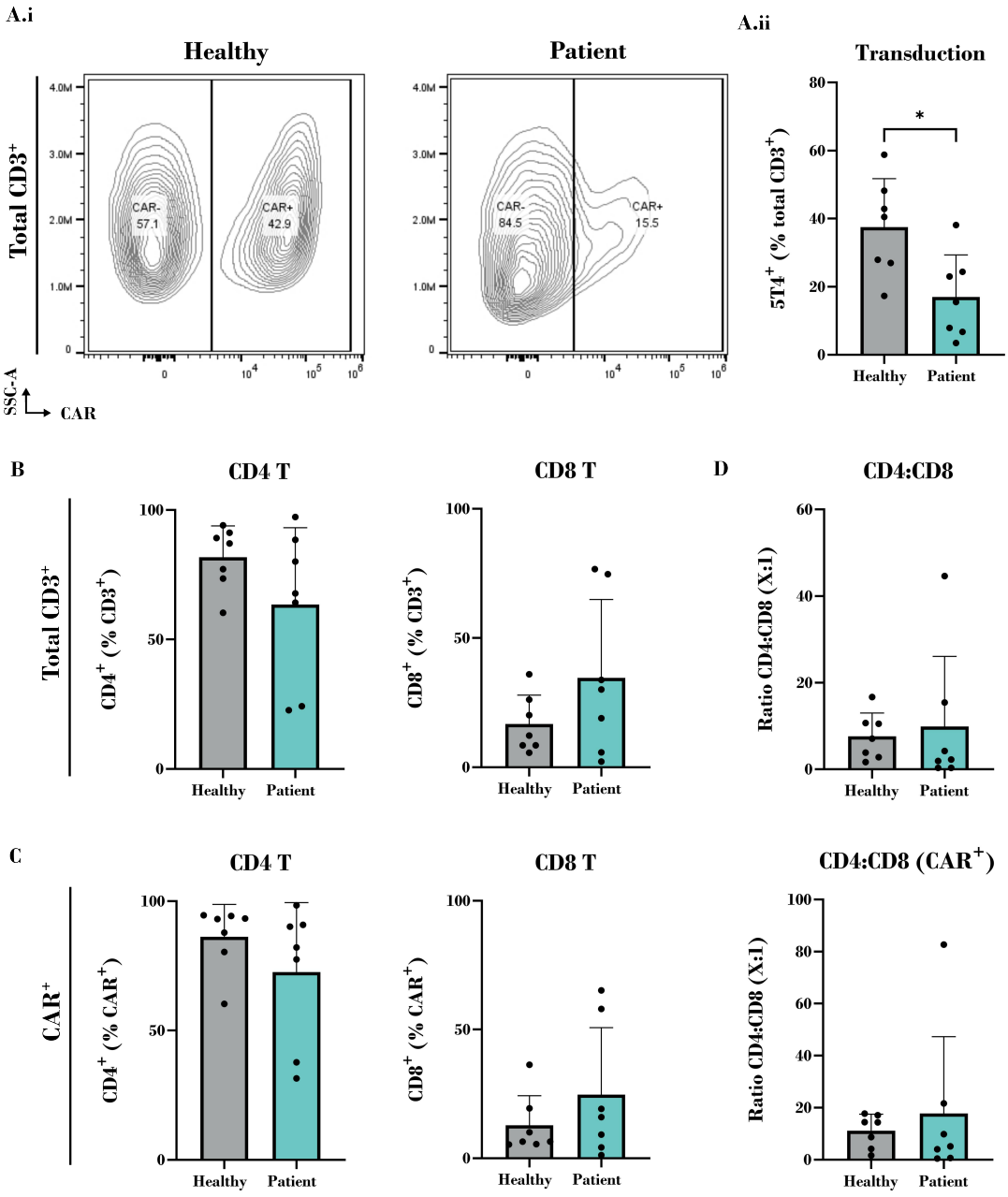


Figure 6.4: CAR transduction efficiency, CD4 and CD8 abundance in healthy and patient donor T cells. (A.i) Representative density plots and (A.ii) quantification of CAR transduction efficiency for healthy (grey) and patient (blue) PBMCs. Density plots show proportions of cells in each population using manual flow cytometry gating. (B) Frequency of CD4 (left) and CD8 (right) T cells among total $CD3^+$ cells. (C) Analysis repeated within the CAR^+ fraction of $CD3^+$ cells. (D) CD4:CD8 ratios calculated for total T cells (top) and transduced cells (bottom). Transduced populations and CD4:CD8 ratios were analysed with Mann Whitney test, all other parameters with unpaired t-test. $^*p < 0.05$. N=7 healthy and patient donor PBMC samples.

6.2.5 T Cell Phenotypic Variation Between Patient and Healthy Donors

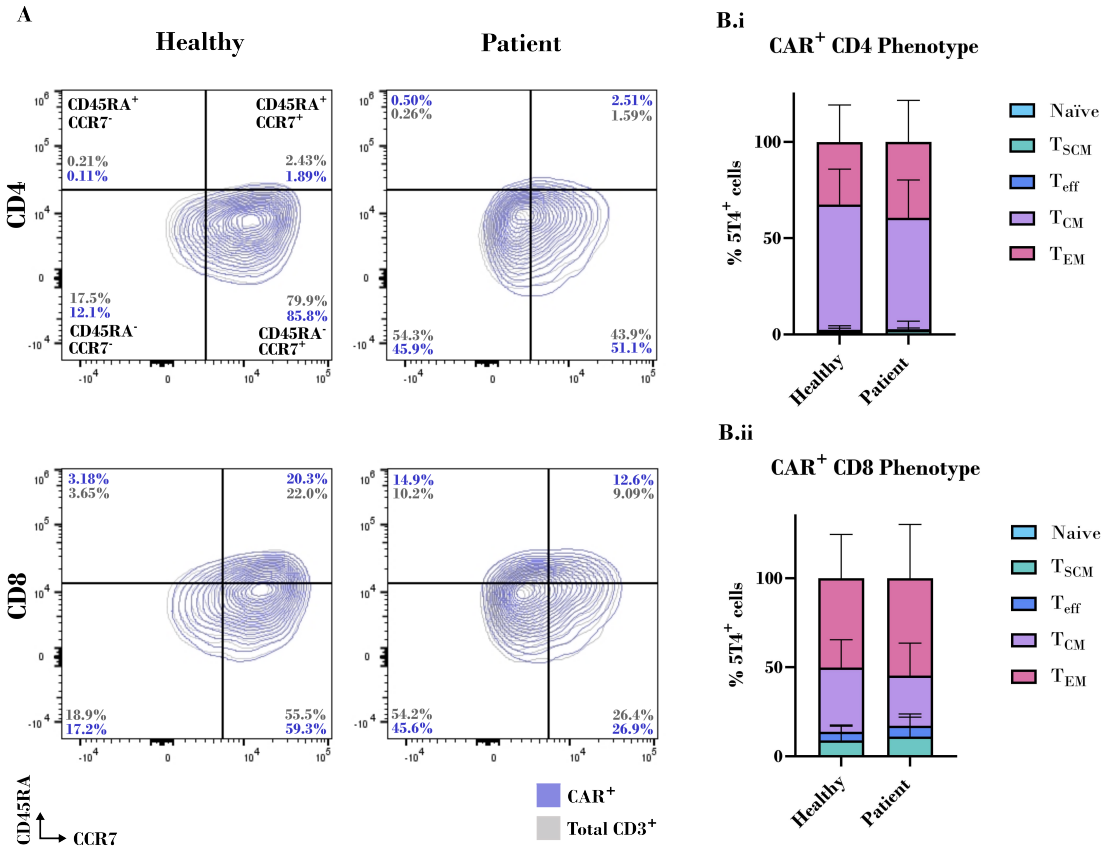


Figure 6.5: Phenotyping healthy and patient donor T cells. (A) Representative density plots of CD4 (top) and CD8 (bottom) T cell phenotype in both total $CD3^+$ cells (grey) and CAR^+ T cells (blue). Density plots show percentages of cells in each population using manual flow cytometry gating. (B) Quantification of phenotype across all healthy and patient donor samples for CD4 (B.i) and CD8 (B.ii) T cells. Mean and standard deviation displayed, data was analysed using 2-way ANOVA with Šidák's multiple comparisons test. N=7 healthy and patient donor PBMC samples.

Within CD4 and CD8 T cell subsets, phenotypic distributions were analysed. These populations were identified by gating initially using CD45RA and CCR7 with CD95 subsequently distinguishing naive and T_{SCM} populations (see Appendix D.2). Figure 6.5A shows density plots of population distributions for total CD4 and CD8 T cells (grey) and CAR^+ fractions (blue). The lack of variation between these two distributions indicates a lack of preferential transduction of any subtypes.

No significant differences were seen between patient and healthy donor CAR-T cell phenotypes in either CD4 (Figure 6.5B.i) or CD8 (Figure 6.5B.ii) T cells.

T_{CM} were the dominant CD4 T cell subset while T_{EM} were dominant among CD8 cells. Higher proportions of both effector T cells and T_{SCM} were seen in CD8 T cells among both donor types with an almost complete absence of both subsets within CD4 T cell populations.

6.2.6 Inhibitory Receptor Expression of Patient and Healthy Donor CAR T Cells

Expression of inhibitory receptors CTLA-4 (Figure 6.6A.i), LAG3 (Figure 6.6A.ii), PD-1 (Figure 6.6A.iii), TIGIT (Figure 6.6A.iv) and TIM3 (Figure 6.6A.v) was evaluated across donor CAR-T cells. Density plots show expression of each inhibitory receptor in CAR^+ CD8 T cells. This expression was confirmed not to vary between total $CD3^+$ cells and the transduced subset as previously.

Both CD4 (Figure 6.6B) and CD8 (Figure 6.6C) CAR T cell expression of each receptor was quantified for all patient and healthy donor samples. Across all inhibitory receptors apart from PD-1 (Figure 6.6B.iii, C.iii), a trend towards higher expression was found in CD8 T cells than in CD4 T cells. LAG3 (Figure 6.6B.ii, C.ii) and TIM3 (Figure 6.6B.v, C.v) were the most highly expressed receptors across both CD4 and CD8 cells. Excluding these, proportions of cells expressing each inhibitory receptor were generally very low.

There were no significant differences in inhibitory receptor expression frequencies between healthy donor and patient CAR-T cells. Only TIM3 showed a trend towards increased expression in patient CAR-T cells across both CD4 and CD8 subsets.

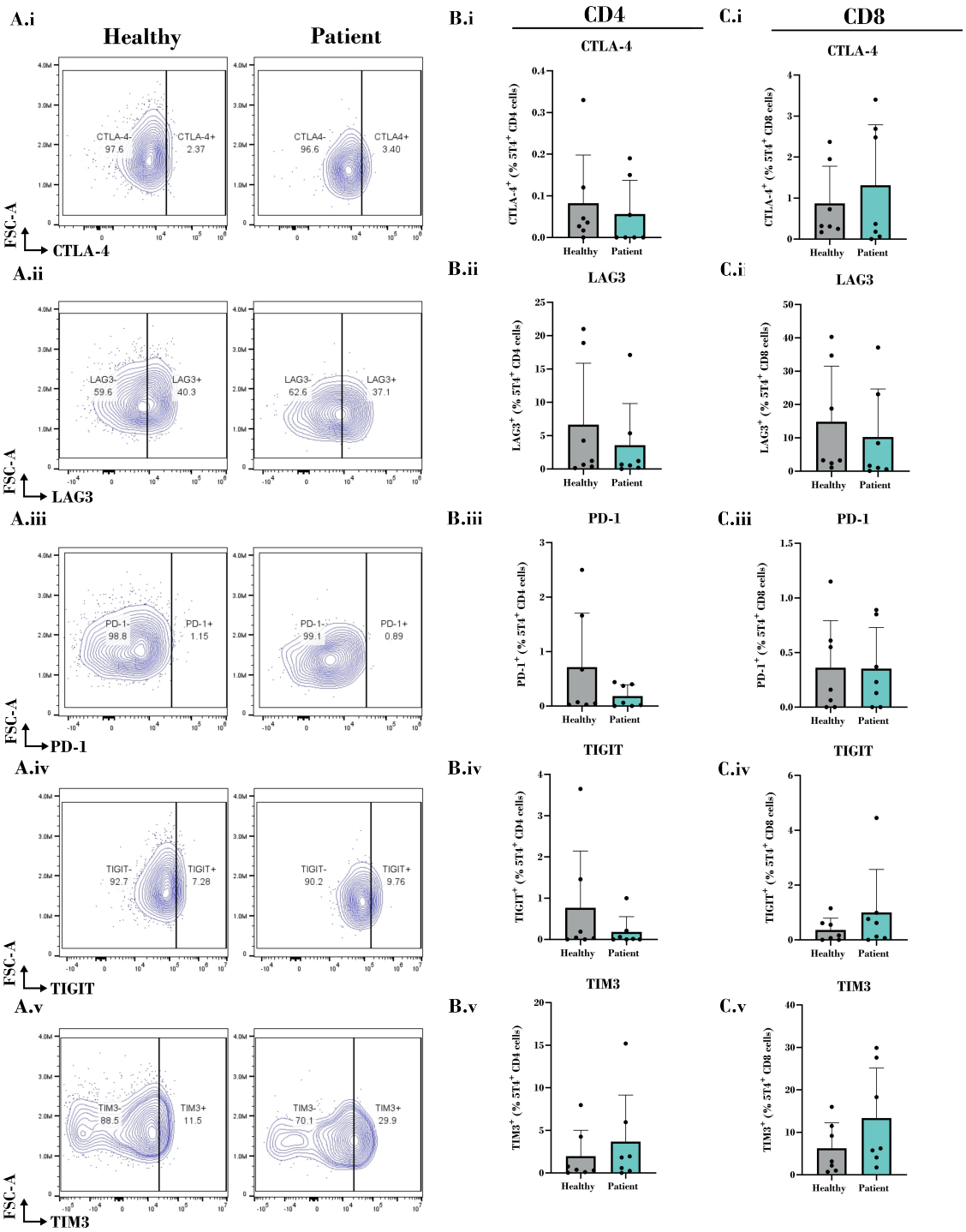


Figure 6.6: Inhibitory receptor expression on patient and healthy donor-derived CAR-T cells. (A) Representative density plots of healthy (left) and patient (right) CD8 CAR-T cell inhibitory receptor expression; (A.i) CTLA-4, (A.ii) LAG3, (A.iii) PD-1, (A.iv) TIGIT and (A.v) TIM3. Quantification shows inhibitory receptor expression across all healthy and patient donor samples for (B) CD4 and (C) CD8 T cells. Mean and standard deviation are displayed, data was analysed using Mann Whitney test. N=7 healthy and patient donor PBMC samples.

6.2.7 TCF1 Expression in Patient and Healthy Donor CAR-T Cells

Inhibitory receptor expression has a dual meaning, signifying both exhaustion and activation, so TCF1 expression was incorporated into analysis to differentiate between subtypes of exhausted cells (Figure 6.1). Initially, TCF1^{+}PD-1^{+} Tpex populations were assessed (Figure 6.7A.i) within CD4 (top) and CD8 (bottom) CAR-T cells to understand potential differences in this prognostically positive population. Density plots represent populations based upon their expression of TCF1 and PD-1.

Given the lack of expression of PD-1 previously seen in both subsets (Figure 6.6B.iii, C.iii), the TCF1^{+}PD-1^{+} fraction was negligible in all patients (Figure 6.7A.ii). This result was similar for the TCF1^{-}PD-1^{+} compartment although one patient displayed a high frequency of TCF1^{-}PD-1^{+} CD8 T cells (bottom) which was not replicated in the CD4 T cell compartment (top). TCF1^{+}PD-1^{-} fractions were high in both healthy donor and patient CAR-T cells but no significant difference was found between them.

We then assessed which T cell phenotypes contributed to each TCF1$^{+/-}$PD-1$^{+/-}$ fraction. Figure 6.7B.i shows pseudocolour plots of TCF1/PD-1 populations overlaid on phenotypic gates CD45RA and CCR7. This analysis was performed for CAR^{+} CD4 (top) and CD8 (bottom) T cells. Quantification (Figure 6.7B.ii) shows that all TCF1/PD-1 populations for CD4 T cells were predominantly derived from T_{CM} cells while in CD8 cells there was more variation in proportions of T_{EM}, T_{CM} and T_{SCM} contributing to each segment. The overall differences between CD4 and CD8 T cell fractions were reflective of the overall phenotypic differences seen in Figure 6.5B.

A significant difference was seen between the subsets producing the small TCF1^{+}PD-1^{+} fraction of CD8 T cells. In healthy donors, this subset was split predominantly between T_{EM}, T_{CM} and T_{SCM} while in patients, the fraction was almost exclusively derived from T_{CM} cells.

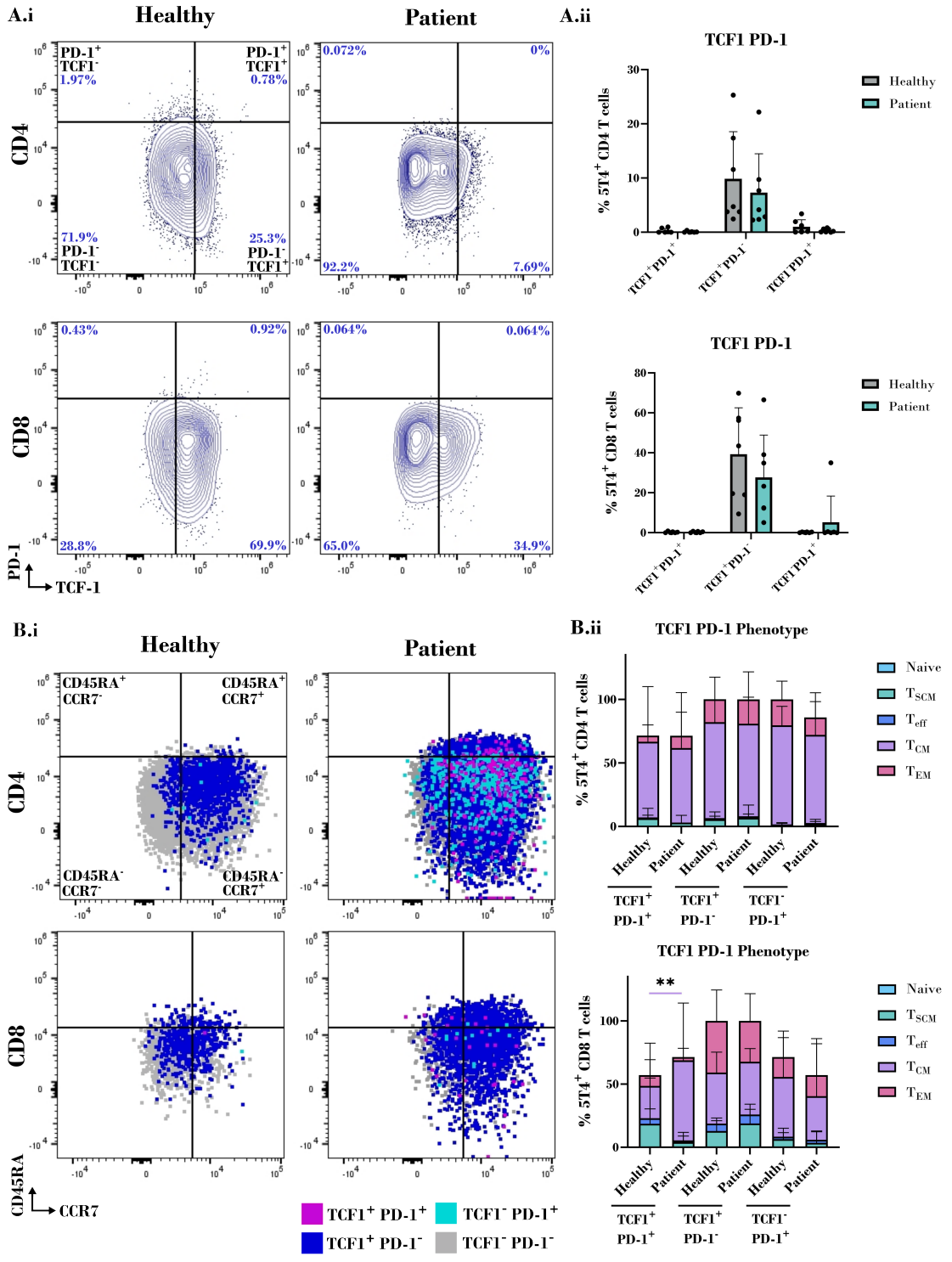


Figure 6.7: Defining exhaustion in patient and healthy donor-derived CAR-T cells. (A.i) Representative density plots of healthy (left) and patient (right) CAR-T cell expression of TCF1 and PD-1. (A.ii) Quantification of PD-1 and TCF1 expression across all samples for CD4 (top) and CD8 (bottom) T cells. (B.i) Pseudocolour plots showing PD-1 and TCF1 expression across T cell phenotypes for CD4 (top) and CD8 (bottom) T cells. (B.ii) Proportions of PD-1 and TCF1 expressing cells in each phenotype. Data was analysed using 2-way ANOVA with multiple comparisons, $^{**}p < 0.01$. N=7 healthy and patient donor PBMC samples.

6.2.8 CAR-T Cell Terminal Exhaustion

In contrast to the progenitor population defined by expression of both TCF1 and PD-1, TCF1 loss in combination with TIM3 is known to define a prognostically negative terminally exhausted T cell fraction. This Tex_{term} population was also evaluated.

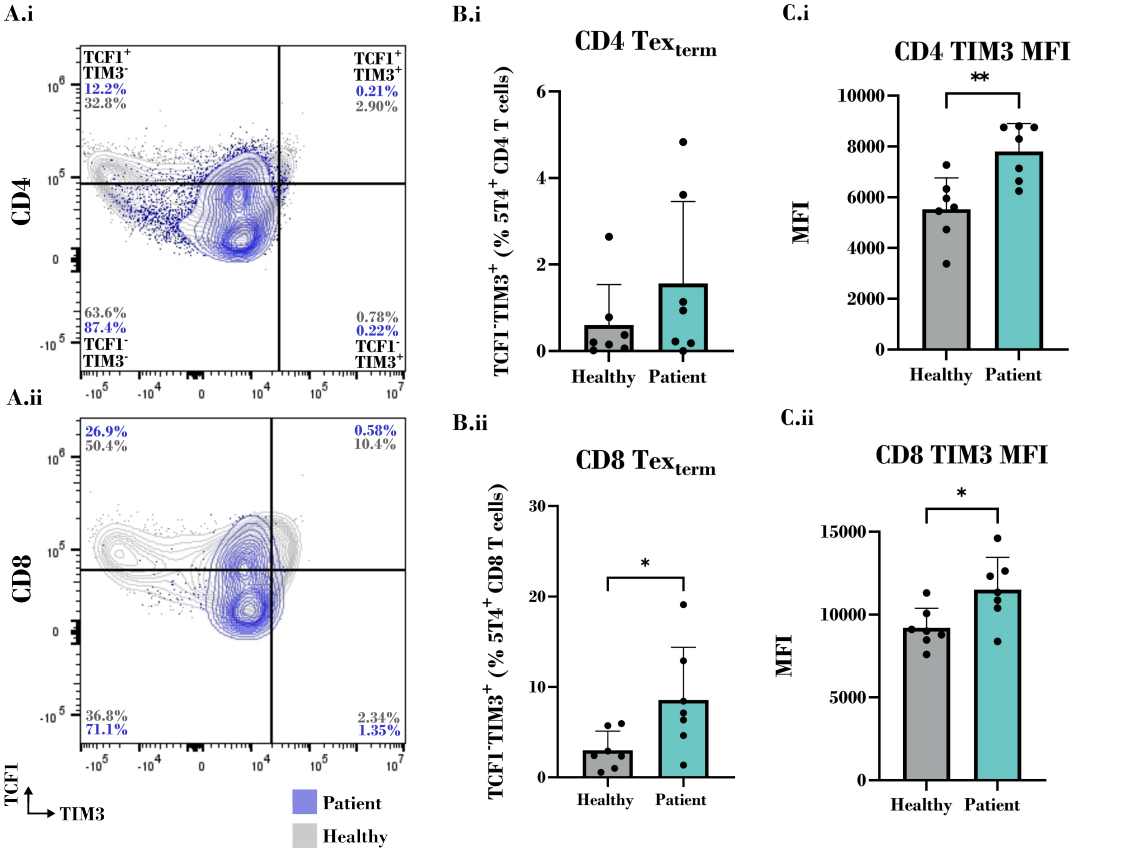


Figure 6.8: Terminally exhausted CAR-T cells from healthy and patient donors. (A) Representative density plots of healthy (grey) and patient (blue) CAR-T cell expression of TCF1 and TIM3 in (A.i) CD4 and (A.ii) CD8 T cell subsets. Density plots show percentages of cells in each population using manual flow cytometry gating. (B) Quantification of $TCF1^{-}TIM3^{+}$ Tex_{term} populations across all healthy and patient donor samples for CD4 (B.i) and CD8 (B.ii) T cells. (C) TIM3 mean fluorescence intensity (MFI) for CD4 (C.i) and CD8 (C.ii) T cells. Mean and standard deviation displayed, data was analysed using unpaired t-test. N=7 healthy and patient donor PBMC samples. $^{**}p < 0.01$,$^{*}p < 0.05$.

Figure 6.8A shows patient (blue) and healthy donor (grey) CAR-T cell expression of TCF1 and TIM3 for both CD4 (Figure 6.8A.i) and CD8 (Figure 6.8A.ii) T cells. Quantification of the $TCF1^{-}TIM3^{+}$ Tex_{term} fraction (Figure 6.8B) showed a significant increase in Tex_{term} cells in the CD8 compartment (Figure 6.8B.i) of patient

CAR-T cells compared to healthy donor CD8 CAR-T cells. No significant difference was seen in expression between the CD4 CAR-T cell fractions (Figure 6.8B.ii) of each donor type. TIM3 MFI was quantified due to an overall shift observed in the populations, showing a significant increase in both CD4 (Figure 6.8C.i) and CD8 (Figure 6.8C.ii) T cell TIM3 MFI in patients compared to healthy donors.

This additional analysis was completed for all other inhibitory receptors but no additional significant changes in MFI were found.

6.2.9 Suppressive Adenosine Signalling

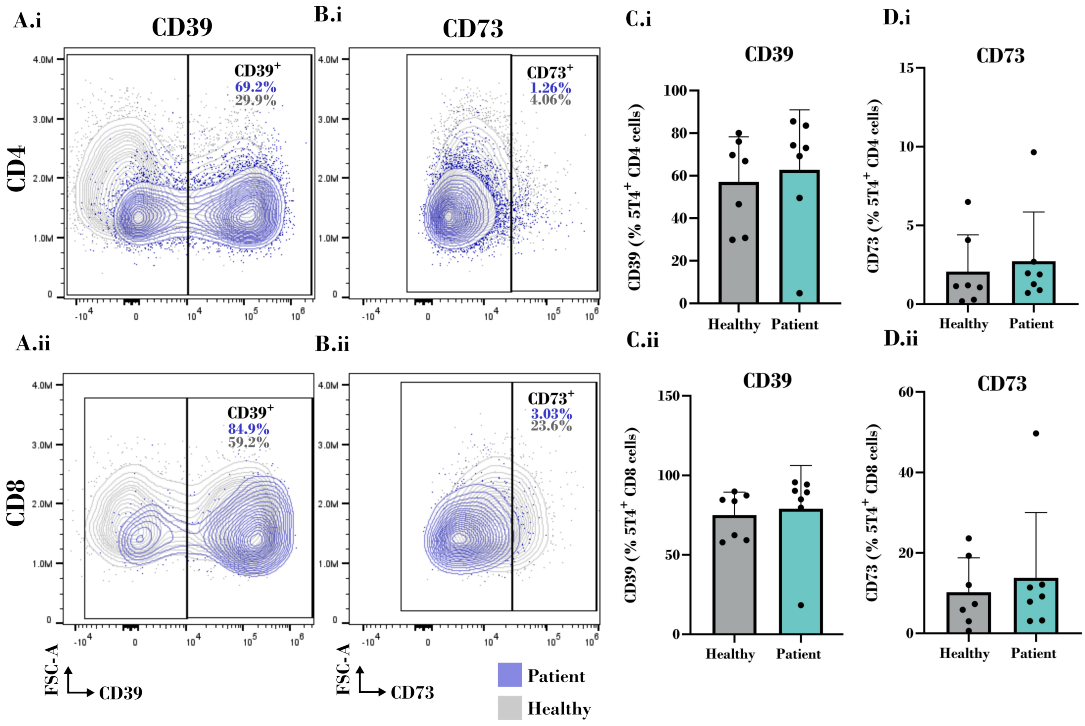


Figure 6.9: Expression of CD39 and CD73 ectonucleotidases. Representative density plots of healthy (grey) and patient (blue) CAR-T cell expression of (A) CD39 and (B) CD73 in (A.i, B.i) CD4 and (A.ii, B.ii) CD8 T cell subsets. Density plots show percentages of cells in each population using manual flow cytometry gating. Quantification of (C) CD39 and (D) CD73 across all healthy and patient donor samples for (C.i, D.i) CD4 and (C.ii, D.ii) CD8 T cells. Mean and standard deviation are displayed. Data was analysed using unpaired t-test. N=7 healthy and patient donor PBMC samples.

The expression of both CD39 and CD73 on the surface of patient and healthy donor T cells was investigated due to the role that each receptor plays in the generation of adenosine and subsequent suppressive effects on T cell activity.

Density plots show the representative expression of CD39 (Figure 6.9A) and CD73 (Figure 6.9B) in patient (blue) and healthy donor (grey) CAR-T cells. Expression was measured within CD4 (Figure 6.9A.i, B.i) and CD8 (Figure 6.9A.ii, B.ii) compartments. Quantification of CD39 (Figure 6.9C) and CD73 (Figure 6.9D) expression showed no significant differences between patient and healthy donor CD4 or CD8 CAR-T cells.

While most donors showed large $CD39^+$ populations and relatively small $CD73^+$ populations, one patient displayed an unusually high $CD73^+$ population and an additional reduction in $CD39^+$ cells compared to all other donors.

6.2.10 UMAP Dimensionality Reduction

Dimensionality reduction with UMAP was used to map the total T cell landscapes across donor types and identify any additional significant markers not detected using manual gating. The clustering algorithm determines the global similarity of cells using physical distance to represent phenotypic difference.

Figure 6.10A shows the UMAP output for the global clustering of all samples gated at the level of $CD45^+$ cells. The pseudocolour plot (top left) shows cell density within each region which can then be segmented by existing population gates or by sample. Donor segmentation (top middle) was performed showing a clear separation between $CD45^+$ cells from healthy donors (blue) and patients (green). When the CAR-T cell expression gates were applied (top right), distinct populations could be seen particularly within the patient-derived CD4 T cell CAR^+ (purple) and CAR^- (blue) populations. The healthy donor CAR-T cell and UTC populations were less differentiated by the clustering.

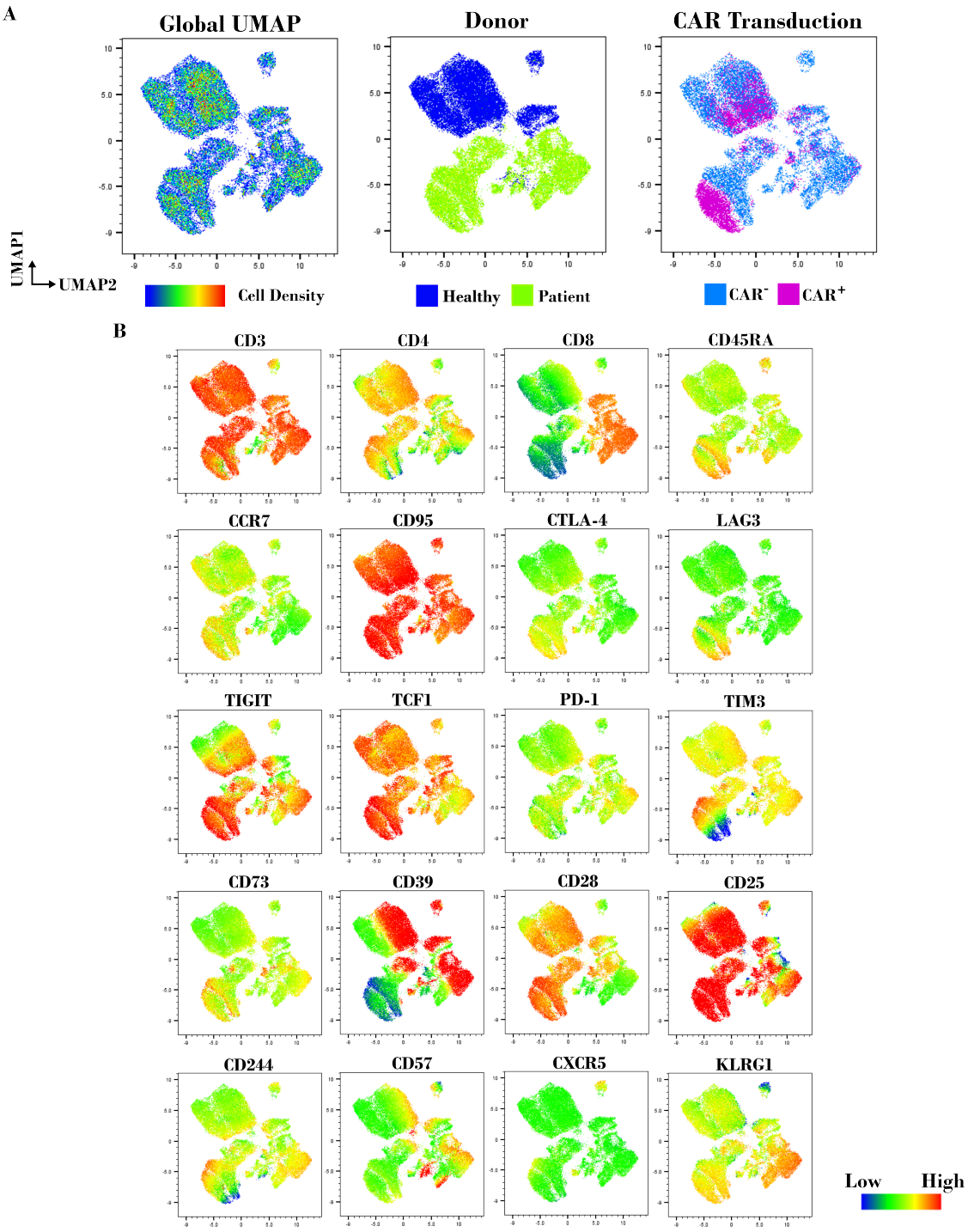


Figure 6.10: UMAP dimensionality reduction. (A) Global Uniform Manifold Approximation and Projection (UMAP). (Left) Global pseudocolour plot applied to all 7 healthy donor and patient samples using the UMAP_R FlowJo Plugin. All parameters except LIVE/DEAD staining and CD45 were included in concatenation and dimensionality reduction. (Middle) UMAP plot was segmented by donor and (right) transduction. Marker identities indicated by key, only live $CD45^+$ cells were used. (B) UMAP plots overlayed with expression of all relevant markers in the panel. N=7 healthy and patient donor PBMC samples.

Following segmentation by donor and transduction, UMAP plots were overlaid with the fluorescence intensity of each marker of interest within the panel (Figure 6.10B). These markers included previously explored subset-defining proteins such as CD4, CD8, CD45RA and CD62L, inhibitory receptors associated with T cell exhaustion; CTLA-4, LAG3, PD-1, TIGIT and TIM3 and ectonucleotidases CD39 and CD73. Also included were markers that were not previously assessed in manual gating analysis, including markers of terminal differentiation and cytotoxicity CD57 and KLRG1, activatory receptors CD28 and CD25 and the lymph node homing marker CXCR5.

CD3 and CD95 were universally highly expressed across the UMAP clusters as expected given the Dynabead selection of $CD3^+$ T cells (Figure 3.7D) and lack of naïve cells seen throughout samples (Figure 6.5B). CD4 and CD8 expression was largely inversely correlated with distinct separation between their respective clusters, although CD8 expression was more clearly defined to a single area than CD4 expression.

The inhibitory receptors associated with T cell exhaustion CTLA-4, LAG3 and PD-1 all clustered similarly while TIGIT was expressed among a larger population of cells. TIM3 expression did not correlate with any other exhaustion marker, showing inverse expression particularly in patient-derived CD4 cells. CD73 expression was sparse while CD39 was highly expressed across a subset of patient and healthy cells within both CD4 and CD8 compartments as seen in Figure 6.9.

The activation markers CD28 and CD25 were similarly distributed and highly expressed among the majority of cells. CD244 expression was sparse with particularly low expression in both patient-derived CD4 and CD8 subsets correlating with areas of high CD25. CXCR5 expression was negligible throughout while KLRG1 was expressed more in patient-derived cells throughout and most highly in the CD8 fraction.

6.3 Discussion

In vitro cytotoxicity of patient-derived CAR-T cells was significantly reduced compared to healthy donor CAR-T cells. Spectral flow cytometry of patient and

healthy donor-derived CAR-T cells revealed reduced transduction efficiency and increased terminally exhausted CD8 CAR-T cell population across patient samples when compared to healthy donors. UMAP dimensionality reduction also revealed an overall separation between patient and healthy donor samples indicating overall phenotypic differences between the two populations.

Differences in cytotoxicity were seen across donor replicates between healthy donor and patient CAR-T cells. These variations were observed not only in the lower 5T4 expressing MIA PaCa-2 cells but also in the high 5T4 expressing PANC-1 cells which were generally killed robustly in other assays. This variation in cytotoxicity in a simple system could potentially have implications for the cytotoxicity of the CAR-T cells in the more complex TME and therefore prompted investigation.

While distinct differences were seen between patient and healthy donor samples, substantial variation was present throughout each donor population. This was evident in fundamental parameters such as CD4:CD8 ratio as well as more nuanced factors including CD39 and CD73 expression. In the patient population this variation could be partially due to previous chemotherapy treatments. While only one patient received neoadjuvant FOLFIRINOX, three patients were reported to have been treated for a previous cancer and are therefore likely to have been exposed to chemotherapy (and possibly radiation) previously. Additionally, inflammatory diseases such as diabetes mellitus are also known to impact T cell fate, leading to increased T_{eff} subsets when compared to healthy controls (Lau et al. 2019). Given that it is estimated that between 4%-65% of PDAC patients have diabetes mellitus (S. Chari and Khan 2022) with a recent study indicating a prevalence of 38.1% (Amri et al. 2023), the effects of this co-morbidity on the T cell population are necessary in determining the potential of CAR-T cell therapy for treatment of PDAC.

Although blood cones are derived from single patients during platelet apheresis donation, demographic information about healthy donors is not available for researchers. This prevents age matching or analysis of any potential conditions which could confound analysis. In future, collection of blood from healthy donors with additional demographic data would aid standardisation.

A notable difference between the two donor populations was transduction efficiency - a factor key in generating sufficient numbers of CAR^+ T cells in a clinical setting. This value is often highly variable, although there is limited data underpinning differences between transduction efficiencies in individual patients. A recent study used a multi-omics approach to identify interferon stimulated gene (ISG) upregulation in untransduced cells following exposure to lentiviral vector. This was contrasted by extracellular signal-regulated kinase (ERK)2 phosphatase upregulation in successfully transduced CAR-T cells. These results were obtained through analysis of healthy donor-derived CAR-T cells but were confirmed by analysis of single-cell RNAseq data for tisagenlecleucel and axicabtagene ciloleucel infusion products. Mimicking the action of the phosphatases using ERK2 inhibitors showed significant increases in transduction efficiency across vectors, highlighting how potential modulation at this stage could increase the proportion of viable CAR-T products (Adabi et al. 2025).

Across inhibitory receptors we observed a lack of differential expression between patient and healthy donor CAR-T cells. This low level of expression is likely underpinned by the lack of prolonged antigen exposure which causes their upregulation (Chow et al. 2022). Generally, receptors were only found to be expressed on a small proportion of cells with the exception of LAG3 and TIM3 which were more highly expressed. UMAP projections showed that there was substantial co-expression of CTLA-4, LAG3 and PD-1 with a similar but more extensive expression pattern displayed by TIGIT. TIM3, on the other hand, was expressed most highly on almost completely different CD4 T cell populations across both patient and healthy donors. Discrepancies in TIGIT abundance between UMAP and manual gating may be due to conservative FMO gating resulting from high spectral overlap leading to a reduction in sensitivity to the antigen.

Given the minimal expression of PD-1 throughout the T cell populations, there were unsurprisingly low numbers of Tpex ($TCF1^+PD\text{-}1^+$) cells present in either of the donor groups. There were, however, a high number of $TCF1^+$ cells overall indicating that proliferative capacity was maintained across donor types. At the

other end of the spectrum of exhausted cells, the TCF1^{-}TIM3^{+} Tex_{term} fraction was more abundant than the progenitor exhausted subset. Elevated proportions of these cells were seen in patient CAR-T cells with a significant increase in CD8 T cells and a positive trend in CD4. While TCF1^{+} populations appeared to remain constant across donor types, these differences were underpinned by a substantial increase in TIM3 MFI displayed by the patient CAR-T cells.

The fact that a significant MFI shift in TIM3 did not result in an increase in TIM3^{+} population detected by gating highlights the challenge of background fluorescence when using a large panel. FMOs (Appendix D.2) may have been influenced by a degree of spectral overlap, preventing the detection of more subtle shifts in marker expression in order to prevent false-positives. A similar effect may have led to the underestimation of the TIGIT^{+} population compared to the UMAP projection. Despite the difference seen in TIM3, no other significant shift in inhibitory receptor MFI was seen between patient and healthy donor CAR-T cells indicating that the lack of sensitivity was not preventing widespread detection of significant changes.

Despite the lack of significant differences observed between patient and healthy donor CAR-T cell expression of CD39 and CD73, UMAP fluorescence intensity revealed a distinct expression pattern of CD39. The receptor was differentially expressed across both donor groups and CD4/CD8 subtypes. No other marker correlated exactly with this segmented expression pattern and future work should involve defining this population.

Additional sub-populations highlighted within the UMAP plots include the small CD244^{-}CD25^{+} region at the base of the patient-derived CD4 T cell cluster which may represent a small Treg population not seen in healthy donor samples. In the context of CAR-T cell clinical efficacy, presence of Tregs has been shown to negatively impact therapy response (Good et al. 2022). *In vitro* depletion of the Treg population was also shown to enhance CAR-T cytotoxicity (Sun et al. 2025) indicating that the population has a directly negative impact.

In a paper highlighting the induction of immunosenescence of CD8 T cells in breast cancer patients, the senescent $CD28^{-}CD57^{+}$ population of CD8 T cells is shown to remain high in cancer patients undergoing DNA-damaging chemotherapy (Brenchley et al. 2003; Onyema et al. 2015). This small $CD28^{-}CD57^{+}$ CD8 cluster was present in the patient-derived lower section of the UMAP plot but absent in the healthy donor-derived cells. Further exploration of these markers could reveal senescence signatures associated with previous chemotherapy or other patient characteristics.

6.3.1 Conclusions

The use of a spectral flow cytometry panel facilitated a broad and unbiased approach to analysis of factors affecting patient-derived CAR-T cell function. Based upon observations of patient-derived cells displaying reduced transduction efficiency and increased Tex_{term} populations along with potentially unique Treg and senescent CD8 T cell subsets, further investigations should focus on relating these parameters back to CAR-T cell functionality, ultimately with the goal of modulating patient-derived CAR-T cells to restore full cytotoxic function.

"Believe that a further shore is reachable from here"

Seamus Heaney

7 Discussion

This thesis sought to evaluate anti-5T4 CAR-T cell therapy using live patient-derived tumour slices as the primary testing platform. In combining these approaches, both the efficacy of the therapy and the utility of live tumour slices in CAR-T cell therapy preclinical testing could be evaluated. The expression of 5T4 across pancreatic malignancies was assessed, confirming surface expression to facilitate potential antigen recognition. Anti-5T4 CAR-T cell cytotoxicity was first investigated *in vitro*, in line with standard preclinical testing methodologies. Observations of high IL-6 cytokine release during these assays prompted investigation into the acute effects of IL-6 exposure on CAR-T cell efficacy. Methods for evaluating autologous CAR-T cell responses in organotypic tumour slices were developed, incorporating analysis of tissue penetration, target engagement, calcium flux, and cytotoxicity. The lack of observable cytotoxicity in this setting prompted investigation into the predominant soluble factors present in tumour slice media and donor-specific differences in CAR-T cell characteristics. This work provides a framework for clinically-relevant evaluation of CAR-T cells prior to clinical testing.

7.1 Contribution to Knowledge

Initial investigations focused on the viability of 5T4 as a CAR-T cell target for PDAC. This was achieved using analysis of total protein expression across a range of pancreatic malignancies and healthy pancreatic tissue samples. Surface expression was validated through flow cytometry, confirming the accessibility of 5T4 for CAR ligation. The presence of acellular 5T4 deposits was observed in some patient samples. Epitope mapping indicated that the membrane-proximal location of the H8 target epitope used in the anti-5T4 CAR is ideal for targeting membrane-bound protein and avoiding cleaved regions. The mechanisms behind these potential cleavage events should be further explored, given their potential role in reducing therapeutic efficacy.

Having confirmed that 5T4 was a suitable target in PDAC, ant-5T4 CAR-T cells were generated and characterised from healthy donor blood. CAR-T cell generation conditions were optimised to maintain high yields of $CD3^+$ CAR^+ cells while aiming to reduce generation times to facilitate rapid production of autologous patient CAR-T cells. A 7-day protocol without prior T cell selection was chosen, yielding high $CD3^+$ selection and consistent transduction. Phenotyping demonstrated that the combination of IL-7 and IL-15 led to high T_{EM} proportions in both CD4 and CD8 T cells. Further optimisation is needed to increase proportions of T_{SCM} cells which are associated with durable responses (Dancy et al. 2018). This could potentially be achieved through replacing the CD28 costimulatory domain with 4-1BB (Kawalekar et al. 2016) or with metabolic manipulation (Foskolou et al. 2020; Song et al. 2024).

Anti-5T4 CAR-T cells were tested *in vitro* for their cytotoxicity and cytokine release. This was performed using standard flow cytometric and impedance-based assays to allow comparison with existing CAR-T cell therapy candidates. Cytotoxicity against non-PDAC cell lines validated at OXB was shown to be 5T4-dependent, with greater efficiency in eradicating the predominantly $5T4^{hi}$ SKOV-3 cell line than the $5T4^{lo}$ Kasumi-1 cells. Elevated IL-2, IFNγ and Granzyme-B were seen and largely correlated with CAR-T cell cytotoxicity. IL-6 was also elevated solely in CAR-T cell co-culture with SKOV-3 indicating production either by the epithelial cell line or CAR-T cells in response to substantial activation.

Impedance-based co-culture with PDAC cell lines confirmed the selectivity of anti-5T4 CAR-T cell cytotoxicity. The higher expressing PANC-1 cells were killed more efficiently than the MIA PaCa-2 cells. This discrepancy was reflected in the cytokine arrays which showed high levels of IFNγ, Granzyme B, IL-2 and TNFα after 24 h of PANC-1 co-culture and extremely low levels in MIA PaCa-2 co-culture. This could be attributed to the later induction of cytotoxicity seen in co-culture with MIA PaCa-2 cells which was evident in the time course plotted for each cell line. Similarly high IL-6 was seen in both PANC-1 and MIA PaCa-2 co-culture, supporting the fact that the cytokine is only produced at these levels in settings of CAR-T cell activity against target-positive epithelial cell lines. The effect of the observed concentrations of IL-6 on CAR-T cell activity was studied due to variable reports of its effects in the literature. No significant differences were seen in CAR-T cell viability or function.

Following *in vitro* analysis, organotypic tumour slice assays were developed to allow *ex vivo* analysis of colocalisation and tumour penetration depth of autologous anti-5T4 CAR-T cells. Autologous patient CAR-T cells successfully colocalised with $5T4^+$ target cells in high 5T4 expressing tumour slices. In all three patients, UTC cells showed significantly greater tumour penetration than CAR-T cells, despite patient 2 having no 5T4 expression in slices used for IF and patient 3 having low 5T4. This difference warrants further investigation, given that the incorporation of the vector is the only difference between the cells. As previously mentioned, this could be due to CAR-T cell sensitivity being greater than assay sensitivity in the detection of 5T4. Using a control CAR-T cell lacking either a functional endodomain or using an alternative irrelevant antigen ectodomain would control for the effects of transduction on T cell phenotype. Live imaging showed calcium fluxes generated upon CAR-T cell contact with $5T4^+$ target cells. Despite this observation, IHC staining of cleaved caspase 3 did not reveal any difference in tumour cell death between slices cultured for 48 h with CAR and UTC cells. Future work will involve use of additional live imaging and flow cytometry to understand where this discrepancy lies.

To investigate potential suppression of cytotoxic function by soluble mediators present in tumour slices, media from the culture of slices was harvested and analysed using a cytokine array. Cytokines of interest were selected based upon their presence in the media sample, which was found to suppress CAR-T cell cytotoxicity *in vitro*, along with their absence in control media samples. CXCL5, CXCL9, CCL20, HGF, adiponectin, osteoprotegerin and angiogenin were all identified as potentially contributing to this suppression.

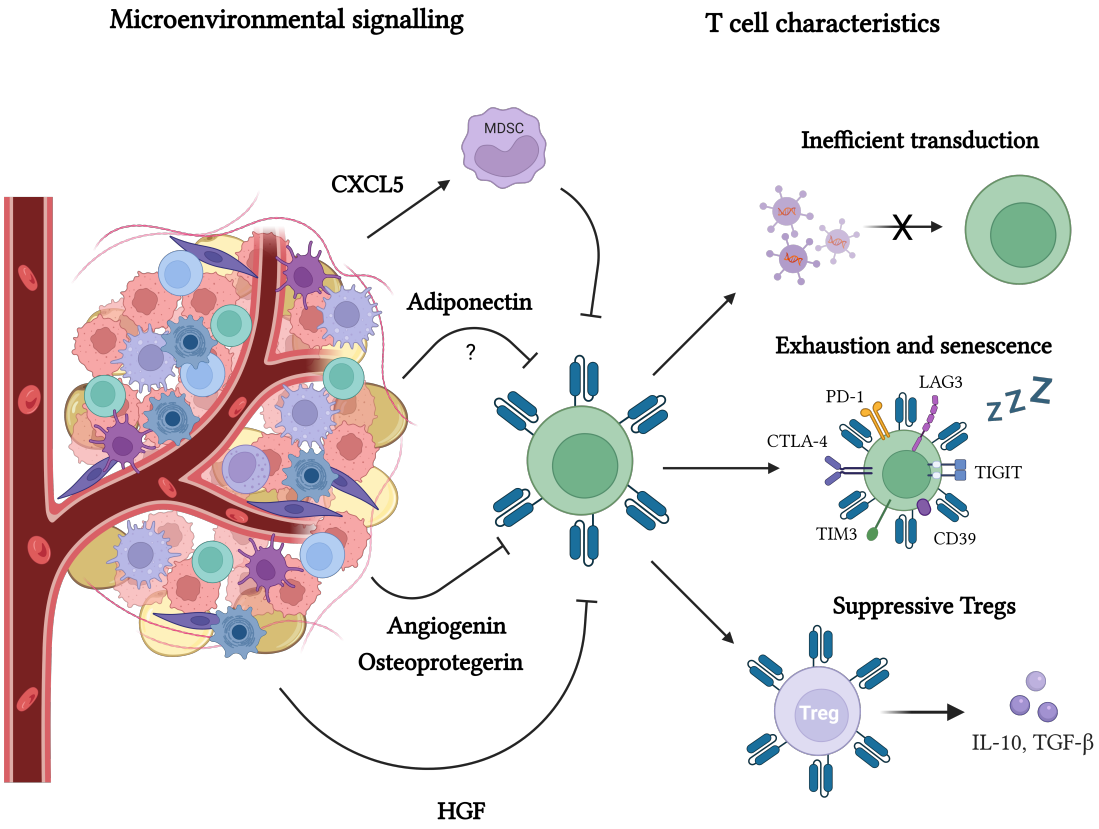


Figure 7.1: Summary of microenvironmental and CAR-T cell-based targeting strategies. (Left) Potential microenvironmental targets identified from cytokine screening of tumour slice conditioned media. (Right) Phenotypic differences identified between healthy donor and patient CAR-T cells using spectral flow cytometry..

Another discrepancy between *in vitro* and *ex vivo* analysis is the source of the donor PBMCs used to make the CAR-T cells. Observations that patient-derived CAR-T cells were less cytotoxic *in vitro* than healthy donor-derived CAR-T cells led to phenotypic analysis using a customised spectral flow cytometry panel. Healthy

donor-derived CAR-T cells had a greater average transduction efficiency and fewer terminally exhausted CD8 T cells than patient-derived CAR-T cells. UMAP analysis also revealed potential CD4 Treg and CD8 immunosenescent populations in patient-derived CAR-T cells alone. These findings along with key microenvironmental factors are summarised in Figure 7.1.

7.2 Opportunities and Limitations

The soluble factors identified in Chapter 5 and donor-specific T cell factors identified in Chapter 6 will form the basis for future work optimising anti-5T4 CAR-T cell efficacy in PDAC. The soluble factors identified through tumour conditioned media cytokine array (Chapter 5) include CXCL9, CXCL5, CCL20, HGF, adiponectin, osteoprotegerin and angiogenin. These factors may not be individually causative in suppressing CAR-T cell cytotoxicity (discussed in Chapter 5.3) but their impact on CAR-T function should be interrogated. CXCL5, HGF, adiponectin, angiogenin and osteoprotegerin are of particular interest due to their high expression and either poorly characterised, or negative, effects on T cell cytotoxicity.

Donor-specific factors of interest identified through CAR-T cell spectral flow cytometry (Chapter 6) include the difference in transduction efficiency between patient and healthy donor-derived CAR-T cells. The mechanisms underlying variable transduction efficiency are poorly characterised but investigating gene signatures associated with transduction (as discussed in Chapter 6.3) could enable mechanistic understanding (Adabi et al. 2025). Future work should also evaluate the effects of the increased Tex_{term} population seen in patient-derived CAR-T cells. The increased proportion of these cells was particularly striking given the lack of repeated antigen exposure at the time of sampling. If this population was consistently limiting cytotoxic potential, strategies could be employed to reinvigorate their proliferative capacity (Ford et al. 2022; Yugang Guo et al. 2021). Additional populations which were identified by UMAP clustering including $CD244^{-}CD25^{+}$ Tregs and senescent $CD28^{-}CD57^{+}$ CD8 T cells should be validated in future assays. These could not be explored by manual gating due to antibody volume limitations preventing generation

of FMOs but could represent key populations underpinning CAR-T cell efficacy discrepancies between donor types.

The calcium flux (Figure 5.4) seen in response to CAR-T cell contact with $5T4^+$ cells provided an indication of successful receptor activation. As previously mentioned, future experiments should incorporate a positive control to determine whether the calcium flux recorded was sufficient to trigger downstream effector functions. Additional measurements of effector function could include cytotoxic granule release through perforin staining (M. Mukherjee et al. 2017), CD107a expression analysis, or Fas-FasL interactions. Whilst there was no evidence of increased cleaved caspase seen with IHC, we planned to incorporate a pan-caspase activity marker into our live imaging panel. This would allow direct observation of whether target-dependent CAR-T cell calcium flux led to caspase-dependent target cell death (Xing Liu and Lieberman 2020).

Flow cytometry of disaggregated tumour slices in co-culture with CAR-T cells could also be used to understand why CAR-T cells can recognise target cells but not induce significant cytotoxicity in tumour slices. Using disaggregated tumour tissue would preserve some of the heterogeneous cell types present in the slices but remove the substantial stromal barriers and reduce suppressive microenvironmental signalling. This was previously not feasible due to the low yields obtained from disaggregation of small volumes of stroma-rich tumour fragments. Multiple studies have similarly found that disaggregation-based methods tend to under-represent cellular populations and bias towards those which are most easily extracted (Steinert et al. 2015; Masuda et al. 2016; W. Li, Germain and Gerner 2019). With sufficient material, a single cell suspension would be a useful tool to understand the barriers preventing cytotoxicity in tumour slices, but the potentially skewed populations should be considered when interpreting results.

The interpatient heterogeneity revealed by organotypic tumour slices is both a unique strength of the model and a challenge for analysis. In Chapter 5, the patients whose slices were co-cultured with autologous CAR-T cells showed substantial variation in their expression of 5T4. This meant that parameters such

as colocalisation could not be directly compared between patients and would limit the power of analyses if patient grouping was required. Despite these challenges, it is essential to consider heterogeneity of target expression when assessing CAR-T cell constructs. Despite the high levels of 5T4 expression seen in the majority of patients (Figure 3.2), the scarcity of antigen seen in autologous CAR-T cell patients 2 (Figure 5.4) and 3 (Figure 5.5) indicates that prior screening would be necessary to stratify patients when using 5T4 as a target. This strategy is common in CAR-T clinical trials, with eligibility screening frequently involving IHC-based expression analysis (NCT06846424, NCT05783089, NCT06010862). The differences in 5T4 expression within individual patient samples (intrapatient heterogeneity) provides additional challenges in standardising analysis. This could be solved by using slice replicates derived from different regions of the biopsy for each assay or applying both CAR and control T cells to the same slice and labelling each population differently. Although there are methods to help overcome these challenges, the variability between individual slices makes the model less useful than a cell line-based system for determining attributes such as T cell potency.

Using autologous patient CAR-T cells for *ex vivo* tumour slice testing allows analysis of the impact of individual patient PBMC populations on response to therapy. Given that across the entirety of the UK only around 2000 patients undergo PDAC resection per year (Rigby 2024), it was challenging to obtain a sufficient number of samples to perform consistent analysis across a patient cohort. This challenge was compounded by the urgency of surgery meaning that bloods were frequently not available 7 days before resection, preventing the generation of autologous CAR-T cells prior to sample acquisition. Working across multiple surgical centres could potentially increase the frequency of samples but would require coordination to ensure that samples were processed quickly without prior degradation. Expansion into other solid tumour types, particularly more common cancers, also has the ability to improve the consistency of sample acquisition. This would have the additional advantage of enabling analysis of similar therapeutic

strategies across a broader range of solid tumours, therefore potentially benefiting a greater number of patients.

Alongside the challenges associated with sample scarcity, the longevity of tumour slices also limits the scope of analysis. Whilst various factors can improve slice viability times, PDAC slices are limited to around 12 days (Hughes et al. 2024; Kokkinos et al. 2021). This timeframe prevents long term analyses necessary for determining CAR-T cell persistence and for potential interrogating of antigen exposure-driven exhaustion. The persistence of CAR-T cells has been shown to be central to durable response (Zhaoyun Liu et al. 2024) and is therefore an important factor to evaluate early in preclinical testing. Murine models are generally used to evaluate this parameter, either simply by measuring CAR^+ cells in circulation (Jonnalagadda et al. 2015; Priceman et al. 2018) or using more complex tumour re-challenge to interrogate the memory function of persistent CAR-T cells (Si et al. 2022). This re-challenge can also be conducted *in vitro* to provide a more simplistic measure of long term efficacy (Klee et al. 2024). Persistence is one example of an important parameter which is best investigated using an alternative model. This is additionally true for the systemic effects of therapy, including CRS and ICANS which are challenging to evaluate even in animal models (Duncan, Dunbar and Ishii 2022). Nouri, Weinkove and Perret (2023) propose *in vitro* co-culture measurement of IL-6 as a proxy, but this does not provide any context about the physiological effects of the cytokine release and only serves as a comparator between constructs (Nouri, Weinkove and Perret 2023). The challenges presented by these factors highlight the need for the integration of multiple model systems to effectively evaluate the efficacy and potential toxicities of CAR-T cell therapies.

Another parameter which is commonly assessed using animal models is the ability of CAR-T cells to infiltrate into tumours following intravenous administration. Given the challenges associated with poorly vascularised tumours, more trials are now using alternative administration routes (discussed in Chapter 1.3.3.6) but intravenous delivery remains standard in clinical practice. CAR-T cell extravasation and tumour infiltration cannot be assessed in isolated tumour slices. Additionally,

administration of CAR-T cells onto slices leads to their engagement with exposed tumour cells at the cut surface. This effectively mimics delivery routes such as intratumoural injection but does not allow investigation of CAR-T cell potential to migrate through an outer stromal layer to access target cells within. Encapsulating tumour slices in a collagen matrix would provide an artificial mimic of the stromal barrier. This technique is frequently employed with organoids due to the need for a supporting scaffold (Feng et al. 2023) but could also be applied to slices.

7.3 Closing Remarks

There are currently still no CAR-T cell therapies licensed for use in solid tumours eight years after Kymriah was licensed for ALL. Although substantial innovation in the field is yet to be translated into widespread clinical efficacy, the recent approvals of both the TIL therapy Amtagvi and the TCR-T Tecelra for treatment of solid tumours (Harrison 2024) demonstrate the feasibility of adoptive cell therapies in this setting. To overcome the challenges that solid tumours present to CAR-T cells, preclinical testing must be conducted with models that truly represent patient tumours. I have demonstrated that live tumour slices are a valuable platform to perform this testing in PDAC. Used alongside other models, organotypic tumour slices can provide unique insights into the therapeutic potential and challenges associated with CAR-T cell therapies. Widespread incorporation of this model into preclinical testing pipelines has the potential to improve the design of CAR-T cell therapies by providing clinically-relevant information before clinical trial.

Appendices

A
Results 1: Appendix

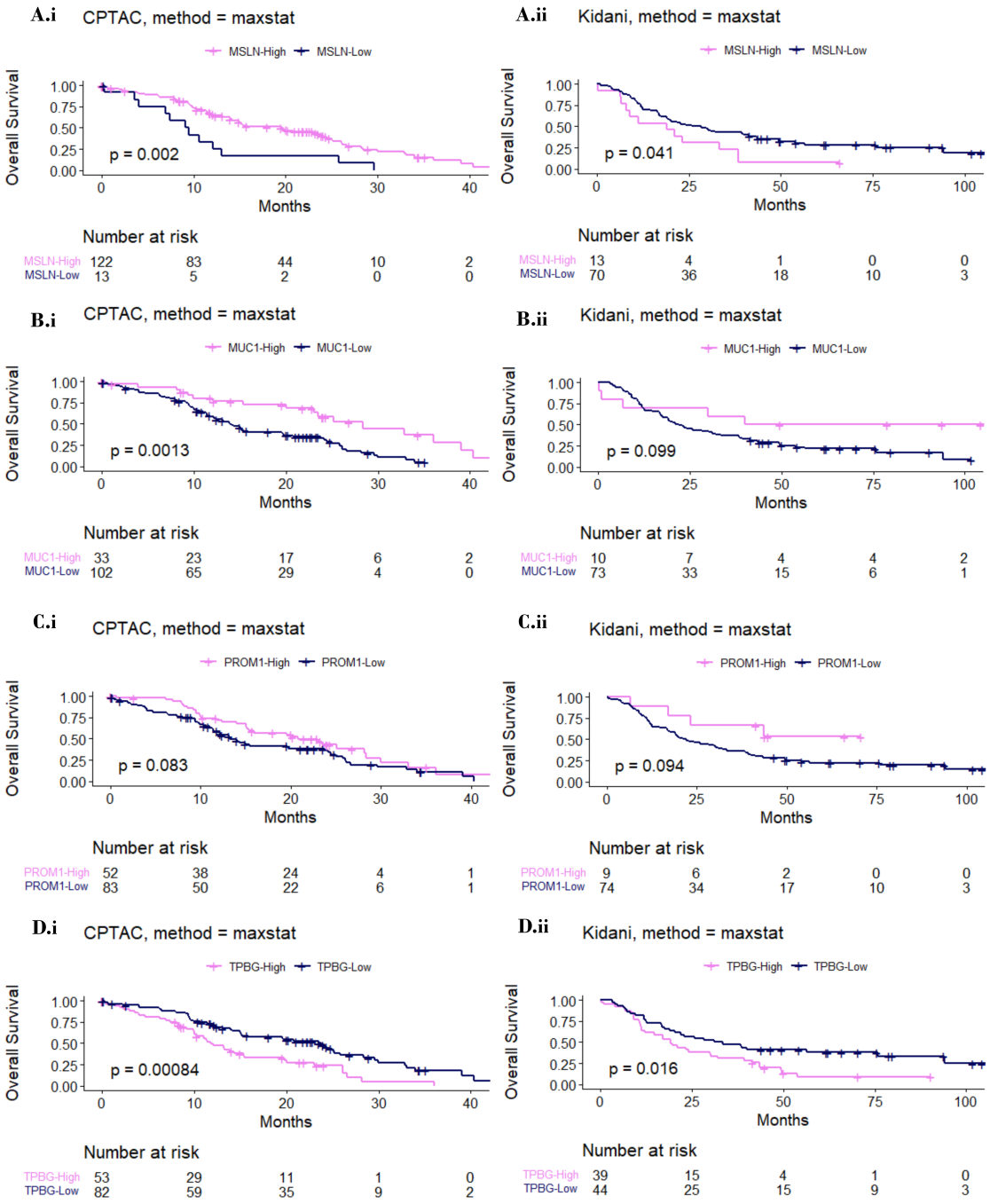
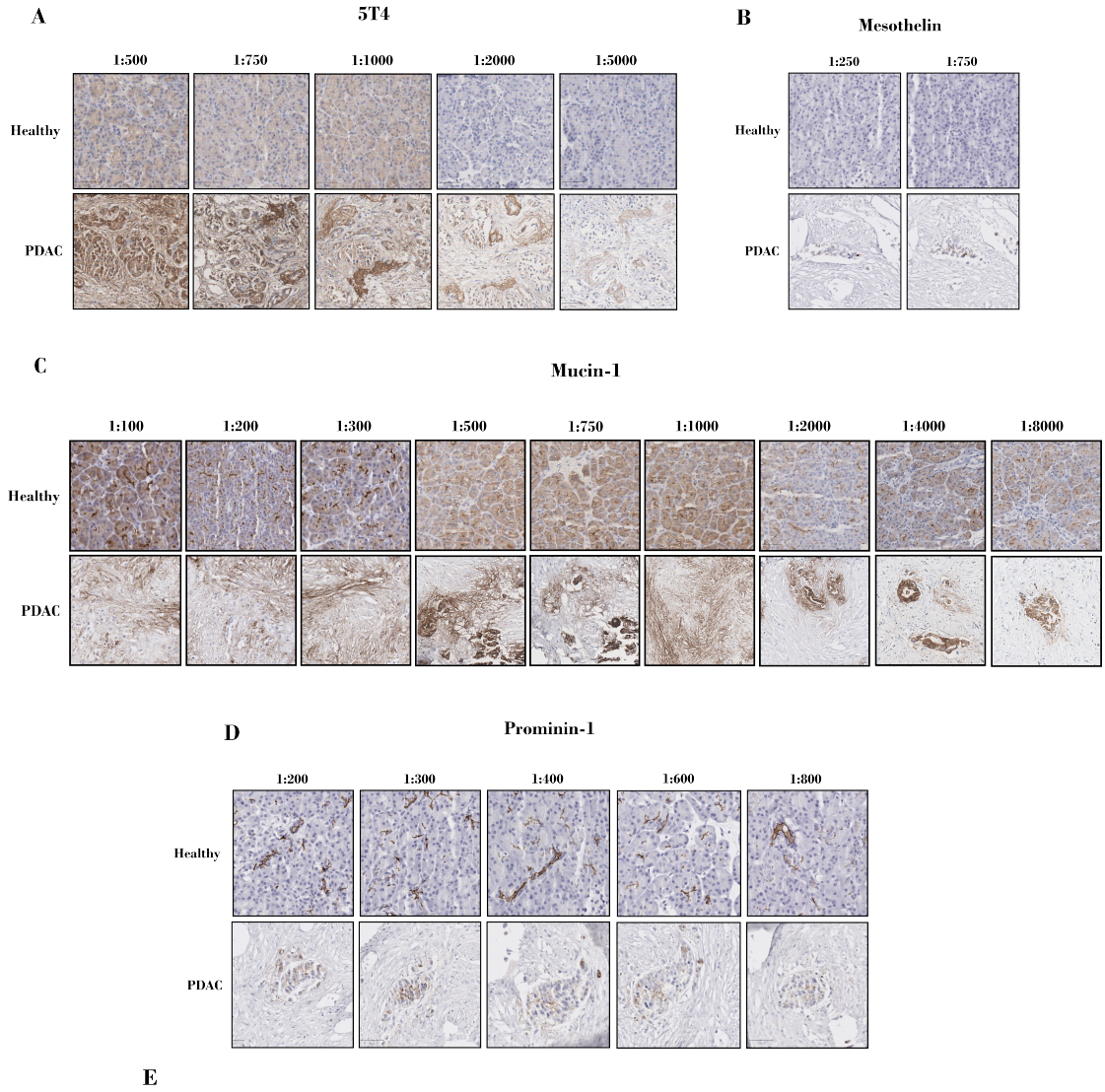


Figure A.1: Survival curves for expression of CAR-T target antigens in PDAC patients. Expression data obtained from the Clinical Proteomic Tumor Analysis Consortium (CPTAC) and Kidani cohort for (Ai, Aii) MSLN, (Bi, Bii) MUC1, (Ci, Cii) PROM1, and (Di, Dii) TPBG segregated using the MAXSTAT function. 'Number at risk' indicates the number of surviving patients at each corresponding timepoint.



E

Antibody	Manufacturer Suggested Dilution	Literature Quoted Dilution	Final Dilution
5T4	1:50 - 1:500	1:200	1:2000
Mucin-1	1:100	1:200	1:4000
Mesothelin	1:250	1:500	1:250
Prominin-1	1:200 - 1:800	1:200 - 1:400	1:300

Figure A.2: Titration of 5T4 antibodies for immunohistochemistry (IHC). (A) 5T4, (B) mesothelin, (C) mucin-1 and (D) prominin-1 antibodies titrated from the manufacturer's recommended dilution using tumour and healthy pancreatic tissue. (E) Table indicating recommended dilution, dilutions used in literature and final dilution based upon titration results. For each antibody n=1 biological replicates were used for the titration.

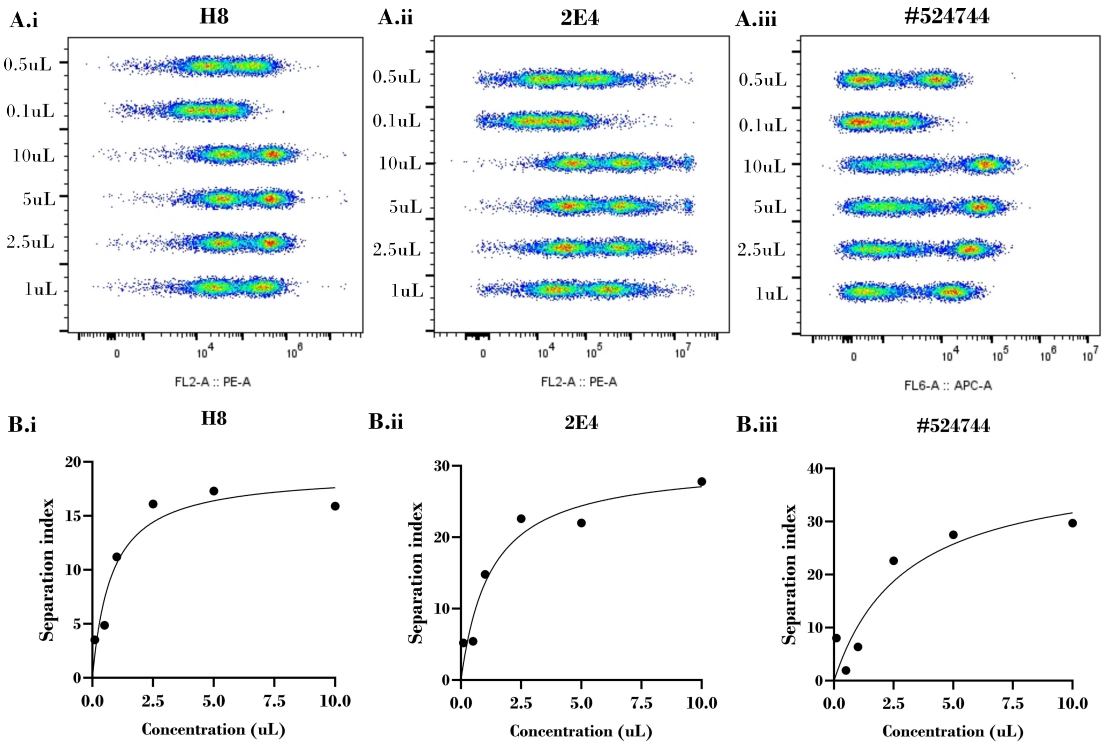


Figure A.3: Titration of 5T4 antibodies for flow cytometry. (A) Separation of 5T4 positive and negative cell populations for (A.i) H8 and (A.ii) 2E4 epitopes provided by Oxford Biomedica and the commercial epitope (A.iii) #524744 using antibody dilutions from 1 in 1000 to 1 in 10. (B) Separation indices for the respective epitopes plotted using least squares fit hyperbolae.

B

Results 2: Appendix

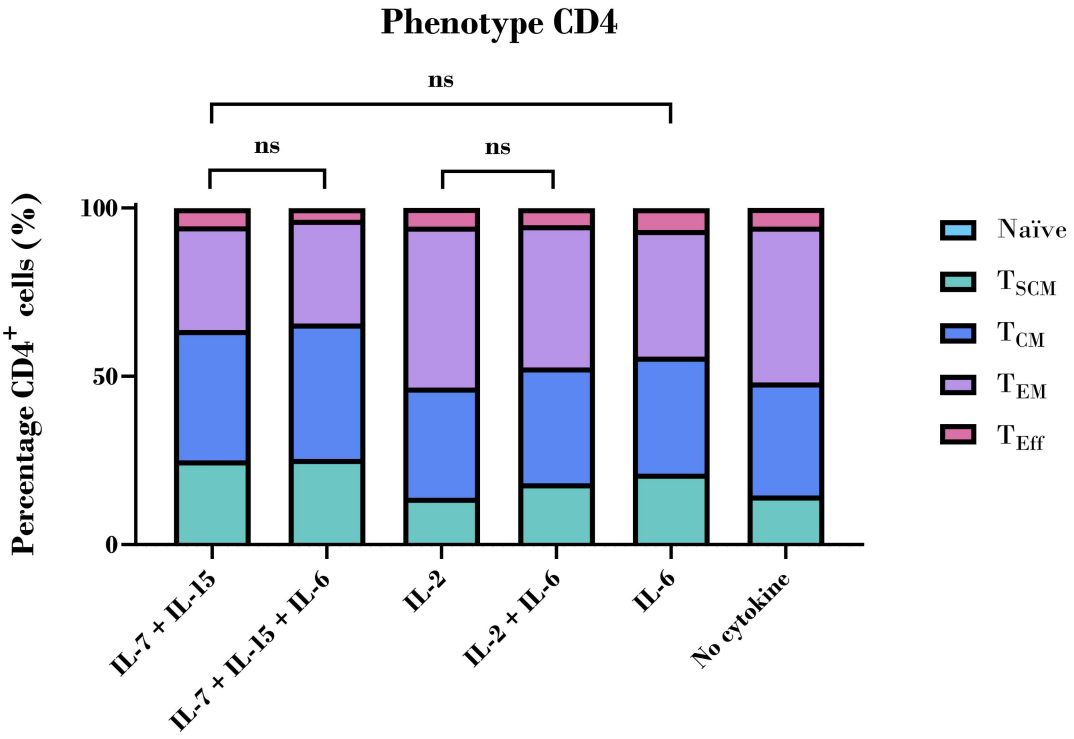


Figure B.1: The *in vitro* effects of IL-6 on CD4 CAR-T cell phenotype. CAR-T cells were generated from n=3 healthy donor PBMC samples in the presence of standard cytokine combinations +/- IL-6 at 10 ng/ml. Phenotyping was performed using flow cytometry and statistical analysis was performed using 2-way ANOVA with Tukey's multiple comparisons.

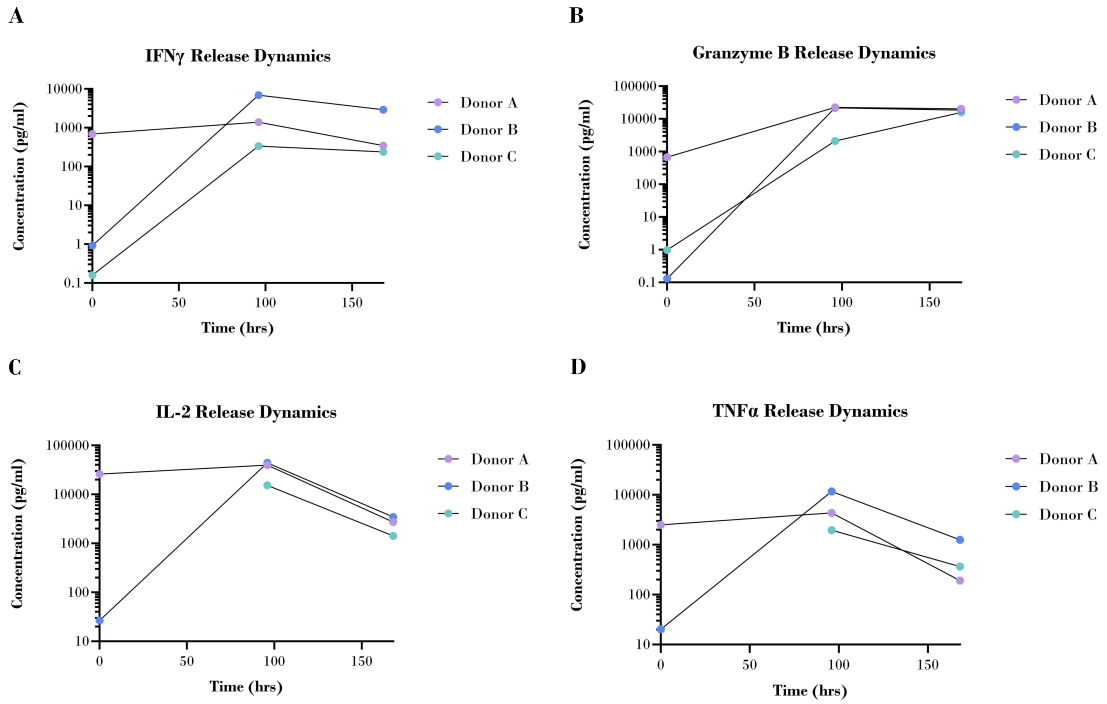


Figure B.2: Dynamics of cytokine release during CAR-T cell generation. Media samples were taken on Day 0, Day 4 and Day 7 of CAR-T cell culture to optimise the timepoint for maximal cytokine release. All samples were taken from the IL-7 and IL-15 culture as this represents the standard protocol. Levels of (A) IFNγ, (B) granzyme B, (C) IL-2, and (D) TNFα were assessed using the cytokine bead array. n=3 healthy donor PBMC samples.

C
Results 3: Appendix

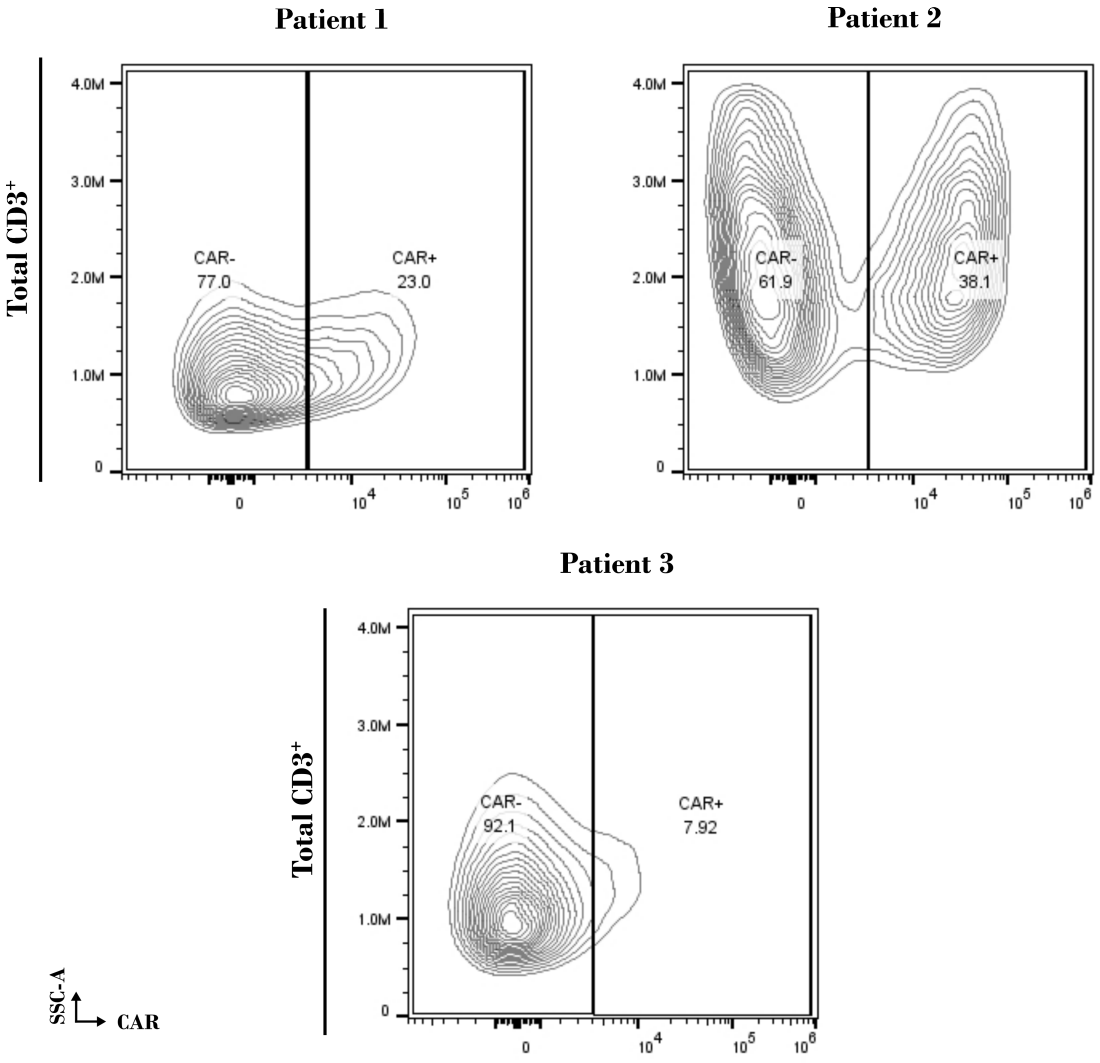


Figure C.1: Transduction of autologous CAR-T cells applied to patient tumour slices. Flow cytometry density plots showing the proportion of transduced cells present in autologous CAR-T cell populations. Only patients whose CAR-T cells were applied to tumour slices (Chapter 5) are displayed. Annotations show CAR^+ and CAR^- populations defined by manual gating from spectral flow cytometry data.

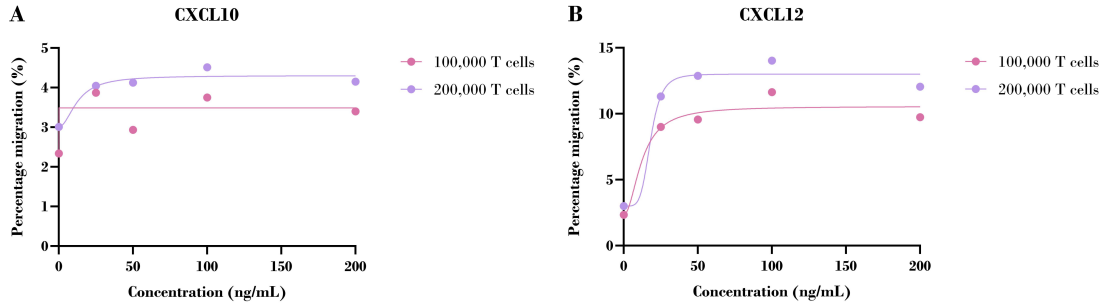


Figure C.2: Chemokine optimisation for transwell migration assays. Transwell migration assays performed with primary human T cells using either 100,000 (pink) or 200,000 (purple) T cells per well. Both (A) CXCL10 and (B) CXCL12 were used as the chemoattractant in the lower chamber of the transwell plate. A non-linear regression was used to generate the curves (Agonist vs. response - variable slope (four parameters)).

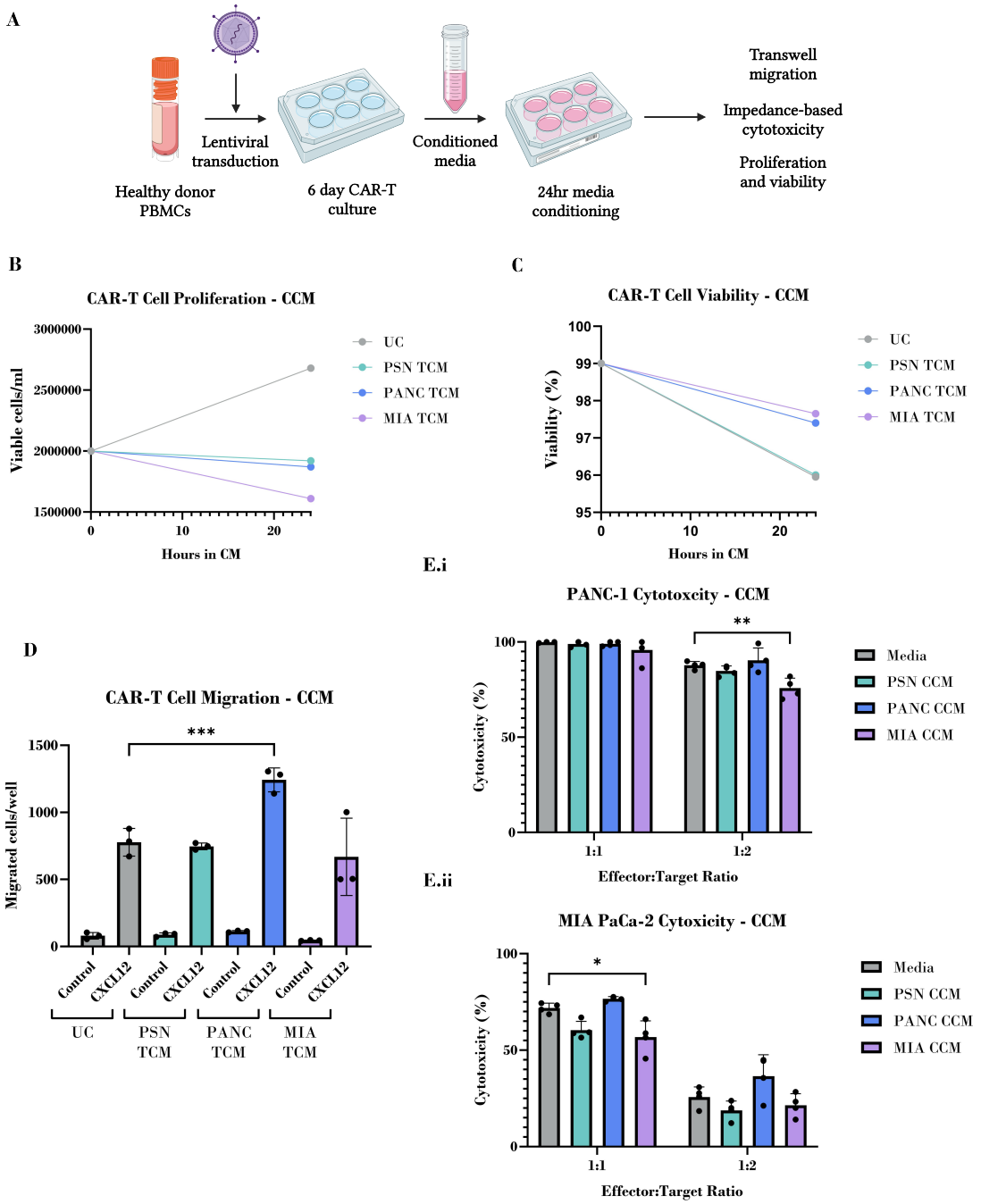


Figure C.3: The *in vitro* effects of cell line conditioned media (CCM) on CAR-T cell growth and functionality. (A) Workflow indicating CCM exposure timeframe and stage in CAR-T cell generation process. (B) Expansion and (C) viability of CAR-T cells exposed to CCM. Viability and expansion measured pre- and post- CCM exposure. (D) CAR-T cell migration measured by flow cytometry and (E) cytotoxicity measured by xCELLigence impedance on Day 7. Migration analysed using 1-way ANOVA and cytotoxicity measured using 2-way ANOVA both with Tukey's multiple comparisons test. For all analyses n=1 healthy PBMC donor-derived CAR-T cells. $^{***}p < 0.001$, $^{**}p < 0.01$, $^{*}p < 0.05$.

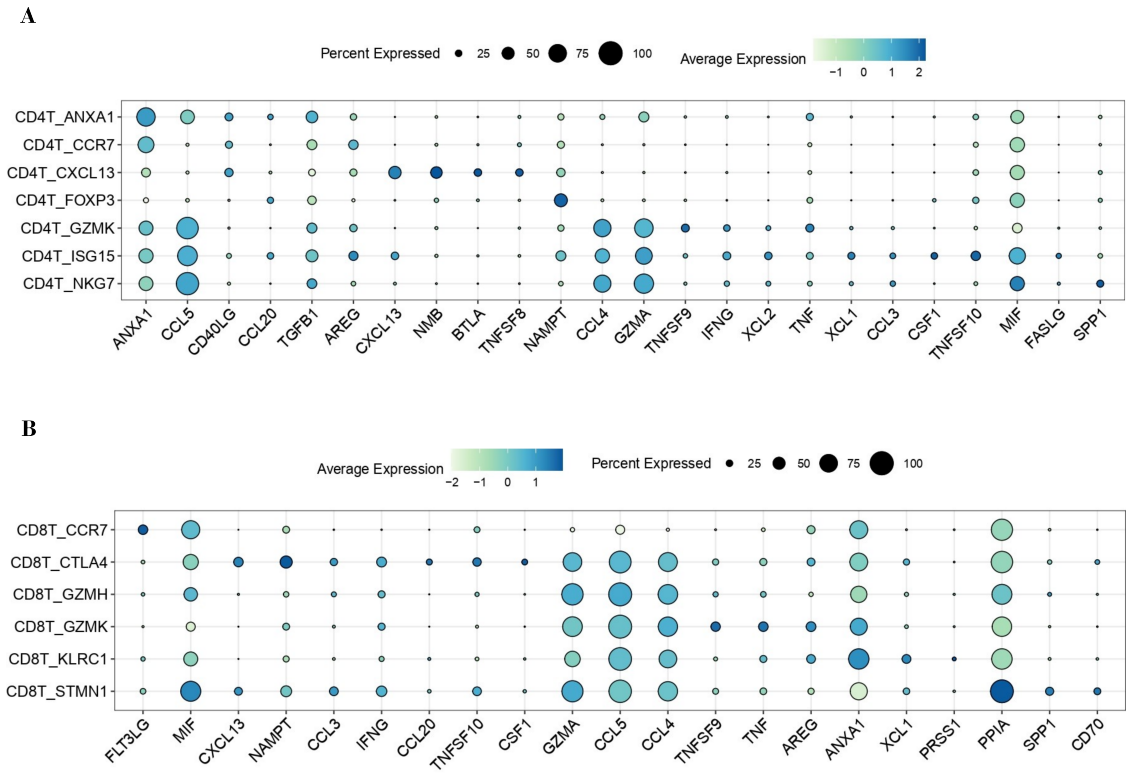


Figure C.4: Differential expression of soluble factors in PDAC patient T cells. Differentially expressed ligands produced by T cells in PDAC patient tumour and healthy adjacent tissue samples from RNAseq data. Ligands expressed by (A) CD4 and (B) CD8 T cells were both filtered for 'secreted signalling' and 'non-protein signalling' using CellChat. Significant genes are shown calculated from a Wilcoxon rank sum test. Analysis carried out by Constantinos Demetriou.

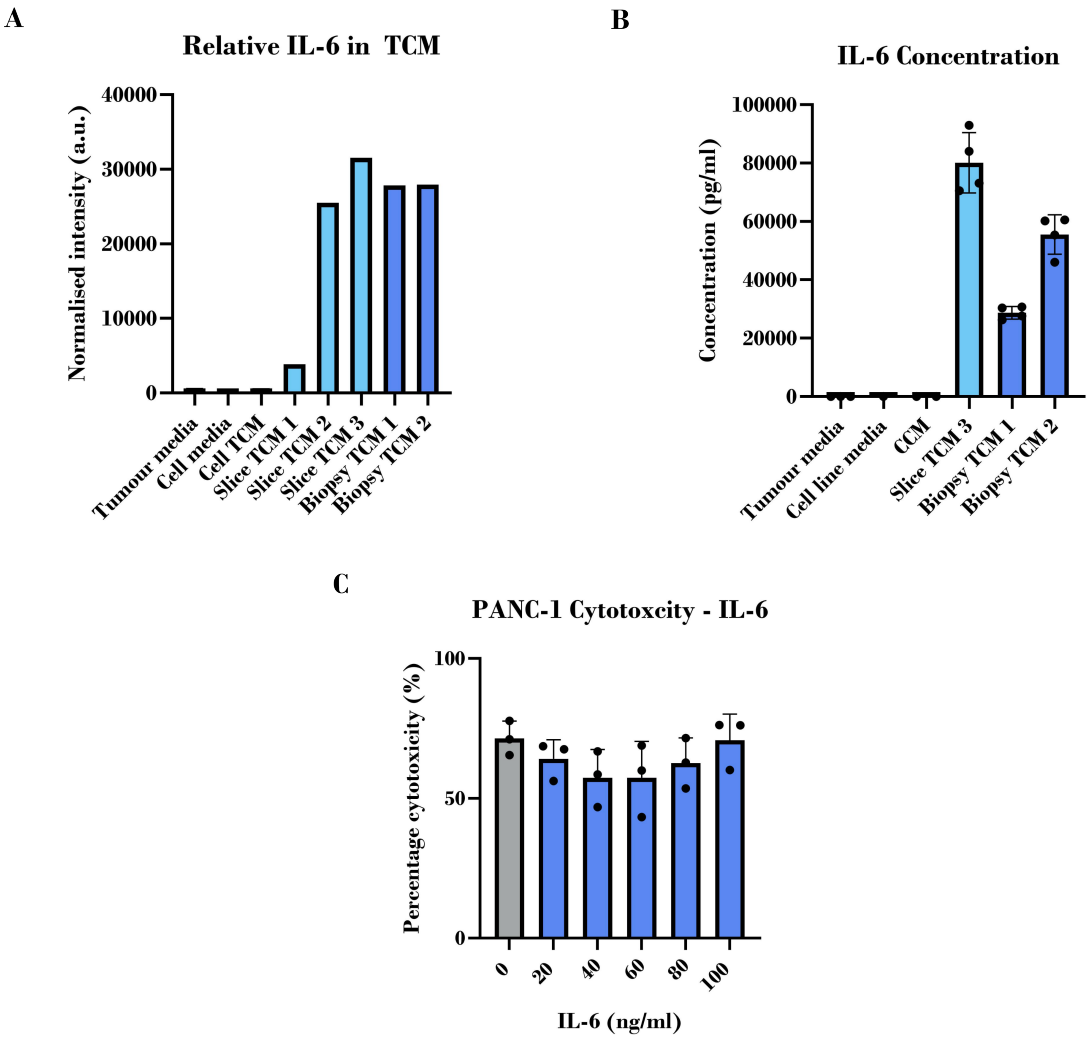


Figure C.5: PDAC tumour concentrations of IL-6 and their effect on *in vitro* CAR-T cell cytotoxicity. (A) Relative quantification of IL-6 in media samples used for cytokine array. (B) Concentration of IL-6 present in tumour conditioned media samples measured by ELISA. (C) *In vitro* impedance-based cytotoxicity assay using 1:1 effector:target ratio of PANC-1 cells with CAR-T cells. Percentage cytotoxicity calculated in the presence of concentrations of IL-6 within the ranges calculated from the tumour conditioned media. Analysed using Kruskal-Wallis test. Duplicates were used to calculate cytokine array values, for ELISA n=4 technical replicates per media sample and for cytotoxicity n=3 healthy donor PBMCs were used to generate CAR-T cells.

D
Results 4: Appendix

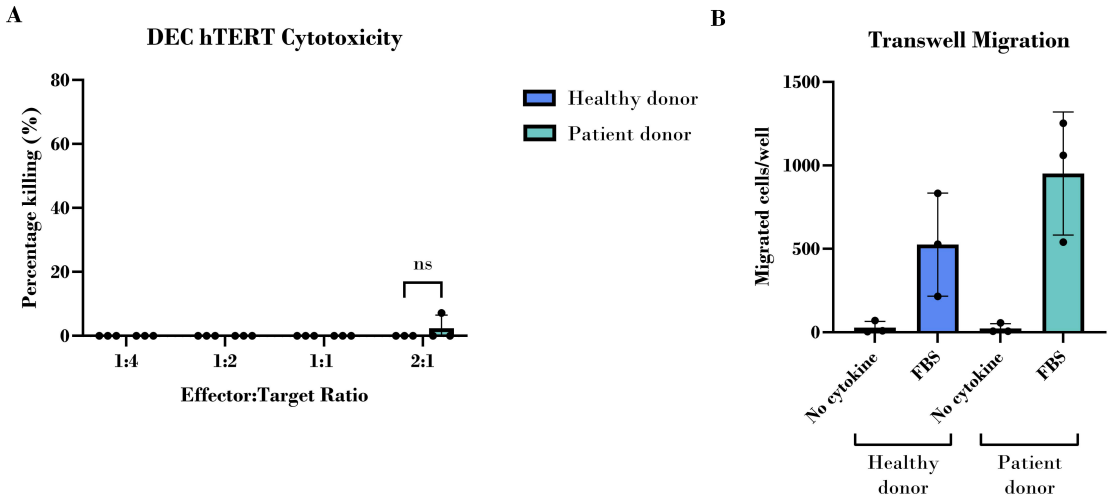


Figure D.1: The *in vitro* functionality of healthy donor and patient-derived CAR-T cells. (A) CAR-T cell cytotoxicity of DEC hTERT cells measured by xCELLigence impedance assay. (B) Migration of cells towards 10% FBS using transwell migration assay. Cytotoxicity analysed with 2-way ANOVA and migration with 1-way ANOVA, both with Tukey's multiple comparisons test. For all analyses n=3 healthy donor and patient donor PBMC samples were used to generate CAR-T cells.

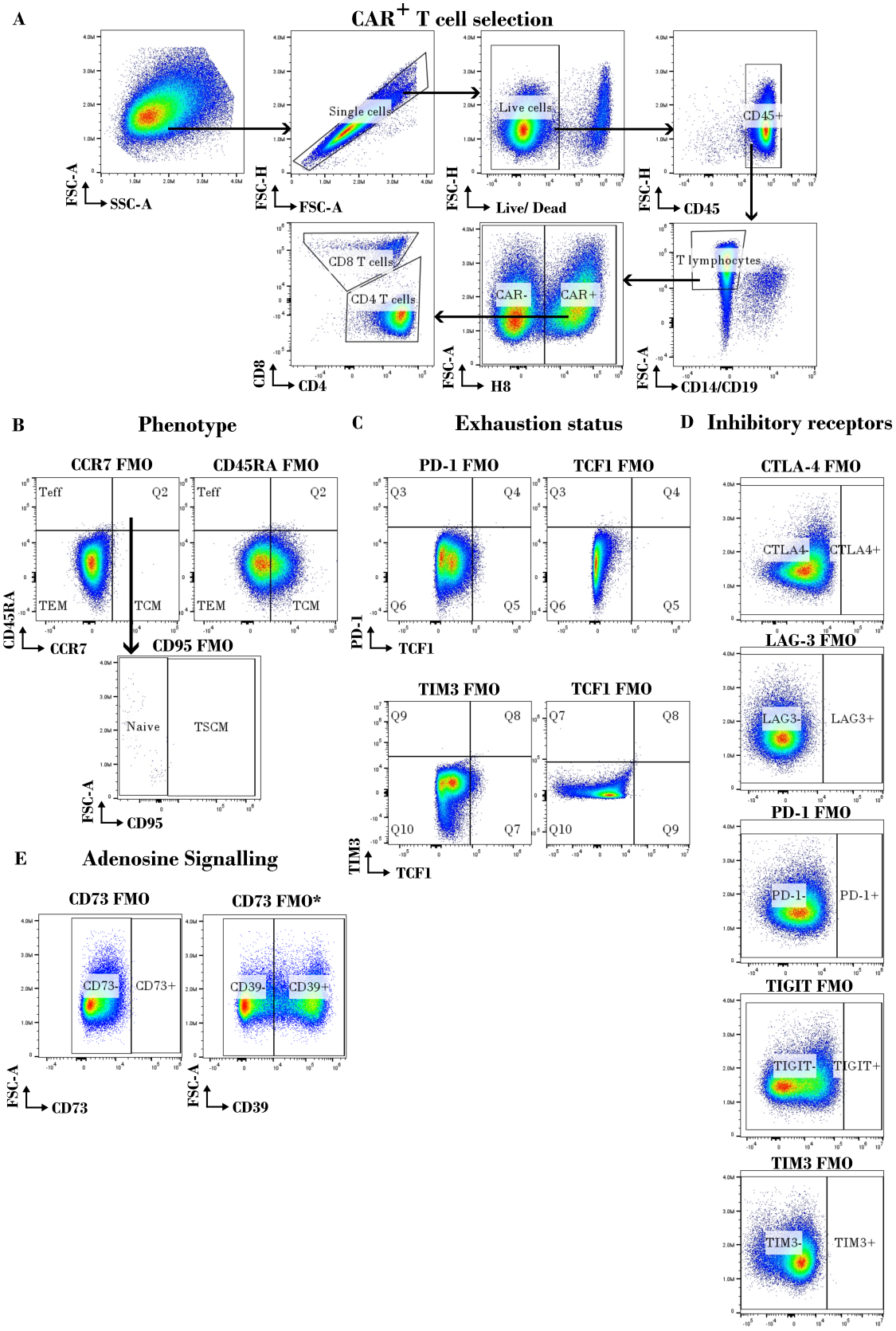


Figure D.2: Gating strategy for spectral flow cytometry. (A) Pseudocolour plots showing gating strategy to select for CAR$^+$ CD4/CD8 T cells. FMO controls used to gate (B) T cell phenotype, (C) exhaustion status, (D) inhibitory marker expression, and (E) adenosine signalling. Plots shown are for CD4 T cells but were gated separately for CD8 T cells. *CD73 FMO was used to gate CD39 as insufficient antibody was available for FMOs for all markers.

References

Abdelhakim, Haitham, Hisham Abdel-Azim and Ayman Saad (June 2017). 'Role of $\alpha\beta$ T cell depletion in prevention of graft versus host disease'. en. In: *Biomedicines* 5.3, p. 35.

Abdo, Luiza, Leonardo Ribeiro Batista-Silva and Martín Hernán Bonamino (June 2025). 'Cost-effective strategies for CAR-T cell therapy manufacturing'. en. In: *Mol Ther Oncol* 33.2, p. 200980.

Abdullah, Kalil G et al. (Apr. 2022). 'Establishment of patient-derived organoid models of lower-grade glioma'. en. In: *Neuro. Oncol.* 24.4, pp. 612–623.

Abiko, K et al. (Apr. 2015). 'IFN-γ from lymphocytes induces PD-L1 expression and promotes progression of ovarian cancer'. en. In: *Br. J. Cancer* 112.9, pp. 1501–1509.

Abraham-Miranda, Julieta et al. (Sept. 2022). 'CAR-T manufactured from frozen PBMC yield efficient function with prolonged in vitro production'. en. In: *Front. Immunol.* 13, p. 1007042.

Abramson, Jeremy S et al. (Sept. 2020). 'Lisocabtagene maraleucel for patients with relapsed or refractory large B-cell lymphomas (TRANSCEND NHL 001): a multicentre seamless design study'. en. In: *Lancet* 396.10254, pp. 839–852.

Acharya, Nandini et al. (Sept. 2020). 'Endogenous glucocorticoid signaling regulates CD8+ T cell differentiation and development of dysfunction in the tumor microenvironment'. en. In: *Immunity* 53.3, 658–671.e6.

Adabi, Elham et al. (Feb. 2025). 'Enhanced conversion of T cells into CAR T cells by modulation of the MAPK/ERK pathway'. en. In: *Cell Rep. Med.* 6.2, p. 101970.

Adusumilli, Prasad S et al. (Nov. 2021). 'A phase I trial of regional mesothelin-targeted CAR T-cell therapy in patients with malignant pleural disease, in combination with the anti-PD-1 agent pembrolizumab'. en. In: *Cancer Discov.* 11.11, pp. 2748–2763.

Agarwal, Sangya et al. (Oct. 2023). 'Deletion of the inhibitory co-receptor CTLA-4 enhances and invigorates chimeric antigen receptor T cells'. en. In: *Immunity* 56.10, 2388–2407.e9.

Aggarwal, Bharat B (Sept. 2003). 'Signalling pathways of the TNF superfamily: a double-edged sword'. en. In: *Nat. Rev. Immunol.* 3.9, pp. 745–756.

Agliardi, Giulia et al. (Jan. 2021). 'Intratumoral IL-12 delivery empowers CAR-T cell immunotherapy in a pre-clinical model of glioblastoma'. en. In: *Nat. Commun.* 12.1, p. 444.

Ahmed, Eman N, Lauren C Cutmore and John F Marshall (Sept. 2024). 'Syngeneic mouse models for pre-clinical evaluation of CAR T cells'. en. In: *Cancers (Basel)* 16.18, p. 3186.

Ahmed, Nabil et al. (May 2015). 'Human epidermal growth factor receptor 2 (HER2) - Specific chimeric antigen receptor - Modified T cells for the immunotherapy of HER2-positive sarcoma'. In: *J. Clin. Oncol.* 33.15, pp. 1688–1696.

Akce, Mehmet et al. (Sept. 2018). 'The Potential of CAR T Cell Therapy in Pancreatic Cancer'. In: *Front. Immunol.* 9.SEP, p. 2166.

Alam, S M K et al. (Feb. 2018). 'Trophoblast Glycoprotein (TPGB/5T4) in Human Placenta: Expression, Regulation, and Presence in Extracellular Microvesicles and Exosomes'. In: *Reprod. Sci.* 25.2, p. 185.

Allen, Elizabeth et al. (Apr. 2017). 'Combined antiangiogenic and anti-PD-L1 therapy stimulates tumor immunity through HEV formation'. en. In: *Sci. Transl. Med.* 9.385.

Alrifai, Doraid, Debashis Sarker and John Maher (2016). 'Prospects for adoptive immunotherapy of pancreatic cancer using chimeric antigen receptor-engineered T-cells'. en. In: *Immunopharmacol. Immunotoxicol.* 38.1, pp. 50–60.

Amatya, Christina et al. (Mar. 2024). 'Optimization of anti-CD19 CAR T cell production for treatment of patients with chronic lymphocytic leukemia'. en. In: *Mol. Ther. Methods Clin. Dev.* 32.1, p. 101212.

Amri, Fakhrddine et al. (Sept. 2023). 'Association between pancreatic cancer and diabetes: insights from a retrospective cohort study'. en. In: *BMC Cancer* 23.1, p. 856.

Arai, Jun et al. (Feb. 2023). 'The immunological role of ADAMs in the field of gastroenterological chronic inflammatory diseases and cancers: a review'. en. In: *Oncogene* 42.8, pp. 549–558.

Aslanian, Harry R, Jeffrey H Lee and Marcia Irene Canto (July 2020). 'AGA clinical practice update on pancreas cancer screening in high-risk individuals: Expert review'. en. In: *Gastroenterology* 159.1, pp. 358–362.

Aspalter, Rosa Maria, Martha Marianne Eibl and Hermann Maximilian Wolf (Oct. 2003). 'Regulation of TCR-mediated T cell activation by TNF-RII'. en. In: *J. Leukoc. Biol.* 74.4, pp. 572–582.

Ayuketang, Francis Ayuk and Ulrich Jäger (Feb. 2022). 'Management of Cytokine Release Syndrome (CRS) and HLH'. In: *The EBMT/EHA CAR-T Cell Handbook*. Cham: Springer International Publishing, pp. 135–139.

Backx, Elyne et al. (Jan. 2022). 'On the origin of pancreatic cancer: Molecular tumor subtypes in perspective of exocrine cell plasticity'. en. In: *Cell. Mol. Gastroenterol. Hepatol.* 13.4, pp. 1243–1253.

Baguet, Clémentine, Jérôme Larghero and Miryam Mebarki (Jan. 2024). 'Early predictive factors of failure in autologous CAR T-cell manufacturing and/or efficacy in hematologic malignancies'. en. In: *Blood Adv* 8.2, pp. 337–342.

Bailey, Stefanie R et al. (Mar. 2022). 'Blockade or deletion of IFNγ reduces macrophage activation without compromising CAR T-cell function in hematologic malignancies'. en. In: *Blood Cancer Discov.* 3.2, pp. 136–153.

Baitsch, Lukas et al. (June 2011). 'Exhaustion of tumor-specific $CD8^+$ T cells in metastases from melanoma patients'. en. In: *J. Clin. Invest.* 121.6, pp. 2350–2360.

Balança, Camille-Charlotte et al. (Jan. 2021). 'PD-1 blockade restores helper activity of tumor-infiltrating, exhausted PD-1hiCD39+ CD4 T cells'. en. In: *JCI Insight* 6.2.

Bandara, Veronika et al. (May 2024). 'Engineered CAR-T cells targeting the non-functional P2X purinoceptor 7 (P2X7) receptor as a novel treatment for ovarian cancer'. en. In: *Clin. Transl. Immunology* 13.5, e1512.

Barroso, Margarida et al. (Oct. 2022). 'A path to translation: How 3D patient tumor avatars enable next generation precision oncology'. In: *Cancer Cell*.

Beatty, Gregory L et al. (July 2018). 'Activity of Mesothelin-Specific Chimeric Antigen Receptor T Cells Against Pancreatic Carcinoma Metastases in a Phase 1 Trial'. In: *Gastroenterology* 155.1, pp. 29–32.

Beavis, Paul A et al. (Mar. 2017). 'Targeting the adenosine 2A receptor enhances chimeric antigen receptor T cell efficacy'. en. In: *J. Clin. Invest.* 127.3, pp. 929–941.

Benmebarek, Mohamed-Reda et al. (Mar. 2019). 'Killing mechanisms of chimeric antigen receptor (CAR) T cells'. en. In: *Int. J. Mol. Sci.* 20.6, p. 1283.

Benslimane-Ahmim, Zahia et al. (July 2013). 'Mechanistic study of the proangiogenic effect of osteoprotegerin'. en. In: *Angiogenesis* 16.3, pp. 575–593.

Bernard, Nick (Dec. 2022). 'Origin of immune checkpoint inhibitors'. en. In: *Nature Research*.

Berrozpe, G et al. (July 1994). 'Comparative analysis of mutations in the p53 and K-ras genes in pancreatic cancer'. en. In: *Int. J. Cancer* 58.2, pp. 185–191.

Biga, Lindsay M et al. (Sept. 2019). '17.9 The Pancreas'. en. In: *Anatomy & Physiology*. OpenStax/Oregon State University.

Blando, Jorge et al. (2019). 'Comparison of immune infiltrates in melanoma and pancreatic cancer highlights VISTA as a potential target in pancreatic cancer'. In: *Proc. Natl. Acad. Sci. U. S. A.* 116.5.

Blank, Christian U et al. (Nov. 2019). 'Defining 'T cell exhaustion''. en. In: *Nat. Rev. Immunol.* 19.11, pp. 665–674.

Bossi, Giovanna and Gillian M Griffiths (Feb. 2005). 'CTL secretory lysosomes: biogenesis and secretion of a harmful organelle'. en. In: *Semin. Immunol.* 17.1, pp. 87–94.

Boucherit, Nicolas, Laurent Gorvel and Daniel Olive (Dec. 2020). '3D Tumor Models and Their Use for the Testing of Immunotherapies'. In: *Front. Immunol.* 11.

Bougherara, Houcine et al. (2015). 'Real-time imaging of resident T cells in human lung and ovarian carcinomas reveals how different tumor microenvironments control T lymphocyte migration'. In: *Front. Immunol.* 6.OCT, p. 500.

Boutet, Marie et al. (Apr. 2016). 'TGFβ Signaling Intersects with CD103 Integrin Signaling to Promote T-Lymphocyte Accumulation and Antitumor Activity in the Lung Tumor Microenvironment'. In: *Cancer Res.* 76.7, pp. 1757–1769.

Bove, Camilla, John Maher and Maya Glover (May 2024). 'The role of CD4+ CAR T cells in cancer immunotherapy'. en. In: *Transl. Cancer Res.* 13.5, pp. 2580–2586.

Brenchley, Jason M et al. (Apr. 2003). 'Expression of CD57 defines replicative senescence and antigen-induced apoptotic death of CD8+ T cells'. en. In: *Blood* 101.7, pp. 2711–2720.

Brooks, Jordan C, Robert M Shavelle and Kate N Vavra-Musser (Feb. 2019). 'Life expectancy in pancreatic neuroendocrine cancer'. en. In: *Clin. Res. Hepatol. Gastroenterol.* 43.1, pp. 88–97.

Broutier, Laura et al. (Sept. 2016). 'Culture and establishment of self-renewing human and mouse adult liver and pancreas 3D organoids and their genetic manipulation'. en. In: *Nat. Protoc.* 11.9, pp. 1724–1743.

Brown, Christine E et al. (Apr. 2024). 'Locoregional delivery of IL-13Rα2-targeting CAR-T cells in recurrent high-grade glioma: a phase 1 trial'. en. In: *Nat. Med.* 30.4, pp. 1001–1012.

Bruggen, P van der et al. (Dec. 1991). 'A gene encoding an antigen recognized by cytolytic T lymphocytes on a human melanoma'. en. In: *Science* 254.5038, pp. 1643–1647.

Brunet, J F et al. (July 1987). 'A new member of the immunoglobulin superfamily–CTLA-4'. en. In: *Nature* 328.6127, pp. 267–270.

Brunner, K T et al. (Feb. 1968). 'Quantitative assay of the lytic action of immune lymphoid cells on 51-Cr-labelled allogeneic target cells in vitro; inhibition by isoantibody and by drugs'. en. In: *Immunology* 14.2, pp. 181–196.

Burton, Jake et al. (Jan. 2025). 'Optimising CAR-T cell sensitivity by engineering matched extracellular sizes between CAR/antigen and CD2/CD58 adhesion complexes'. en. In: *bioRxiv*, p. 2025.01.06.631424.

Burton, Jake I D et al. (Jan. 2023). 'Inefficient exploitation of accessory receptors reduces the sensitivity of chimeric antigen receptors'. In: *Proceedings of the National Academy of Sciences* 120.2, e2216352120.

Cachot, Amélie et al. (Feb. 2021). 'Tumor-specific cytolytic CD4 T cells mediate immunity against human cancer'. en. In: *Sci. Adv.* 7.9, eabe3348.

Cappell, Kathryn M and James N Kochenderfer (Nov. 2021). 'A comparison of chimeric antigen receptors containing CD28 versus 4-1BB costimulatory domains'. en. In: *Nat. Rev. Clin. Oncol.* 18.11, pp. 715–727.

— (June 2023). 'Long-term outcomes following CAR T cell therapy: what we know so far'. en. In: *Nat. Rev. Clin. Oncol.* 20.6, pp. 359–371.

Cappuccini, Federica et al. (2020). 'Safety and immunogenicity of novel 5T4 viral vectored vaccination regimens in early stage prostate cancer: A phase I clinical trial'. In: *Journal for ImmunoTherapy of Cancer* 8.1.

Carpenter, Eileen S et al. (June 2023). 'Analysis of donor pancreata defines the transcriptomic signature and microenvironment of early neoplastic lesions'. en. In: *Cancer Discov.* 13.6, pp. 1324–1345.

Caruso, Hillary G et al. (Sept. 2015). 'Tuning sensitivity of CAR to EGFR density limits recognition of normal tissue while maintaining potent antitumor activity'. en. In: *Cancer Res.* 75.17, pp. 3505–3518.

Castelletti, Laura et al. (Feb. 2021). 'Anti-Mesothelin CAR T cell therapy for malignant mesothelioma'. en. In: *Biomark. Res.* 9.1, p. 11.

Cekic, Caglar et al. (Nov. 2013). 'Extracellular adenosine regulates naive T cell development and peripheral maintenance'. en. In: *J. Exp. Med.* 210.12, pp. 2693–2706.

Ceniceros, Lucía, Susana Prados and Rafael Alvarez Gallego (2021). 'Jaundice in Pancreatic Cancer'. In: *Textbook of Pancreatic Cancer*. Cham: Springer International Publishing, pp. 1215–1225.

Chamoto, Kenji et al. (Oct. 2023). 'Insights from a 30-year journey: function, regulation and therapeutic modulation of PD1'. en. In: *Nat. Rev. Immunol.* 23.10, pp. 682–695.

Chang, Evelyn, Kelly Cavallo and Samuel M Behar (Mar. 2025). 'CD4 T cell dysfunction is associated with bacterial recrudescence during chronic tuberculosis'. en. In: *Nat. Commun.* 16.1, p. 2636.

Chang, Yun et al. (Apr. 2023). 'CAR-neutrophil mediated delivery of tumor-microenvironment responsive nanodrugs for glioblastoma chemo-immunotherapy'. en. In: *Nat. Commun.* 14.1, p. 2266.

Chari, Suresh and Anam Khan (2022). 'Pancreatic Cancer and Diabetes Mellitus'. en. In: *Pancreatic Cancer: A Multidisciplinary Approach*. Cham: Springer International Publishing, pp. 33–37.

Chari, Suresh T et al. (Feb. 2022). 'Early Detection Initiative: A randomized controlled trial of algorithm-based screening in patients with new onset hyperglycemia and diabetes for early detection of pancreatic ductal adenocarcinoma'. en. In: *Contemp. Clin. Trials* 113.106659, p. 106659.

Charkhchi, Parsa et al. (Dec. 2020). 'CA125 and ovarian cancer: A comprehensive review'. en. In: *Cancers (Basel)* 12.12, p. 3730.

Chatila, T et al. (Aug. 1989). 'Mechanisms of T cell activation by the calcium ionophore ionomycin'. en. In: *J. Immunol.* 143.4, pp. 1283–1289.

Chen, A, Z Velickovic and J Rasko (May 2020). 'Vector copy number quality control testing for CAR T-cells: critical validation parameters'. en. In: *Cytotherapy* 22.5, S142.

Chen, Gregory M et al. (Sept. 2021). 'Integrative bulk and single-cell profiling of premanufacture T-cell populations reveals factors mediating long-term persistence of CAR T-cell therapy'. en. In: *Cancer Discov.* 11.9, pp. 2186–2199.

Chen, Inna Markovna et al. (June 2023). 'Randomized phase 2 study of nab-paclitaxel and gemcitabine with or without tocilizumab as first-line treatment in patients with advanced pancreatic cancer (PACTO)'. en. In: *J. Clin. Oncol.* 41.16_suppl, pp. 4147–4147.

Chen, Joyce et al. (Mar. 2019). 'NR4A transcription factors limit CAR T cell function in solid tumours'. en. In: *Nature* 567.7749, pp. 530–534.

Chen, Quanyu et al. (Jan. 2023). 'Hepatocyte growth factor-mediated apoptosis mechanisms of cytotoxic CD8+ T cells in normal and cirrhotic livers'. en. In: *Cell Death Discov.* 9.1, p. 13.

Cheng, Xiang et al. (Oct. 2012). 'Adiponectin induces pro-inflammatory programs in human macrophages and CD4+ T cells'. en. In: *J. Biol. Chem.* 287.44, pp. 36896–36904.

Chow, Andrew et al. (Dec. 2022). 'Clinical implications of T cell exhaustion for cancer immunotherapy'. en. In: *Nat. Rev. Clin. Oncol.* 19.12, pp. 775–790.

Chu, Gerard J et al. (Dec. 2023). 'The 4-1BBζ costimulatory domain in chimeric antigen receptors enhances CD8+ T-cell functionality following T-cell receptor stimulation'. en. In: *Cancer Cell Int.* 23.1, p. 327.

Chu, Xianjing et al. (July 2024). 'Cancer stem cells: advances in knowledge and implications for cancer therapy'. en. In: *Signal Transduct. Target. Ther.* 9.1, p. 170.

Cigalotto, Lavinia and Denis Martinvalet (Apr. 2024). 'Granzymes in health and diseases: the good, the bad and the ugly'. en. In: *Front. Immunol.* 15, p. 1371743.

Coley, William B The American Journal of The Medical Sciences (May 1893). 'THE TREATMENT OF MALIGNANT TUMORS BY REPEATED INOCULATIONS OF ERYSIPELAS: WITH A REPORT OF TEN ORIGINAL CASES.1: BIBLIOGRAPHY'. en. In: 105.6, p. 1827.

Colina, Alfredo S et al. (Feb. 2024). 'Current advances in experimental and computational approaches to enhance CAR T cell manufacturing protocols and improve clinical efficacy'. en. In: *Front. Mol. Med.* 4, p. 1310002.

Corral, Juan E et al. (Jan. 2019). 'Diagnostic yield from screening asymptomatic individuals at high risk for pancreatic cancer: A meta-analysis of cohort studies'. en. In: *Clin. Gastroenterol. Hepatol.* 17.1, pp. 41–53.

Crawford, Alison et al. (Feb. 2014). 'Molecular and transcriptional basis of $CD4^+$ T cell dysfunction during chronic infection'. en. In: *Immunity* 40.2, pp. 289–302.

Cruceriu, Daniel et al. (Feb. 2020). 'The dual role of tumor necrosis factor-alpha (TNF-α) in breast cancer: molecular insights and therapeutic approaches'. en. In: *Cell. Oncol.* 43.1, pp. 1–18.

D'Cruz, Jason R et al. (Jan. 2025). 'Pancreaticoduodenectomy (Whipple procedure)'. en. In: *StatPearls*. Treasure Island (FL): StatPearls Publishing.

Daher, May and Katayoun Rezvani (Jan. 2021). 'Outlook for new CAR-based therapies with a focus on CAR NK cells: What lies beyond CAR-engineered T cells in the race against cancer'. en. In: *Cancer Discov.* 11.1, pp. 45–58.

Dancy, Ehren et al. (Nov. 2018). 'Clinical predictors of T cell fitness for CAR T cell manufacturing and efficacy in multiple myeloma'. en. In: *Blood* 132.Supplement 1, pp. 1886–1886.

Deaglio, Silvia et al. (June 2007). 'Adenosine generation catalyzed by CD39 and CD73 expressed on regulatory T cells mediates immune suppression'. en. In: *J. Exp. Med.* 204.6, pp. 1257–1265.

Deer, Emily L et al. (May 2010). 'Phenotype and genotype of pancreatic cancer cell lines'. en. In: *Pancreas* 39.4, pp. 425–435.

Deng, Jie et al. (Aug. 2022). 'CXCL5: A coachman to drive cancer progression'. en. In: *Front. Oncol.* 12, p. 944494.

Depil, S et al. (Mar. 2020). ''Off-the-shelf' allogeneic CAR T cells: development and challenges'. en. In: *Nat. Rev. Drug Discov.* 19.3, pp. 185–199.

Deshwar, Amar B et al. (Feb. 2018). 'Diagnostic intervals and pancreatic ductal adenocarcinoma (PDAC) resectability: a single-center retrospective analysis'. en. In: *Ann. Pancreat. Cancer* 1, p. 13.

Di Virgilio, Francesco et al. (Oct. 2018). 'Extracellular ATP and P2 purinergic signalling in the tumour microenvironment'. en. In: *Nat. Rev. Cancer* 18.10, pp. 601–618.

Du, Bing et al. (Apr. 2025). 'CAR-T therapy in solid tumors'. en. In: *Cancer Cell* 43.4, pp. 665–679.

Duan, Deming et al. (Mar. 2021). 'The BCMA-targeted fourth-generation CAR-T cells secreting IL-7 and CCL19 for therapy of refractory/recurrent multiple myeloma'. en. In: *Front. Immunol.* 12, p. 609421.

Dudley, Mark E et al. (Oct. 2002). 'Cancer regression and autoimmunity in patients after clonal repopulation with antitumor lymphocytes'. en. In: *Science* 298.5594, pp. 850–854.

Duijneveldt, Gemma van, Michael D W Griffin and Tracy L Putoczki (Aug. 2020). 'Emerging roles for the IL-6 family of cytokines in pancreatic cancer'. en. In: *Clin. Sci. (Lond.)* 134.16, pp. 2091–2115.

Duncan, Brynn B, Cynthia E Dunbar and Kazusa Ishii (Dec. 2022). 'Applying a clinical lens to animal models of CAR-T cell therapies'. en. In: *Mol. Ther. Methods Clin. Dev.* 27, pp. 17–31.

E. Poruk, K et al. (Feb. 2013). 'The clinical utility of CA 19-9 in pancreatic adenocarcinoma: Diagnostic and prognostic updates'. In: *Curr. Mol. Med.* 13.3, pp. 340–351.

Elsaesser, Heidi, Karsten Sauer and David G Brooks (June 2009). 'IL-21 is required to control chronic viral infection'. en. In: *Science* 324.5934, pp. 1569–1572.

Elta, Grace H et al. (Apr. 2018). 'ACG clinical guideline: Diagnosis and management of pancreatic cysts'. en. In: *Am. J. Gastroenterol.* 113.4, pp. 464–479.

Ene-Obong, Abasi et al. (Nov. 2013). 'Activated pancreatic stellate cells sequester CD8+ T cells to reduce their infiltration of the juxtatumoral compartment of pancreatic ductal adenocarcinoma'. en. In: *Gastroenterology* 145.5, pp. 1121–1132.

Escobar, Giulia, Davide Mangani and Ana C Anderson (Nov. 2020). 'T cell factor 1: A master regulator of the T cell response in disease'. en. In: *Sci. Immunol.* 5.53, eabb9726.

Eshhar, Z et al. (Jan. 1993). 'Specific activation and targeting of cytotoxic lymphocytes through chimeric single chains consisting of antibody-binding domains and the gamma or zeta subunits of the immunoglobulin and T-cell receptors'. en. In: *Proc. Natl. Acad. Sci. U. S. A.* 90.2, pp. 720–724.

Espie, David et al. (2023). 'Live Imaging of CAR T Cell Ca2+ Signals in Tumor Slices Using Confocal Microscopy'. en. In: *Methods Mol. Biol.* 2654, pp. 453–462.

Ethun, Cecilia G et al. (Apr. 2017). 'Distal cholangiocarcinoma and pancreas adenocarcinoma: Are they really the same disease? A 13-institution study from the US Extrahepatic Biliary Malignancy consortium and the central pancreas consortium'. en. In: *J. Am. Coll. Surg.* 224.4, pp. 406–413.

Eyquem, Justin et al. (Mar. 2017). 'Targeting a CAR to the TRAC locus with CRISPR/Cas9 enhances tumour rejection'. en. In: *Nature* 543.7643, pp. 113–117.

Fallah-Mehrjardi, Keyvan et al. (July 2020). 'Pharmacological targeting of immune checkpoint A2aR improves function of anti-CD19 CAR T cells in vitro'. en. In: *Immunol. Lett.* 223, pp. 44–52.

Fayad, L et al. (Jan. 2001). 'Interleukin-6 and interleukin-10 levels in chronic lymphocytic leukemia: correlation with phenotypic characteristics and outcome'. en. In: *Blood* 97.1, pp. 256–263.

Feig, Christine et al. (Dec. 2013). 'Targeting CXCL12 from FAP-expressing carcinoma-associated fibroblasts synergizes with anti-PD-L1 immunotherapy in pancreatic cancer'. en. In: *Proc. Natl. Acad. Sci. U. S. A.* 110.50, pp. 20212–20217.

Feng, Bo et al. (Dec. 2023). 'Collagen-based biomaterials in organoid technology for reproductive medicine: composition, characteristics, and applications'. en. In: *Collagen & Leather* 5.1, pp. 1–26.

Feola, Sara et al. (June 2020). 'Uncovering the tumor antigen landscape: What to know about the discovery process'. en. In: *Cancers (Basel)* 12.6, p. 1660.

Fernandez, Jessica Lage et al. (Nov. 2023). 'A comparative analysis of orthotopic and subcutaneous pancreatic tumour models: Tumour microenvironment and drug delivery'. en. In: *Cancers (Basel)* 15.22, p. 5415.

Flugel, Christian L et al. (Jan. 2023). 'Overcoming on-target, off-tumour toxicity of CAR T cell therapy for solid tumours'. en. In: *Nat. Rev. Clin. Oncol.* 20.1, pp. 49–62.

Ford, B Rhodes et al. (Aug. 2022). 'Tumor microenvironmental signals reshape chromatin landscapes to limit the functional potential of exhausted T cells'. en. In: *Sci. Immunol.* 7.74, eabj9123.

Foskolou, Iosifina P et al. (Sept. 2020). 'The S enantiomer of 2-hydroxyglutarate increases central memory CD8 populations and improves CAR-T therapy outcome'. en. In: *Blood Adv.* 4.18, pp. 4483–4493.

Fraietta, Joseph A et al. (May 2018). 'Determinants of response and resistance to CD19 chimeric antigen receptor (CAR) T cell therapy of chronic lymphocytic leukemia'. en. In: *Nat. Med.* 24.5, pp. 563–571.

Frank, Richard C et al. (May 2021). 'A PAncreatic cancer screening study in individuals with New-onset or DeteriOrating diabetes MEllitus (PANDOME study)'. en. In: *J. Clin. Oncol.* 39.15_suppl, TPS10607–TPS10607.

Freeman, A E and R M Hoffman (Apr. 1986). 'In vivo-like growth of human tumors in vitro'. en. In: *Proc. Natl. Acad. Sci. U. S. A.* 83.8, pp. 2694–2698.

Freeman, G J et al. (Oct. 2000). 'Engagement of the PD-1 immunoinhibitory receptor by a novel B7 family member leads to negative regulation of lymphocyte activation'. en. In: *J. Exp. Med.* 192.7, pp. 1027–1034.

Fu, Yaojie et al. (Feb. 2018). 'The critical roles of activated stellate cells-mediated paracrine signaling, metabolism and onco-immunology in pancreatic ductal adenocarcinoma'. en. In: *Mol. Cancer* 17.1, p. 62.

Gallimore, A et al. (May 1998). 'Induction and exhaustion of lymphocytic choriomeningitis virus-specific cytotoxic T lymphocytes visualized using soluble tetrameric major histocompatibility complex class I-peptide complexes'. en. In: *J. Exp. Med.* 187.9, pp. 1383–1393.

Gao, Dong et al. (Sept. 2014). 'Organoid cultures derived from patients with advanced prostate cancer'. en. In: *Cell* 159.1, pp. 176–187.

Gao, Yan et al. (Sept. 2023). 'Single-cell transcriptomics identify TNFRSF1B as a novel T-cell exhaustion marker for ovarian cancer'. en. In: *Clin. Transl. Med.* 13.9, e1416.

Gattinoni, Luca, Christopher A Klebanoff and Nicholas P Restifo (Oct. 2012). 'Paths to stemness: building the ultimate antitumour T cell'. en. In: *Nat. Rev. Cancer* 12.10, pp. 671–684.

Gerlach, M M et al. (Jan. 2014). 'Slice cultures from head and neck squamous cell carcinoma: A novel test system for drug susceptibility and mechanisms of resistance'. In: *Br. J. Cancer* 110.2, pp. 479–488.

Geyer, Marlene et al. (Jan. 2023). 'A microfluidic-based PDAC organoid system reveals the impact of hypoxia in response to treatment'. en. In: *Cell Death Discov.* 9.1, p. 20.

Ghoneim, Hazem E et al. (June 2017). 'De Novo epigenetic programs inhibit PD-1 blockade-mediated T cell rejuvenation'. en. In: *Cell* 170.1, 142–157.e19.

Gkountakos, Anastasios et al. (Feb. 2023). 'Extrahepatic distal cholangiocarcinoma vs. Pancreatic ductal adenocarcinoma: Histology and molecular profiling for differential diagnosis and treatment'. en. In: *Cancers (Basel)* 15.5, p. 1454.

Glumac, Paige M and Aaron M LeBeau (July 2018). 'The role of CD133 in cancer: a concise review'. en. In: *Clin. Transl. Med.* 7.1, p. 18.

Goggins, Michael et al. (Jan. 2020). 'Management of patients with increased risk for familial pancreatic cancer: updated recommendations from the International Cancer of the Pancreas Screening (CAPS) Consortium'. en. In: *Gut* 69.1, pp. 7–17.

Gold, P and S O Freedman (Sept. 1965). 'Specific carcinoembryonic antigens of the human digestive system'. en. In: *J. Exp. Med.* 122.3, pp. 467–481.

Goloudina, Anastasia et al. (June 2025). 'Shared neoantigens for cancer immunotherapy'. en. In: *Mol Ther Oncol* 33.2, p. 200978.

Gong, Ke et al. (Feb. 2021). 'Tumor necrosis factor in lung cancer: Complex roles in biology and resistance to treatment'. en. In: *Neoplasia* 23.2, pp. 189–196.

Good, Zinaida et al. (Sept. 2022). 'Post-infusion CAR TReg cells identify patients resistant to CD19-CAR therapy'. en. In: *Nat. Med.* 28.9, pp. 1860–1871.

Govindaraj, Chindu et al. (Oct. 2013). 'Impaired Th1 immunity in ovarian cancer patients is mediated by TNFR2+ Tregs within the tumor microenvironment'. en. In: *Clin. Immunol.* 149.1, pp. 97–110.

Gros, Alena et al. (Nov. 2015). 'Selection of circulating PD-1+ lymphocytes from cancer patients enriches for tumor-reactive and mutation-specific lymphocytes'. In: *Journal for Immunotherapy of Cancer* 3.Suppl 2, O2.

Grosskopf, Abigail K et al. (Apr. 2022). 'Delivery of CAR-T cells in a transient injectable stimulatory hydrogel niche improves treatment of solid tumors'. en. In: *Sci. Adv.* 8.14, eabn8264.

Grossman, William J et al. (Nov. 2004). 'Differential expression of granzymes A and B in human cytotoxic lymphocyte subsets and T regulatory cells'. en. In: *Blood* 104.9, pp. 2840–2848.

Guedan, Sonia et al. (Jan. 2018). 'Enhancing CAR T cell persistence through ICOS and 4-1BB costimulation'. en. In: *JCI Insight* 3.1, e96976.

Gunderson, Andrew J et al. (Apr. 2020). 'TGFβ suppresses CD8+ T cell expression of CXCR3 and tumor trafficking'. en. In: *Nat. Commun.* 11.1, p. 1749.

Gunti, Sreenivasulu et al. (Feb. 2021). 'Organoid and spheroid tumor models: Techniques and applications'. en. In: *Cancers (Basel)* 13.4, p. 874.

Guo, Yelei et al. (Nov. 2023). 'Reciprocal activation of antigen-presenting cells and CAR T cells triggers a widespread endogenous anti-tumor immune response through sustained high-level IFNγ production'. en. In: *Cancer Biol. Med.* 20.11, pp. 1–4.

Guo, Yugang et al. (June 2021). 'Metabolic reprogramming of terminally exhausted CD8+ T cells by IL-10 enhances anti-tumor immunity'. en. In: *Nat. Immunol.* 22.6, pp. 746–756.

Haabeth, Ole Audun Werner et al. (Apr. 2014). 'How do CD4(+) T cells detect and eliminate tumor cells that either lack or express MHC class II molecules?' en. In: *Front. Immunol.* 5, p. 174.

Haas, Andrew R et al. (Nov. 2019). 'Phase I study of Lentiviral-transduced chimeric antigen receptor-modified T cells recognizing mesothelin in advanced solid cancers'. en. In: *Mol. Ther.* 27.11, pp. 1919–1929.

Hain, Elisabeth et al. (Nov. 2016). 'Management of gastrinoma'. fr. In: *Presse Med.* 45.11, pp. 986–991.

Halbrook, Christopher J et al. (Apr. 2023). 'Pancreatic cancer: Advances and challenges'. en. In: *Cell* 186.8, pp. 1729–1754.

Harper, Jay et al. (Aug. 2017). 'Preclinical evaluation of MEDI0641, a pyrrolobenzodiazepine-conjugated antibody-drug conjugate targeting 5T4'. en. In: *Mol. Cancer Ther.* 16.8, pp. 1576–1587.

Harris, Daniel T et al. (Feb. 2018). 'Comparison of T cell activities mediated by human TCRs and CARs that use the same recognition domains'. en. In: *J. Immunol.* 200.3, pp. 1088–1100.

Harrison, Charlotte (Oct. 2024). 'TCR cell therapies vanquish solid tumors - finally'. en. In: *Nat. Biotechnol.* 42.10, pp. 1477–1479.

Harrop, Richard, Daniel G Blount et al. (Oct. 2024). 'Targeting the tumour antigen 5T4 using CAR-T cells for the treatment of Acute Myeloid Leukaemia'. en. In: *Mol. Cancer Ther.*, OF1–OF12.

Harrop, Richard, Noel Drury et al. (July 2008). 'Vaccination of colorectal cancer patients with TroVax given alongside chemotherapy (5-fluorouracil, leukovorin and irinotecan) is safe and induces potent immune responses'. en. In: *Cancer Immunol. Immunother.* 57.7, pp. 977–986.

Haskins, K et al. (Apr. 1983). 'The major histocompatibility complex-restricted antigen receptor on T cells. I. Isolation with a monoclonal antibody'. en. In: *J. Exp. Med.* 157.4, pp. 1149–1169.

Hay, Zachary L Z and Jill E Slansky (Feb. 2022). 'Granzymes: The molecular executors of immune-mediated cytotoxicity'. en. In: *Int. J. Mol. Sci.* 23.3, p. 1833.

Hayashida, Kazutaka et al. (June 2010). 'Molecular and cellular mechanisms of ectodomain shedding'. en. In: *Anat. Rec. (Hoboken)* 293.6, pp. 925–937.

Heinemann, V (Dec. 2002). 'Gemcitabine in the treatment of advanced pancreatic cancer: A comparative analysis of randomized trials'. en. In: *Semin. Oncol.* 29.6, pp. 9–16.

Hernandez, Inmaculada, Vinay Prasad and Walid F Gellad (July 2018). 'Total costs of chimeric antigen receptor T-cell immunotherapy'. en. In: *JAMA Oncol.* 4.7, pp. 994–996.

Hernandez-Lopez, Rogelio A et al. (Mar. 2021). 'T cell circuits that sense antigen density with an ultrasensitive threshold'. en. In: *Science* 371.6534, pp. 1166–1171.

Hill, Joshua A, Sergio Giralt et al. (Nov. 2019). 'CAR-T - and a side order of IgG, to go? - Immunoglobulin replacement in patients receiving CAR-T cell therapy'. en. In: *Blood Rev.* 38.100596, p. 100596.

Hill, Joshua A, Daniel Li et al. (Jan. 2018). 'Infectious complications of CD19-targeted chimeric antigen receptor-modified T-cell immunotherapy'. en. In: *Blood* 131.1, pp. 121–130.

Hill, Joshua A and Susan K Seo (Aug. 2020). 'How I prevent infections in patients receiving CD19-targeted chimeric antigen receptor T cells for B-cell malignancies'. en. In: *Blood* 136.8, pp. 925–935.

Himer, Leonóra et al. (Aug. 2010). 'Adenosine A2A receptor activation protects CD4+ T lymphocytes against activation-induced cell death'. en. In: *FASEB J.* 24.8, pp. 2631–2640.

Hingorani, Sunil R et al. (May 2005). 'Trp53R172H and KrasG12D cooperate to promote chromosomal instability and widely metastatic pancreatic ductal adenocarcinoma in mice'. en. In: *Cancer Cell* 7.5, pp. 469–483.

Hole, N and P L Stern (Mar. 1988). 'A 72 kD trophoblast glycoprotein defined by a monoclonal antibody'. en. In: *Br. J. Cancer* 57.3, pp. 239–246.

Holmberg Olausson, Karl et al. (Sept. 2014). 'Prominin-1 (CD133) defines both stem and non-stem cell populations in CNS development and gliomas'. en. In: *PLoS One* 9.9, e106694.

Horvat, Natalie K et al. (Jan. 2024). 'Clinically relevant orthotopic pancreatic cancer models for adoptive T cell transfer therapy'. en. In: *J. Immunother. Cancer* 12.1, e008086.

Hothorn, Torsten (Apr. 2001). *maxstat: Maximally Selected Rank Statistics*. Title of the publication associated with this dataset: CRAN: Contributed Packages.

Hou, Andrew J, Laurence C Chen and Yvonne Y Chen (July 2021). *Navigating CAR-T cells through the solid-tumour microenvironment*.

Hou, Diyu et al. (Dec. 2023). 'Interleukin-6 facilitates acute myeloid leukemia chemoresistance via mitofusin 1-mediated mitochondrial fusion'. en. In: *Mol. Cancer Res.* 21.12, pp. 1366–1378.

Houston, Aileen and Joe O'Connell (Aug. 2004). 'The Fas signalling pathway and its role in the pathogenesis of cancer'. en. In: *Curr. Opin. Pharmacol.* 4.4, pp. 321–326.

Huang, Steve et al. (Aug. 1997). 'Role of A2a extracellular adenosine receptor-mediated signaling in adenosine-mediated inhibition of T-cell activation and expansion'. en. In: *Blood* 90.4, pp. 1600–1610.

Hughes, Daniel et al. (July 2024). 'Development of human pancreatic cancer avatars as a model for dynamic immune landscape profiling and personalized therapy'. en. In: *Sci. Adv.* 10.27, eadm9071.

Huinen, Zowi R et al. (Aug. 2021). 'Anti-angiogenic agents - overcoming tumour endothelial cell anergy and improving immunotherapy outcomes'. en. In: *Nat. Rev. Clin. Oncol.* 18.8, pp. 527–540.

Hull, Ashleigh et al. (Dec. 2020). 'The Expression Profile and Textural Characteristics of C595-Reactive MUC1 in Pancreatic Ductal Adenocarcinoma for Targeted Radionuclide Therapy'. In: *Cancers* 13.1, p. 61.

Hwu, P et al. (Aug. 1995). 'In vivo antitumor activity of T cells redirected with chimeric antibody/T-cell receptor genes'. en. In: *Cancer Res.* 55.15, pp. 3369–3373.

Im, Se Jin et al. (Sept. 2016). 'Defining CD8+ T cells that provide the proliferative burst after PD-1 therapy'. en. In: *Nature* 537.7620, pp. 417–421.

Ishida, Y et al. (Nov. 1992). 'Induced expression of PD-1, a novel member of the immunoglobulin gene superfamily, upon programmed cell death'. en. In: *EMBO J.* 11.11, pp. 3887–3895.

Ismaiel, Abdulrahman et al. (Sept. 2024). 'The role of adipokines in chronic pancreatitis. A systematic review and meta-analysis'. en. In: *J. Gastrointestin. Liver Dis.* 33.3, pp. 394–404.

Iwai, Yoshiko et al. (Sept. 2002). 'Involvement of PD-L1 on tumor cells in the escape from host immune system and tumor immunotherapy by PD-L1 blockade'. en. In: *Proc. Natl. Acad. Sci. U. S. A.* 99.19, pp. 12293–12297.

Jacoberger-Foissac, Célia et al. (Jan. 2023). 'CD73 inhibits cGAS-STING and cooperates with CD39 to promote pancreatic cancer'. en. In: *Cancer Immunol. Res.* 11.1, pp. 56–71.

Jedema, Inge et al. (Apr. 2004). 'New CFSE-based assay to determine susceptibility to lysis by cytotoxic T cells of leukemic precursor cells within a heterogeneous target cell population'. en. In: *Blood* 103.7, pp. 2677–2682.

Jiang, Hua et al. (Dec. 2017). 'Efficient growth suppression in pancreatic cancer PDX model by fully human anti-mesothelin CAR-T cells'. In: *Protein and Cell* 8.12, pp. 926–931.

Jiang, Yu-Li, Ren-Chao Zhang and Yu-Cheng Zhou (Aug. 2019). 'Comparison of overall survival and perioperative outcomes of laparoscopic pancreaticoduodenectomy and open pancreaticoduodenectomy for pancreatic ductal adenocarcinoma: a systematic review and meta-analysis'. en. In: *BMC Cancer* 19.1, p. 781.

Jiang, Xiuyun et al. (July 2017). 'Long-lived pancreatic ductal adenocarcinoma slice cultures enable precise study of the immune microenvironment'. In: *Oncoimmunology* 6.7.

Jiang, Yan and Davendra P S Sohal (Jan. 2023). 'Pancreatic adenocarcinoma management'. en. In: *JCO Oncol. Pract.* 19.1, pp. 19–32.

Jin, Qili et al. (Mar. 2018). 'Rapid flow cytometry-based assay for the evaluation of $\gamma\delta$ T cell-mediated cytotoxicity'. en. In: *Mol. Med. Rep.* 17.3, pp. 3555–3562.

Jin, Xin et al. (Mar. 2020). 'HLA-matched and HLA-haploidentical allogeneic CD19-directed chimeric antigen receptor T-cell infusions are feasible in relapsed or refractory B-cell acute lymphoblastic leukemia before hematopoietic stem cell transplantation'. en. In: *Leukemia* 34.3, pp. 909–913.

Joedicke, Jara J et al. (Mar. 2022). 'Accelerating clinical-scale production of BCMA CAR T cells with defined maturation stages'. en. In: *Mol. Ther. Methods Clin. Dev.* 24, pp. 181–198.

Jonnalagadda, Mahesh et al. (Apr. 2015). 'Chimeric antigen receptors with mutated IgG4 Fc spacer avoid fc receptor binding and improve T cell persistence and antitumor efficacy'. en. In: *Mol. Ther.* 23.4, pp. 757–768.

Jorgovanovic, Dragica et al. (Sept. 2020). 'Roles of IFN-γ in tumor progression and regression: a review'. en. In: *Biomark. Res.* 8.1, p. 49.

Jost, Tanja Rezzonico et al. (June 2016). 'Role of CXCR4-mediated bone marrow colonization in CNS infiltration by T cell acute lymphoblastic leukemia'. en. In: *J. Leukoc. Biol.* 99.6, pp. 1077–1087.

Joy, Joash D et al. (Aug. 2024). 'Human 3D ovarian cancer models reveal malignant cell-intrinsic and -extrinsic factors that influence CAR T-cell activity'. en. In: *Cancer Res.* 84.15, pp. 2432–2449.

Ju, Yixin et al. (Sept. 2024). 'Barriers and opportunities in pancreatic cancer immunotherapy'. en. In: *NPJ Precis. Oncol.* 8.1, p. 199.

Julve, M et al. (Mar. 2025). 'Solid tumour cellular therapy - principles of toxicity management'. en. In: *Immunooncol. Technol.* 25, p. 100737.

Kadomoto, Suguru, Kouji Izumi and Atsushi Mizokami (July 2020). 'The CCL20-CCR6 axis in cancer progression'. en. In: *Int. J. Mol. Sci.* 21.15, p. 5186.

Kagermeier-Schenk, Birgit et al. (Dec. 2011). 'Waif1/5T4 inhibits Wnt/β-catenin signaling and activates noncanonical Wnt pathways by modifying LRP6 subcellular localization'. en. In: *Dev. Cell* 21.6, pp. 1129–1143.

Kallendrusch, Sonja et al. (May 2017). 'Long-Term Tissue Culture of Adult Brain and Spleen Slices on Nanostructured Scaffolds'. In: *Adv. Healthc. Mater.* 6.9, p. 1601336.

Kanda, Mitsuro et al. (Apr. 2012). 'Presence of somatic mutations in most early-stage pancreatic intraepithelial neoplasia'. en. In: *Gastroenterology* 142.4, 730–733.e9.

Kantari-Mimoun, Chahrazade et al. (Dec. 2021). 'CAR T-cell Entry into Tumor Islets Is a Two-Step Process Dependent on IFNg and ICAM-1'. In: *Cancer Immunology Research* 9.12, pp. 1425–1438.

Kanzaki, Hirotaka et al. (Apr. 2013). 'Mutations in K-Ras linked to levels of osteoprotegerin and sensitivity to TRAIL-induced cell death in pancreatic ductal adenocarcinoma cells'. en. In: *Exp. Mol. Pathol.* 94.2, pp. 372–379.

Karimi, Mobin A et al. (Feb. 2014). 'Measuring cytotoxicity by bioluminescence imaging outperforms the standard chromium-51 release assay'. en. In: *PLoS One* 9.2, e89357.

Karpińska, Monika and Marian Czauderna (Mar. 2022). 'Pancreas-its functions, disorders, and physiological impact on the mammals' organism'. en. In: *Front. Physiol.* 13, p. 807632.

Kato, Hiroyuki and Nabeel Bardeesy (Oct. 2024). 'Illuminating the path to pancreatic cancer'. en. In: *Cell Res.* 34.10, pp. 681–682.

Kato, Tomonori et al. (Nov. 2011). 'Correlation of serum IL-6 level with exhaustion of Cytomegalovirus-specific T cells after hematopoietic stem cell transplantation'. en. In: *Blood* 118.21, pp. 360–360.

Kawalekar, Omkar U et al. (Feb. 2016). 'Distinct signaling of coreceptors regulates specific metabolism pathways and impacts memory development in CAR T cells'. en. In: *Immunity* 44.2, pp. 380–390.

Keerthivasan, Shilpa et al. (Feb. 2014). 'β-Catenin promotes colitis and colon cancer through imprinting of proinflammatory properties in T cells'. en. In: *Sci. Transl. Med.* 6.225, 225ra28.

Kershaw, Michael H et al. (Oct. 2006). 'A phase I study on adoptive immunotherapy using gene-modified T cells for ovarian cancer'. en. In: *Clin. Cancer Res.* 12.20 Pt 1, pp. 6106–6115.

Khalaf, Natalia and Basim Ali (Sept. 2022). 'New-onset diabetes as a signpost of early pancreatic cancer: The role of screening'. en. In: *Clin. Gastroenterol. Hepatol.* 20.9, pp. 1927–1930.

Kiesgen, Stefan et al. (Mar. 2021). 'Comparative analysis of assays to measure CAR T-cell-mediated cytotoxicity'. en. In: *Nat. Protoc.* 16.3, pp. 1331–1342.

Kimura, Wataru et al. (Apr. 2014). 'A pancreaticoduodenectomy risk model derived from 8575 cases from a national single-race population (Japanese) using a web-based data entry system: the 30-day and in-hospital mortality rates for pancreaticoduodenectomy'. en. In: *Ann. Surg.* 259.4, pp. 773–780.

Kirsh, Sarah M, Sydney A Pascetta and James Uniacke (2023). 'Spheroids as a 3D model of the hypoxic tumor microenvironment'. en. In: *Methods Mol. Biol.* 2614, pp. 273–285.

Klee, Clara Helena et al. (Jan. 2024). 'In vitro re-challenge of CAR T cells'. en. In: *Methods Cell Biol.* 183, pp. 335–353.

Klichinsky, Michael et al. (Aug. 2020). 'Human chimeric antigen receptor macrophages for cancer immunotherapy'. en. In: *Nat. Biotechnol.* 38.8, pp. 947–953.

Kohli, Karan, Venu G Pillarisetty and Teresa S Kim (Jan. 2022). 'Key chemokines direct migration of immune cells in solid tumors'. en. In: *Cancer Gene Ther.* 29.1, pp. 10–21.

Kokkinos, John et al. (Dec. 2021). 'Ex vivo culture of intact human patient derived pancreatic tumour tissue'. In: *Sci. Rep.* 11.1.

Kong, Weimin et al. (Aug. 2021). 'BET bromodomain protein inhibition reverses chimeric antigen receptor extinction and reinvigorates exhausted T cells in chronic lymphocytic leukemia'. en. In: *J. Clin. Invest.* 131.16, e145459.

Kpeglo, Delanyo et al. (June 2022). 'Modeling the mechanical stiffness of pancreatic ductal adenocarcinoma'. en. In: *Matrix Biol. Plus* 14.100109, p. 100109.

Kranz, Emiko et al. (July 2022). 'Efficient derivation of chimeric-antigen receptor-modified TSCM cells'. en. In: *Front. Immunol.* 13, p. 877682.

Kuwana, Y et al. (Dec. 1987). 'Expression of chimeric receptor composed of immunoglobulin-derived V regions and T-cell receptor-derived C regions'. en. In: *Biochem. Biophys. Res. Commun.* 149.3, pp. 960–968.

Lahusen, Anton et al. (Apr. 2024). 'A pancreatic cancer organoid-in-matrix platform shows distinct sensitivities to T cell killing'. en. In: *Sci. Rep.* 14.1, p. 9377.

Lappas, Courtney M, Jayson M Rieger and Joel Linden (Jan. 2005). 'A2A adenosine receptor induction inhibits IFN-gamma production in murine CD4+ T cells'. en. In: *J. Immunol.* 174.2, pp. 1073–1080.

Larsen, Brian M et al. (July 2021). 'A pan-cancer organoid platform for precision medicine'. en. In: *Cell Rep.* 36.4, p. 109429.

Larson, Rebecca et al. (Nov. 2021). '221 CRISPR screen identifies loss of IFNγR signaling and downstream adhesion as a resistance mechanism to CAR T-cell cytotoxicity in solid but not liquid tumors'. en. In: *J. Immunother. Cancer* 9.Suppl 2, A234–A234.

Lau, E Y M et al. (Aug. 2019). 'Type 2 diabetes is associated with the accumulation of senescent T cells'. en. In: *Clin. Exp. Immunol.* 197.2, pp. 205–213.

Leach, D R, M F Krummel and J P Allison (Mar. 1996). 'Enhancement of antitumor immunity by CTLA-4 blockade'. en. In: *Science* 271.5256, pp. 1734–1736.

Ledergor, Guy et al. (July 2024). 'CD4+ CAR T-cell exhaustion associated with early relapse of multiple myeloma after BCMA CAR T-cell therapy'. en. In: *Blood Adv.* 8.13, pp. 3562–3575.

Lee, Jae W et al. (June 2016). 'Genetically Engineered Mouse Models of Pancreatic Cancer: The KPC Model (LSL-Kras(G12D/+) ;LSL-Trp53(R172H/+) ;Pdx-1-Cre), Its Variants, and Their Application in Immuno-oncology Drug Discovery'. en. In: *Curr. Protoc. Pharmacol.* 73, pp. 14.39.1–14.39.20.

Lee, Sang Yun et al. (Nov. 2023). 'CD8+ chimeric antigen receptor T cells manufactured in absence of CD4+ cells exhibit hypofunctional phenotype'. en. In: *J. Immunother. Cancer* 11.11, e007803.

Lei, Wen et al. (Nov. 2022). 'Safety and feasibility of anti-CD19 CAR-T expressing IL-7 and CCL19 in patients with relapsed or refractory large B-cell lymphoma'. en. In: *Blood* 140.Supplement 1, pp. 12722–12722.

Leighton, J (Dec. 1951). 'A sponge matrix method for tissue culture; formation of organized aggregates of cells in vitro'. en. In: *J. Natl. Cancer Inst.* 12.3, pp. 545–561.

Lenzo, Felicia L et al. (Jan. 2021). 'Immune profiling and immunotherapeutic targets in pancreatic cancer'. en. In: *Ann. Transl. Med.* 9.2, p. 119.

Leung, Po Sing (2010). 'Overview of the pancreas'. en. In: *Adv. Exp. Med. Biol.* 690, pp. 3–12.

Levin, Aron M et al. (Mar. 2012). 'Exploiting a natural conformational switch to engineer an interleukin-2 'superkine''. en. In: *Nature* 484.7395, pp. 529–533.

Li, Bofeng, Lindsay L Jones and Terrence L Geiger (Nov. 2018). 'IL-6 promotes T cell proliferation and expansion under inflammatory conditions in association with low-level RORγt expression'. en. In: *J. Immunol.* 201.10, pp. 2934–2946.

Li, Weizhe, Ronald N Germain and Michael Y Gerner (Apr. 2019). 'High-dimensional cell-level analysis of tissues with Ce3D multiplex volume imaging'. In: *Nature Protocols 2019 14:6* 14.6, pp. 1708–1733.

Liadi, Ivan et al. (May 2015). 'Individual motile CD4(+) T cells can participate in efficient multikilling through conjugation to multiple tumor cells'. en. In: *Cancer Immunol. Res.* 3.5, pp. 473–482.

Lieber, Michael et al. (May 1975). 'Establishment of a continuous tumor-cell line (PANC-1) from a human carcinoma of the exocrine pancreas'. In: *International Journal of Cancer* 15.5, pp. 741–747.

Lim, Chae Yoon, Jae Hyuck Chang, Won Sun Lee, Jeana Kim et al. (Dec. 2021). 'CD40 Agonists Alter the Pancreatic Cancer Microenvironment by Shifting the Macrophage Phenotype toward M1 and Suppress Human Pancreatic Cancer in Organotypic Slice Cultures'. In: *Gut Liver*.

Lim, Chae Yoon, Jae Hyuck Chang, Won Sun Lee, Kang Min Lee et al. (Dec. 2018). 'Organotypic slice cultures of pancreatic ductal adenocarcinoma preserve the tumor microenvironment and provide a platform for drug response'. In: *Pancreatology* 18.8, pp. 913–927.

Lindner, S E et al. (May 2020). 'Chimeric antigen receptor signaling: Functional consequences and design implications'. en. In: *Sci. Adv.* 6.21, eaaz3223.

Liu, Guodi et al. (Dec. 2021). 'Disruption of adenosine 2A receptor improves the anti-tumor function of anti-mesothelin CAR T cells both in vitro and in vivo'. en. In: *Exp. Cell Res.* 409.1, p. 112886.

Liu, Xing and Judy Lieberman (Apr. 2020). 'Knocking 'em Dead: Pore-Forming Proteins in Immune Defense'. en. In: *Annu. Rev. Immunol.* 38.1, pp. 455–485.

Liu, Xiufen et al. (Dec. 2020). 'Multiple proteases are involved in mesothelin shedding by cancer cells'. en. In: *Commun. Biol.* 3.1, p. 728.

Liu, Zhao et al. (Jan. 2023). 'Biological and clinical impacts of glucose metabolism in pancreatic ductal adenocarcinoma'. en. In: *Cancers (Basel)* 15.2, p. 498.

Liu, Zhaoyun et al. (Feb. 2024). 'Challenges and strategies associated with CAR-T cell therapy in blood malignancies'. en. In: *Exp. Hematol. Oncol.* 13.1, p. 22.

Loi, Sherene et al. (July 2013). 'CD73 promotes anthracycline resistance and poor prognosis in triple negative breast cancer'. en. In: *Proc. Natl. Acad. Sci. U. S. A.* 110.27, pp. 11091–11096.

Loyher, Pierre-Louis et al. (Nov. 2016). 'CCR2 influences T regulatory cell migration to tumors and serves as a biomarker of cyclophosphamide sensitivity'. en. In: *Cancer Res.* 76.22, pp. 6483–6494.

Lukashev, Dmitriy E et al. (June 2003). 'Analysis of A2a receptor-deficient mice reveals no significant compensatory increases in the expression of A2b, A1, and A3 adenosine receptors in lymphoid organs'. en. In: *Biochem. Pharmacol.* 65.12, pp. 2081–2090.

Maher, John et al. (Jan. 2002). 'Human T-lymphocyte cytotoxicity and proliferation directed by a single chimeric TCRzeta /CD28 receptor'. en. In: *Nat. Biotechnol.* 20.1, pp. 70–75.

Maitra, Anirban, N Volkan Adsay et al. (Sept. 2003). 'Multicomponent analysis of the pancreatic adenocarcinoma progression model using a pancreatic intraepithelial neoplasia tissue microarray'. en. In: *Mod. Pathol.* 16.9, pp. 902–912.

Maitra, Anirban, Ayush Sharma et al. (2018). 'A prospective study to establish a new-onset diabetes cohort: From the Consortium for the study of Chronic Pancreatitis, diabetes, and Pancreatic Cancer'. en. In: *Pancreas* 47.10, pp. 1244–1248.

Majumder, Biswanath et al. (Feb. 2015). 'Predicting clinical response to anticancer drugs using an ex vivo platform that captures tumour heterogeneity'. en. In: *Nat. Commun.* 6.1, p. 6169.

Malandro, Nicole et al. (Jan. 2016). 'Clonal abundance of tumor-specific CD4(+) T cells potentiates efficacy and alters susceptibility to exhaustion'. en. In: *Immunity* 44.1, pp. 179–193.

Malik, Shivani et al. (Dec. 2021). 'CXCL12 in pancreatic cancer: Its function and potential as a therapeutic drug target'. en. In: *Cancers (Basel)* 14.1, p. 86.

Mallya, Kavita et al. (Aug. 2021). 'Modeling pancreatic cancer in mice for experimental therapeutics'. en. In: *Biochim. Biophys. Acta Rev. Cancer* 1876.1, p. 188554.

Mantzavinou, Artemis et al. (May 2022). 'Robotic versus open pancreaticoduodenectomy, comparing therapeutic indexes; a systematic review'. en. In: *Int. J. Surg.* 101.106633, p. 106633.

Martin, Steve Z et al. (Nov. 2019). 'Ex vivo tissue slice culture system to measure drug-response rates of hepatic metastatic colorectal cancer'. In: *BMC Cancer 2019 19:1* 19.1, pp. 1–14.

Masuda, Ayako et al. (Apr. 2016). 'An improved method for isolation of epithelial and stromal cells from the human endometrium'. en. In: *J. Reprod. Dev.* 62.2, pp. 213–218.

Melenhorst, J Joseph et al. (Feb. 2022). 'Decade-long leukaemia remissions with persistence of CD4+ CAR T cells'. en. In: *Nature* 602.7897, pp. 503–509.

Mercogliano, María Florencia et al. (Apr. 2020). 'Tumor necrosis factor α blockade: An opportunity to tackle breast cancer'. en. In: *Front. Oncol.* 10, p. 584.

Metropulos, Anastasia E, Hidayatullah G Munshi and Daniel R Principe (Dec. 2022). 'The difficulty in translating the preclinical success of combined TGFβ and immune checkpoint inhibition to clinical trial'. en. In: *EBioMedicine* 86.104380, p. 104380.

Meuer, S C et al. (Feb. 1983). 'Clonotypic structures involved in antigen-specific human T cell function. Relationship to the T3 molecular complex'. en. In: *J. Exp. Med.* 157.2, pp. 705–719.

Miron, Michelle et al. (Oct. 2018). 'Human lymph nodes maintain TCF-1hi memory T cells with high functional potential and clonal diversity throughout life'. en. In: *J. Immunol.* 201.7, pp. 2132–2140.

Misra, Sougat et al. (Dec. 2019). 'Ex vivo organotypic culture system of precision-cut slices of human pancreatic ductal adenocarcinoma'. In: *Sci. Rep.* 9.1, p. 2133.

Mitra, Aroshi et al. (May 2023). 'From bench to bedside: the history and progress of CAR T cell therapy'. en. In: *Front. Immunol.* 14, p. 1188049.

Modica, Chiara et al. (July 2021). 'HGF/MET axis induces tumor secretion of tenascin-C and promotes stromal rewiring in pancreatic cancer'. en. In: *Cancers (Basel)* 13.14, p. 3519.

Monici, Monica (Jan. 2005). 'Cell and tissue autofluorescence research and diagnostic applications'. en. In: *Biotechnol. Annu. Rev.* 11, pp. 227–256.

Moradi, Vahid, Azadeh Omidkhoda and Naser Ahmadbeigi (Dec. 2023). 'The paths and challenges of "off-the-shelf" CAR-T cell therapy: An overview of clinical trials'. en. In: *Biomed. Pharmacother.* 169.115888, p. 115888.

Moritz, D et al. (May 1994). 'Cytotoxic T lymphocytes with a grafted recognition specificity for ERBB2-expressing tumor cells'. en. In: *Proc. Natl. Acad. Sci. U. S. A.* 91.10, pp. 4318–4322.

Moro, Carlos Fernández et al. (Aug. 2022). 'Drug-induced tumor-specific cytotoxicity in a whole tissue ex vivo model of human pancreatic ductal adenocarcinoma'. In: *Front. Oncol.* 12.

Moulin, David et al. (Apr. 2025). 'The role of the immune system in osteoarthritis: mechanisms, challenges and future directions'. en. In: *Nat. Rev. Rheumatol.* 21.4, pp. 221–236.

Mukherjee, Malini et al. (Aug. 2017). 'Quantitative imaging approaches to study the CAR immunological synapse'. en. In: *Mol. Ther.* 25.8, pp. 1757–1768.

Murakawa, Masaaki et al. (Aug. 2023). 'Risk factors for early recurrence in patients with pancreatic ductal adenocarcinoma who underwent curative resection'. en. In: *World J. Surg. Oncol.* 21.1, p. 263.

Naganuma, Hiroshi et al. (Mar. 2002). 'Oncofetal antigen 5T4 expression as a prognostic factor in patients with gastric cancer'. en. In: *Anticancer Res.* 22.2B, pp. 1033–1038.

Nath, Sritama and Pinku Mukherjee (June 2014). 'MUC1: a multifaceted oncoprotein with a key role in cancer progression'. en. In: *Trends Mol. Med.* 20.6, pp. 332–342.

Neelapu, Sattva S et al. (Dec. 2017). 'Axicabtagene ciloleucel CAR T-cell therapy in refractory large B-cell lymphoma'. en. In: *N. Engl. J. Med.* 377.26, pp. 2531–2544.

Netto, Daniel et al. (Sept. 2024). 'Systemic therapy for metastatic pancreatic cancer-current landscape and future directions'. en. In: *Curr. Oncol.* 31.9, pp. 5206–5223.

Nguyen, Duc-Huy T et al. (Aug. 2019). 'A biomimetic pancreatic cancer on-chip reveals endothelial ablation via ALK7 signaling'. en. In: *Sci. Adv.* 5.8, eaav6789.

Nouri, Yasmin, Robert Weinkove and Rachel Perret (Aug. 2023). 'An in vitro model to assess CRS potential of CAR T cells using a tumor cell line and autologous monocytes'. en. In: *Curr. Protoc.* 3.8, e864.

Nywening, Timothy M et al. (June 2018). 'Targeting both tumour-associated CXCR2+ neutrophils and CCR2+ macrophages disrupts myeloid recruitment and improves chemotherapeutic responses in pancreatic ductal adenocarcinoma'. en. In: *Gut* 67.6, pp. 1112–1123.

Öhlund, Daniel et al. (Mar. 2017). 'Distinct populations of inflammatory fibroblasts and myofibroblasts in pancreatic cancer'. In: *J. Exp. Med.* 214.3, pp. 579–596.

Okabayashi, Takehiro et al. (Feb. 2013). 'Diagnosis and management of insulinoma'. en. In: *World J. Gastroenterol.* 19.6, pp. 829–837.

Olubajo, Farouk, Shailendra Achawal and John Greenman (Jan. 2020). 'Development of a Microfluidic Culture Paradigm for Ex Vivo Maintenance of Human Glioblastoma Tissue: A New Glioblastoma Model?' In: *Transl. Oncol.* 13.1, pp. 1–10.

Onyema, Oscar Okwudiri et al. (Mar. 2015). 'Chemotherapy-induced changes and immunosenescence of CD8+ T-cells in patients with breast cancer'. en. In: *Anticancer Res.* 35.3, pp. 1481–1489.

Ooft, Salo N et al. (Oct. 2019). 'Patient-derived organoids can predict response to chemotherapy in metastatic colorectal cancer patients'. en. In: *Sci. Transl. Med.* 11.513, eaay2574.

Otero-Mateo, Marc et al. (Mar. 2025). 'KPC pancreatic cancer cells are a novel immunocompetent murine model supporting human adenovirus replication and tumor oncolysis'. en. In: *Mol Ther Oncol* 33.1, p. 200928.

Owens, Gemma L et al. (Apr. 2018). 'Preclinical Assessment of CAR T-Cell Therapy Targeting the Tumor Antigen 5T4 in Ovarian Cancer'. en. In: *J. Immunother.* 41.3, pp. 130–140.

Palani, Hamenth Kumar et al. (June 2025). 'Safety, efficacy and total cost of point-of-care manufactured anti-CD19 CAR-T cell therapy in India: VELCART trial'. en. In: *Mol Ther Oncol* 33.2, p. 200977.

Pampaloni, Francesco, Emmanuel G Reynaud and Ernst H K Stelzer (Oct. 2007). 'The third dimension bridges the gap between cell culture and live tissue'. en. In: *Nat. Rev. Mol. Cell Biol.* 8.10, pp. 839–845.

Pankova, Daniela et al. (July 2019). 'RASSF1A controls tissue stiffness and cancer stem-like cells in lung adenocarcinoma'. en. In: *EMBO J.* 38.13, e100532.

Papa, Sophie et al. (June 2023). 'Intratumoral pan-ErbB targeted CAR-T for head and neck squamous cell carcinoma: interim analysis of the T4 immunotherapy study'. en. In: *J. Immunother. Cancer* 11.6, e007162.

Park, Julie R et al. (Apr. 2007). 'Adoptive transfer of chimeric antigen receptor re-directed cytolytic T lymphocyte clones in patients with neuroblastoma'. en. In: *Mol. Ther.* 15.4, pp. 825–833.

Passariello, Margherita et al. (Feb. 2025). 'Tri-specific tribodies targeting 5T4, CD3, and immune checkpoint drive stronger functional T-cell responses than combinations of antibody therapeutics'. en. In: *Cell Death Discov.* 11.1, p. 58.

Patel, Ashna et al. (Jan. 2024). 'Using CombiCells, a platform for titration and combinatorial display of cell surface ligands, to study T-cell antigen sensitivity modulation by accessory receptors'. en. In: *EMBO J.* 43.1, pp. 132–150.

Paul, Jeddeo et al. (June 2024). 'Trends in prices of checkpoint inhibitors in the US, 2016-2023'. en. In: *J. Clin. Oncol.* 42.16_suppl, pp. 11075–11075.

Peng, Zheng et al. (Mar. 2025). '3D tumor cultures for drug resistance and screening development in clinical applications'. en. In: *Mol. Cancer* 24.1, p. 93.

Peper, Janet Kerstin et al. (Mar. 2014). 'An impedance-based cytotoxicity assay for real-time and label-free assessment of T-cell-mediated killing of adherent cells'. en. In: *J. Immunol. Methods* 405, pp. 192–198.

Peranzoni, Elisa, Houcine Bougherara et al. (Dec. 2017). 'Ex Vivo Imaging of Resident CD8 T Lymphocytes in Human Lung Tumor Slices Using Confocal Microscopy'. In: *J. Vis. Exp.* 2017.130, p. 55709.

Peranzoni, Elisa, Jean Lemoine et al. (Apr. 2018). 'Macrophages impede CD8 T cells from reaching tumor cells and limit the efficacy of anti–PD-1 treatment'. In: *Proc. Natl. Acad. Sci. U. S. A.* 115.17, E4041–E4050.

Pesaresi, Martina et al. (Feb. 2021). 'The chemokine receptors Ccr5 and Cxcr6 enhance migration of mesenchymal stem cells into the degenerating retina'. en. In: *Mol. Ther.* 29.2, pp. 804–821.

Peters, Mary Linton B et al. (Dec. 2018). 'Progression to pancreatic ductal adenocarcinoma from pancreatic intraepithelial neoplasia: Results of a simulation model'. en. In: *Pancreatology* 18.8, pp. 928–934.

Petersen, Christopher T et al. (Feb. 2018). 'Improving T-cell expansion and function for adoptive T-cell therapy using ex vivo treatment with PI3Kδ inhibitors and VIP antagonists'. en. In: *Blood Adv.* 2.3, pp. 210–223.

Petrelli, Fausto et al. (July 2020). 'Outcomes following immune checkpoint inhibitor treatment of patients with microsatellite instability-high cancers: A systematic review and meta-analysis: A systematic review and meta-analysis'. en. In: *JAMA Oncol.* 6.7, pp. 1068–1071.

Piraner, Dan I et al. (Feb. 2025). 'Engineered receptors for soluble cellular communication and disease sensing'. en. In: *Nature* 638.8051, pp. 805–813.

Poirot, Laurent et al. (Sept. 2015). 'Multiplex genome-edited T-cell manufacturing platform for "off-the-shelf" adoptive T-cell immunotherapies'. en. In: *Cancer Res.* 75.18, pp. 3853–3864.

Porter, David L et al. (Aug. 2011). 'Chimeric antigen receptor-modified T cells in chronic lymphoid leukemia'. en. In: *N. Engl. J. Med.* 365.8, pp. 725–733.

Posey, Avery D et al. (June 2016). 'Engineered CAR T Cells Targeting the Cancer-Associated Tn-Glycoform of the Membrane Mucin MUC1 Control Adenocarcinoma'. In: *Immunity* 44.6, pp. 1444–1454.

Postow, Michael A et al. (May 2015). 'Nivolumab and ipilimumab versus ipilimumab in untreated melanoma'. en. In: *N. Engl. J. Med.* 372.21, pp. 2006–2017.

Pothula, Srinivasa P et al. (Dec. 2020). 'Targeting HGF/c-MET axis in pancreatic cancer'. en. In: *Int. J. Mol. Sci.* 21.23, p. 9170.

Priceman, Saul J et al. (2018). 'Co-stimulatory signaling determines tumor antigen sensitivity and persistence of CAR T cells targeting PSCA+ metastatic prostate cancer'. en. In: *Oncoimmunology* 7.2, e1380764.

Procaccini, Claudio et al. (Oct. 2013). 'Role of adipokines signaling in the modulation of T cells function'. en. In: *Front. Immunol.* 4, p. 332.

Qasim, Waseem et al. (Jan. 2017). 'Molecular remission of infant B-ALL after infusion of universal TALEN gene-edited CAR T cells'. en. In: *Sci. Transl. Med.* 9.374.

Qdaisat, Sadeem et al. (Sept. 2025). 'Sensitization of tumours to immunotherapy by boosting early type-I interferon responses enables epitope spreading'. en. In: *Nat. Biomed. Eng.* 9.9, pp. 1437–1452.

Raglow, Zoe et al. (Sept. 2022). 'Targeting glycans for CAR therapy: The advent of sweet CARs'. en. In: *Mol. Ther.* 30.9, pp. 2881–2890.

Rakshit, Srabanti et al. (Nov. 2014). 'Interferon-gamma induced cell death: Regulation and contributions of nitric oxide, cJun N-terminal kinase, reactive oxygen species and peroxynitrite'. en. In: *Biochim. Biophys. Acta* 1843.11, pp. 2645–2661.

Rappa, Germana et al. (Apr. 2013). 'Wnt interaction and extracellular release of prominin-1/CD133 in human malignant melanoma cells'. en. In: *Exp. Cell Res.* 319.6, pp. 810–819.

Rappaport, Amy R et al. (Apr. 2024). 'A shared neoantigen vaccine combined with immune checkpoint blockade for advanced metastatic solid tumors: phase 1 trial interim results'. en. In: *Nat. Med.* 30.4, pp. 1013–1022.

Rašková, Magdalena et al. (Nov. 2022). 'The role of IL-6 in cancer cell invasiveness and metastasis-overview and therapeutic opportunities'. en. In: *Cells* 11.22, p. 3698.

Ravi, Vidhya M et al. (Aug. 2019). 'Human organotypic brain slice culture: a novel framework for environmental research in neuro-oncology'. In: *Life Science Alliance* 2.4.

Ray, Arja et al. (Feb. 2022). 'Stromal architecture directs early dissemination in pancreatic ductal adenocarcinoma'. In: *JCI Insight* 7.3.

Reinherz, E L, R E Hussey and S F Schlossman (Oct. 1980). 'A monoclonal antibody blocking human T cell function'. en. In: *Eur. J. Immunol.* 10.10, pp. 758–762.

Ren, Bing, Xiaoying Liu and Arief A Suriawinata (Jan. 2019). 'Pancreatic ductal adenocarcinoma and its precursor lesions: Histopathology, cytopathology, and molecular pathology'. en. In: *Am. J. Pathol.* 189.1, pp. 9–21.

Rice, A J et al. (July 2017). 'Matrix stiffness induces epithelial-mesenchymal transition and promotes chemoresistance in pancreatic cancer cells'. en. In: *Oncogenesis* 6.7, e352.

Richardson, Gavin D et al. (July 2004). 'CD133, a novel marker for human prostatic epithelial stem cells'. en. In: *J. Cell Sci.* 117.Pt 16, pp. 3539–3545.

Rigby, Fiona (Sept. 2024). *National Pancreatic Cancer Audit Report 2024 (NPaCA)*. en. `https://www.hqip.org.uk/resource/npaca-sotn-2024/`. Accessed: 2025-5-20.

Rizvi, Sumera and Gregory J Gores (Dec. 2013). 'Pathogenesis, diagnosis, and management of cholangiocarcinoma'. en. In: *Gastroenterology* 145.6, pp. 1215–1229.

Rizwani, Wasia, Amanda E Allen and Jose G Trevino (Sept. 2015). 'Hepatocyte growth factor from a clinical perspective: A pancreatic cancer challenge'. en. In: *Cancers (Basel)* 7.3, pp. 1785–1805.

Robb, R J, A Munck and K A Smith (Nov. 1981). 'T cell growth factor receptors. Quantitation, specificity, and biological relevance'. en. In: *J. Exp. Med.* 154.5, pp. 1455–1474.

Roberts, Nicholas J et al. (Oct. 2011). 'Systemic use of tumor necrosis factor alpha as an anticancer agent'. en. In: *Oncotarget* 2.10, pp. 739–751.

Rodriguez, A D et al. (May 2020). 'A microfluidic platform for functional testing of cancer drugs on intact tumor slices'. In: *Lab Chip* 20.9, pp. 1658–1675.

Rodriguez-Garcia, Alba et al. (June 2020). 'CAR-T Cells Hit the Tumor Microenvironment: Strategies to Overcome Tumor Escape'. en. In: *Front. Immunol.* 11, p. 548227.

Rodríguez-Merced, Nelson J, Mackenzie K Callaway and Paolo P Provenzano (Mar. 2023). 'Protocol to culture and image pancreatic ductal adenocarcinoma tumor slices to study T cell migration'. In: *STAR Protocols* 4.1, p. 102135.

Romero-Leguizamón, César R et al. (Feb. 2019). 'Increasing cellular lifespan with a flow system in organotypic culture of the Laterodorsal Tegmentum (LDT)'. In: *Scientific Reports 2019 9:1* 9.1, pp. 1–11.

Röper, K, D Corbeil and W B Huttner (Sept. 2000). 'Retention of prominin in microvilli reveals distinct cholesterol-based lipid micro-domains in the apical plasma membrane'. en. In: *Nat. Cell Biol.* 2.9, pp. 582–592.

Roselli, Emiliano et al. (Oct. 2021). '4-1BB and optimized CD28 co-stimulation enhances function of human mono-specific and bi-specific third-generation CAR T cells'. en. In: *J. Immunother. Cancer* 9.10, e003354.

Rosenberg, S (Oct. 1985). 'Lymphokine-activated killer cells: a new approach to immunotherapy of cancer'. en. In: *J. Natl. Cancer Inst.* 75.4, pp. 595–603.

Rosenberg, S A, B S Packard et al. (Dec. 1988). 'Use of tumor-infiltrating lymphocytes and interleukin-2 in the immunotherapy of patients with metastatic melanoma. A preliminary report'. en. In: *N. Engl. J. Med.* 319.25, pp. 1676–1680.

Rosenberg, S A, P Spiess and R Lafreniere (Sept. 1986). 'A new approach to the adoptive immunotherapy of cancer with tumor-infiltrating lymphocytes'. en. In: *Science* 233.4770, pp. 1318–1321.

Runge, Annette et al. (Sept. 2022). 'Patient-derived head and neck tumor slice cultures: a versatile tool to study oncolytic virus action'. In: *Scientific Reports 2022 12:1* 12.1, pp. 1–14.

Rutihinda, Cleopatra et al. (Nov. 2021). '597 The role of CCL20 in mediating regulatory T cell infiltration and resistance to radiotherapy in head and neck squamous cell carcinoma'. en. In: *J. Immunother. Cancer* 9.Suppl 2, A627–A627.

Saadi, Mahdiyar Iravani et al. (Sept. 2021). 'Expression levels of IL-6 and IL-18 in acute myeloid leukemia and its relation with response to therapy and acute GvHD after bone marrow transplantation'. en. In: *Indian J. Surg. Oncol.* 12.3, pp. 465–471.

Sade-Feldman, Moshe et al. (Nov. 2018). 'Defining T cell states associated with response to checkpoint immunotherapy in melanoma'. en. In: *Cell* 175.4, 998–1013.e20.

Saftig, Paul and Karina Reiss (June 2011). 'The "A Disintegrin And Metalloproteases" ADAM10 and ADAM17: novel drug targets with therapeutic potential?' en. In: *Eur. J. Cell Biol.* 90.6-7, pp. 527–535.

Salas, Ana et al. (Mar. 2020). 'Organotypic culture as a research and preclinical model to study uterine leiomyomas'. In: *Scientific Reports 2020 10:1* 10.1, pp. 1–12.

Salem, Dalia A et al. (Aug. 2018). 'Quantification of B-cell maturation antigen, a target for novel chimeric antigen receptor T-cell therapy in Myeloma'. en. In: *Leuk. Res.* 71, pp. 106–111.

Salmikangas, Paula, Niamh Kinsella and Paul Chamberlain (May 2018). 'Chimeric antigen receptor T-cells (CAR T-cells) for cancer immunotherapy - moving target for industry?' en. In: *Pharm. Res.* 35.8, p. 152.

Salmon, Hélène et al. (Mar. 2012). 'Matrix architecture defines the preferential localization and migration of T cells into the stroma of human lung tumors'. In: *J. Clin. Invest.* 122.3, p. 899.

Salter, Alexander I et al. (Aug. 2018). 'Phosphoproteomic analysis of chimeric antigen receptor signaling reveals kinetic and quantitative differences that affect cell function'. en. In: *Sci. Signal.* 11.544, eaat6753.

Sarfaty, Elad et al. (Sept. 2023). 'Surgical management of pancreatic ductal adenocarcinoma: a narrative review'. en. In: *Transl. Gastroenterol. Hepatol.* 8, p. 39.

Sato, Toshiro et al. (Nov. 2011). 'Long-term expansion of epithelial organoids from human colon, adenoma, adenocarcinoma, and Barrett's epithelium'. en. In: *Gastroenterology* 141.5, pp. 1762–1772.

Savoldo, Barbara et al. (May 2011). 'CD28 costimulation improves expansion and persistence of chimeric antigen receptor-modified T cells in lymphoma patients'. en. In: *J. Clin. Invest.* 121.5, pp. 1822–1826.

Schadendorf, Dirk et al. (June 2015). 'Pooled analysis of long-term survival data from phase II and phase III trials of ipilimumab in unresectable or metastatic melanoma'. en. In: *J. Clin. Oncol.* 33.17, pp. 1889–1894.

Scheurich, P et al. (Mar. 1987). 'Immunoregulatory activity of recombinant human tumor necrosis factor (TNF)-alpha: induction of TNF receptors on human T cells and TNF-alpha-mediated enhancement of T cell responses'. en. In: *J. Immunol.* 138.6, pp. 1786–1790.

Schmitt, Saskia et al. (Mar. 2024). 'Abstract 2623: Enabling 5T4 for targeted cancer therapy: TUB-030, a novel ADC built with ethynylphosphonamidate conjugation chemistry, shows long-lasting anti-tumor activity via Topoisomerase-I inhibition with an optimized therapeutic index'. en. In: *Cancer Res.* 84.6_Supplement, pp. 2623–2623.

Schneider, Enja et al. (Oct. 2021). 'CD73-mediated adenosine production by CD8 T cell-derived extracellular vesicles constitutes an intrinsic mechanism of immune suppression'. en. In: *Nat. Commun.* 12.1, p. 5911.

Schuster, Brooke et al. (Oct. 2020). 'Automated microfluidic platform for dynamic and combinatorial drug screening of tumor organoids'. In: *Nat. Commun.*

Schuster, Stephen J et al. (Jan. 2019). 'Tisagenlecleucel in adult relapsed or refractory diffuse large B-cell lymphoma'. en. In: *N. Engl. J. Med.* 380.1, pp. 45–56.

Schuth, Sebastian et al. (Oct. 2022). 'Patient-specific modeling of stroma-mediated chemoresistance of pancreatic cancer using a three-dimensional organoid-fibroblast co-culture system'. en. In: *J. Exp. Clin. Cancer Res.* 41.1, p. 312.

Seo, Yongwoo David et al. (2019). 'Mobilization of CD8+ T cells via CXCR4 blockade facilitates PD-1 checkpoint therapy in human pancreatic cancer'. In: *Clin. Cancer Res.* 25.13, p. 3934.

Seufferlein, T et al. (Jan. 2023). 'Perioperative or only adjuvant gemcitabine plus nab-paclitaxel for resectable pancreatic cancer (NEONAX)-a randomized phase II trial of the AIO pancreatic cancer group'. en. In: *Ann. Oncol.* 34.1, pp. 91–100.

Sharma, Ankur et al. (Oct. 2022). 'Oncofetal reprogramming in tumour development and progression'. en. In: *Nat. Rev. Cancer* 22.10, pp. 593–602.

Shaw, David M et al. (Apr. 2002). 'Glycosylation and epitope mapping of the 5T4 glycoprotein oncofoetal antigen'. en. In: *Biochem. J* 363.Pt 1, pp. 137–145.

Sheth, Vipul S and Jordan Gauthier (Mar. 2021). 'Taming the beast: CRS and ICANS after CAR T-cell therapy for ALL'. en. In: *Bone Marrow Transplant.* 56.3, pp. 552–566.

Shewade, Ashwini (Dec. 2023). 'Real-World Incidence, Characteristics and Management of Cytokine Release Syndrome Induced By Chimeric Antigen Receptor T-Cell Therapy across Hematologic Malignancies'. en. In: *65th ASH Annual Meeting & Exposition*. ASH.

Shichi, Yuuki et al. (May 2022). 'Epithelial and mesenchymal features of pancreatic ductal adenocarcinoma cell lines in two- and three-dimensional cultures'. en. In: *J. Pers. Med.* 12.5, p. 746.

Shin, E C et al. (July 2001). 'IFN-gamma induces cell death in human hepatoma cells through a TRAIL/death receptor-mediated apoptotic pathway'. en. In: *Int. J. Cancer* 93.2, pp. 262–268.

Shinkins, Bethany et al. (Mar. 2017). 'The diagnostic accuracy of a single CEA blood test in detecting colorectal cancer recurrence: Results from the FACS trial'. en. In: *PLoS One* 12.3, e0171810.

Shirakabe, Kyoko et al. (Apr. 2017). 'Mechanistic insights into ectodomain shedding: susceptibility of CADM1 adhesion molecule is determined by alternative splicing and O-glycosylation'. en. In: *Sci. Rep.* 7.1, p. 46174.

Shouse, Acacia N, Kathryn M LaPorte and Thomas R Malek (Mar. 2024). 'Interleukin-2 signaling in the regulation of T cell biology in autoimmunity and cancer'. en. In: *Immunity* 57.3, pp. 414–428.

Si, Xiaohui et al. (Mar. 2022). 'Preclinical evaluation of CAR T cell function: In vitro and in vivo models'. en. In: *Int. J. Mol. Sci.* 23.6, p. 3154.

Siddiqui, Imran et al. (Jan. 2019). 'Intratumoral Tcf1+PD-1+CD8+ T cells with stem-like properties promote tumor control in response to vaccination and checkpoint blockade immunotherapy'. en. In: *Immunity* 50.1, 195–211.e10.

Siegel, Rebecca L, Kimberly D Miller and Ahmedin Jemal (Jan. 2018). 'Cancer statistics, 2018'. en. In: *CA Cancer J. Clin.* 68.1, pp. 7–30.

Silveira, Caio Raony Farina et al. (Sept. 2022). 'Cytokines as an important player in the context of CAR-T cell therapy for cancer: Their role in tumor immunomodulation, manufacture, and clinical implications'. en. In: *Front. Immunol.* 13, p. 947648.

Singh, Jassimran et al. (May 2025). 'Pancreatic neuroendocrine tumors-A descriptive study of the presenting features in a 20-year surgical resection cohort at a tertiary institution'. en. In: *Pancreas* 54.5, e423–e429.

Siret, Carole et al. (2019). 'Deciphering the crosstalk between myeloid-derived suppressor cells and regulatory T cells in pancreatic ductal adenocarcinoma'. en. In: *Front. Immunol.* 10, p. 3070.

Sivakumar, Ramya et al. (Dec. 2019). 'Organotypic tumor slice cultures provide a versatile platform for immuno-oncology and drug discovery'. In: *Oncoimmunology* 8.12.

Smith, Tyrel T et al. (June 2017). 'Biopolymers codelivering engineered T cells and STING agonists can eliminate heterogeneous tumors'. In: *J. Clin. Invest.* 127.6, p. 2176.

Sockolosky, Jonathan T et al. (Mar. 2018). 'Selective targeting of engineered T cells using orthogonal IL-2 cytokine-receptor complexes'. en. In: *Science* 359.6379, pp. 1037–1042.

Song, Hannah W et al. (July 2024). 'CAR-T cell expansion platforms yield distinct T cell differentiation states'. en. In: *Cytotherapy* 26.7, pp. 757–768.

Sontheimer-Phelps, Alexandra, Bryan A Hassell and Donald E Ingber (Feb. 2019). 'Modelling cancer in microfluidic human organs-on-chips'. en. In: *Nat. Rev. Cancer* 19.2, pp. 65–81.

Southall, P J et al. (Jan. 1990). 'Immunohistological distribution of 5T4 antigen in normal and malignant tissues'. en. In: *Br. J. Cancer* 61.1, pp. 89–95.

Spolski, Rosanne, Peng Li and Warren J Leonard (Oct. 2018). 'Biology and regulation of IL-2: from molecular mechanisms to human therapy'. en. In: *Nat. Rev. Immunol.* 18.10, pp. 648–659.

Springfeld, Christoph et al. (May 2023). 'Neoadjuvant therapy for pancreatic cancer'. en. In: *Nat. Rev. Clin. Oncol.* 20.5, pp. 318–337.

Starnes, C O (May 1992). 'Coley's toxins in perspective'. en. In: *Nature* 357.6373, pp. 11–12.

Starzynska, T, V Rahi and P L Stern (Nov. 1992). 'The expression of 5T4 antigen in colorectal and gastric carcinoma'. en. In: *Br. J. Cancer* 66.5, pp. 867–869.

Starzyńska, T et al. (May 1994). 'Prognostic significance of 5T4 oncofetal antigen expression in colorectal carcinoma'. In: *Br. J. Cancer* 69, pp. 899–902.

Steinert, Elizabeth M et al. (May 2015). 'Quantifying memory CD8 T cells reveals regionalization of immunosurveillance'. en. In: *Cell* 161.4, pp. 737–749.

Stern, Peter L and Richard Harrop (Apr. 2017). '5T4 oncofoetal antigen: an attractive target for immune intervention in cancer'. In: *Cancer Immunol. Immunother.* 66.4, pp. 415–426.

Sterner, Robert C and Rosalie M Sterner (Apr. 2021). 'CAR-T cell therapy: current limitations and potential strategies'. en. In: *Blood Cancer J.* 11.4, p. 69.

Suh, Hyung C et al. (Nov. 2018). 'Bioengineered autologous dendritic cells enhance CAR T cell cytotoxicity by providing cytokine stimulation and intratumoral dendritic cells'. en. In: *Blood* 132.Supplement 1, pp. 3693–3693.

Sun, Yunyan et al. (Apr. 2025). 'Depletion of Tregs from CD4+ CAR-T cells enhances the tumoricidal effect of CD8+ CAR-T cells in anti-CD19 CAR-T therapy'. en. In: *FEBS J.* 292.8, pp. 1904–1919.

Sutherland, R M, J A McCredie and W R Inch (Jan. 1971). 'Growth of multicell spheroids in tissue culture as a model of nodular carcinomas'. en. In: *J. Natl. Cancer Inst.* 46.1, pp. 113–120.

Svoboda, J et al. (June 2023). '17th international conference on malignant lymphoma, Palazzo dei congressi, Lugano, Switzerland, 13 - 17 June, 2023'. en. In: *Hematol. Oncol.* 41 Suppl 2.S2, pp. 35–37.

Tabu, Kouichi et al. (2013). 'Gene regulation of prominin-1 (CD133) in normal and cancerous tissues'. en. In: *Adv. Exp. Med. Biol.* 777, pp. 73–85.

Taher, Mustafa Yassin, David Marc Davies and John Maher (Dec. 2018). 'The role of the interleukin (IL)-6/IL-6 receptor axis in cancer'. en. In: *Biochem. Soc. Trans.* 46.6, pp. 1449–1462.

Tamaki, Stanley et al. (Sept. 2002). 'Engraftment of sorted/expanded human central nervous system stem cells from fetal brain'. en. In: *J. Neurosci. Res.* 69.6, pp. 976–986.

Tang, Lin et al. (Nov. 2023). 'Arming CAR-T cells with cytokines and more: Innovations in the fourth-generation CAR-T development'. en. In: *Mol. Ther.* 31.11, pp. 3146–3162.

Tang, Na et al. (Feb. 2020). 'TGF-β inhibition via CRISPR promotes the long-term efficacy of CAR T cells against solid tumors'. en. In: *JCI Insight* 5.4.

Tang, Tiffany C Y et al. (Apr. 2022). 'Donor T cells for CAR T cell therapy'. en. In: *Biomark. Res.* 10.1, p. 14.

Taves, Matthew D and Jonathan D Ashwell (Apr. 2021). 'Glucocorticoids in T cell development, differentiation and function'. en. In: *Nat. Rev. Immunol.* 21.4, pp. 233–243.

Tawbi, Hussein A et al. (Jan. 2022). 'Relatlimab and nivolumab versus nivolumab in untreated advanced melanoma'. en. In: *N. Engl. J. Med.* 386.1, pp. 24–34.

Taylor, Chelsea Alice, Maya Glover and John Maher (Aug. 2024). 'CAR-T cell technologies that interact with the tumour microenvironment in solid tumours'. en. In: *Expert Rev. Clin. Immunol.* 20.8, pp. 849–871.

Teleanu, Raluca Ioana et al. (Dec. 2019). 'Tumor angiogenesis and anti-angiogenic strategies for cancer treatment'. en. In: *J. Clin. Med.* 9.1, p. 84.

Thommen, Daniela S et al. (July 2018). 'A transcriptionally and functionally distinct PD-1+ CD8+ T cell pool with predictive potential in non-small-cell lung cancer treated with PD-1 blockade'. en. In: *Nat. Med.* 24.7, pp. 994–1004.

Tian, Yonggui et al. (Nov. 2022). 'CXCL9-modified CAR T cells improve immune cell infiltration and antitumor efficacy'. en. In: *Cancer Immunol. Immunother.* 71.11, pp. 2663–2675.

Torjesen, Ingrid (Nov. 2021). 'HPV vaccine cut cervical cancer rates in England by 87'. en. In: *BMJ* 375, n2689.

Tousley, Aidan M et al. (Mar. 2023). 'Co-opting signalling molecules enables logic-gated control of CAR T cells'. en. In: *Nature* 615.7952, pp. 507–516.

Tsang, Julia Yuen Shan et al. (May 2011). 'Novel immunomodulatory effects of adiponectin on dendritic cell functions'. en. In: *Int. Immunopharmacol.* 11.5, pp. 604–609.

Tu, Taojian et al. (Mar. 2025). 'Proinflammatory macrophages release CXCL5 to regulate T cell function and limit effects of αPD-1 in steatosis-driven liver cancer'. en. In: *JHEP Rep.* 0.101385, p. 101385.

Turtle, Cameron J et al. (June 2016). 'CD19 CAR-T cells of defined CD4+:CD8+ composition in adult B cell ALL patients'. en. In: *J. Clin. Invest.* 126.6, pp. 2123–2138.

Uhlen, Mathias et al. (Aug. 2017). 'A pathology atlas of the human cancer transcriptome'. en. In: *Science* 357.6352.

Valencia, Xavier et al. (July 2006). 'TNF downmodulates the function of human CD4+CD25hi T-regulatory cells'. en. In: *Blood* 108.1, pp. 253–261.

Valenzano, Giampiero et al. (Oct. 2024). 'Using spectral flow cytometry to characterize anti-tumor immunity in orthotopic and subcutaneous mouse models of cancer'. en. In: *Curr. Protoc.* 4.10, e70032.

Versteijne, Eva et al. (Apr. 2022). 'Neoadjuvant chemoradiotherapy versus upfront surgery for resectable and borderline resectable pancreatic cancer: Long-term results of the Dutch randomized PREOPANC trial'. en. In: *J. Clin. Oncol.* 40.11, pp. 1220–1230.

Vianello, Fabrizio et al. (Mar. 2006). 'Murine B16 melanomas expressing high levels of the chemokine stromal-derived factor-1/CXCL12 induce tumor-specific T cell chemorepulsion and escape from immune control'. en. In: *J. Immunol.* 176.5, pp. 2902–2914.

Voabil, Paula et al. (July 2021). 'An ex vivo tumor fragment platform to dissect response to PD-1 blockade in cancer'. en. In: *Nat. Med.* 27.7, pp. 1250–1261.

Wainberg, Zev A, Gulam Abbas Manji et al. (Jan. 2024). 'ARC-8: Phase 1/1b randomized study of quemliclustat + gemcitabine/nab-paclitaxel ± zimberelimab in patients with treatment-naive metastatic pancreatic adenocarcinoma'. en. In: *J. Clin. Oncol.* 42.3_suppl, pp. 665–665.

Wainberg, Zev A, Davide Melisi et al. (Oct. 2023). 'NALIRIFOX versus nab-paclitaxel and gemcitabine in treatment-naive patients with metastatic pancreatic ductal adenocarcinoma (NAPOLI 3): a randomised, open-label, phase 3 trial'. en. In: *Lancet* 402.10409, pp. 1272–1281.

Walunas, T L et al. (Aug. 1994). 'CTLA-4 can function as a negative regulator of T cell activation'. en. In: *Immunity* 1.5, pp. 405–413.

Wang, Dan et al. (Aug. 2019). 'Colorectal cancer cell-derived CCL20 recruits regulatory T cells to promote chemoresistance via FOXO1/CEBPB/NF-κB signaling'. en. In: *J. Immunother. Cancer* 7.1, p. 215.

Wang, Jiasheng and John Doran (Mar. 2021). 'The many faces of cytokine release syndrome-related coagulopathy'. en. In: *Clin. Hematol. Int.* 3.1, pp. 3–12.

Wang, Kemeng, Guoqing Wei and Delong Liu (Nov. 2012). 'CD19: a biomarker for B cell development, lymphoma diagnosis and therapy'. en. In: *Exp. Hematol. Oncol.* 1.1, p. 36.

Wang, Ruixue et al. (2018). 'A novel 5T4-targeting antibody-drug conjugate H6-DM4 exhibits potent therapeutic efficacy in gastrointestinal tumor xenograft models'. In: *Am. J. Cancer Res.* 8.4, p. 610.

Wang, Xiuyan and Isabelle Rivière (June 2016). 'Clinical manufacturing of CAR T cells: foundation of a promising therapy'. en. In: *Mol. Ther. Oncolytics* 3.16015, p. 16015.

Ware, Michael Brandon, Bassel F El-Rayes and Gregory B Lesinski (Aug. 2020). 'Mirage or long-awaited oasis: reinvigorating T-cell responses in pancreatic cancer'. en. In: *J. Immunother. Cancer* 8.2, e001100.

Weber, Rebekka et al. (Jan. 2021). 'IL-6 as a major regulator of MDSC activity and possible target for cancer immunotherapy'. en. In: *Cell. Immunol.* 359.104254, p. 104254.

Weiss, Ronald et al. (Oct. 2021). 'Comparison of three CD3-specific separation methods leading to labeled and label-free T cells'. en. In: *Cells* 10.11, p. 2824.

Wessels, Alette M et al. (Feb. 2020). 'Efficacy and safety of lanabecestat for treatment of early and mild Alzheimer disease: The AMARANTH and DAYBREAK-ALZ randomized clinical trials: The AMARANTH and DAYBREAK-ALZ randomized clinical trials'. en. In: *JAMA Neurol.* 77.2, pp. 199–209.

Wherry, E John, Sang-Jun Ha et al. (Oct. 2007). 'Molecular signature of CD8+ T cell exhaustion during chronic viral infection'. en. In: *Immunity* 27.4, pp. 670–684.

Wherry, E John, Volker Teichgräber et al. (Mar. 2003). 'Lineage relationship and protective immunity of memory CD8 T cell subsets'. en. In: *Nat. Immunol.* 4.3, pp. 225–234.

Wilk, Sabrina et al. (Aug. 2011). 'Adiponectin is a negative regulator of antigen-activated T cells'. en. In: *Eur. J. Immunol.* 41.8, pp. 2323–2332.

Wilkie, Scott et al. (Apr. 2008). 'Retargeting of human T cells to tumor-associated MUC1: the evolution of a chimeric antigen receptor'. en. In: *J. Immunol.* 180.7, pp. 4901–4909.

Williamson, Steve (May 2019). *Implementing CAR T cell therapy in the NHS*. Tech. rep. NHS England.

Wu, Jie et al. (Oct. 2020). 'High expression of CD39 is associated with poor prognosis and immune infiltrates in clear cell renal cell carcinoma'. en. In: *Onco. Targets. Ther.* 13, pp. 10453–10464.

Wu, Xian-Rui et al. (Aug. 2012). 'High expression of CD73 as a poor prognostic biomarker in human colorectal cancer: CD73 and Prognosis of Colorectal Cancer'. en. In: *J. Surg. Oncol.* 106.2, pp. 130–137.

Wullkopf, Lena et al. (Oct. 2018). 'Cancer cells' ability to mechanically adjust to extracellular matrix stiffness correlates with their invasive potential'. en. In: *Mol. Biol. Cell* 29.20, pp. 2378–2385.

Xi, Biao et al. (Nov. 2019). 'A real-time potency assay for chimeric antigen receptor T cells targeting solid and hematological cancer cells'. en. In: *J. Vis. Exp.* 153.

Xinopoulos, D et al. (July 2008). 'Gemcitabine as palliative treatment in patients with unresectable pancreatic cancer previously treated with placement of a covered metal stent. A randomized controlled trial'. en. In: *J. BUON* 13.3, pp. 341–347.

Xu, Shan et al. (July 2014). 'Construction and characteristics of an E-cadherin-related three-dimensional suspension growth model of ovarian cancer'. en. In: *Sci. Rep.* 4.1, p. 5646.

Xu, X et al. (July 1998). 'IFN-gamma induces cell growth inhibition by Fas-mediated apoptosis: requirement of STAT1 protein for up-regulation of Fas and FasL expression'. en. In: *Cancer Res.* 58.13, pp. 2832–2837.

Yamada, Hisashi et al. (Oct. 1986). 'Establishment of a human pancreatic adenocarcinoma cell line (PSN-1) with amplifications of both c-myc and activated c-Ki-ras by a point mutation'. In: *Biochem. Biophys. Res. Commun.* 140.1, pp. 167–173.

Yan, Xin et al. (Nov. 2022). 'CD58 loss in tumor cells confers functional impairment of CAR T cells'. en. In: *Blood Adv.* 6.22, pp. 5844–5856.

Yazdanifar, Mahboubeh et al. (Sept. 2019). 'Overcoming immunological resistance enhances the efficacy of A novel anti-tMUC1-CAR T cell treatment against pancreatic ductal adenocarcinoma'. en. In: *Cells* 8.9, p. 1070.

Yin, A H et al. (Dec. 1997). 'AC133, a novel marker for human hematopoietic stem and progenitor cells'. en. In: *Blood* 90.12, pp. 5002–5012.

Yin, Jiaxin et al. (Sept. 2022). 'What is the optimal duration of immune checkpoint inhibitors in malignant tumors?' en. In: *Front. Immunol.* 13, p. 983581.

Yu, Qing, Archna Sharma, Amalendu Ghosh et al. (Apr. 2011). 'T cell factor-1 negatively regulates expression of IL-17 family of cytokines and protects mice from experimental autoimmune encephalomyelitis'. en. In: *J. Immunol.* 186.7, pp. 3946–3952.

Yu, Qing, Archna Sharma, Sun Young Oh et al. (Sept. 2009). 'T cell factor 1 initiates the T helper type 2 fate by inducing the transcription factor GATA-3 and repressing interferon-gamma'. en. In: *Nat. Immunol.* 10.9, pp. 992–999.

Yuki, Kanako et al. (Aug. 2020). 'Organoid Models of Tumor Immunology'. In: *Trends Immunol.* 41.8, pp. 652–664.

Yunis, Adel A, Grace K Arimura and David J Russin (Jan. 1977). 'Human pancreatic carcinoma (mia paca-2) in continuous culture: Sensitivity to asparaginase'. In: *International Journal of Cancer* 19.1, pp. 128–135.

Zajac, A J et al. (Dec. 1998). 'Viral immune evasion due to persistence of activated T cells without effector function'. en. In: *J. Exp. Med.* 188.12, pp. 2205–2213.

Zarour, Hassane M et al. (2003). 'Categories of Tumor Antigens'. In: *Holland-Frei Cancer Medicine. 6th edition.* BC Decker.

Zhang, David K Y et al. (Feb. 2025). 'Subcutaneous biodegradable scaffolds for restimulating the antitumour activity of pre-administered CAR-T cells'. en. In: *Nat. Biomed. Eng.* 9.2, pp. 268–278.

Zhang, Meiyin et al. (May 2025). 'Advances in cancer immunotherapy: historical perspectives, current developments, and future directions'. en. In: *Mol. Cancer* 24.1, pp. 1–48.

Zhang, Yuanyuan and Zemin Zhang (Aug. 2020). 'The history and advances in cancer immunotherapy: understanding the characteristics of tumor-infiltrating immune cells and their therapeutic implications'. en. In: *Cell. Mol. Immunol.* 17.8, pp. 807–821.

Zhang, Yugu et al. (Sept. 2023). 'Exploring CAR-T cell therapy side effects: Mechanisms and management strategies'. en. In: *J. Clin. Med.* 12.19, p. 6124.

Zhao, Zeguo, Maud Condomines et al. (Oct. 2015). 'Structural design of engineered costimulation determines tumor rejection kinetics and persistence of CAR T cells'. en. In: *Cancer Cell* 28.4, pp. 415–428.

Zhao, Zeguo and Michel Sadelain (Oct. 2023). 'CAR T cell design: approaching the elusive AND-gate'. en. In: *Cell Res.* 33.10, pp. 739–740.

Zhou, Yan et al. (Feb. 2008). 'IFN-gamma induces apoptosis in HL-60 cells through decreased Bcl-2 and increased Bak expression'. en. In: *J. Interferon Cytokine Res.* 28.2, pp. 65–72.

Zoetemelk, Marloes et al. (May 2019). 'Short-term 3D culture systems of various complexity for treatment optimization of colorectal carcinoma'. en. In: *Sci. Rep.* 9.1, p. 7103.